Viral vector-mediated RNA interference in the retina

Anastasios Georgiadis

A thesis submitted for the degree of
Doctor of Philosophy

2009

Division of Molecular Therapy
Institute of Ophthalmology
University College London

I, Anastasios Georgiadis confirm that the work presented in this thesis is my own. Where information has been derived from other sources, I confirm that this has been indicated in the thesis.

Abstract

RNA interference (RNAi) is a highly conserved post-transcriptional gene silencing process triggered by double-stranded RNA (dsRNA) in eukaryotic cells. Elucidation of the RNAi regulatory pathway and its components has led to the identification of endogenous dsRNA molecules, termed microRNAs (miRNAs), which are transcribed as a single hairpin molecule prior to their maturation into a cytoplasmic dsRNA. The efficient gene silencing achieved by these short hairpin RNA (shRNA) molecules and the cumulative understanding of the RNAi pathway has prompted the development of hairpin expression vectors capable of mediating stable gene silencing *in vitro* and *in vivo*. The aim of this thesis is to evaluate the efficacy of viral vector-mediated RNAi in the retina using recombinant adeno-associated viruses (AAV) and lentiviruses that contain silencing hairpin cassettes to target four genes in murine photoreceptors and the retinal pigment epithelium (RPE).

A detailed assessment of the utility and extend of RNAi in the retina using different viral vectors and hairpin designs is presented in this thesis. Lentiviral and AAV vectors were firstly used to silence GFP *in vitro* and *in vivo* as a proof of concept for vector mediated RNAi in the retina. Subsequently, we used lentivirally-mediated RNAi to study disease processes in the retina concentrating on tight junction (TJ) modulators ZO-1 and ZONAB and their role in RPE homeostasis, cell-cycle progression and epithelial-mesenchymal transition (EMT). Here we demonstrated how TJ misregulation can lead to RPE loss, proliferation or dedifferentiation; processes involved in pathological conditions such as atrophic age-related macular degeneration (AMD) and proliferative vitroretinopathy (PVR).

Whilst lentivirally-mediated RNAi was used to elucidate aspects of retinal function and disease, AAV-mediated RNAi was used to probe the therapeutic potential of shRNAs by silencing *Peripherin-2* (*Prph2*), the second most abundant retinal protein, using a miRNA-based hairpin. AAV2/8 particles

were used to target endogenous Prph2 and evasion of silencing was demonstrated using an engineered *Prph2* cDNA that could be used in a suppression and replacement approach for the treatment of dominant retinal disorders.

Table of contents

Figures

Tables

Acknowledgements

I would like to thank Robin Ali for giving me the opportunity to do my PhD in his group as well as for his guidance, interest and support throughout all these years. I also thank Sander Smith for his advice and valuable input for all the projects I was involved in; Jim Bainbridge and Scott Robbie for the injections; Maria Balda and Karl Matter for their enthusiasm and collaboration. I would also like to extend my gratitude to Adrian Thrasher and Christine Kinnon for the opportunity to work in their group in the early stages of this project, and to all in Molecular Therapy.

My love goes to my parents, Dimos and Ioanna, for their support and love and my brother, Vassilis, for being always on my side and his constant encouragement. Finally I am grateful to Marion Tschernutter for all the endless help in the lab and especially her love and affection during all these years.

1 Introduction

1.1 Aims of study

RNA interference (RNAi) is a powerful technique for the downregulation of endogenous expression that is mediated by short double-stranded RNA molecules. Since its discovery about a decade ago, RNAi has proved to be an invaluable tool for characterising gene function and has been used *in vivo* to ablate specific mRNAs in various tissues. In this study, the utility of vector-mediated RNAi in the eye is assessed. The eye is a good candidate for genetic intervention because of its confined environment and accessibility and here we employed RNAi to test the potency of genetic silencing in different parts of the retina using different viral vectors.

Initially, we tested the technology in different parts of the retina using either AAV or lentiviral vectors to downregulate a reporter gene *in vivo* (see Chapter 3). Subsequently, lentiviruses were used to silence the tight-junction genes ZO-1 and ZONAB in the RPE to study disease processes and the importance of RPE cell-cycle regulation in retinal homeostasis. The role of the ZO-1/ZONAB pathway in epithelial-mesenchymal transition also highlighted the connection between RPE cell-cycle deregulation and gliotic retinal scarring in proliferative vitroretinopathy (see Chapter 4). Finally, we assessed the potential of RNAi for treating dominantly inherited retinal disorders. To date, there are no gene-based therapies for dominant retinopathies mainly because dominant disorders are more complex to treat than recessive ones due to the nature of the genetic mutation. Here, AAV2/8 vectors were used to silence Peripherin-2, one of the most highly expressed genes in the retina mutations in which are mainly involved in dominant retinopathies, indicating the potential of AAV2/8 vectors expressing RNAi cassettes for the treatment of dominant retinopathies (see Chapter 5).

In brief, the aim of this study is to further assess the potential of viral-mediated RNAi in the eye for the elucidation of disease mechanisms and for the treatment of dominant retinal disorders using the two most commonly used ocular gene therapy vectors, AAV and lentiviruses, to mediate efficient genetic silencing in photoreceptors and retinal pigment epithelium, respectively.

1.2 The eye

The eye is regarded as one of the most highly specialised organs in biology; an attribute based both on its structure and function. It is part of the central nervous system (CNS) and is in effect an extension of the brain. During embryogenesis, the first morphological manifestation of the eye structure is marked by the appearance of the optic pit, resulting from the invagination of the diencephalon. The optic pit gives rise to the early optic cup in which the neural retina and the RPE are formed from developmentally distinct regions. Meanwhile, inductive signals between the forming eye cup and the surface ectoderm initiate an invagination of the latter into what will form the lens vesicle and the cornea. At a later stage, the iris and ciliary body develop from the point where neural retina and RPE meet in the developing eye cup. At this time, the RPE is thin and is in contact with the extraocular mesenchyme. The ventral and dorsal areas of the optic stalk fuse into the choroidal fissure, which acts as the channel through which blood vessels pass and neuronal axons exit. From this point onwards, the neuroretina progressively thickens as cells proliferate and differentiate to give rise to different retinal cell types. The point at which the RPE associates with the neuroretina is a vital one for the future viability of photoreceptors as from that moment onwards the retina is isolated and relies on the RPE for its maintenance (see section 1.2.1.3 and Chapter 4 for RPE structure and its role in retinal homeostasis). A good review on early eye development is provided by Chow & Lang, 2001 [1].

There is a vast morphological variety of eye structures in the animal kingdom. However, physical laws and natural selection have restricted the general optic design of the eye into eight main types [2]. The mammalian eye lies in the chambered-refractive type where light is focused onto specialised nerve receptors. It is divided into three layers: the outer layer consists of the fibrocollagenous sclera and the transparent cornea that enables light to enter the eye; the middle vascular layer is called uvea and consists of the choroid,

the ciliary body and the iris that provide support and nutrients; the inner layer includes the neuroretina and the RPE where the visual cycle takes place. At the posterior side of the cornea lies the lens which acts as the refractive medium that focuses incoming light onto the retina. For a schematic overview of the human eye see Figure 1.1.

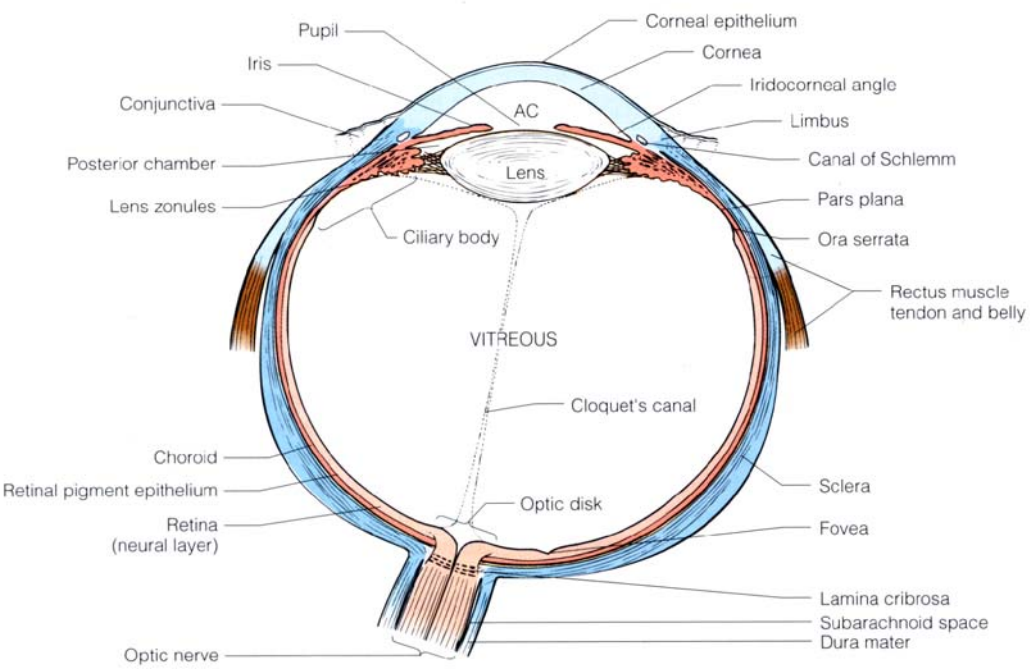

Figure 1.1: Anatomy of the eye. A schematic cross-section view of the human eye. The murine eye has a significantly larger lens that occupies the majority of the vitreous space and lacks a central cone-rich macula or fovea. AC; anterior chamber. (Forrester J.V., *The Eye: Basic Sciences in Practice*, 2002)

The retina is the innermost layer of the eye. It is divided into the neuroretina, which is the photosensitive tissue that includes the photoreceptor cells, and the RPE.

1.2.1 The retina

The organisation of the mammalian retina is indicative of its highly specialised function of phototransduction. The murine retina consists of approximately 55 distinct cell types [3] and it is structurally divided into ten different layers (Figure 1.2).

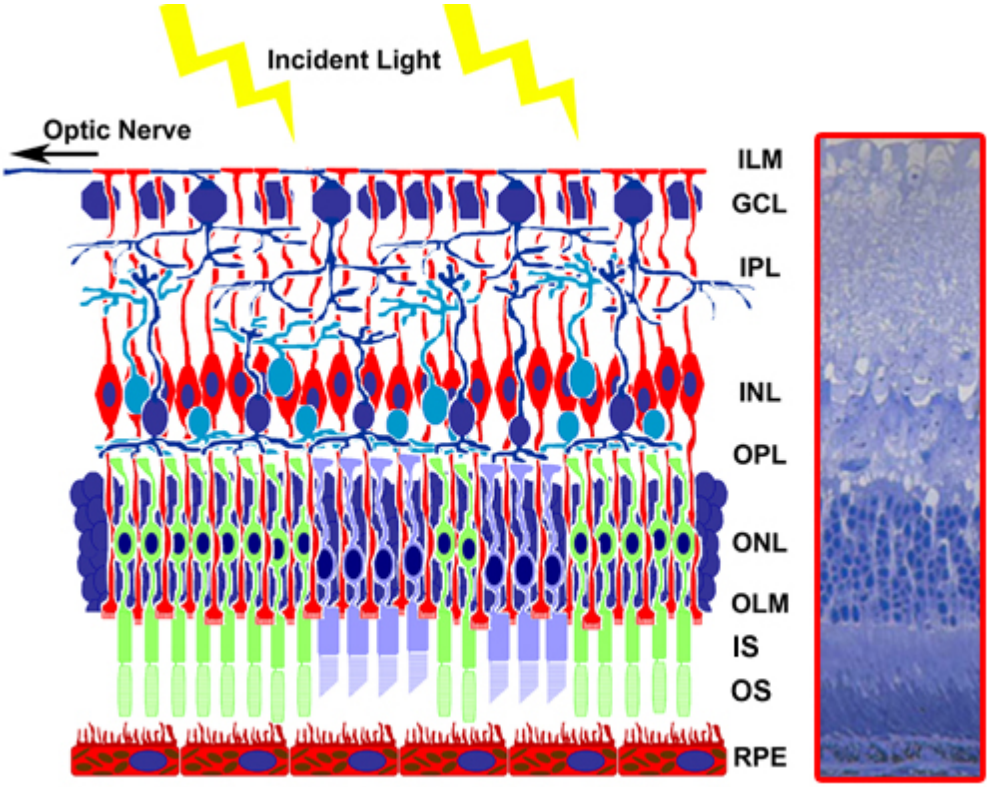

Figure 1.2: Structure of the murine retina. Schematic diagram of the retinal layers and corresponding light micrograph of a semithin section. **RPE**; retinal pigment epithelium. **OS**; (photoreceptor) outer segments; **IS**; (photoreceptor) inner segments. **OLM**; outer limiting membrane consisting of intercellular junctions. **ONL**; outer nuclear layer consisting of photoreceptor cell nuclei. **OPL**; outer plexiform layer consisting of synaptic connections between photoreceptor cells and nerve cells. **INL**; inner nuclear layer consisting of the nuclei of nerve and support cells. **IPL**; inner plexiform layer which is build up of synapses. **GC**; ganglion cell layer. **ILM**; inner limiting membrane which forms the border between the retina and the vitreous. (Adapted from West *et al.*, 2009) [4]

1.2.1.1 The neuroretina

In the neuroretina, there are three principal neuronal cells that relay impulses generated by light: photoreceptors, bipolar cells and ganglion cells. The activity of these cells is modulated by other neuronal cell types including horizontal cells and amacrine cells. Up to 11 different types of bipolar cells exist and they are primarily responsible for transmitting signals from photoreceptors to ganglion cells. In the primate central retina (*fovea centralis*), the ratio of cones to bipolar cells to ganglion cells can be as high as 1:1:1, while in the peripheral retina one bipolar cell can receive stimuli from up to 50-100 rods. In the latter situation, multiple bipolar cell dendrites reach out to various photoreceptors, while only a single axon synapses with ganglion and amacrine cells. This process is called signal summation. Their axonal input can be initiated through GABAergic or ionotropic glutamate receptors.

Horizontal cells exist as two main types and cross-connect numerous photoreceptor cells. They are thought to be part of a feedback system that modulates contrast in vision. Horizontal axons inhibit excited photoreceptors as well as neighbouring ones, adding to the sharpness of the initial signal. They constitute 5 % of the inner retina neurons and are situated mainly at the borders of outer plexiform layer (OPL) and outer nuclear layer (ONL).

The amacrine cell, although not considered to be one of the principal retinal neurons, is the most diverse and one of the most abundant. There are up to twenty-nine distinct types of amacrine cells and they outnumber horizontal, ganglion or Müller cells. They contribute to most of the ganglion cell synapses and their broad range of function is reflected in the variety of signalling mechanisms they use, including dopaminergic, cholinergic and GABAergic signalling along with paracrine regulated modulation through gap junctions. Although the function of each type of amacrine cell is not fully elucidated, they play an essential role in creating and shaping the retina's final physiological output. They are situated along the inner nuclear layer (INL).

Müller cells provide the scaffolding around which the retinal architecture is built. They are a retinal glial cell and maintain retinal homeostasis by neurotrophic factor secretion, support of retinal blood vessels and scavenging of signalling endproducts. Although they do not take part in the visual transduction pathway directly, the constant supply of cytokines and modulation of inner retinal vascular permeability renders them indispensable for the structure and function of the retina as a whole. It has also been suggested that these cells are an additional source of 11-cis retinal for cone cells [5]. A complex network of adherens junctions at the foot processes of Müller cells forms the inner limiting membrane (ILM) that separates the neuroretina from the vitreous. A similar junctional network between Müller cell end processes and the photoreceptor inner segments forms the outer limiting membrane (OLM) that provides structural support to the ONL.

Retinal ganglion cells (RGC) exist as up to ten distinct types according to their branching level and their dendritic arbour width. There is a difference in size with the smaller cells referred to as midget – a classification also seen in bipolar cells – as well as summing and non-summing responsive cell types. Ganglion cell dendrites receive impulses from bipolar cells and amacrine cells which they subsequently pass on through their axons to the visual cortex of the brain via the optic nerve. All ganglion cell axons are collected in the nerve fibre layer (NF) and are orientated towards the optic disc.

1.2.1.2 Photoreceptors

Photoreceptors occupy the innermost layers of the neuroretina with their outer segments adjacent to the apical membrane of the RPE, and their cell bodies in the ONL. There are two distinct types of photoreceptors: the rods and the cones. Their differences lie both in their structure (Figure 1.3) and function. Rods are the prominent type of photoreceptors in the mammalian retina outnumbering cones by approximately 20-fold [3]. They are

responsible for sensing motion, contrast and brightness through their highly sensitive visual pigment, rhodopsin. Cones, on the other hand, are necessary for spatial resolution, colour vision and fine detail; their visual pigments are the cone opsins. In primates, they exist in three types according to the wavelength of light they absorb. L-cones respond to long wavelengths of light (red light), M-cones to medium wavelengths (green light) and S-cones respond to short wavelengths (blue light) [3] (see Figure 1.4).

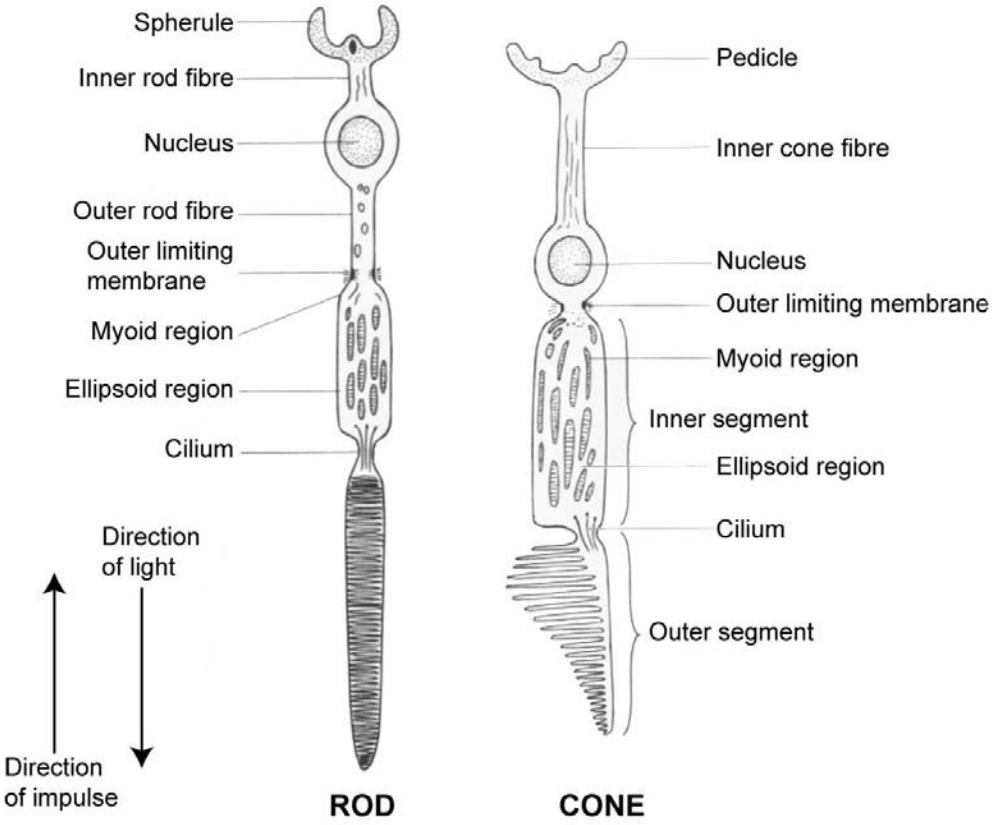

Figure 1.3: Structure of photoreceptor cells. Schematic representation of rod and cone photoreceptor cells. The distinct structural features of each cell type are annotated as well as the direction of light and electrical impulse they elicit. (Adapted from http://www.cis.rit.edu)

The opsins are located in the outer segments (OS) of the photoreceptor cells where the phototransduction cascade is initiated (see section 1.2.3). The outer segments in rods are formed by a dense network of membrane discs, whereas in cones they are formed by membrane infolds. The outer segments

provide a tightly-packed scaffold for the phototransduction cascade to take place. This increases the surface area per cell, thereby aiding in the potency of the visual signal. The main structural components of the outer segments are rhodopsin and Peripherin-2 (Prph2) (see section 5.1 for more detailed description of outer segments). The inner segments are rich in mitochondria and generate the energy for the demanding process of phototransduction. The spherules and pedicles form the synapses with horizontal and bipolar cells where neurotransmitters pass on the neural impulse generated by the photoreceptors.

The distribution of cones varies in the retina. In humans, there is a central cone-rich area in the retina, called macula, which contributes most to the visual acuity (Figure 1.4). In the centre of the macula is the fovea which consists exclusively of cones. There the supporting nerve cells are displaced so that light is directed straight onto this area. This structuring is essential for the high levels of visual acuity in primates and its understanding is vital for the characterisation of disease patterns in humans (see section 1.3). Mice, however, lack a central cone-rich region and the two types of cones (M- and S- type) are distributed all over the retina. However, the distribution of murine M- and S- cones is not equal in the dorsal-ventral orientation. The majority of M-cones are distributed in the dorsal hemisphere (M-field) whereas the majority of S-cones occupy the ventral hemisphere (S-field) [6,7].

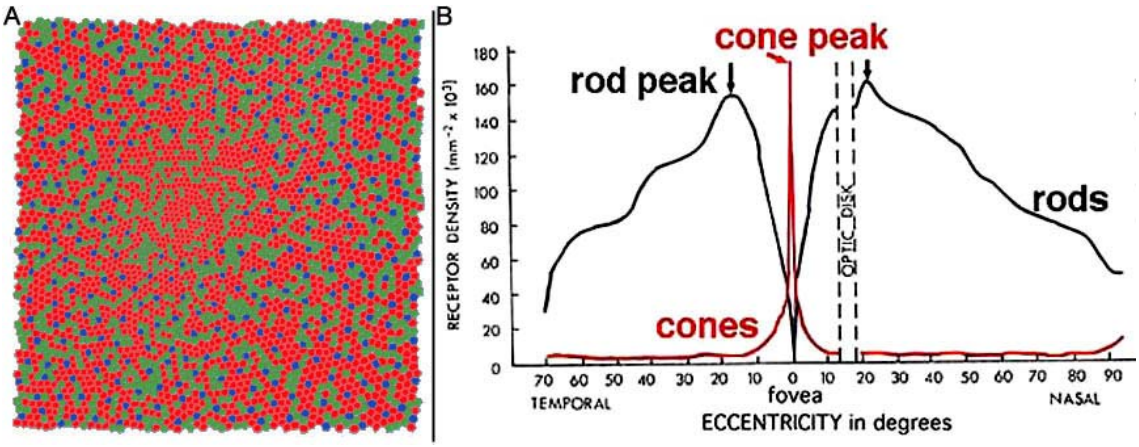

Figure 1.4: Rod and cone distribution in the human fovea. (A) Schematic representation of the cone mosaic. An area of 1° visual angle is represented. S-cones (blue) comprise 7% of the area, whereas the L-cone (red): M-cone (green) ratio is 1.5. The central area of 0.34° is S-cone free. **(B)** Diagram showing the densities of rods and cones along the horizontal meridian. (Adapted from http://webvision.med.utah.edu)

1.2.2 The retinal pigment epithelium

The RPE lies posterior to the neuroretina. It consists of melanin-containing, cuboidal, epithelial cells that form a rigid interconnected cell layer regulated by epithelial tight junctions (TJ), gap junctions (GJ) and adherens junctions (AJ). Cellular junctions within the RPE are vital for intracellular and paracellular signalling. Junctional components such as ZO-1, ZONAB, β-catenin and their importance in RPE function are discussed in depth in Chapter 4. The basal membrane of the RPE lies on the Bruch's membrane and its apical membrane forms microvilli presented towards the inter-photoreceptor matrix (IPM) and surrounding photoreceptor OS. The RPE plays a vital role in forming the blood-retinal barrier (BRB), physically assisting the structure of the neuroretina and maintaining photoreceptor cells through phagocytosis of their OS debris. In addition, it is involved in the turnover of by-products of the visual cycle (see section 1.2.3) as well as the production of neurotrophic factors essential for photoreceptor cell viability. Furthermore, the melanin layer confers higher visual acuity by inhibiting scattering of the light focused on the retina by the lens. Thus, the RPE is an essential non-neuronal cell layer directly involved in the retinal integrity and

the phototransduction pathway. A structurally or functionally compromised RPE leads to retinal degeneration and loss of vision.

1.2.2.1 Blood-retina barrier

The CNS maintains its homeostasis through the stability and function of the blood-neural barrier (BNB) that protects the CNS from surrounding blood or cerebrospinal fluid. The blood-retina barrier (BRB) is the ocular part of BNB and it is composed of the retinal vascular endothelium (inner BRB) and the RPE (outer BRB) [8]. The BRB is maintained mainly through tight, adherens and gap junctions between the vascular endothelial cells and between the pigmented epithelial cells (see section 4.1). Leakage or breakage of the BRB is thought to play a role in numerous ocular disorders. Experimental autoimmune uveoretinitis (EAU) serves as a model for human posterior uveitis where inflammation of the choroid, neovascularisation and BRB leakage leads to retinal scarring. In EAU, TJ function is compromised in the retinal vascular endothelium (RVE) and RPE leading to leukocyte infiltration. Disregulation of TJs not only compromises the BRB but also the polarity of the RPE. Oxidative stress, implicated in the pathogenesis of age-related macular degeneration (AMD), has also been shown to affect RPE polarity *in vitro* and causes downregulation of major TJ and AJ components like ZO-1, occludin and β–catenin [9]. Typical symptoms of diabetic retinopathy such as macular oedema and retinal neovascularisation are also associated with BRB breakage [10]. A number of molecules have been shown to affect BRB stability through their effect on TJs. Vascular endothelial growth factor (VEGF), tumour necrosis factor alpha (TNF-α) and interleukin 1 beta (IL1$_\beta$) have been shown to cause BRB dysfunction by destabilising TJ formation [8]. Mutations in *CLDN19*, a claudin family gene and important TJ anchor protein, cause renal failure and optic disc misdevelopment [11].

1.2.3 The visual cycle

Vertebrate visual responses are initiated in the photoreceptor OS by a photon-activated chemical cascade. This results in the propagation of a neuronal signal that crosses the neuroretina and is transferred to the brain for processing. The chemical cascade is a complex pathway that involves the continuous recycling of its substrates, hence the term visual cycle. Defects in any of the many genes encoding components of the visual cycle can result in a form of retinal dystrophy (see section 1.3)

Rhodopsin is the light-absorbing photopigment of rods and is located in the disc membrane of OS. It consists of a seven-pass transmembrane domain protein, opsin, as well as the Vitamin A analogue chromophore, 11-*cis* retinal. Upon light absorption it isomerises to all-*trans* retinal resulting in a subtle change in the conformation of rhodopsin. The conformational change in the molecule exposes a binding site on its cytoplasmic domain for a guanosine-5'-triphosphate (GTP) binding protein (G protein) called transducin. The α-subunit of transducin molecule then dissociates and activates a photoreceptor-specific disc-bound phosphodiesterase (PDE) by interacting with its inhibitory γ-subunit. The phase of the R*→G-protein→PDE cascade is greatly amplified at each step, with each molecule activating multiples of its downstream substrate. In effect, a single photon creates a relatively potent signal in comparison to its initial biochemical impact [12] (see Figure 1.5 for a summary).

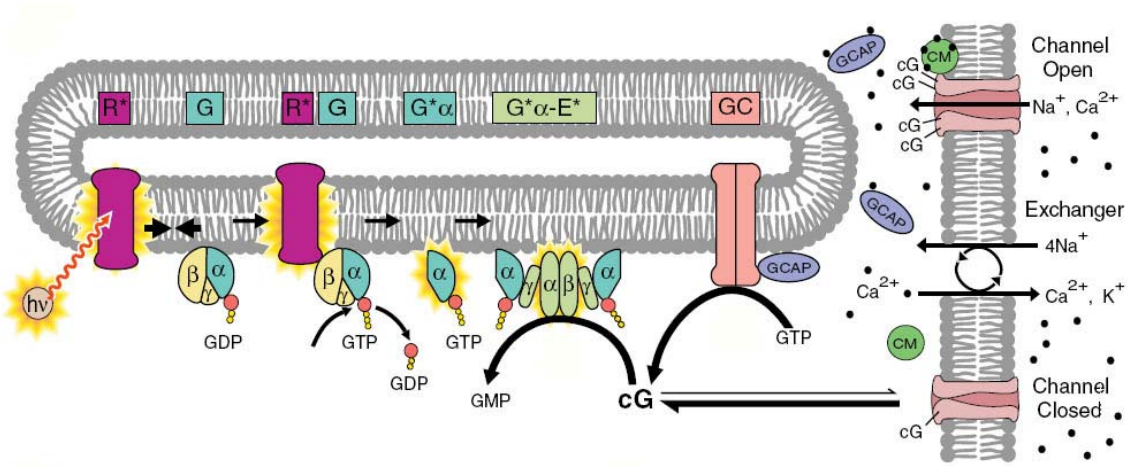

Figure 1.5: The phototransduction cascade. Schematic representation of the activation cascade. The cascade initiates with a photon (hv) activating rhodopsin (R*) which in turn binds a G protein (G) called transducin. The activated α-subunit of transducin (G*α) binds to PDE forming a complex activating the γ-subunit of PDE (G*α-E*). The cGMP gated channel function is illustrated under high Ca^{2+} concentration (top right) and low Ca^{2+} concentration (bottom right). GC; guanylate cyclase. CM; calmodulin. cG; cGMP. (Adapted from Pugh & Lamb, 2000) [12]

The change of intracellular cGMP concentration results in the closure of cGMP-gated channels, thus causing hyperpolarisation. The modulation of Ca^{2+} gated channels is essential for the onset of hyperpolarisation and the recovery that follows. At the height of activation, the intracellular Ca^{2+} concentration is at its lowest due to the closure of the cGMP-gated channels. After the visual signal has been generated and propagated, there are two remaining steps to complete the visual cycle: recovery of the cation gradient in the photoreceptor matrix and regeneration of 11-*cis* retinal – hence rhodopsin. At low Ca^{+2} concentration, a cGMP-channel binding protein called calmodulin, dissociates, increasing the affinity of the intracellular channel domains to cGMP. That leads to reopening of the Ca^{+2} channels. In addition, a calmodulin-like calcium-binding protein, called guanylate cyclase activator protein (GCAP), is free to associate with the activating domain of retinal guanylate cyclase (retGC). At low Ca^{+2} concentrations, Ca^{2+} dissociates from GCAP which is free to binds to its epitope on retGC, activating the conversion of GTP to cGMP. This step further increases the reopening Ca^{+2} channel cascade for the final recovery step of intracellular Ca^{2+} concentration.

The recovery phase of all-*trans* retinal recycling to 11-*cis* retinal occurs in the RPE. At this point Vitamin A from the diet can enter the cycle as well. Once within the RPE cell, it is esteryfied by lecithin-retinol acyltransferase (LRAT) and the all-*trans* retinyl ester is converted to 11-*cis* retinal by the iron-dependent isomerohydrolase RPE65 and 11-*cis*-RDH [13].. Finally, 11-*cis* retinal is transported back into the OS to re-enter the visual cycle as part of the inactivated rhodopsin [14,15] (Figure 1.6).

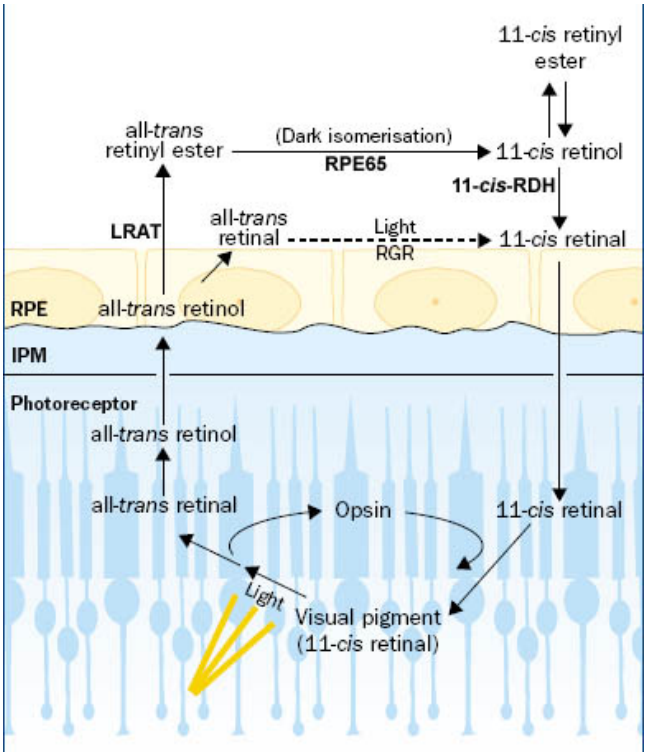

Figure 1.6: The visual pigment cycle. Schematic diagram of the 11-*cis* retinal cycle in the photoreceptor cell and the RPE. Upon light excitation, 11-*cis* retinal alters its conformation to all-*trans* retinal. After release from opsin, it is reduced to all-*trans* retinol and is transported to the RPE through the inter-photoreceptor matrix (IPM). In the RPE, it undergoes esterification by LRAT. A further isomerisation step and hydrolysis of the ester group is carried out by RPE65. Finally, the resulting alcohol group is oxidised to the 11-*cis* retinal aldehyde by 11-*cis* RDH and is transported back into the photoreceptor OS to re-enter the visual cascade. (Adapted from Pepperberg & Crouch, 2001) [16]

1.3 Retinal disorders

Retinal disorders can be categorised into different classes depending on their underlying cause. Disease in the retina can be acquired, inherited or complex. Acquired retinal disorders cover a broad range of retinal conditions caused by exogenous factors such as infection or injury. Complex retinal disorders are multifactorial and the factors leading to them are usually both genetic and environmental. Inherited retinal disorders, which are covered more extensively below, may be caused by a defect in any one of a large number of genes. The complexity of pathways involved in retinal function adds to the heterogeneity of the disorders arising from mutations in the genes involved. Currently, there are no effective treatments for inherited retinopathies that affect 1/3000 people worldwide [17]. The last 20 years have seen an increase in the genetic analysis of vision; extensive gene mapping and cloning has lead to the identification of 197 genes, of which 150 have been cloned (Retnet Database update: June 2009, http:// www.sph.uth.tmc.edu/Retnet) (also see Figure 1.7). In the following sections, inherited retinal disorders are separated based on the effect of the underlying mutation on retinal function.

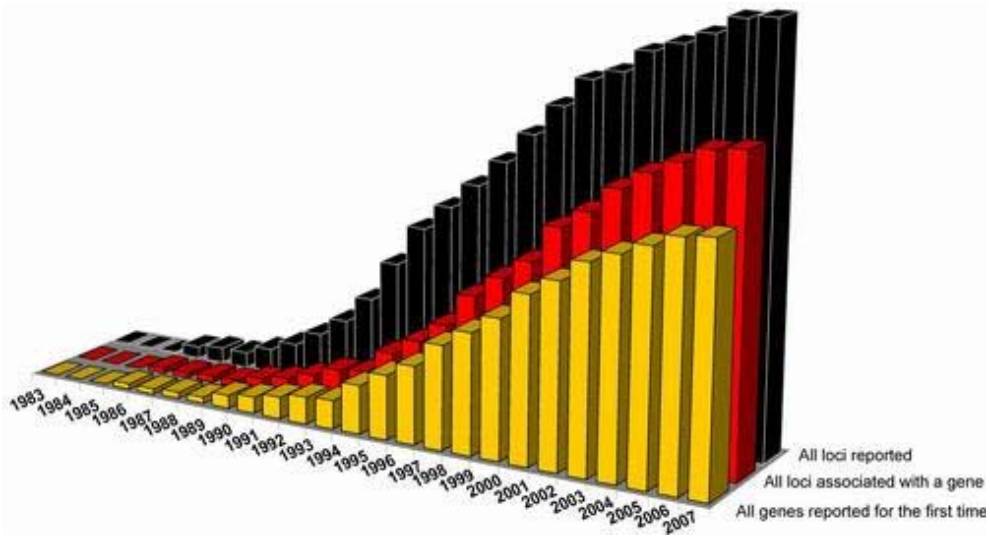

Figure 1.7: Compiled graph listing of mapped genes. Advances in gene mapping technologies during the last decade enabled for increased gene identification in retinal disorders (Retina International Scientific Newsletter, http://www.retina-international.org).

Retinitis pigmentosa, macular dystrophies and cone-rod dystrophies are three of the main disease categories and between them encompass more than 80 of the genes that are known to cause recessive, dominant or X-linked dystrophies. Since the focus of this study with regard to inherited retinal degeneration is on dominantly inherited conditions, the following section will focus mainly on disorders caused by gain of function mutations (see table 1 for a summary of genes involved in dominant eye disorders; Retnet Database update: October 2008, http:// www.sph.uth.tmc.edu/Retnet).

Table 1: Genes involved in autosomal dominant retinal dystrophies. A number of gene mutations have been shown to cause dominant retinopathies. Different mutations in the same genes may alter the inheritance pattern or even the type of disease (diseases in brackets). ad; autosomal dominant. ar; autosomal recessive. RP; retinitis pigmentosa. CORD; cone-rod dystrophy. LCA; Leber's congenital amaurosis. MD; macular degeneration (Retnet Database up-to-date: June 2009).

GENE	DISEASE	FUNCTION
RHO	adRP (also arRP)	Rod photoreceptor chromophore
RDS	adRP (also digenic)	Photoreceptor structural protein; localises in outer segments; associated with ROM-1
ROM-1	Digenic adRP	Photoreceptor structural protein; localises in outer segments; associated with RDS
NRL	adRP (also arRP)	Transcription factor expressed in retina; regulates rod development
RP1	adRP	Microtubule-associated protein; vital for photoreceptors
CRX	adRP (also adCORD)	Homeobox transcription factor; associated with NRL; involved in circadian rhythm regulation
PRPF-31 (RP11)	adRP	Pre-mRNA splicing factor, ubiquitously expressed
IMPDH1	adRP (also adLCA)	Dehydrogenase essential for *de novo* guanine synthesis
GUCY2D	adCORD (also arLCA)	Guanylate cyclase; converts GTP to cGMP during visual cycle
RPGR	adCORD (also xlRP)	Stabilising photoreceptor connecting cilium; associated with RPGRIP
ABCA4	adCORD (also ar-Stargard)	ATP-binding transporter; involved in photopigment recovery
ELOVL4	Stargard-like dystrophy (dominant)	Elongase of long fatty-acid molecules; also expressed in epidermis
VMD2	Best dystrophy	RPE chloride channel component; associated with paracellular exchange
AIPL1	adCORD	Molecular chaperone, involved in protein folding
TIMP3	Sorby fundus dystrophy	Proteolytic enzyme inhibitor; involved in extracellular matrix turnover
TJ genes (e.g.CLDN19)	MD? Uveitis?	Cell-cell adhesion, cell cycle, paracellular permeability and BRB

1.3.1 Retinitis pigmentosa (rod-cone dystrophies)

Retinitis pigmentosa (RP) is a broad class of retinal disorders that involves progressive degeneration of the photoreceptors. It affects 1 in 4000 people worldwide resulting in 1.5 million visually disabled patients [17-19]. Typically, degeneration starts at the periphery of the retina and advances towards the macula at varying rates depending on the type of the mutation. Night blindness is the first sign of impact on the patient's vision caused by degeneration of rod photoreceptors. Decreasing visual fields and tunnel vision are the signs of progressing RP that eventually leads to legal or complete blindness by middle age. At the later stages of the disease, cones are also severely compromised as well as the inner nuclear layer of the retina which leads to greatly diminished scotopic (rod induced) and photopic (cone induced) vision and RP can therefore be regarded as a rod-cone dystrophy. Clinical examinations reveal abnormal fundi with pigmented bone-spicule deposits and attenuated retinal vessels in the mid-periphery [19,20].

The inheritance patterns of RP are autosomal recessive (arRP), autosomal dominant (adRP), X-linked (xlRP) and digenic. In general terms, the rate of progression is thought to be faster in xlRP, followed by arRP, while adRP shows the slowest progression in retinal degeneration [21]. In xlRP, the only copy of the gene is mutated in male patients leading to the fastest rate of degeneration. In arRP cases, fast degeneration occurs due to complete lack of function due to mutations in both autosomal copies of the gene with Leber's congenital amaurosis (LCA) cases showing the fastest rate of degeneration than any other retinal dystrophies. In adRP, a dominantly inherited mutation in one of the two gene copies leads to either haploinsufficiency or a gain-of-function that is toxic to the affected cell. RP can also be classified as syndromic, where non-ocular tissues are also affected and more commonly non-syndromic, where only ocular tissues are affected. Usher's syndrome is the most frequent form of syndromic RP in which RP symptoms are usually associated with hearing impairment [19]. The first RP causing mutation was reported in 1990 [22]. It resulted in a single amino-acid change in rhodopsin. Since then, around 100 different

mutations have been identified in rhodopsin that account for a total of 25% of all forms of adRP [23]. To date, mutations in twelve different genes have been shown to cause adRP. These genes include rhodopsin (*RHO*), neural retina leucine zipper transcription factor (*NRL*) [24], *RP1* [25], cone-rod otx-like homeobox (*CRX*), peripherin-2 (*RDS*) and retinal outer segment membrane protein-1 (*ROM-1*) (see Chapter 4), ubiquitously expressed pre-mRNA splicing factors *PRPF-31* [26], *HPRP3* and *PRPC8* [20], and the inosine monophosphate dehydrogenase 1 gene (*IMPDH1*) which is expressed in the retina, lung, thymus and brain [27]. Many of the screened adRP causing mutations in NRL, RP1, CRX, RDS and IMPDH1 are missense mutations that alter a single amino acid in the protein polypeptide. Amino-acid changes often result in gain-of-function mutations as they affect the folding of the protein leading to toxic saturation in the cell, or by affecting the rate of function of the protein when they occur in catalytic domains. Exon deletions or insertions, as in the case of PRPF-31, can cause adRP mainly due to the haploinsufficiency that rises from loss of function rather than a gain-of-function effect.

1.3.2 Cone-rod dystrophies

Cone-rod dystrophies (CORDs) are another group of pigmentary retinopathies with a collective frequency of 1/40,000 [28]. Fundus examination reveals pigmented deposits that are mainly localised in the macular region of the patient. The reason why CORDs are diagnostically separated from RP is the order of events during retinal degeneration. In contrast to RP, in CORDs cones are primarily affected with rod involvement occurring as the disease progresses. Consequently, visual loss follows the opposite sequence of events to that in RP; visual acuity and sensitivity of the central visual field are initially compromised reflecting the loss of cones, followed by night blindness as rods begin to degenerate. In general, retinal degeneration is more severe in CORDs than in RP.

To date, around twelve genes have been identified that can cause non-syndromic CORD and a number of these genes is also involved in other retinopathies [29]. Missense gain-of-function mutations in *CRX* usually cause autosomal dominant CORD (adCORD) [28,30]. More severe frameshift mutations that abolish the function of *CRX* result in LCA. Most *GUCY2D* mutations cause adCORD and are comprised of missense gain-of-function mutations in exon 13 of the gene that affects the dimerisation of the proteins. However, similarly with *CRX*, some mutations in *GUCY2D* that lead to loss of function cause autosomal recessive LCA. Missense mutations don't always cause gain-of-function mutations in dominantly-inherited disease. For example, ABCA4 truncating mutations are associated with adCORDs due to their deleterious effect that results in haploinsufficiency in contrast with amino acid changes that lead to a milder phenotype and are associated with Stargardt disease. Genes usually associated with RP (e.g. Peripherin-2 and RPGR) or LCA (AIPL1 and RPGRIP1) can also cause adCORDS although the underlying mechanisms of the mutations have not been elucidated yet.

1.3.3 Macular degeneration (cone dystrophies)

Macular dystrophies are a broad group of retinal diseases characterised by loss of central vision and degeneration of the macular region [31]. Inherited maculopathies are mostly inherited dominantly and, to date, mutations in seven genes have been implicated (Retnet Database update: June 2009, http:// www.sph.uth.tmc.edu/Retnet).

Autosomal dominant Stargardt-like macular dystrophy is an early-onset maculopathy that appears after 20 years of age [32]. Vision loss due to geographical RPE atrophy and the presence of yellow macular flecks are the main clinical features. Pallor of the optic nerve can usually distinguish the disease from other dominant maculopathies. Mutations in the gene *elongase of very long chain fatty acids-4* (*ELOVL4*) have been linked to affected pedigrees. The underlying mutations have been often found to be exonic deletions that cause a frame-shift leading to dominant disease. *ELOVL4* is

expressed in rod and cone inner segments and is involved in retinal fatty acid metabolism. ELOVL4 malfunctions due to missense gain-of-function mutations lead to lipofuscin accumulation in the subretinal space as well as epidermal barrier malformation as it has been observed in a recent animal model with an *ELOVL4* knock-in mutation [33].

Best macular degeneration (VMD2) is a juvenile-onset dominantly inherited maculopathy characterised by a yellow subretinal macular lesion due to lipofuscin accumulation in the RPE. Atrophy of the RPE, especially in the fovea, leads to loss of vision. Peri-macular retinal involvement can also occur but the progression of the disease is slow with most patients maintaining reading vision past the fifth decade of life. The gene product of *VMD2*, bestrophin, is an RPE chloride channel component and it is localised at the basolateral membrane [34]. Mutational analysis of VMD2 has indicated that the putative second transmembrane domain of the protein is of major importance and even single amino acid changes are enough to trigger dominant Best's disease. *In vitro* analysis has shown that its malfunction affects paracellular exchange and leads to debris and lipofuscin accumulation between the RPE and Bruch's membrane [35].

Sorsby fundus dystrophy (SFD) is a late-onset dominant macular dystrophy that appears after 30 years of age and is characterised by the macular accumulation of white-yellow drusen, sub-retinal haemorrhage and CNV. The gene implicated in SFD is the tissue inhibitor of metalloproteinase-3 (*TIMP3*) that is expressed in endothelial cells of the choriocapillaries and its protein localises in Bruch's membrane [36]. Metalloproteinases are proteolytic enzymes that regulate the turnover of the extracellular matrix and their deregulation can result in abnormal deposits between RPE and Bruch's membrane. Single point-mutations in TIMP3 have been associated with SFD when they cause amino-acid changes. Proteolytic enzymes are highly dependent on their tertiary structure and mutations in key residues that affect bond formation can abolish the function of the enzyme. A malfunctioning TIMP3 can lead to subsequent thickening of the Bruch's membrane that has been also thought to hamper vitamin A absorption by the neuroretina. The

inhibitory function of *TIMP3* on vascular endothelial growth factor (*VEGF*) also accounts for the occurrence in CNV [37].

It is evident that the nature of retinal disease is not only dependent on the affected gene, but mostly on the type of mutation. As described above, the genetic causes for each type of disorder are not always distinct with many genes involved in more than one type of dystrophy. A deletion leading to a frame-shift or a key amino acid change that causes a gain-of-function, rather a loss-of-function in the affected protein, often alters the phenotype of the disorder (dominant vs. recessive) and hence the therapeutic strategies required for its treatment.

1.4 Therapies for retinal disorders

Although to date there have been no effective treatments for retinal degenerations, advances in our understanding of the pathophysiology of these disorders and the advances in gene and stem cell therapy technologies increases the prospects for at least some of these disorders. In the next section a brief account of the development of pharmacological and cell-based therapies will be given, before reviewing the progress in gene therapy, particularly with regard to treating dominant retinopathies.

1.4.1 Pharmacological and cell-based treatments

A number of studies have examined whether vitamin A supplementation might confer protection against retinal degeneration. Initial findings of a clinical trial suggested that vitamin A intake combined with docosahexaenoic acid, reduced loss of function over a period of two years in RP patients but a follow up of the patient cohort indicated that the effect was not significant after that period [38,39]. It has also been suggested that calcium channel blockers, antioxidants and neurotrophic factors might also be used to slow retinal degeneration following studies using mouse models. However, the amelioration is always transient and repeated administration is required [40-49]. To date, the administration of pharmacological agents as a sole therapeutic strategy for the treatment of retinal dystrophies has proved largely ineffective in delaying visual loss. In humans, allo-transplantation of RPE cells has had a long history but has produced relatively poor results and autologous (from the host) transplantation techniques are currently being investigated. In AMD patients, RPE from an unaffected area of the midperiphery can be transplanted into the macula, in a process called RPE translocation [50]. Cell suspensions or patches of RPE and choroid are isolated and inserted into the central retina after submacular surgery. Long-term follow up of four patients after undergoing RPE choroidal translocation

indicated that the transplanted tissue survived up to six years in the submacular space but the gain in visual function had been transient and short-lived [51,51]. Since the developed retina might lack the environmental cues to drive the lineage of an unspecified stem or progenitor cell, transplantation of post-mitotic precursors may prove promising. A breakthrough in photoreceptor cell transplantation was recently reported by MacLaren and colleagues using retinal precursor cells from the post-natal murine retina. Although previous studies failed to show effective integration of photoreceptors [52-54], this study described an optimal ontogenic stage at which donor cells were more likely to integrate into the host retina. They used a transgenic model that expressed GFP under a *Nrl* promoter. *Nrl* is an early rod-specific marker and therefore GFP expression is localised in cells that have entered the rod lineage. By assessing the levels of GFP-positive cell integration, they demonstrated that the early postnatal period is optimal for harvesting rod precursor cells for transplantation [55]. After subretinal delivery into the rhodopsin knockout mouse, increased levels of photoreceptor integration (i.e. thousands of integrated cells) were observed in conjunction with an improvement in visual function [55].

To date, the most promising study involving stem cell differentiation has been carried out by Osakada and colleagues using conditional pre-differentiation of mouse, human and monkey embryonic stem cells [56]. The investigators were able to successfully differentiate the cells into mature photoreceptor and RPE cells but their integrative potential into a host retina was not investigated. Stem cells might have a promising future for certain types of neuronal transplants and corneal engraftments but until there are improvements in the efficiency of differentiation and integration, it is unlikely they will provide an effective treatment for retinal degeneration.

1.4.2 Gene therapy

Genetic engineering, molecular virology and understanding the genetic basis of disease paved the way for the development of gene delivery vectors to treat the underlying causes – and not just the symptoms – of genetic disorders. Briefly, a therapeutic transgene is placed under the regulation of a constitutive, tissue specific or conditional promoter and is delivered *in vivo* or *ex vivo* to the affected tissue using viral and sometimes non-viral vectors. There are three main issues to be addressed when developing gene therapy approaches for treating genetic defects:

1. Efficient gene delivery to the appropriate target cells. Specificity can be obtained through the use of specific vectors, promoters and routes of administration.
2. Appropriate levels of transgene expression.
3. Avoidance of host immune responses to either vector or transgene product.

Gene therapy vectors for the treatment of X-linked chronic granulomatous disease (X-CGD) [57], Parkinson's disease [58] and cystic fibrosis [59] are advancing into the clinic. To date, the most successful gene therapy applications in the clinic focus on treating forms of severe combine immunodeficiency (SCID). X-linked SCID (xlSCID) and adenosine deaminase-deficient SCID (ADA-SCID) are characterised by abnormal leukocyte development and patients usually do not live past adulthood. Because of their severely compromised immune system, patients of xlSCID have to live in a protective sterile "bubble" to minimise infection. Using gamma retroviruses, Alan Fischer and Adrian Thrasher demonstrated the first ever successful gene therapy treatment of patients. Two boys with xlSCID were effectively cured from the disease after *ex vivo* gene delivery in haematopoietic stem cells that were subsequently engrafted to their bone marrow [60-62]. Since then, more successful *ex vivo* gene therapy trials for ADA-SCID [63] and xlSCID [64] have been carried out in a number of young patients but with post-operative side effects in some xlSCID patients [65].

Insertional mutagenesis is currently hindering patient treatments due to incidents of T cell acute lymphoblastic leukaemia caused by “semi-random” integration of the proviral cassette into transcriptionally active areas of the genome. Ongoing studies in self-inactivating vectors and site-specific viral integration in conjunction with the use of ubiquitously-acting chromatin opening elements (UCOE) might aid in the development of a safe gene therapy strategy using integrative viral vectors [66,67].

The eye as a target for gene therapy provides the advantage of accessibility and immune privilege. Both administration of vector as well as the follow up of the phenotypic effect can be carried out with relatively minimal surgical intervention. In addition, the BRB acts to inhibit the release of exogenously delivered agents into the systemic circulation reducing the levels of active or passive immune responses. Gene therapy approaches have been successful in treating monogenic recessive disorders in various animal models of retinal disease and recently the first clinical trials to treat a recessive retinal dystrophy were initiated. Corrective gene replacement of *RPE65* is currently in phase I/II in Leber’s congenital amaurosis patients after viral vector safety was confirmed in canine models of the disease [68,69]. Early data indicate that there are no adverse effects caused by vector administration while some significant amelioration in central visual acuity was reported for a number of patients [70-74].

The different virus vector types and their potential use for ocular gene therapy is presented in depth in section 1.4.2.2.

1.4.2.1 Non-viral vectors for gene delivery to the eye

Injection of naked plasmid DNA does not result in cellular uptake because cells will not actively take up naked nucleic acids in their vicinity. Therefore, cationic liposomes that bind DNA, forming an enclosed protective vesicle, have been used to transduce cells both *in vitro* and *in vivo*. The most

promising nucleic acid encapsulating technology for retinal transfection is DNA nanoparticle encapsulation. Polyethylene glycol (PEG)-substituted lysine peptides encapsulate a single DNA molecule per vesicle and have been shown to transfect murine photoreceptors after subretinal delivery [75]. Persistence of expression ranges from a few days to a few months depending on promoter and plasmid construction.

The overall negative charge of DNA molecules is advantageous not only for DNA encapsulation techniques but also for plasmid electroporation in the retina. Naked nucleic acids can be injected intravitreally or subretinally followed by a series of electrical pulses – ranging from 30 V to 100 V depending on age and species – that cause the DNA to migrate through the cellular membrane. The direction of the current is applied in such way that the DNA moves into the desirable adjacent cell layer (i.e. polarity is inverted between intravitreal and subretinal DNA delivery). Transgene expression that persists for 50 days in transfected photoreceptor cells has been demonstrated in both rat and mice after subretinal injection and electroporation in P0 pups [76]. The main drawbacks of retinal DNA electroporation are the relatively low efficiency for transfecting high numbers of photoreceptors and the inability of the DNA to enter other tissues apart from the RPE in adult mice.

The majority of non-viral delivery methods are mostly inefficient in providing stable and high transgene expression in the eye or other tissues [77-79], hence the focus of gene delivery studies is currently on viral vectors. Since non-viral gene therapy vectors have the advantage of delivering very large DNA molecules, further optimisation with regard to expression levels and persistence may enable gene therapy applications that are not feasible using viral vectors.

1.4.2.2 Viral vectors for gene delivery to the eye

Viral vector technology has been optimised for efficient transduction and expression in various tissues. Viral technology confers an advantage with regard to gene delivery to cells in comparison to non-viral techniques due to the innate ability of virions to infect a cell and deliver their genome into the host's nucleus.

Upon viral vector construction, part of the viral genome is removed to allow space for the transgene expression cassette and to prevent replication of the vector. The latter aspect of vector design is essential for the safety of the vector and to diminish any host immune responses. Since the virus has lost its ability to replicate, production of the recombinant virus particles requires "packaging cell lines" that contain trans-acting viral genes needed for vector replication and packaging.

Depending on the type of virus used, the transgene cassette is introduced episomally into the host nucleus or is integrated mainly into the host's euchromatin – the transcriptionally active chromosomal regions. Integration of the transgene in the host genome enables the expression in the daughter cells of actively dividing, transduced cells. Episomal delivery in the same population would not provide a therapeutic long-term effect as the transgene would be lost after cell division. In contrast, episomal gene delivery in post-mitotic cells can lead to equal long-term expression levels in comparison to integrative delivery.

Viral gene therapy in the eye has come a long way during the last 20 years with a variety of vectors being developed that efficiently transduce most ocular tissues. The majority of the developed retina consists of post-mitotic (arrested at G0 of the cell cycle) neuronal cells and non-neuronal glia, endothelial and epithelial cells, like the RPE. The overall efficiency of viral vector transduction in the eye has been demonstrated by the therapeutic effect of virally delivered transgenes into animal models of monogenic retinal degeneration.

The two most potent expression vectors used in the eye are based on AAV and lentiviruses. Their characteristics as well as their progress and prospects in treating ocular disorders are described later in detail. HSV and adenovirus-based vector technology, some of which preceded and aided to the construction of the latest AAV and lentiviral vectors, is briefly introduced.

1.4.2.2.1 Herpes simplex virus-based vectors

Herpes simplex virus (HSV) is a neurotropic virus with a single stranded DNA genome and a broad host cell range. Although they can package large inserts, the main drawback of HSV in ocular gene transfer is its inability to transduce photoreceptors [80]. In the eye, when HSV vectors are delivered intravitreally they allow for rapid but transient expression in the murine RPE. Reporter gene expression has been observed just one day after delivery but declined after two days reaching undetectable levels at six weeks [81]. In another study, intravitreal delivery of HSV vectors carrying an expression cassette for FGF2 failed to preserve visual function in a rat model with light-induced damage two weeks after treatment [82]. The reason for the lack of persistence of expression after HSV vector administration lies on the immunogenicity of the HSV virion. It has been suggested that upon cell entry and within three hours, a rapid immune response is raised against the HSV particles mediated by IL-6 and NFkB [83]. Another reason for lack of persistence could be viral latency were the inserted provirus lies “dormant” in the transduced cells. The high immunogenicity, inability to infect photoreceptors and lack of vector persistence render HSV vectors inadequate for gene replacement therapy approaches. However, if a less immunogenic HSV vector is developed it could be delivered to the anterior of the eye to treat acute conditions where fast and robust – but not persistent – expression of a therapeutic transgene/neurotrophin is needed.

1.4.2.2.2 Adenoviral vectors

As with HSV-based vectors, adenoviral (Ad) vectors can accommodate large transgenic inserts ranging from 8 kb to 38 kb, but their immunoreactivity has raised concerns over the years. The need for safe Ad vectors was made clear in 1998 when a patient suffering from ornithine transcarbmalayse (OTC) deficiency died within 96 h from massive systemic immune responses after receiving a systemic dose of Ad vector [84].

The reason why Ad vectors are not widely used in retinal gene transfer is, apart from their immunogenicity, due to their inability to transduce photoreceptor cells [85]. After subretinal injection Ad vectors transduce the RPE whereas after intravitreal injection they transduce Müller cells [86]. Ad-mediated delivery of transgenes in the retina has failed to date to demonstrate persistent expression of transgenes in photoreceptors. Transgene delivery to the *rd* mouse, that carries a mutation in the β-PDE gene, has been attempted using either first or third generation adenoviral vectors [87,88]. In both studies, no evidence of photoreceptor transduction was presented. The short-term amelioration in the retinal morphology of the *rd* mouse might be explained by intercellular trafficking of β-PDE from the RPE to the photoreceptors [89]. The first Ad-based ocular clinical trial was carried out in patients with CNV caused by advanced AMD, using a second generation Ad vector expressing *PEDF* but after 3 months no significant stabilisation or improvement of CNV lesions were detected [90].

Recently it was shown that by modifying a domain on the Ad vector's capsid, it is possible to increase the vector's tropism to transduce photoreceptors after subretinal delivery [91]. Although this study demonstrated the highest levels of reporter gene expression in photoreceptors following Ad-mediated delivery, the levels of expression are not comparable to those obtained after transduction of photoreceptors using adeno-associated viral vectors.

1.4.2.2.3 Adeno-associated viral vectors

Adeno-associated viruses (AAV) belong to the family of parvoviruses, which are among the smallest, simplest eukaryotic viruses. Essentially, they fall into two groups, defective viruses that are dependent on helper virus for replication and autonomous, replication-competent viruses. AAVs are helper-dependent single-stranded DNA viruses that are not associated with any human disease and therefore are considered to be one of the most promising vectors for gene delivery in the retina. The wtAAV genome is 4.6 kb long flanked by inverted terminal repeats (ITRs) that drive viral replication. The genome is composed of two multi-cistronic genes, *rep* and *cap*. *Rep* is involved in the site-specific integration of AAV during latency that occurs via non-homologous recombination in chromosome 19 (AAVS1), as well as in viral replication and packaging [92]. *Cap* expresses three proteins (VP 1, 2 and 3) that form the 20 nm icosahedral viral capsid. AAV exist in different serotypes that differ in their cell surface receptors, heparin sulphate and sialic acids, which results in different cell tropism of viruses. Therefore, it is possible to use different serotypes to target specific cells in *vivo*. Chimeric virions can be produced by using the regulatory element *rep* of one serotype (usually from AAV2) in conjunction with the capsid element cap from another serotype (e.g. AAV5; the resulting chimeric virus is termed AAV2/5). In effect, recombinant AAV particles are produced that are capable of trasducing different retinal layers depending on the capsid pseudotyping and route of administration [93]. Following subretinal injection, serotype 1 transduced the RPE and has an onset of expression after 3 days, whereas serotypes 5 and 8 target both RPE and photoreceptors initiating expression after 2 weeks. Serotype 2 transduces RPE and photoreceptors when delivered subretinally but it is capable of transducing the ganglion cells when delivered intravitreally with onset of expression at 4 weeks after delivery. Approximately fifteen serotypes have been isolated from different species and six of them have been isolated from humans [94]. Depending on the serotype, between 10^8-10^9 infectious viral particles can lead to transduction of approximately 50 % of the murine photoreceptors after subretinal delivery.

Recombinant AAV (rAAV) vectors retain only the viral ITRs and allow for ~4.5 kb inserts to be cloned between them. *In vitro* vector production requires the presence of *rep* and *cap* products in *trans* together with a helper Ad or HSV virus or a plasmid that provides Ad or HSV functions (see Figure 1.8). The need for high-titre, pure AAV preparations of different serotypes has led to the development of various purification techniques. Heparin [95], mucin [96] and ion-exchange chromatography binding matrices [97,98] provide up to 10^{13} particles per ml of rAAV virions with 99 % purity. In order to reduce the time needed for the onset of transgene expression, self-complementary AAV (scAAV) vectors have been developed. scAAV carries a double-stranded genome and mutated ITRs to evade the rate-limiting step of second-strand synthesis after transduction. Although the size of the insert is reduced to 2.4 kb, scAAV vectors mediate earlier and stronger expression than their single-stranded counterparts of the same serotype [99,100].

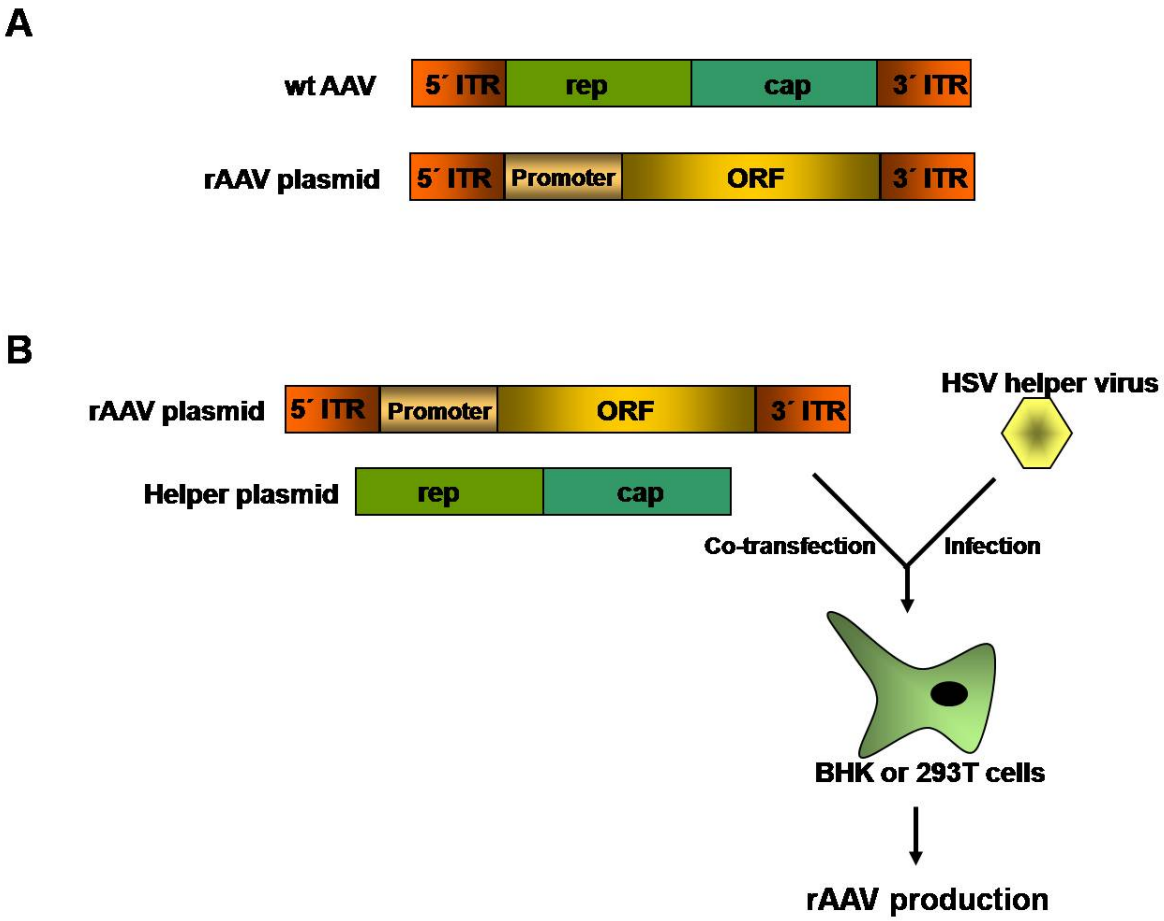

Figure 1.8: AAV genome and vector components. (A) Schematic diagram of the wtAAV genome and the rAAV expression cassette. ORF; open reading frame. The promoter can be an RNA polymerase III or II, ubiquitous or tissue specific, constitutive or conditional depending on the nature of the ORF: long cDNA transgene (pol II) or short RNA transcript (pol III). **(B)** Schematic diagram of rAAV production. The rAAV plasmid and a plasmid carrying the *rep* and *cap* genes are co-transfected into 293T or BHK cells followed by infection with a helper virus (HSV or Ad). rAAV is harvested 72 h and purified using the appropriate binding matrix according to its serotype.

rAAV vectors have provided the platform for numerous successful gene replacement therapies in ocular gene therapy. Investigators demonstrated the potential of AAV to transduce retinal tissues [101,102] mediating efficient expression of therapeutic genes [103]. Since then, rAAV2/2, 2/5 and 2/8 have been used to rescue mice models of monogenic ocular disorders with mutations in *rds* [103], *rpe65* [104], *RPGRIP* [105], AIPL1 [106], *Gnat2* (achromatopsia) [107] and *Rs1h* (retinoschisin) [108]. In addition, AAV-mediated delivery of neurotrophic factors (*Fgf2* [44], *Cntf* [49], *Gdnf* [42]) has

been shown to ameliorate the phenotype of mouse models after delivery of the neurotrophic factor alone or in conjunction with a replacement cassette. Although the majority of studies has been carried out in mice or rats, expression in canine [69,109] and primate [110,111] models has also demonstrated the ability of rAAV vectors to efficiently transduce various tissues in larger animals.

The lack of human pathogenicity together with their broad tropism has placed rAAV vectors at the front of pre-clinical gene therapy research. However, recently a few studies have raised concerns about rAAV vector safety following systemic, hepatic or intramuscular delivery. Yuasa and colleagues demonstrated transgene-specific immunotoxicity in the canine skeletal muscles after rAAV2/2 delivery of the micro-dystrophin gene [112]. They concluded that the immunogenicity was associated with the transgene and the poor transduction efficiency (i.e. muscular absorption) of the vector, rather than a specific AAV-targeted immune response. Although the absence of the *rep* cistron is thought to abolish specific integration in the AAVS1 site with 5 % of vector randomly integrating into the host genome [92], Donsante and colleagues reported rAAV2/2-mediated insertional mutagenesis in mice following systemic delivery [113]. Hepatocellular carcinomas were found to be caused by upregulation of genes adjacent to the integration locus. However, other research groups have failed to replicate the study by Donsante *et al.* or to show integration after rAAV administration concluding that rAAVs mainly persist as an episome. Recently, Pien et al. have demonstrated that hepatic toxicity can be mediated by the capsid of the AAV and not the transgene. In their study, AAV2/2 capsids were found to sensitise hepatocytes for cytotoxic T-cell mediated destruction [114]. Another issue with regard to intracellular AAV particles has been raised by Stieger and colleagues. They reported that AAV virions persist in the retinae of dogs and primates six years after subretinal injection [115]. Although no immune responses were raised against the persisting virions possibly due to the immune privilege of the eye, the authors suggested that future clinical trials should address the issue of intracellular virion clearance.

In spite of the recent issues raised about rAAV biosafety for certain tissues, phase I clinical trials have been initiated using rAAV2/2 vectors for the treatment of Parkinson's disease [58] and LCA (*Rpe65*) [70,72,116]. In the LCA studies, patients were subretinally injected with approximately 10^8 rAAV2/2 particles diluted in either 100µl or 1000µl. So far, no immune responses have been raised in the patients while some of the patients have shown visual improvement. The CNS is a good target for AAV-mediated gene delivery and establishment of a safe clinical protocol will pave the way for further gene therapy clinical trials in other organs. Future trials may also employ rAAV2/8 vectors which are being increasingly used in gene therapy research. Although the clinical safety of serotype 8 viruses will need to be assessed pre-clinically after reports of trans-synaptic transmission to the visual cortex following subretinal delivery in dogs [117], they are a favourite candidate for the treatment of early-onset retinal disorders due to their ability to mediate rapid and high levels of transgene expression [99].

1.4.2.2.4 Lentiviral vectors

Lentiviruses are a sub-category of retroviruses, RNA-based virions that carry a diploid single-stranded RNA genome. Retroviruses are generally highly pathogenic, infect dividing cells and integrate their genome into their host's. Lentiviruses are also capable of infecting cells at the post-mitotic G_0 phase of the cell cycle, providing an advantage for the development of a gene delivery vector. Lentiviruses have a 9-10 kb genome flanked by long terminal repeats (LTRs) that are essential for integration and the initiation of gene expression [118,119]. Feline immunodeficiency virus (FIV), equine infectious anaemia virus (EIAV) and the human immunodeficiency virus type I (HIV-1) are various lentivirus family members used in vector construction, with the latter being the most widely used in research. In lentiviral vectors most of the genome is deleted leaving space for expression cassettes up to 9 kb in size to be incorporated. In the latest 3rd generation HIV-based vectors, most of the lentiviral genes are deleted and some are delivered in *trans* during vector

production [120,121] (see Figure 1.9). The *gag*, *pol* and *env* genes encode for the capsid, polymerase/integrase and envelope components, respectively. The remaining genes of the lentiviral genome (like *vpu*, *vif*, *vpr* and *tat*) encode for “accessory proteins” that enhance proviral expression and are mostly removed. The *cis*-acting packaging element, ψ, remains present in the vector plasmid to enable recombinant viral particle formation. The 3’-LTR is partially deleted to ensure it does not elicit any promoter activity of downstream genes but retaining the sequence required for reverse transcription and integration of the proviral DNA. Vectors with the 3’-LTR deletion reduce the risk for ectopic host gene activation as well as the risk of vector mobilisation in the host and are called self-inactivating (SIN) vectors. Capsid pseudotyping is essential in order to induce the desired cell tropism of the vector and it is achieved by cloning the *gag* gene from the genome of another virus. Vesicular-stomatitis virus G-protein (VSV-G) pseudotyping is the most widely used in HIV-based lentiviruses as it confers a broad host-cell range.

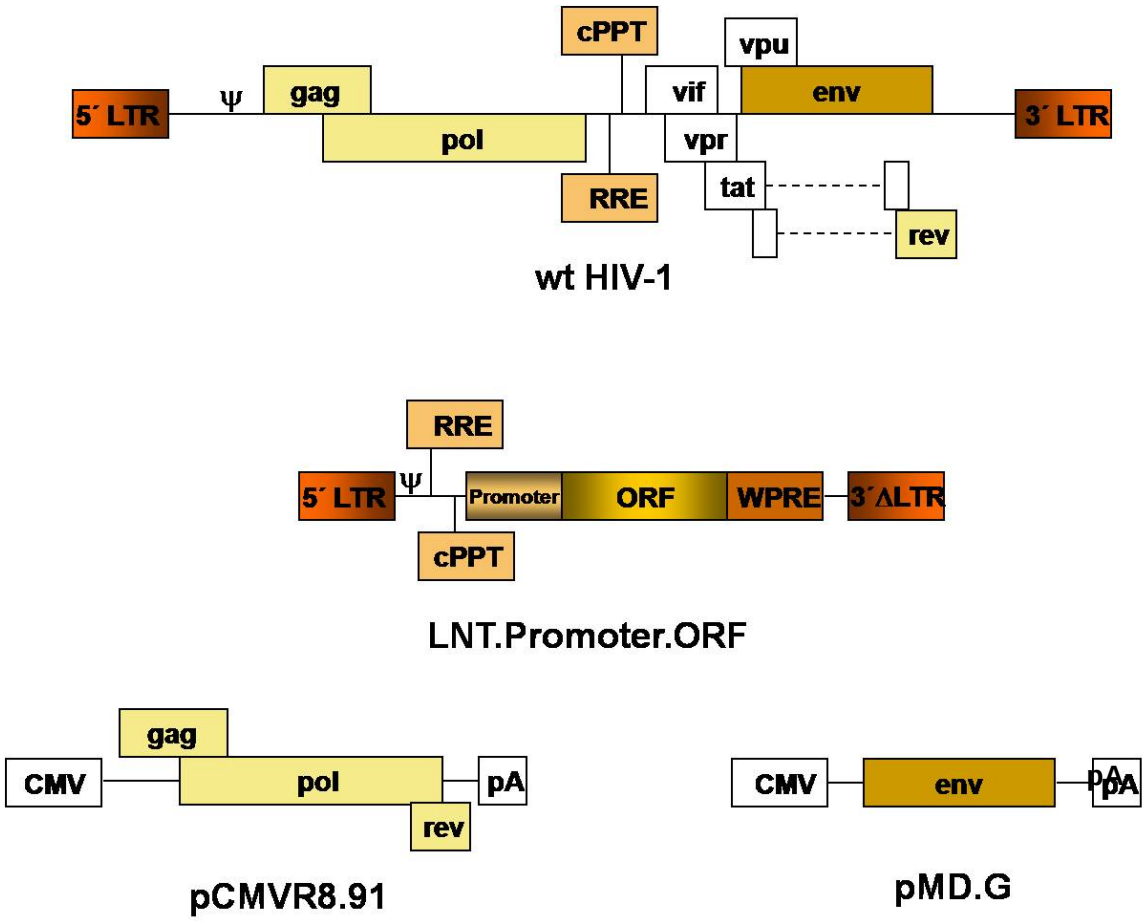

Figure 1.9: HIV-1 genome and lentiviral vector constructs. Schematic diagram of the wtHIV-1 genome, the lentiviral vector plasmid (LNT.promoter.ORF) and the helper plasmids with the viral polymerase (pCMVR8.91) and envelope (PMD.G) genes. The Woodchuck hepatitis virus post-transcriptional element (WPRE) is often used in pol II expression cassettes to increase gene expression. The three plasmids are co-transfected into 293T cells and the virus is purified after 48 h through ultracentrifugation. cPPT; central polypurine tract. RRE; rev-responsive element. 3'ΔLTR; partially-deleted 3' LTR. CMV; cytomegalovirus promoter.

Following subretinal injection, VSV-G pseudotyped HIV-based lentiviruses specifically transduce the RPE in mice [122] and dogs [123]. Inneficient photoreceptor and INL transduction has been seen at the injection site or after subretinal delivery in mice neonates [124]. Depending on the gene, therapeutic levels of transgene expression in the RPE are achieved after subretinal delivery of at least 10^5 viral particles. Lentivirus-mediated gene therapy has been successfully applied in the *RCS* rat [125,126], and the

Rpe65$^{-/-}$ mouse [123,126] to rescue the retinal degenerations caused by lack of expression of the RPE-specific *Mertk* and *Rpe65* genes, respectively.

The retina contains mainly non-dividing neurons and transgene expression is not diluted by cell proliferation. The integrative ability of retroviruses makes lentiviral vectors a promising vehicle for efficient transduction of dividing cells in other tissues. Episomal transgene expression is diluted in an actively dividing population since the episome is not transferred to the daughter cells after cell division. However, lentiviral-mediated integration is non-specific and occurs at random in euchromatic regions. The risk of insertional mutagenesis was demonstrated in a retroviral-based clinical trial for the treatment of X-SCID, where activation of a downstream host oncogene resulted in leukaemic neoplasia [65]. Although the occurrence of insertional mutagenesis is not high [61], there is a need for an optimised non-integrating vector that transduces dividing cells.

Non-integrating lentiviral vectors have been designed carrying a mutation in the *pol* gene that prevents integration of the provirus. The vectors retain their tropism and expression levels but persist episomally [127]. Such vectors are useful for transduction of mitotic tissues were the risk for insertional mutagenesis is high even though integrase-deficient lentiviral vectors have also been shown to efficiently transduce post-mitotic cells in the retina and brain [126]. However, these vectors do not address the problem of transgene dilution across mitotic daughter cells and recent studies on vector technology concentrate on the generation of a site-specific or tightly-regulated lentivirus. The chicken β-globin insulator element has been used to "shield" the integrated cassette from position-effect variegation, or ectopic downstream activation [128]. Similarly, Zhang and colleagues demonstrated that a vector encompassing a ubiquitously-acting chromatin opening element (UCOE) offers stable transgene expression without ectopic activation [67]. UCOEs consist of methylation-free CpG islands and drive the expression of the downstream gene without activating adjacent genes or being silenced by site-specific factors. Even though the post-mitotic environment of the retina

protects against transcriptional silencing, in mitotic tissues epigenetic regulation often hampers lentiviral transduction [129] and maintaining the activity of the transgene cassette is as essential as the abolishment of insertional mutagenesis.

Development of the next generation of lentiviral vectors aims to combine tightly regulated promoters with site-specific scaffold regions for specific locus integration, overcoming the current safety issues raised in the clinic.

1.4.3 Approaches for treating gain of function mutations

Gene replacement therapy approaches have been used successfully for treating animal models of recessive monogenic retinal disorders where there is a deficiency in a functional gene product. In some dominant disorders, however, the mutated gene product may have a toxic impact on the cell, as a result interfering adversely with its normal cellular pathway. Therefore, supplementing the cell with a normal copy of the gene would not necessarily reduce the negative effect of the mutation. Ablating the mutated gene's expression is essential for the treatment of gain of function dominantly inherited disorders and if haploinsufficiency results after the silencing of the mutation, it can be treated with a replacement gene therapy approach. The term "suppresion and replacement" was coined by Jane Farrar and Peter Humphreys (Trinity College, Dublin) to describe this concept and its application is described later (see section 1.5.3) [130]. To date, three main approaches for the ablation of a toxic gene product have been devised: antisense nucleotides, ribozyme technology and RNA interference.

Antisense RNAs are ssRNA molecules that can range in size up to a few hundred base pairs and they hybridise with the target mRNA. The aim of antisense technology is to cause host-induced mRNA degradation. The antisense nucleotides either alter the secondary structure of the mRNA in a way that hinders translation, or form an RNA double helix that elicits RNase-

specific degradation. The drawback with delivering antisense RNA molecules is their instability. RNA has a high turnover in the cell and the effect from a single administration is transient. Stabilising the molecule and increasing its persistence has been achieved by modifying the phosphate bonds in the RNA backbone [131]. Sugar modifications, like oxetane or deoxyribose, can be introduced in the nucleosides of the backbone. In this way, the molecule persists in the cell for longer hence providing extended target silencing. Antisense oligodeoxynucleotides (ADN) 20 base pairs (bp) long have been used to target VEGF production in laser-induced CNV lesions in primates [132]. Intravitreal delivery of ADN reduced neovascularisation in treated eyes three days after the CNV lesion. Similarly, antisense nucleotides have been used to silence TNF-α in mice with HSV-induced retinitis resulting in reduced inflammation after one and four days following subconjuctival injection [133]. The fast degradation of naked RNA in retinal cells abolishes any therapeutic effect after a few days rendering them inefficient for long-term treatments. However, a transient targeting may be promising for the treatment of an acute condition but not for the treatment of a genetic defect.

Ribozymes are small RNA molecules that catalyse the cleavage of a targeted mRNA and are derived from viruses, lower eukaryotes and bacteria [134]. Although some, such as the Group I intron ribozymes, can cleave the phosphate backbone of the RNA and reattach it at a different point, others cleave the RNA molecule without re-ligating the broken ends and hence leading to silencing of the transcript. Hammerhead ribozymes are 30 bp long and are the smallest ribozyme molecules long enough for their intramolecular secondary structure to provide the epitope for mRNA binding. An advantage that ribozymes present over ADNs is the fact that they can be transcribed as hairpin molecules providing a stable supply in the affected tissue overcoming the issue of rapid RNA degradation. Expression cassettes encoding ribozymes can be delivered with various vectors providing silencing of a mutation and can be highly specific as to target a point-mutation in an allele-specific manner. Ribozymes have been shown to specifically target mutations *in vitro* when delivered synthetically [135] or virally [136]. The

efficiency of ribozymes in treating dominant ocular disorders has been shown on a rat model for dominant RP expressing the *P23H* rhodopsin mutation where a partial rescue of the model was demonstrated for up to 3 months after AAV-mediated delivery [137]. The *P23H* rats have a murine rhodopsin transgene with an amino-acid changing mutation leading to loss of 50 % of the photoreceptors within three months of age [138]. In a different study, AAV2/2-mediated delivery of a hammerhead ribozyme targeting the P23H mutation reduced ONL degeneration for eight months and partially improved the ERG response for three months after treatment [139]. Rats were treated at either P15 or P45 and were followed for eight months. In another study, the same model was treated with an AAV2/5 vector expressing a rhodopsin-targeting ribozyme cassette. A 46 % reduction in expression of the P23H allele *in vivo* after three months was demonstrated [140]. In all efforts to rescue the P23H rat, the amelioration of the phenotype was transient and a functional rescue did not exceed three months after treatment. In addition, treatment for dominantly inherited disorders in the early postnatal period would not be possible in patients due to ethical concerns rendering ribozymes inefficient to reverse or halt the progression of the dominant phenotype. Apart from the P23H rat model were an optimal ribozyme clievage site was engineered in the P23H mutant murine allele to increase efficiency, ribozyme technology has not shown to deliver stable silencing *in vivo*.

During the last decade a novel technique emerged on the field of gene silencing whose efficiency surpasses the knockdown achieved with ribozymes [136]. RNA interference is probably the most efficient way to silence the expression of a gene and is rapidly advancing into the clinic. Below the main principles, vector design and therapeutic applications of RNA interference are discussed.

1.5 RNA interference

RNA interference (RNAi) is the term given to post-transcriptional gene silencing induced by double-stranded RNA (dsRNA) in eukaryotic cells. In 1998, Fire and colleagues demonstrated that the introduction of dsRNA molecules into the nematode, *C. elegans*, leads to specific silencing of a fully complementary mRNA [141]. Furthermore, the extent of mRNA silencing was far more potent than that achieved after the introduction of single-stranded RNA (ssRNA) molecules. In their landmark publication, they also reported that the interference between dsRNA and mRNA was not stochiometric and that a small quantity of dsRNA molecules within the cell could provide almost total mRNA knockdown indicating a catalytic pathway. Further studies revealed that RNAi utilises an endogenous highly conserved trans-kingdom pathway, developed as a defence mechanism by eukaryotes against transposons and viral infections. Whereas in lower organisms the dsRNA molecules can vary in size, in mammalian cells long dsRNA molecules trigger a toxic, non-specific global knockdown that leads to cell death. Short-interfering RNA (siRNA) molecules 19-21 bp long have been found to specifically silence the complementary mRNA in mammalian cells by becoming incorporated into a large multicomponent RNA-protein complex called the RNA induced silencing complex (RISC) [142,143]. The siRNA guides the RISC to the complementary mRNA which is then catalytically cleaved. The specific size requirements of siRNAs (19-21 bp) together with the low tolerance for size deviations was clarified with the discovery of Dicer, an RNase III endonuclease that cleaves long dsRNA molecules into siRNAs [144,145].

The potential therapeutic implications of harnessing this natural defence mechanism are apparent and studies on the two main components of RNAi, RISC and Dicer, led to the elucidation of the catalytic cleavage mechanism as well as to the analysis of siRNA design down to every nucleotide of the molecule. However, the discovery of endogenous cellular short RNA

(microRNA) molecules that are not derived from transgenic or parasitic dsRNA introduction, suggested the existence of other yet unknown pathways. Since then, a whole “panoply” of small noncoding RNA (ncRNA) molecules has been found to control gene silencing and chromatin structure indicating that they might constitute the most important group of regulatory molecules in the cell. The discovery of microRNAs (miRNAs) has led to a better understanding of the endogenous pathways that in turn have aided the design of more potent therapeutic siRNAs. For this reason, miRNAs will be discussed first before addressing their impact on siRNA technology.

1.5.1 MicroRNAs (miRNAs)

Of the total transcriptional output of the cell, 97 % is ncRNA. Transfer RNA (tRNA), ribosomal RNA (rRNA), untranslated regions (UTRs), introns and transposable elements make up the majority of the previously known ncRNAs. With the emergence of RNAi, a new group of highly conserved small ncRNAs, called small temporal RNA or microRNA (miRNA) molecules, was found to be involved in gene regulation. miRNAs are 20-22 nucleotides (nt) long ssRNA molecules formed after nuclear and cytoplasmic processing of longer transcripts [146-148]. Lagos-Quintana and colleagues first observed miRNA function in *C. elegans* by studying miRNAs lin-4 and let-7 [149]. Expression of miRNAs was found to be variable during embryogenesis suggesting a regulatory role in differentiation and tissue development. Further studies in Drosophila and human tissue confirmed the existence of miRNAs as temporal gene expression regulators that cause the translational repression of their complementary mRNA. To date, at least 800 miRNAs have been found in the human genome [146,150].

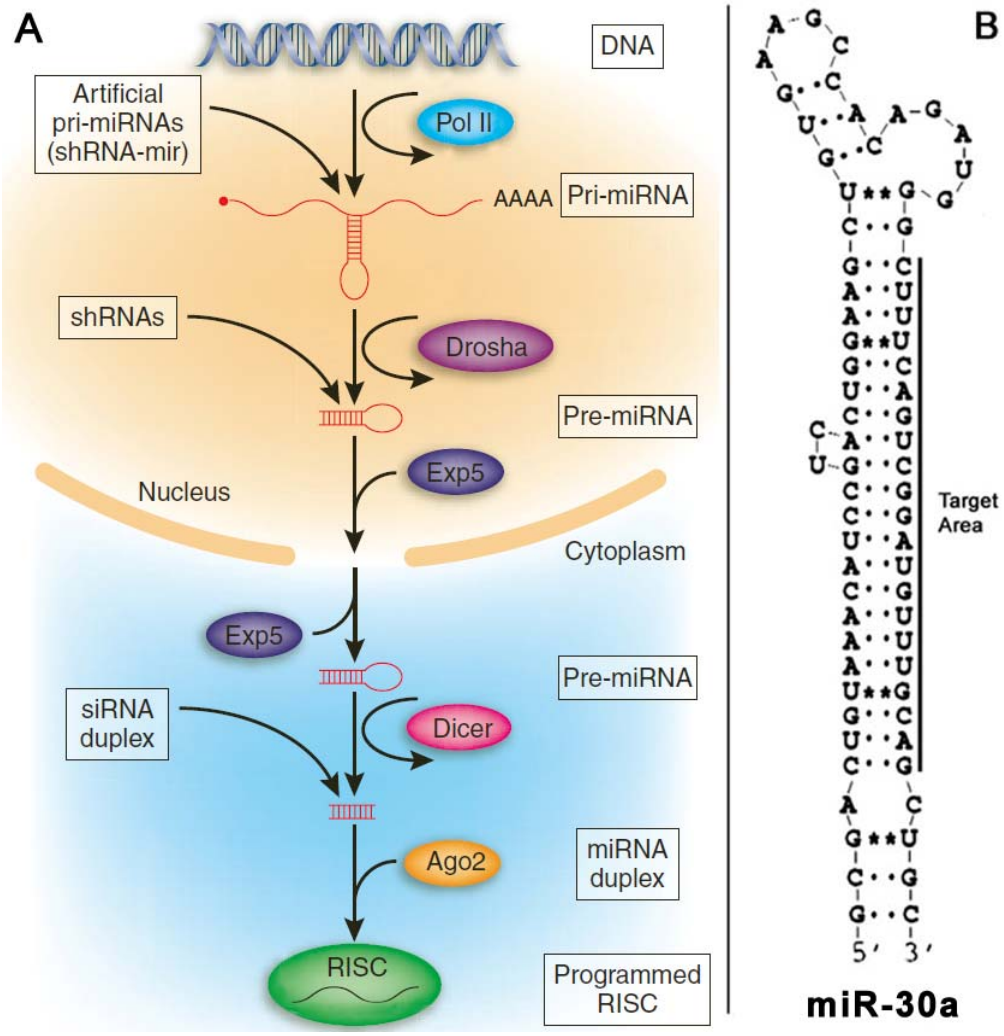

Figure 1.10: The miRNA biogenesis pathway. (A) Schematic representation of miRNA transcription (pri-miRNA), nuclear processing (pre-miRNA) and cytoplasmic maturation (miRNA duplex) steps. On the left side of the diagram, the steps where exogenously delivered molecules enter the pathway are annotated (see section 1.5.2). Exp5; Exportin 5. Ago2; Argonaute 2 (not the only one; indicative of the whole family). RISC; RNA-induced silencing complex. (Adapted from Cullen, 2005) [146] **(B)** Secondary structure of the human pre-miR-30, one of the most studied miRNA molecules. *; G-U wobble nucleotide bonding (Adapted from Boden et al., 2004) [151]

MicroRNAs are transcribed from RNA pol II promoters in clusters that are several kb long. Each miRNA sequence contains a palindrome whose secondary structure is a non-perfect hairpin. The initial primary miRNA (pri-miRNA) transcript is processed in the nucleus by an RNase III enzyme called Drosha. Drosha catalyses the excision of miRNA hairpins from the primary

transcript by recognising the hairpin structure in the pri-miRNA transcript and cleaving ~22 nt away from the hairpin loop. The ~70 nt long pre-miRNA hairpin bears a 2 nt 3' overhang after Drosha cleavage that acts as a recognition site for its interaction with Exportin-5 [152] (Figure 1.10). Exportin-5 is a nuclear export factor that mediates the transfer of the pre-miRNA to the cytoplasm where a second RNase III enzyme, namely Dicer, catalyses the final step in the formation of a mature miRNA duplex. Dicer recognises the 2 nt 3' overhang of the pre-miRNA and cleaves ~22 nt away from the last base excising the terminal loop and leaving another 2 nt 3' overhang [144,153,154]. The strand with the least thermodynamically stable 5' end incorporates an effector complex called miRNA ribonucleoprotein (miRNP) complex that includes RISC [155]. miRNPs consist of a number of miRNAs and RNA binding proteins mainly from within the Argonaute (Ago) family. Recent studies on Ago proteins reveal that they are key factors in many different RNA silencing pathways through the interactions of their PAZ (Piwi Argonaute and Zwille) and PIWI domains with RNA molecules [156]. PAZ is a 130 amino acids (aa) domain that recognises the 3' overhang of the miRNA strand whereas the PIWI domain (300 aa) forms the core of the protein than guides mRNA alignment to the miRNPs [156,157]. Through PIWI induced coupling of the miRNA strand and the 3' UTR of the target mRNA, translational repression occurs. Although PIWI domains have been shown to have endonuclease capacity, in the miRNA silencing pathway the mRNA is not degraded upon recognition. Instead, the miRNA strand forms a non-perfect duplex at the 3' UTR hindering translation. This is the main characteristic of the miRNA pathway: translational repression as opposed to mRNA degradation (in siRNA pathway) or chromatin rearrangements (in piRNA pathway).

The targeting of an mRNA by its corresponding miRNA depends on the free energy value of the miRNA:mRNA duplex. More specifically, the first 6-8 nt of the miRNA's 5' end are used as a "seed region" for mRNA coupling [146,158]. In addition, non-perfect complementarity between miRNA and mRNA creates nucleotide wobbles that can have an additional effect apart from influencing total free energy values. Guanine:Uracil (G:U) wobbles in

particular greatly reduce translational repression when present within the 5' "seed region" whereas other mismatches are more tolerated [158]. Further upstream of the miRNA biogenesis pathway, the pri-miRNA hairpin loop has been shown to affect its nuclear processing. Polymorphisms within the loop sequence have an impact on Drosha processing and therefore on cytoplasmic miRNA concentration [159]. The existence of sequence polymorphisms with functional effects indicates the dynamic role of the miRNA pathway in development as well as in disease. Expression levels of miRNAs have been shown to be altered in cancer and indeed in retinal degenerations [148,160-163]. This finding presents a new therapeutic platform for the treatment of certain diseases. For example, in cases of miRNA overexpression, stable synthetic "anti-miR" molecules can be introduced to the cell to reduce the concentration of an endogenous active miRNA. Antagomirs are 2'-*O*-Methyl modified RNA molecules that bind the active miRNA strand preventing its incorporation into miRNPs, hence influencing mRNA translation [160,164].

The expression levels of pri-miRNAs and their target mRNAs, the number of targeting miRNAs per mRNA as well as the variable processing of each miRNA depending on tissue and developmental timing, indicates that miRNAs provide a finely tuned mechanism for the regulation of gene expression.

1.5.1.1 Piwi-interacting RNAs (piRNAs)

Apart from miRNAs another ncRNA group called Piwi-interacting RNAs (piRNAs), or repeat-associated siRNAs (rasiRNAs), has recently beem discovered.

piRNAs are slightly longer than miRNAs and siRNAs ranging between 26-31nt [165]. They are associated with chromatin rearrangements during gamete formation and their presence has been confirmed in nematodes

[165], insects [166,167] and mammals [168-170]. piRNAs are thought to be transcribed from long ssRNA transcripts and gene clusters of piRNAs have been found in Drosophila [166] as well as mouse [168,170] and rat [169] testes. The main structural difference to miRNAs or siRNAs is not the gene clustering but the absence of antisense piRNA strands or hairpin formation within the multicistronic piRNA transcript [165]. However, the process and the components that mediate the excision and generation of an active piRNA as well as the pathway through which they trigger epigenetic modifications are not known yet. RNA involvement in genomic rearrangements has been previously reported in *Tetrahymena* through what was thought to be an RNAi-dependent pathway [171]. Yao and colleagues demonstrated that genome-wide DNA rearrangements that persist in the progeny of protozoa can be induced by introducing dsRNA. The targeted region was not merely translationally repressed but excised from the genome. Germline DNA rearrangements alter chromatin structure through histone modifications to silence parasitic repetitive elements like transposons. The pathway through which piRNAs trigger DNA rearrangements is not fully understood but Argonaute-based complexes (similar to miRNPs and RISC) have been found to be involved.

The Argonaute family can be divided into the Ago and Piwi subfamilies based on aa sequence variations. In general, the Ago subfamily is ubiquitously expressed and associated with the miRNA and siRNA pathways. The Piwi subfamily is restricted to the germline and stem cells where it is associated with genomic rearrangement pathways [168]. It seems possible that, apart from Argonaute based RISC complexes, piRNAs also interact with as yet unknown enzymatic methyltransferases or acetylases that induce histone modifications based on an RNA-based template.

Further studies on the catalytic function of piRNAs may in the future enable the construction of novel siRNA molecules that when provided in the host cell together with Piwi components, could mediate not only RNA silencing but also specific genomic DNA rearrangements.

1.5.2 Short-interfering RNAs (siRNAs)

1.5.2.1 Mechanism and components of siRNAs

The presence of dsRNA in the cytoplasm triggers its degradation by Dicer into ~22 nt siRNAs. The main difference between the miRNA and siRNA pathway is the pattern of cleavage by Dicer and the recruitment of an RNA-binding helicase, RDE-4, in the siRNA pathway [172]. In the miRNA pathway Dicer cleaves the pre-miRNA molecule on the basis of the Drosha-generated hairpin. In the siRNA pathway, Dicer can degrade a long dsRNA into consecutive ~22 nt siRNAs [143,145]. After Dicer maturation, the majority of miRNAs and siRNAs are virtually identical in size (~22 nt) and structure (3' 2 nt overhangs). They both incorporate into a large ribonucleoprotein complex that acts as the effector molecule for transcriptional repression. RISC is a large 500 kDa complex that mediates siRNA: mRNA association through Ago-2 [143]. Prior to mRNA silencing, RISC degrades the sense (passenger) strand and retains the antisense (guide) strand as a template for mRNA recognition. Of all the Argonaute family members, Ago-2 demonstrates splicer activity that can lead to the cleavage of the complementary mRNA [156]. Furthermore, Ago-2 mediated mRNA cleavage occurs when the level of complementarity between mRNA and siRNA is very high. In contrast to the miRNA pathway, non-perfect mRNA:siRNA duplexes do not lead to transcriptional repression but instead greatly reduce the degradation of the non-perfect transcript. The fact that the majority of Ago proteins (Ago 1,3,4) do not demonstrate splicer activity might suggest that most of the transcriptional repression is brought about *via* the miRNA and not the siRNA pathway [156]. However, understanding the basis of the siRNA pathway's high stringency can aid to develop a highly efficient targeting therapeutic molecule.

1.5.2.2 Design of siRNAs and stringency of silencing

RNAi pathways rely on certain key steps in the maturation of the targeting molecule and its target coupling. These steps involve nuclear Drosha processing and Exportin-5 trafficking as well as cytoplasmic Dicer maturation and RISC activation *via* strand selection and target recognition. The main optimisation points for efficient RNAi design are summarised below (also see Table 2).

Each mature siRNA duplex consists of two strands: the passenger and guide strands. The RISC cannot distinguish between the two strands for incorporation, therefore each strand has equal chances of RISC binding given they have equal thermodynamic stability. Various studies have shown that the strand with the least thermostable 5'- end is more likely to enter RISC [173-176]. In fact, high adenine/uracil (A/U) content in the 5'-end of the guide strand as opposed to high G/C content in the 5'-end of the passenger strand can drive antisense strand RISC incorporation as well as eliminate sense strand incorporation. G:U wobble mutations have also been recruited to aid in strand selection [177].

Once the guide strand is incorporated in the active RISC, the knockdown efficiency depends on mRNA complementarity and the catalytic function of Ago-2. Although the exact catalytic epitopes of Ago-2 and their function relative to siRNA:mRNA coupling have not been elucidated, there are certain sequence biases that increase the silencing efficiency of an siRNA. Optimal GC content has been estimated at 36 – 52 % and the siRNA guide strand should be devoid of strong internal secondary structures like hairpins caused by palindromes [173,175]. These two characteristics ensure for efficient strand separation aided by RISC's helicase activity and correct guide strand placement in the PAZ and PIWI domains of Ago. Furthermore, the presence (or absence) of certain nucleotides in certain positions seems to increase silencing efficiency: U at position 11, A at position 1 and position 16 of the guide strand are preferable for siRNA function [175,178,179]. The absence of G/C at position 7 is also favourable. In addition, position 10 and position 16 of

the guide strand have been shown to play an essential role in the catalytic activity of Ago-2 [180]. The catalytic role of these central nucleotides is stringent enough to distinguish between point mutations when purine:purine mismatches occur at these positions [180]. In this way, it is possible to silence an allele with a point mutation while the wild-type allele remains unaffected [181,182]. Alternatively, supplementation with a gene carrying a wobble mutation at the point of target is also possible [183].

Apart from ensuring efficient knockdown of the targeted mRNA, siRNA design should also concentrate in minimising off-target silencing. The 5'-end of the guide strand, and especially positions 2-8, is the "seed region" and is associated with siRNA target recognition [173]. On the other hand, the 3' end of the guide strand and especially the central nucleotides (positions 10-16) are involved in the catalytic function of the siRNA. Off-targeting has been associated with "seed region" complementarity between siRNA and 3' UTRs [184,185]. These observations are taken into account in algorithm-based siRNA designing software for target prediction in order to narrow down the selection criteria for any given gene target.

Finally, other design strategies concentrate on the flanking sequences of the active siRNA in order to enhance nuclear Drosha and cytoplasmic Dicer processing prior to RISC incorporation. Synthetic hairpins, 29 nt in size rather than the standard 19-21 nt, have been shown to act as a more efficient substrate for Dicer because of their similarity to the natural miRNA hairpins [186]. These "miRNA mimetics" have been further optimised by incorporating flanking sequences of pre-miRNAs or pri-miRNAs to facilitate Drosha as well as Dicer processing [187-189]. However, the pre- and pri-miRNA templates are too large to be delivered synthetically and since their presence is required in the nucleus, they are provided in expression cassettes driven from RNA pol III promoters.

Table 1: Summary of siRNA design strategies. The main design criteria employed for siRNA design are listed together with their underlying molecular rationales. Their accumulation has been progressive and recent sequence prediction software may use some or all of them. Note that these criteria increase the *probability* of efficient siRNA design and *do not guarantee* it. Likewise, sequences derived without the previously mentioned criteria in mind might be successful in a specific cellular context. SNP; single nucleotide polymorphism.

DESIGN CRITERION	RATIONALE	REFERENCES
5' reduced thermostability	Increasing the chance for RISC incorporation	[173-176]
36 – 52 % GC content	Although RISC has helicase activity, a high siRNA GC content might delay incorporation	[173,175]
Absence of strong siRNA secondary structure	Palindromes lead to hairpin formation that hinders Ago binding and mRNA recognition	[175,178]
High A/U frequency at 5' U at pos. 11 A at pos. 1 & 16 Not G/C at pos. 7 SNP targeting at pos. 16	Certain positions within the siRNA are more crucial than others. Probably because of Ago-2 epitope association	[175-178,180-183]
Avoid "seed region" complementarity with 3' UTR of non-target mRNAs	3 or more consecutive nucleotide matches should be avoided as 3'UTRs are more prone to off-targeting	[173,184,185]
Use pre- and pri-miRNA hairpins as templates	Natural design enhances Drosha and Dicer processing	[186-189]
Avoid immunostimulatory sequences in the siRNA	Certain sequences 5-9 nt in size may activate Toll-like receptors	[178]

1.5.2.3 Alternative design of hairpins

The majority of hairpin-based RNAi studies employ a standard design rationale for the construction of an expression cassette that drives the transcription of sense and antisense strands separated by a loop sequence. The shRNA hairpin produced by the cassette is not processed in the nucleus after transcription but instead is transported to the cytoplasm where the loop sequence is cleaved by Dicer. The only variable part of the expression cassette apart from the target area is the loop sequence as it can vary between three and twelve nucleotides. The variations in the size of the loop have arisen from different studies that concentrated on the loop sequence as a means of increasing the silencing potential of the shRNA molecule [190-192].

In an effort to further improve shRNA processing, various groups have examined the endogenous regulatory miRNA pathway and its components (see section 1.5.1). As the endogenous miRNA pathway was being deciphered and key enzymes in the miRNA pathway were identified, it was apparent that the initial transcript of a miRNA undergoes three main stages of maturation to reach the cytoplasmic siRNA duplex state. Sequence analysis of initial (pri-miRNA) and intermediate (pre-miRNA) states indicated that apart from an extended loop sequence, the miRNA molecules contained 5' and 3'-unspecific sequences that although did not contribute to the target area *per se*, they did influence nuclear processing and cytoplasmic end concentration [152,159]. The term "miRNA mimetics" is used to describe the mimicking of naturally occurring flanking sequences when designing an shRNA expression cassette. The aim is to use the nuclear machinery to process the hairpin molecule more efficiently, increasing its cytoplasmic concentration and thus its potency [193]. In addition, miRNA-based hairpins have also been shown to reduce non-specific toxicity in host cells. The same target areas incorporated into standard shRNAs induced toxicity caused by high hairpin concentration [194]. miRNA-based design should improve the silencing capacity of any hairpin; something which could prove useful in applications where the choice of target area is limited. For example, in

conventional siRNA studies the whole span of a given mRNA sequence is targeted and the most efficient candidate is used for the construction of a hairpin cassette. However, in the case of point mutation targeting there is minimal flexibility in siRNA selection. Similarly, when targeting a highly expressed gene, the most efficient siRNA candidate may still not be efficient enough to achieve total silencing.

With the advancement of tissue miRNA profiling, a number of highly expressed miRNAs have been identified in most tissues and range from universal miRNAs (house-keeping regulators) to tissue-specific miRNAs (tissue-specific regulators). The structure of these miRNAs can be mimicked in hairpin design and increase the levels of gene knockdown. miR-30 is one molecule which has been used in miR-based hairpin design [151,195,196]. As in all miRNAs, miR-30 contains 3' and 5' flanking sequences as well as an extended loop sequence (Figure 1.10). In addition, mismatches decrease the energy stability of the molecule at various positions. This feature has already been used in standard siRNA design as a means of increasing the ratio of antisense-sense strand Dicer incorporation.

1.5.2.4 Evading silence using the degeneracy of the genetic code

The degeneracy of the genetic code is a powerful asset for DNA transcription as it "shields" the cell from the accumulation of random mutations over time. In effect, 61 codons correspond to 20 amino acids resulting in each amino acid being incorporated into a polypeptide by a range of codons (from a minimum of one codon, only in the case of tryptophan and methionine, to a maximum of six codons in the case of arginine, leucine and serine). With regard to RNAi design, when selecting target sequences randomly, the chances that the target area is situated in the ORF of the gene are higher as it often exceeds the 3' or 5'-UTRs in size. The stringency with which siRNA molecules function renders the degeneracy of the genetic code a powerful tool to evade silencing for "suppression and replacement" approaches.

Alternatively, specifically targeting intragenic polymporphisms or UTRs while altering the 3' and 5'-UTRs in the replacement construct could lead to similar levels of silencing [130]. When targeting within the ORF, by manipulating the third nucleotide of the codons in the target area it is possible to produce an altered transgene that is not silenced by the mismatched siRNA, while at the same time it encodes the same polypeptide as the siRNA's target. One precaution that needs to be taken into consideration prior to inserting the codon-altering mutations, is the relative abundances of their respective tRNAs. In each species, the tRNAs carrying the amino acids for each corresponding codon do not exist in equal cytoplasmic concentrations [197]. The reason for this is that certain codons are far more common than others and equimolar cellular tRNA concentrations hamper mRNA translation. When considering codon exchanges within a polypeptide, the codon with the lowest relative abundance (i.e. the rarest) in the original cDNA should first be identified. Since the rarest codon is the rate limiting factor during mRNA translation, the substituted codons in the area of interest should not have lower relative abundances. Slower production of the polypeptide might be deleterious especially when high transgene expression levels are needed.

1.5.2.5 Hairpin expression cassettes and viral vectors

Synthetic siRNA administration provides a transient knockdown of the target mRNA as its cytoplasmic turnover is very fast. Expression cassettes that transcribe a hairpin RNA can be more persistent than synthetic siRNA transfection and the incorporation of a hairpin cassette into a viral vector can prolong the short hairpin RNA (shRNA) expression even further depending on the nature of the virus and the transduced tissue.

Plasmid shRNA expression requires an RNA pol III promoter such as U6 or H1 to drive the transcription of the sense and antisense strand which are separated by a oligonucleotide loop sequence that enables hairpin formation. Brummelkamp and colleagues have demonstrated that plasmid-based

shRNA expression in human breast cancer cells leads to an almost 90 % knockdown of p53 and CDH1 [198]. In addition, they performed a loop size analysis indicating that a 9 nt long loop provides better knockdown than hairpins with 5 or 7 nt. The loop size can vary from 3 nt to large miRNA based ones and it should allow for efficient hairpin formation [190]. RNA pol III promoters can also be enhanced for increased or selective expression. A CMV enhancer has been shown to increase shRNA expression from the U6 promoter in 293T cells and has been used to target an allele-specific *SOD1* mRNA point mutation [192]. Doxycyclin and tetracycline H1 inducible promoters have been successfully used in human colorectal cancer cells to target β–catenin [199] and DNMT1 [200] expression, respectively. Silencing of these genes was greater than 2-fold and resulted in growth arrest of the cancer cell line.

A main advantage of RNAi expression cassettes is their relatively small size (~500 bp) that enables their cloning in viral vectors often in bicistronic configuration together with a reporter gene expression cassette. Lentiviruses expressing shRNA cassettes have been used to effectively target luciferase [201] and the *K-RAS* oncogene [202] in human cells. The efficient virally-induced silencing of *K-RAS* was also demonstrated *in vivo* in athymic mice by preventing tumour progression [202]. When miRNA-based design is employed together with lentiviral expression, the silencing of the target gene can be even more potent and stable. Lentiviral transduction of 293T cells with a miRNA-based cassette targeting the HIV-specific *tat* gene resulted in 80 % reduction of the p24 antigen titration value [151]. The potency of lentiviral miRNA-based hairpin expression was further demonstrated by Shin and colleagues on mouse embryonic fibroblasts and macrophages. At an MOI of 1, efficient and stable tetracycline-regulated silencing of G protein subunits was observed in both cell lines [203]. In addition, multicistronic miRNA cassettes were efficiently transcribed from one promoter leading to equal levels of silencing for two different G protein subunits. AAV-based hairpin expression has also proved to be effective *in vitro* and *in vivo* for the targeting of cancer or neural cell specific expression [204-206].

1.5.2.6 Hairpin toxicity and off-targeting

Although the efficiency of siRNAs or shRNA expression cassettes has been widely demonstrated in various studies, any non-specific off-targeting or toxic effect that these molecules might have is not always assessed. In mammalian cells, the presence of dsRNA might activate cellular defence mechanisms through the interferon response pathway resulting in non-specific RNA degradation. A few studies employed microarray profiling or interferon stimulated gene (ISG) expression analysis to answer the question of siRNA non-specificity. Efficient knockdown of chromatin regulating *MORFL* genes in human lung fibroblasts increased the expression of 2'5'-oligoadenylate synthetase (*OAS1*), a classic interferon target gene, by 50-fold [207]. Although the effect might depend on the nature of the targeted gene, the cell line or indeed immunostimulatory sequences in the siRNA [208], the authors of the study point out that many cancerous cell lines, which are often used in RNAi experiments, have a defective interferon response and hence an immunostimulatory effect may not be observed. In human glioblastoma cells, laminin siRNA transfection resulted in multiple ISG overexpression through a pathway independent from PKR, a dsRNA-dependent protein kinase, and RNase L, the main dsRNA interferon triggers [209]. It has been speculated that toll-like receptor 3 (TLR3) activation may be the cause of siRNA immunoreactivity but this has not been confirmed [210]. TLR3 is a cell surface double-stranded viral RNA sensor that protects the cell from viral infections. Naked siRNAs are able to activate the extracellular part of TLR3 causing non-specific mRNA degradation and eventually leading to cell death. This process is initiated by TLR3 and propagated through the interferon response system for the protection of the host. Kleinman *et al.* also demonstrated that the minimum siRNA length required for TLR3 activation was 21 nt of conventional design [210]. Smaller siRNAs did not activate the receptor. Although the authors clearly demonstrated TLR3 activation by naked RNA, they did not test corresponding shRNAs or siRNAs delivered using transfection reagents. Although U6 and H1 are the most popular promoters used to drive RNAi expression, other RNA pol III promoters can be used for shRNA transcription.

However, the bacteriophage T7 promoter has been found to induce an interferon response due to a GGG triphosphate addition at the beginning of the hairpin [211]. It is, however, possible to prevent the immune response by using an additional two 3' adenosine residues at the end of the hairpin that abolishes coupling with the GGG at the 5'-end allowing RNAse T1 to cleave them.

Apart from initiating an interferon response, it has been suggested that off-targeting may result in siRNAs acting as miRNAs on non-perfect complementary mRNAs [212]. RISC incorporation does not determine whether the short RNAs progress down the siRNA or miRNA pathway, instead it is the complementarity with the target mRNA that determines this. However, the exact process by which RISC distinguishes between miRNA and siRNA guide strands, is not yet known. Jackson and colleagues carried out an extensive microarray analysis on off-targeting after siRNA transfection targeting *MAPK14* and *IGF1R* in HeLa cells. A number of mRNAs with a minimum complementarity of 11 consecutive nucleotides to the siRNA were also downregulated [213]. However, all the nucleotide identities were located towards the 5' end of the guide strand indicating binding of the siRNA "seed region" to the 3'UTR of the off-targets. This study further highlights the importance of safe siRNA design and the need for updated sequence predicting software.

A recent study suggested that RNAi toxicity may be due in large part to the levels of shRNA/miRNA expression rather than their silencing effect on gene expression. Grimm and colleagues used AAV2/8 vectors to drive miRNA-based cassettes targeting 49 different areas within 6 mRNA targets [214]. Systemic delivery of the viruses in mice resulted in dose-dependent liver injury (36 viruses) and/or death (23 viruses). The saturation of the endogenous miRNA pathway that resulted in the downregulation of liver-specific miRNAs was found to be the reason of toxicity. Exportin-5, in particular, is the key protein that chaperones pre-miRNAs to the cytoplasm and was mostly affected. Supplementation with an *Exportin-5* transgene restored endogenous miRNA processing indicating toxicity was caused by a

reversible saturation event. It is evident that when using a combination of potent vector (AAV2/8) and expression cassette (miRNA-based), an optimal dosage is essential to minimise toxicity and at the same time maintain the desired silencing. Therefore, safe design as well as appropriate choice of vector and hairpin template are the main prerequisites to ensure successful application of this technology.

1.5.3 Applications of RNAi

RNAi-mediated knockdown has been successfully applied *in vitro* and *in vivo* using various delivery methods. Oncogenes [215-218], HIV-1 regulatory elements [151,219,220] and triplet-repeat expansion mutations [221-224] have been silenced in various animal models. In the eye, viral-mediated RNAi has been used to efficiently silence photoreceptor-specific genes in mouse models of dominant RP.

Inhibition of an angiogenic factor in the retina to combat neovascularisation has been the first effort to efficiently treat an ocular condition using RNAi [178,225,226]. *VEGF* has been silenced using synthetic [227,228] or viral hairpin cassettes [229] resulting in reduced neovascularisation in a mouse model for CNV. The first clinical trial using a synthetic siRNA downregulating *VEGF* expression to treat AMD patients is currently in progress and is expected to enter phase II soon. Administration of siRNA via intravitreal injection requires minimal surgery and is the favoured route of administration for repeated siRNA delivery in the eye. The advantage of using synthetic siRNAs to target VEGF over shRNA expression cassettes relies on the fact that shRNA delivery to the retina is still being optimised in terms of choice of vector and regulation of expression. Intravitreal injections are routinely performed and even though repeated administration of siRNAs is required, their short period of action eliminates many possible side-effects of prolonged expression. Since angiogenesis is part of healthy retinal development, constitutive downregulation of angiogenic factors like VEGF might not be

desirable. Temporary inhibition can provide protection against aberrant neovascularisation where permanent silencing would not be favourable since VEGF is an important component of vascular regulation. Although the majority of anti-angiogenic studies concentrate on VEGF, other molecules involved in the neovascularisation pathway, like HIF-1, have recently attracted attention as they act upstream of VEGF in the angiogenesis pathway [230].

Another area of interest is the silencing of major photoreceptor genes. Palfi and colleagues used a plasmid based shRNA expression cassette to silence ~80 % of *Prph2* mRNA in retinal explants and transfected COS-7 cells [231]. They also demonstrated replacement of PRPH2 through the expression of an alternate *Prph2* cDNA with 8 point mutations within the siRNA target area. Subsequent silencing of other photoreceptor genes (*rho* silenced by 50 %, *pde* silenced by 20 %) that had no homology to the targeted area of *Prph2* were attributed to secondary effect after *Prph2* depletion rather than off-targeting [231]. Although this explanation is quite possible, partial complementarity with these genes' 3'UTR should also be investigated.

RNAi-mediated knockdown of rhodopsin has been studied more extensively as *Rho* mutations account for the majority of adRP mutations. Cashman and colleagues used human embryonic retinoblasts to demonstrate *Rho* knockdown after plasmid transfection with an shRNA cassette. Robust silencing of ~95 % of *Rho* expression was observed in the transfected cells [232] although it is not clear how expression levels in embryonic retinoblasts compare with that in adult photoreceptors. The hairpin used in this study silenced both wild-type *Rho* mRNA and *Rho* mRNA carrying the P23H mutation while a *Rho* cDNA mutated within the target area of the hairpin using the degeneracy of the code was left unaffected. *In vivo*, *Rho* knockdown has been attempted using subretinally injected AAV2/5 vectors by two different research groups. Gorbatyuk and colleagues showed wild-type *Rho* knockdown in $rho^{+/-}$ mice resulting in 40 % reduction of scotopic ERG values and a reduction in ONL thickness (53 – 86 %) 2 months after injection [233]. Although the feasibility of *in vivo Rho* knockdown was clearly

demonstrated, Tessitore and colleagues failed to rescue a transgenic rat expressing a *Rho* mRNA carrying the P23H mutation using an allele-specific shRNA cassette [234]. Despite mRNA and protein level depletion three weeks after *in vivo* delivery there was no morphological amelioration in the treated eyes after four months possibly because of non-specific knockdown of *Rho* mRNAs. The authors suggested that the *in vivo* level of silencing was not high enough and the construction of a more robust shRNA cassette for the treatment of dominant *Rho* mutations would be required. O'Reilly and colleagues recently published the most promising study on *Rho* mutation-independent silencing for the treatment of the P23H dominant mutation [235]. They constructed a number of shRNAs that targeted *Rho* at different regions achieving ~90 % silencing in retinal explants. *Rho* cDNAs mutated at the target area of the shRNA remained unaffected *in vitro* and in retinal explants. Morphological amelioration was observed in 2 month-old transgenic mice carrying the P23H mutated allele on a *rho*+/- background after subretinal injection at P10 of an AAV2/5 expressing *Rho* shRNA and replacement cDNA. The thickness of the ONL in treated eyes was ~33 % thicker than the control eGFP injected eyes [235]. Electrophysiological responses were not included in the study although it would be interesting to compare the morphological rescue with a possible amelioration in visual responses. However, the efficiency of *in vivo* "suppression and replacement" in mammalian photoreceptors has been demonstrated in this study and its follow up successfully targeting the Pro357Ser *Rho* mutation in mice [236]. In that study, the efficient downregulation of the Pro357Ser mutation was coupled with a doubling of the ERG amplitudes in comparison to control eyes ten weeks after subretinal delivery, demonstrating that AAV-mediated RNAi can reduce the rate of retinal degeneration and lead to functional amelioration in models of adRP.

The emergence of RNAi and the discovery of a broad range of novel ncRNAs have shaped the field of molecular therapeutics during the past decade. In the future, RNAi technology employing vectors with regulated targeting hairpin and gene supplementation cassettes may lead to clinical applications

of somatic gene therapy for the correction of monogenic dominant disorders which up to now has not been possible.

2 Materials and Methods

2.1 Hairpin RNA design

Upon designing a short-interfering RNA various factors must be considered in order to maximise the silencing potential of the molecule. For a detailed analysis on sequence, size and intramolecular dynamics, see Chapter 1.4.2. The target sequences of the *egfp* and *peripherin-2* genes were obtained from one of the numerous sequence prediction websites available in the internet (www.dharmacon.com).

The target sequences for *ZO-1* and *ZONAB* were kindly provided by Karl Mater, IOO.

The hairpins where designed so as to contain the sense and anti-sense stands of the target sequence separated by either a 3nt (ATG) or a 9nt loop (TTCAAGAGA) or by the miR-30 human micro RNA loop. The miR-30 full sequence is 5' – GCGA**CUGUAAACAUCCGUCACUGGAAG** *CUGUGAAGCCACAGAUGGG***CUUUCAGUCGGAUGUUUGCAG**CUGC – 3'. The sequence in bold indicates the natural miR-30 sequence and was substituted by the target sequence of interest (see Table 1). The sequence in italics indicates the stem loop.

2.2 Cloning

2.2.1 DNA electrophoresis

After restriction digests or PCR reactions, DNA fragments were separated on a 1-2 % (w/v) agarose gel, according to the size of the DNA fragment, using 1x TBE buffer. Ethidium bromide (1 µl of 10 mg/ml concentration per 50 ml of gel) was added to visualise nucleic acid bands. Samples were loaded onto the gel using gel-loading buffer (6x; 0.25 % (w/v) bromophenol blue in water and a 1 kb DNA ladder (Bioline Ltd., UK) was run at the same time to provide a size marker. The voltage was set between 50-90 V considering the separation time of fragments of the expected size. The gels were photographed on an ultraviolet transilluminator.

Ethidium bromide concentration was reduced to a 1:100 dilution when attempting difficult clonings in order to reduce DNA chelation that hinders ligation.

2.2.2 DNA extraction from agarose gels

The required DNA fragments were excised from the agarose gel and the DNA was extracted using QIAquick™ Gel Extraction Kit (QIAGEN Ltd., UK) following the manufacturer's instructions. The concentration of the eluted DNA was measured by photospectroscopy using a NanoDrop® ND-1000 Spectrophotometer (LabTech Int., UK).

2.2.3 Cloning ligations

The ligation of gel purified DNA fragments was carried out at 25°C for 3 hr or at 16°C overnight. T4 DNA ligase (New England Biolabs Ltd. UK), the supplied buffer, the vector backbone and the insert of interest were added in accordance with the manufacturer's instructions at a final volume of 20µl. To

check whether the ligation was successful, the ligated plasmid was transformed in *E.Coli* bacteria. DNA was isolated from the bacterial cultures using GenElute™ Plasmid Miniprep Kit (Sigma, UK) and analysed by the appropriate restriction enzyme digests and subsequent gel electrophoresis. Bacterial cultures of positive clones (680 µl) were mixed with glycerol (180 µl) (Sigma, UK) and kept in -80°C for long-term storage. All cloning end-products were subsequently sent for sequencing at MWG Biotech, UK together with appropriate primers in order to obtain sequencing reading from both DNA strands. The insert together with part of the backbone was thoroughly sequenced for all cloned plasmids presented in this study.

2.2.4 Transformation and recovery of plasmids

DH5α™ competent cells (Invitrogen Ltd., UK) were defrosted on ice. After the bacterial suspension had thawed on ice, the ligation solution was added and the transformation mix was incubated on ice for 15-30 min. Samples were then heat-shock treated for 90 sec at 42°C in a water bath, quickly transferred for 15 min on ice, and 500 µl LB (Luria Bertani, Merck Ltd, UK) medium was added. All plasmids used included the ampicillin or kanamycin resistance gene as a selection marker for successfully transformed colonies. To ensure efficient expression of the resistance gene, transformed bacteria were incubated for 1 hr at 37°C before they were spread on selective LB agar plates. LB agar plates were prepared containing 20 g Bacteriological agar (Oxoid Ltd., UK) per litre of water, 15 g/l yeast extract (Oxoid Ltd., UK), 10g/l NaCl (Sigma, UK), 10g/l peptone from casein and 100 µg/ml ampicillin or 50 µg/ml kanamycin (1000x; Sigma, UK). Plates were incubated overnight at 37°C to allow resistant bacteria to grow.

Bacterial colonies were inoculated into 5 ml of LB medium containing 100 µg/ml ampicillin or 50 µg/ml kanamycin (1000x; Sigma, UK) the following day and were incubated at 37°C overnight to allow for growth. For small scale preparations, plasmids were recovered using GenElute™ Plasmid Miniprep Kit (Sigma, UK). For large scale preparation 50 µl of the 5 ml culture were

used to inoculate 500-1000 ml LB medium and bacteria were grown as described above. DNA was then recovered using QIAGEN® Plasmid Mega Kit (QIAGEN Ltd., UK). For transformation and preparation of highly recombinogenic plasmids, all the incubations were carried out at room temperature for 30 hrs.

2.2.5 Basic RNAi expression vector (mu6pro)

The target sequences for RNAi on the genes of interest where converted into DNA hairpin oligonucleotides (see Table 1) in order to be cloned into the mU6pro expression plasmid. The oligonucleotides were designed so that the sense and antisense strands of the target area are separated by a 3 or 9 nt loop sequence (ATG or TTCAAGAGA), and after primer annealing the restriction site overhangs of *BbsI* and *XbaI* form at the 5' and 3' end of the fragment, respectively. In this way, the hairpin sequence can be cloned exactly downstream of the U6 promoter. For the miR-30 based hairpins, the same nucleotide overhangs were used when incorporating the target sequence into the microRNA template.

Table 2: Hairpin RNA design. The two strands of the hairpin sequences for each gene are displayed in 5' to 3' orientation. The sense and guide strand of the hairpin target area (bold) are separated by the loop sequence and flanked by the sequences of the restriction enzymes *BbsI* and *XbaI*. Hairpins with the **sh** prefix have the standard 3 or 9 nt loop design. The **miR** prefix indicates miR-30 based design. miRshCON and shCON target area is a control non-targeting sequence.

NAME (TARGET GENE)	HAIRPIN SEQUENCE (OF EACH DNA STRAND)
shGFP (*egfp*)	TTTG**GTTCATCTGCACCACCGGCAAGT**TTCAAGAGA **GCTTGCCGGTGGTGCAGATGAAC**TTTT
	CTAGAAAA**GTTCATCTGCACCACCGGCAAGC**TCTCTTGAA **ACTTGCCGGTGGTGCAGATGAAC**
miRGFP (*egfp*)	TTTGGCGA**GTTCATCTGCACCACCGGCAAGT**CTGTGAAGCCACAGATGGG **GCTTGCCGGTGGTGCAGATGAAC**CTGCTTTT
	CTAGAAAAGCAG**GTTCATCTGCACCACCGGCAAGC**CCCATCTGTGGCTTCACAG **ACTTGCCGGTGGTGCAGATGAAC**TCGC
shRDS4 (*rds*)	TTTG**TCGACATGCTCCAGATTGA**ATG**TCAATCTGGAGCATGTCGA**TTTT
	CTAGAAAA**TCGACATGCTCCAGATTGA**CAT**CAATCTGGAGCATGTCGA**
shRDS5 (*rds*)	TTTG**ATAATTCTGAGAGCCACTT**ATG**AAGTGGCTCTCAGAATTAT**TTTT
	CTAGAAAA**ATAATTCTGAGAGCCACTT**CAT**AAGTGGCTCTCAGAATTAT**
shRDS6 (*rds*)	TTTG**CTACAGCTATGACCATCAT**ATG**CTGATGGTCATAGCTGTAG**TTTT
	CTAGAAAA**CTACAGCTATGACCATCAT**CAT**CTGATGGTCATAGCTGTAG**
miRDS6 (*rds*)	TTTGGCGA**CTACAGCTATGACCATCAT**CTGTGAAGCCACAGATGGG **CTGATGGTCATAGCTGTAG**CTGCTTTT
	CTAGAAAAGCAG**CTACAGCTATGACCATCAG**CCCATCTGTGGCTTCACAG **ATGATGGTCATAGCTGTAG**TCGC
shZO-1 (*ZO-1*)	TTTG**AAGATAGTTTGGCAGCAAGAG**ATG**CTCTTGCTGCCAAACTATCTT**TTTT
	CTAGAAAA**AAGATAGTTTGGCAGCAAGAG**CAT**CTCTTGCTGCCAAACTATCTT**
shZONAB (*ZONAB*)	TTTG**AACTTACCGCCCAAGGTACCG**ATG**CGGTACCTTGGGCGGTAAGTT**TTTT
	CTAGAAAA**AACTTACCGCCCAAGGTACCG**CAT**CGGTACCTTGGGCGGTAAGTT**
shCON	TTTG**GATCGGACACTCCTCATAA**ATG**TTATGAGGAGTGTCCGATC**TTTT
	CTAGAAAA**GATCGGACACTCCTCATAA**CAT**TTATGAGGAGTGTCCGATC**
miRCON	TTTGGCGA**GATCGGACACTCCTCATAA**CTGTGAAGCCACAGATGGG **TTATGAGGAGTGTCCGATC**CTGCTTTT
	CTAGAAAAGCAG**GATCGGACACTCCTCATAA**CCCATCTGTGGCTTCACAG **TTATGAGGAGTGTCCGATC**TCGC

2.2.6 Peripherin-2 site-directed mutagenesis PCR

Prph-2 cDNA was amplified from our pre-existing pD10.Rho.Rds plasmid using 2 sets of primers. The two step PCR was used to introduce 3 nucleotide changes in the *Prph-2* cDNA targeted by our shRDS6 and miRDS6 hairpins (pos: 906-927). The primers used were:
P1 – CACCGCACTCGGTAAGCATGGCG – (5' outer forward),
P2 – TCAGCCAGCCTCTGG – (3' outer reverse),
P3 – TA**T**AG**T**TA**C**GACCATCAGACTGAGGAGCTCAAC – (middle forward),
P4 – AGTCTGATGGTC**G**TA**A**CT**A**TAGTGCGCCGAGTTG – (middle reverse).
Nucleotides in bold indicate point mutations. PCR reactions were performed in a total volume of 30 µl, 0.2 mM dNTPs (Promega, UK), 3 µl of buffer, 30 pM of each primer and 1 U of Expand High Fidelity PCR System polymerase (Roche, UK) were with 100-200 ng of plasmid template DNA or 50-100 ng of PCR product. Initially, primers P1&P3 and P2&P4 were used in pairs on the plasmid template to generate two halves of the mutated *Prph-2* cDNA. The two PCR products were then mixed together and P1&P2 were used to generate the full length cDNA. The final amplified fragment (mutRDS) was then sequenced also using outer primers P1 and P2 to confirm point mutation incorporation (MWG Biotech, UK).

CYCLING CONDITIONS:

Initial denaturation	3 min at 95°C	
Denaturation	1 min at 95°C	40 cycles
Annealing	30 sec at 51°C	
Extension	1 min at 72°C	
Final extension	10 min at 72°	

2.3 Tissue Culture

2.3.1 Cell lines and culture of cells

Baby hamster kidney (BHK) cells were grown in BHK-21 medium supplemented with 10 % heat inactivated foetal bovine serum (FBS), 100 U/ml penicillin and 0.1 mg/ml streptomycin, 5 % tryptose phosphate broth, 2 mM L-glutamine and 0.25 mg/ml geneticin G418. 293T cells were cultured in Dulbecco's Modified Eagle's Medium (DMEM) supplemented with 10 % FBS, 100 U/ml penicillin and 0.1 mg/ml streptomycin. Madin-Darby canine kidney (MDCK) cells were cultured in a 1:1 mixture of DMEM and Ham's F-12 nutrient medium supplemented with 10 % FBS, 100 U/ml penicillin and 0.1 mg/ml streptomycin. ARPE-19 cells were grown in a 1:1 mixture of DMEM and Ham's F-12 nutrient medium supplemented with 10 % FBS, 100 U/ml penicillin, 0.1 mg/ml streptomycin and 56 mM sodium bicarbonate. HeLa cells were grown in DMEM. 10 % FBS, 100 U/ml penicillin, 0.1 mg/ml streptomycin and 0.25 mg/ml geneticin G418 and were added to the medium (all reagents were purchased from Invitrogen Ltd., UK). Cells were grown in a Sanyo CO_2 incubator at 37°C with 5 % CO_2.

2.3.2 Passaging of cell cultures

Confluent cell cultures were split usually 1:2 or 1:7 to maintain healthy colonies. The old medium was removed and cells were washed twice with 1x PBS (10 phosphate buffered saline tablets (Oxoid Ltd., UK) dissolved in 1 l sterile dH_2O) before trypsin-EDTA (Invitrogen Ltd., UK) was added until all cells were covered. Plates were then incubated for approximately 10 min at 37°C to allow cells to dissociate. The process was stopped by adding FCS containing growth medium before the cells being split into new plates in the appropriate ratio.

2.3.3 Cell line long-term storage

For long-term storage cells were trypsinised and pelleted by centrifugation. Approximately 5 x 10^6 cells/ml were resuspended in 1 ml growth medium with 20 % FCS and 10 % dimethylsulfoxide (DMSO; Invitrogen Ltd., UK). The cryovials were pre-cooled on ice and once the cells were aliquoted they were kept overnight at -80°C in a storage container with isopropanol. The following day the frozen cultures were transferred to liquid nitrogen.

Frozen cells can be re-cultured by thawing the cryovials in a water bath at 37°C. Cells were then pelleted by centrifugation and the DMSO containing medium was removed. The process was repeated washing the cells with 1x PBS before resuspending them in the appropriate medium.

2.3.4 Infections

Cells were split the day before at appropriate concentrations and at low confluency. The multiplicity of infection (MOI) was calculated using the number of cells plated and the titre of the virus in transducing units per ml. The virus suspension was mixed with the medium and added onto the cells. Microscope imaging of reporter gene expression was carried out after 24hr when using a lentiviral vector. For fluorescent microscopy and nucleic acid or protein extraction, the cells were left for 4 to 7 days. For FACS sorting, pellets were recovered through centrifugation at 2000 xg for 5 min and resuspended in 400 µl PBS with 4 % PfA. The cells were kept on ice and sorted using an Epics XL flow cytometer (Beckman Coulter, UK).

2.3.5 Transfections

Similarly to the conditions prior to infection, the cells were split the day before at appropriate concentrations and at 60 to 70 % confluency. A total amount of

1-2 µg of plasmid DNA was mixed in Opti-MEM® (Invitrogen Ltd., UK) with 2 µl Lipofectin reagent (Invitrogen Ltd., UK) and incubated at room temperature for 20 min. The cells were washed with 1x PBS after removal of the growth medium and the transfection medium (DNA–Lipofectin) was added onto the cells. After 4 hr incubation at 37°C, the transfection medium were removed and replaced with normal growth medum. The following day the cells were visualised under a fluorescent microscope to assay the transfection efficiency based on reporter gene expression. At 72 hr after transfection, the cells were trypsinised and pellets were recovered through centrifugation at 2000 xg for 5 min prior to their resuspension in 400 µl PBS with 4 % PfA. The cells were kept on ice and sorted using an Epics XL flow cytometer (Beckman Coulter, UK).

2.3.6 Generation of peripherin-2 and egfp expressing stable cell lines

293T cells were seeded in a 24 well-plate the day before. LNT.SFFV.RDS or LNT.SFFV.EGFP was added at limiting MOI in each well and the cells were left to grow for 6 days splitting them once in between. The cells were then seeded in a 96 well-plate at limiting dilutions and left to grow colonies. For the *peripherin-2* expressing cells, pellets were recovered through centrifugation at 2000 xg for 5 min and resuspended in 2x Laemni buffer. The protein was prepared for western blotting and the cell clone with the highest *peripherin-2* expression and viability was selected and propagated. For the *egfp* expressing cells, pellets were recovered similarly and resuspended in 200µl PBS with 5 % BSA. The cells were kept on ice and sorted using a Beckman Coulter Epics Altra cell sorter with Expo32 software (Beckman Coulter, UK). The single-cell clone with the highest *egfp* expression was selected, using UV microscopy, and propagated.

2.3.7 Cell immunofluorescent staining

For immunofluorescence staining, MDCK or ARPE-19 cells were grown on glass coverslips and after infection were fixed with methanol at –20°C or with PfA at room temperature. The samples were then rehydrated with PBS, permeabilised with Triton X-100 (1 %) and blocked for 1hr with 0.5 % BSA solution. The 1° antibody was then added at the appropriate concentration and incubated for 1hr at room temperature. The cells were washed with PBS and the 2° antibody was added for 50 min at room temperature. After rinsing with 1x PBS, the samples were analysed using fluorescent microscopy.

2.3.8 3-D cultures

MDCK cell cysts were grown in 3-D collagen gels. Briefly, MDCK cells were trypsinised, diluted 1:3 with serum-containing medium to inactivate trypsin, spun, and then resuspended to a single cell suspension and counted. Cells (20,000 in 5 µl) were mixed with 100 µl collagen-Matrigel master mix that was prepared by neutralizing 60 µl of ice-cold solution containing 1 mg/ml calf skin type I collagen (Sigma, UK) with 10 µl 10x DMEM, 2 µl HEPES 1 M (pH 7.4), and 2 to 3 µl of 2 M NaOH that was then mixed with 10 µl of 100 % fetal bovine serum and 16 µl of Matrigel (growth factor reduced; BD Biosciences, UK). The cell-collagen-Matrigel mix was plated in a well of a 48-well dish containing a coverslip that had been covered with 100 µl of the collagen-Matrigel master mix for 1 hr at 37°C. The plated mixture was then allowed to form a solidified gel at 37°C prior to the addition of culture medium. The medium was replaced every 2 days, and the cysts were allowed to develop over 5 to 6 days. For fluorescence labelling, cells were fixed with 3 % PfA for 20 min at room temperature and were then washed twice with PBS. Then, the cells were blocked and permeabilised for 30 min at room temperature with 2 % BSA, 1 % Triton X-100, and 25 mM Tris in PBS, followed by incubation overnight at 4°C with a goat anti-beta-catenin antibody. After three washes with 2 % BSA, 1 % Triton, 25 mM Tris in PBS, the samples were

incubated with a Cy3-conjugated anti-goat antibody, fluorescein isothiocyanate (FITC)-phalloidin and Hoechst 33528. After three washes with PBS, cells were mounted with Mowiol. For quantification of the different structures, low-magnification pictures from the actin stainings were taken. Ten pictures of each cell line and condition were quantified from two experiments.

2.4 Adeno-associated viral vectors

2.4.1 RNAi Constructs

The RNAi hairpin cassettes (U6 promoter + hairpins) were cloned into a pD10.CBA.RFP backbone using the *AscI* and *BstZ17I* restriction sites in the pD10.CBA.RFP plasmid and *AscI* and *SnaBI* to excise them from the donor mU6pro plasmid. The pD10.CBA.RFP plasmid also drives expression of *rfp* through a CBA promoter. The resulting plasmids were verified by sequencing (MWG Biotech, UK) and AAV virus particles were made for each hairpin vector.

2.4.2 Production and purification of rAAV2/2

Production of recombinant AAV2/2 (rAAV2/2) was carried out by co-transfection of two plasmids in the presence of a helper virus in BHK cells as previously described [95]. BHK cells were seeded into 150 mm plates at a concentration of 10^6 cells/plate. The plates were incubated overnight so that they reach 70 % confluency the following day. The cells were transfected with the aforementioned pD10 constructs that contained the RNAi and RFP expression cassettes flanked by AAV-based ITRs and the helper plasmid pHAV7.3 that contains the viral *rep* and *cap* genes. The two plasmids were mixed in a 1:1 weight ratio (60 µg total/plate) in 6 ml Opti-MEM®/plate. In a separate tube, 240 µg of a β-integrin-targeting peptide used to improve the binding of the DNA [(K16)GACRRETAWACG)], was mixed with 45 µl of Lipofectin reagent (Invitrogen Ltd., UK). The two tubes were mixed and incubated at room temperature for 1 hr in order for the DNA to bind the Lipofectin-peptide complex. The medium was removed from the plates and the cells were washed with Opti-MEM® prior to the addition of the transfection solution. The plates were then incubated at 37°C for 4 hr. After incubation, the transfection solution was replaced by normal growth medium containing a helper PS1 HSV helper virus at an MOI (multiplicity of infection = average

number of particles that infect a single cell) of 10. The cells were incubated at 37°C for a further 36 hr, to allow the completion of the lytic cycle and were subsequently scraped and centrifuged before being resuspended in serum-free medium. The viral particles were released from the harvested cells by 3 freeze-thaw cycles at -80°C and 37°C. Vigorous vortexing for 5 min in between ensured adequate cell lysis. Treatment with 50 U of benzonase (Sigma, UK) to eliminate any plasmid DNA was followed by centrifugation and retention of the supernatant. The supernatant was further treated with 0.5 % deoxycholic acid and filtered through 5 µm and 0.8 µm syringe filters before proceeding with the rAAV particle concentration. The cell lysate was bound on a heparin-agarose column (Sigma, UK) that had been equilibrated with 10 ml PBS-MK. After the loading of the virus, the column was washed with 10 ml PBS-MK + 0.1 M NaCl and the rAAV particles were eluted in 6 ml PBS-MK + 0.4 M NaCl (the first two ml were discarded). The eluate was concentrated using Centricon 100 columns (Millipore, USA) by centrifugation at 5000 xg for 25 min followed by a wash with PBS-MK. The Centricon columns were then turned upside down and the concentrated rAAV was spun into a collection tube. The average yield of the rAAV2/2 production protocol is approximately 100 µl of concentrated virus (10^{12} viral particles/ml) per 10 plates of transfected BHK cells. The virus was then aliquoted and frozen at -80°C.

2.4.3 Production and purification of rAAV2/8

Production of recombinant AAV2/8 (rAAV2/8) was carried out by co-transfection of three plasmids in 293T cells. In addition to the pD10-based plasmids, pAAV8 (that carries the *rep* and *cap* genes) and pHGTI (that carries helper accessory genes) plasmids were used in a $CaCl_2$-based transfection. 293T cells were seeded into 150 mm plates at a concentration of 10^6 cells/plate. The plates were incubated overnight so that they reach 70 % confluency the following day. The transfection medium was prepared using the following amounts:

For 10 plates:

pAAV8	→	100 µg
pHGTI	→	30 µg
pD10-RNAi	→	100 µg
$CaCl_2$ 2.5M	→	1.25 ml
dH_2O	→	up to 12.5 ml

The same amount in volume (i.e. 12.5 ml) of 2x HBS buffer was added dropwise to the plasmid solution followed by 25 ml of full DMEM medium. Five ml of the transfection solution was then added to the 293T plates without removing the old medium and the cells were incubated for 36 hrs before scraping and harvesting in TD buffer. The freeze-thaw cycles, benzonase and deoxycholic acid treatments were carried out in the same way as performed in the rAAV2/2 production. The lysate was then filtered through a 0.45 µm syringe filter before proceeding with the exchange chromatography purification using an ÄKTA^{TM}prime FPLC apparatus (Amersham, UK) to bind the rAAV2/8 particles on an anionic sephacryl S300 and a POROS 50HQ column. The FPLC purification was carried out in Dr Amit Nathwani's laboratory (UCL) with the assistance of Dr Jenny McIntosh. FPLC purification is carried out by binding the viral lysate first to the anionic column followed by the POROS 50HQ column and eluted using an increasing salt gradient (Buffer A and B; see Buffers & solutions). Approximately 15 ml of eluate are produced by 10 plates which are subsequently concentrated in Centricon 100 columns to a final volume of approximately 200 µl. The virus was then aliquoted and frozen at -80°C.

2.4.4 Genomic titration by dot-blot analysis

One and 5 µl samples from the rAAV preparations were treated with 100 µg proteinase K (Promega, UK) in 100 µl 2 x proteinase K buffer and 100 µl dH_2O. After 1 hr incubation at 37°C, viral DNA was precipitated by adding

1/10 volume of 3M sodium acetate, 40 µg glycogen (Sigma, UK) and 2.5 volumes of 96 % ethanol and left at -80°C for 30 min. DNA was pelleted by centrifugation at 5000 xg for 30 min at 4°C. Each DNA pellet was washed with 200 µl of 70 % ethanol, air dried and resuspended in 200 µl 0.4 M NaOH + 10 mM EDTA solution.

A dilution series of plasmid DNA (usually the pD10-based plasmid) ranging from 10^{12} to 10^{7} molecules was used to produce a standard ladder. The samples were prepared with 0.4 M NaOH + 10 mM EDTA solution in a total volume of 200 µl. The rAAV DNA and standard ladder samples were denatured at 100°C for 2 min and then cooled for 2 min on ice. The samples were then applied onto a pre-wet 0.45 µm Hybond^{TM}-N+ membrane (Amersham, UK) in a Dot-blot apparatus (Bio-Rad, UK). Each well of the manifold that would have a sample loaded onto it was pre-washed with 0.2 ml of dH_2O and vacuum dried before sample loading. After the DNA samples were bound onto the membrane, 0.2 ml of 0.4 M NaOH and 10 mM EDTA was added to each well and was subsequently vacuum dried. The membrane was then moistened with dH_2O, placed in a hybridisation tube and heated to 65°C in a hybridisation oven to cross-link the DNA on the membrane. A hybridisation bottle was pre-heated in a hybridisation rotisserie oven at 65°C, together with Church buffer. The blot membrane was transferred to the pre-heated bottle between hybridisation mesh and pre-hybridised for 30 min.

Meanwhile the probe DNA (CBA promoter fragment) was excised from the plasmid and isolated from an agarose gel. The extracted probe DNA was denatured at 95°C for 5 min followed by incubation on ice for 2 min. Biotinylation of the probe DNA was carried out using the NeoBlot Phototope Kit (New England Biolabs Ltd., UK) according to the manufacturer's instructions. In brief, a reaction with a total volume of 50 µl was performed by adding to the probe DNA 5x Labelling mix (containing random octamer primers), 10µM dNTP mix (containing a biotinylated dATP) and 1 µl Klenow polymerase. The probe was incubated at 37°C for 1 hr followed by the addition of 5 µl 0.2 M EDTA, pH 8 to terminate the biotinylation reaction. DNA precipitation was carried out by incubating the probe at -20°C for 30 min in

the presence of 3 M NaOAc (5 µl) and 100 % ethanol (150 µl). After centrifugation at 5000 xg for 10 min at 4°C, the DNA pellet was washed with 70 % ethanol and precipitated again. The final probe DNA pellet was resuspended in 20 µl dH_2O and stored at -20°C.

Five µl of the probe were added to the pre-hybridised membrane and incubated at 65°C overnight to ensure hybridisation to the viral samples and the standard ladder. The blot was then washed three times with 50 ml 33 mM sodium phosphate buffer, pH 8 for 5 min per wash. Block solution was then added onto the blot ensuring that it is covered and it was incubated on a shaking platform at room temperature for 1 hr. Streptavidin incubation was carried out by diluting the supplied stock 1:1000 in Block solution and applying it onto the drained blot at room temperature for 20 min. Two rounds of washing in Wash solution I for 5 min were followed by a 5 min room temperature incubation with pre-diluted (1:1000 in Block solution) biotin-conjugated alkaline phosphatase. Two rounds of washing in Wash solution II were followed by the addition of the CDP-Star reagent directly onto the blot covering the area that with blotted samples. The blot was immediately wrapped in cling film and exposed to an X-ray film for a variable amount of time (usually 3 min but depends on the strength of the signals). Viral titre determination was then possible by comparison between the viral samples and the standard ladder.

2.5 Lentiviral vectors

2.5.1 RNAi Constructs

The RNAi hairpin cassettes shCON, shGFP, miRGFP, shRDS5, shRDS6, shZO-1 and shZONAB were cloned into the pHR'SIN third generation lentiviral backbone using *AscI* and *Acc65I* restriction sites. The SFFV promoter and WPRE were removed before cloning the RNAi cassette in. The rest of the backbone sequence is identical to the construct pHR'SIN-cPPT-CEW as described by Bainbridge *et al.* [122]. The resulting plasmids were verified by sequencing (MWG Biotech, UK) and lentivirus particles were made for each hairpin cassette.

2.5.2 Peripherin-2 or ZONAB construct

The *peripherin-2* or *ZONAB* cDNA was cloned into the pENTR® vector and the Gateway® cloning kit was used to make LNT.SFFV.RDS or LNT.SFFV.ZONAB, respectively. The mutated *peripherin-2* cDNA (dRDS) (see 2.2.6) was cloned into the pENTR/D-TOPO® vector. Likewise, LNT.SFFV.dRDS was made using the Gateway® cloning kit.

2.5.3 Production of recombinant lentivirus

For the production of recombinant lentivirus, 293T cells were seeded the day before in 175 cm^2 flasks so that the cells are 80-90 % confluent prior to transfection (30-40x10^6 cells per flask). The cells were transfected with 60 µg of the lentiviral recombinant construct per flask in addition to the lentivirus helper constructs pMD.G (21 µg) and the packaging plasmid p8.91 (39 µg) using the following protocol. The aforementioned plasmid amounts were added to 6 ml Opti-MEM®. In a separate tube, 1 µl of a 10 mM stock of

polyethylenimine (PEI, Sigma, UK) was also added to 6 ml of Opti-MEM®. DNA and PEI solutions were mixed 1:1 and left at room temperature for 20 min. The cells were washed in Opti-MEM® and then 12 ml of the PEI and DNA complexes were added to each flask. The cells were incubated at 37°C, 5 % CO_2 for 4 hr. The medium was then replaced with complete DMEM (25 ml/plate). Twenty-four hours after transfection the medium was removed and replaced with fresh medium (15 ml per plate). The virus was harvested the following day by centrifugation of the harvested medium at 2500 rpm for 10 min and then filtered through a 0.45 µm filter. The filtered medium was transferred to polyallomer ultra-centrifuge tubes (11.5 ml/tube for TH641 rotor or 33 ml/tube for Surespin rotor) and were ultra-centrifuged at 4°C, for 2 hr at 23,000 rpm (TH641 rotor) or 22,000 rpm (Surespin rotor). The supernatant was decanted off and the tubes maintained upside down on tissue paper to drain the remaining supernatant. The last drops around the rim were dried with paper. Then, 50 µl (TH641 rotor tubes) or 125 µl (Surespin rotor tubes) of DMEM without serum were added per tube and pipetted ten times. Parafilm was placed over the top and the tubes were left on ice for 1 hr.

The medium were then pipetted another 10 times to resuspend the virus and were transferred to an eppendorf. The average yield of the lentivirus production protocol is approximately 500 µl of concentrated virus (10^9 viral particles/ml) per 10 plates of transfected 293T cells. The virus was then centrifuged for 10 min at 4000 rpm to remove cell debris, aliquoted and stored at -80°C.

2.6 Quantification of Expression

2.6.1 Total RNA isolation

Cell pellets (10^5 cells), FACS sorted cells (10^4 cells) or whole retinas (quick frozen in liquid N_2) were resuspended in 500 ml TRI-BD® reagent (Sigma, UK). Vigorous resuspension with a pipette (or a homogeniser) is essential to ensure breaking down of the cell wall. When the solution was homogenous, 200 µl chloroform were added and the samples were mixed by inversion. Straight after, the samples were centrifuged at 5000 xg for 15 min at 4°C. The clear top phase (contains RNA) was removed to another tube and the organic phases were kept for protein isolation (see 2.6.3). Equal amount of isopropanol was added to the clear phase and the samples were frozen for a minimum of 2 hr at -80°C. Overnight incubation at -20°C is favourable, however, because it increases the amount of RNA precipitation. Then, the samples were spun at 5000 xg for 10 min at 4°C. The supernatant was carefully decanted without disturbing the pellet. One ml of ethanol was added and the RNA pellets were spun at 5000 xg for 5 min at 4°C. The ethanol was removed and the samples were left to air dry for 5 min at room temperature. Each pellet was resuspended in 20 µl dH_2O. Alternatively, the RNeasy Mini Kit (QIAGEN Ltd., UK) was used for RNA extraction of cell pellets or laser dissected cells (approximately 100 cells dissected using ZEISS PALM RoboMover Axiovert 200) according to the manufacturer's instructions. The RNA concentration was measured using a NanoDrop® ND-1000 spectrophotometer (LabTech Int., UK). Total RNA was stored in -80°C.

2.6.2 Generation of cDNA & Relative quantification

For cDNA generation the QuantiTect® Reverse Transcription Kit (QIAGEN Ltd., UK) was used according to the manufacturer's instructions. Briefly, the RNA samples were thawed on ice and up to 12 µl (or up to 1 µg) were added

to 2 µl of gDNA Wipeout Buffer. The reaction was made up to 14 µl with water and incubated at 42°C for 2 min. In a separate tube, 1 µl of Quantiscript Reverse Transcriptase, 4 µl of Quantiscript RT Buffer and 1 µl of RT Primer mix (containing random octamers and dT nucleotide mix) were mixed before adding them to the template RNA. The reaction tube (20 µl final volume) was incubated at 42°C for 1 hr to enable reverse transcription, followed by a 3 min incubation at 95°C to inactivate the Quantiscript Reverse Transcriptase. The efficiency of the reaction provides a 1:1 conversion ratio of RNA:cDNA, hence up to 1 µg of cDNA was made per sample. Total cDNA was stored in -20°C.

Fifty ng (or 1 µl approximately) of total cDNA from each sample, was loaded onto a 96 well-plate with 2x FastStart TaqMan® Probe Mastermix (ROX) (Roche, UK), forward and reverse primers for amplification of gene of interest (Final concentration: 900 nM each), appropriate hydrolysis probe that binds the amplified area (Final concentration: 250 nM; Roche, UK), ROX reference dye (Final concentration: 400 nM; Roche, UK) and dH_2O to make the final reaction volume up to 50 µl. The amount of cDNA template used in each reaction ranged from 5-500 ng with 50 ng being the usual loading amount. Quantitative real-time PCR was run on an ABI Prism 7900HT Fast Real-time Sequence Detection System (Applied Biosystems, UK) and the manufacturer's software (SDS 2.2.2) was used to obtain Ct values for the reactions. The relative expression between comparable samples in relation to the expression of the genes of interest was calculated through the formula: $2^{-\Delta\Delta Ct}$.

2.6.3 Total Protein isolation

Cell pellets of 10^5 cells were resuspended vigorously with a pipette in 25 µl of PBS and 25 µl of 2x Laemni buffer. The organic phases from chloroform treatment (see 2.6.1) were precipitated using 150 µl of 100 % ethanol. The samples were mixed by inversion and incubated at room temperature for 3

min. Centrifugation was carried out at 4000 xg for 5 min at 4°C. The supernatant was transferred to a new tube and 3 V acetone were added. The samples were mixed and incubated at room temperature for 10 min and spun at 5000 xg for 10 min at 4°C and the pellet was washed with 70 % ethanol. The samples were then spun at 5000 xg for 5 min and the pellet was resuspended in 25 µl PBS and 25 µl 2x Laemni buffer. The protein concentration was measured using a NanoDrop® ND-1000 spectrophotometer (LabTech Int., UK). Total protein samples were stored in -20°C.

2.6.4 Western Blot

Polyacryramide gels were made as two discontinuous gels, a 12 % separating and a 4 % stacking gel. Eight µg of each sample were made up to 15 µl with 1x Laemni buffer and bromophenol blue was added to 0.05 % concentration. The samples were boiled for 5 min and loaded on the gel together with a pre-stained molecular weight marker (Bio-Rad, UK). The gel was run in Running buffer until bromophenol blue run out of the gel (200 V for 50 min). The glass plates were separated and the stacking gel was removed. The separating gel was marked (cut at corner) and equilibrated in Transfer buffer for 20 min. Immobilon P membrane (Amersham, UK) was cut at the size of the gel and put in methanol for 15 sec. Then it was rinsed in water for 2 min, and equilibrated in Transfer buffer for 5 min. The transfer formation was set up on the appropriate apparatus in the order: anode – Immobilon P – Gel – Cathode with 4 pieces of Whatman 3 MM paper in between. It was run for 30 min at 10 V. Immediately after transfer, the membrane was washed with PBS and immersed in methanol for 10 sec. Then it was dried on filter paper and blocked with Blocking solution for 2 hr at 4°C. The membrane was washed 3 times with PBS and the 1° antibody was incubated in Hybridisation solution at appropriate concentration overnight at 4°C. The following day, the membrane was washed 3 times with PBS and the horse-radish peroxidase (HRP)–conjugated 2° antibody was incubated in Hybridisation solution for 50

min at room temperature. The membrane was washed 3 final times with PBS and put on a plate. ECL reagents (Amersham, UK) were mixed and added onto the membrane for 1 min. The western blot was imaged either using a UVIchemi Chemiluminometer (UVItec ltd., UK) or by exposing and developing of photographic film.

2.7 In vivo experiments

2.7.1 Animals

Wild-type C57BL/6 or *GFP*$^{CBA+/+}$ transgenic 6-8 week old female mice were used for this study. All animals were cared for in accordance with the Animal Scientific Procedures Act 1986 and procedures were in accordance with the ARVO Statement for the Use of Animals in Ophthalmic and Vision Research.

2.7.2 Anaesthesia

For intraocular procedures animals were anaesthetised by intraperitoneal injections of Dormitor (1 mg/ml, Pfizer Pharmaceuticals, UK) and ketamine (100 mg/ml, Fort Dodge Animal Health, UK) mixed with sterile water in the ratio 5:3:42. Young adult mice weighing 200 g received 0.2 ml of the anaesthetic solution. After treatment (see 2.7.3), 1 % Chloramphenicol (FDC International ltd., UK) was carefully applied topically on the cornea. To reverse the anaesthesia 0.2 ml of Antiseden (0.10 mg/ml, Pfizer Pharmaceuticals, UK) was injected intraperitoneally and the mice were placed into an oxygenated chamber until they regained consciousness.

2.7.3 Subretinal injections

Surgery was performed under direct retinoscopy through an operating microscope. The pupils were dilated with 1 % Tropicamide (Chauvin Pharmaceuticals, UK) topically administered. The eye was protruded by gentle pressure on either side of the eye and held in position by holding a section of the conjunctiva and extraocular muscle with a pair of forceps. The fundus was visualised using a contact lens system consisting of a drop of a coupling medium solution on the cornea (Viscotears, Novartis

Pharmaceuticals, UK) and a cover slip. The tip of a 1.5 cm, 34-gauge hypodermic needle mounted on a 5 µl Hamilton syringe (Hamilton, Switzerland) was guided underneath the cover slip to the sclera of the eye and then inserted tangentially through it, causing a self-sealing wound tunnel. The needle tip was brought into focus between the retina and the RPE and 2 µl of virus suspension containing around 10^8-10^9 particles of rAAV or 10^5-10^6 particles of lentivirus were injected to produce a bullous retinal detachment in the superior hemisphere. Where necessary, a second injection was performed subsequently to produce a similar detachment in the inferior hemisphere. Where appropriate, 0.2 ml of a 100 ng/ml 5-bromo-2-deoxyuridine solution (BrdU; Sigma, UK) was injected intraperitoneally following the subretinal vector administration.

2.7.4 Fluorescein angiography

Five minutes after the induction of anaesthesia, 0.2 ml of 2 % fluorescein sodium diluted in dH_2O was administered by intraperitoneal injection. A Kowa Genesis small animal fundus camera equipped with appropriate excitation and barrier filters was used to obtain fluorescein angiograms at early (90 s after fluorescein injection) and late (7 min) phases of dye transit. At the early phase, the retinal vasculature is clearly defined by the intravascular fluorescein dye. At the late phase, any extravascular leakage or RPE loss is evident as patches of topical hyperfluorescence. Both the superior and inferior hemispheres were individually photographed in rapid succession (within 15 s). The contralateral eye was then immediately photographed.

2.8 Histological Analysis

2.8.1 Cryosections

At various time points, treated animals were sacrificed by exposure to carbon dioxide and the eyes were retrieved and immediately immersed in a fixation solution of 4 % PfA for 2 hr. After fixation the eyes were embedded in O.C.T. (R.A. Lamb, E. Sussex, UK) and frozen in isopentane which had been pre-cooled in liquid nitrogen. Specimens were stored at -20°C and 12 µm thick sections were cut using a Bright cryostat. Slides were stored at -20°C.

2.8.1.1 Immunohistochemistry

For immunofluorescence, cryosections were air-dried for 10 min and marked with a hydrophobic marker pen. They were then blocked for 1 hr with a TBS-T solution containing 1 % BSA, Triton-X (0.5 %), and 5 % serum of the species the 2° antibody was raised in. The 1° antibody was then added at the appropriate concentration and left overnight at 4°C. After washing six times with TBS-T, sections were incubated with the 2° antibody diluted at the appropriate concentration in blocking solution for 2 hr at room temperature. The slides were then washed six times with TBS-T. In order to visualise cell nuclei, sections were usually counterstained with 1:1000 dilution of Hoescht33342 (Sigma, UK) and mounted on mounting medium (DAKO) prior to placing a coverslip on top. Analysis was performed from 30 min afterwards or preferably the following day using confocal (see 2.8.1.2) or fluorescent microscopy before capturing images with a Leica DC 500 digital camera mounted on the microscope. Slides were stored at 4°C.

2.8.1.2 Confocal Imaging

Cryosections were analysed using the 3-laser ZEISS LSM 510UV Confocal Imager and its software was used to capture images at x40 and x60 objective, at various thickness layers (Z-stack) of the section. The images of the Z-stack were either used individually or as projected composite of each other.

2.8.2 Fixation of eyes for semithin and ultrathin sections

At various time points, eyes were retrieved from treated animals and immediately orientated with a nasal stitch. Then eyes were immersion fixed in 3 % glutaraldehyde and 1 % PfA buffered to pH 7.4 with 0.07 M sodium cacodylate-HCl buffer (Karnovsky's; 0.2 M $(CH_3)_2AsO_2Na.3H_2O$ with 0.2 M HCl). After 12 hr the anterior part of the eye was removed by microdissection. The posterior segments were then osmicated for 2.5 hr in a 1 % aqueous solution of osmium tetroxide, followed by a dehydration series through ascending alcohols (50 – 100 %, 10 min per step). After 3 changes of 100 % ethanol, specimens were passed through propylene oxide (3x 10 min) and left overnight in a 50:50 mixture of propylene oxide and araldite. Following a single change to fresh araldite (5 hr with rotation) the specimens were embedded in resin and cured for 48 hr at 60°C.

2.8.3 Semithin Sections

Semithin sections (0.7 µm) were cut using a Leica ultracut S microtome fitted with a diamond knife (Diatome histoknife). Sections were stained with toluidine blue stain (25 ml 2 % hydrated sodium borate, 25 ml 100 % ethanol, 0.5 g toluidine blue, SPI-Chem^{TM}) and slides were mounted with DPX after the sections had dried. Sections were analysed using a Leitz Diaplan microscope for observation and imaged with a Leica DC 500 digital camera.

2.8.4 Ultrathin sections

Ultrathin sections (70 nm) were cut using a Leica ultracut S microtome fitted with a diamond knife for ultrathin sections (Diatome histoknife for ultrathin sections). Sections were taken of treated areas of retinae and collected onto grids. Sections were stained with uranyl acetate for 10 min and lead citrate for 7 min and then washed with dH_2O. After the sections had dried they were analysed by electron microscopy (JEOL 1010 TEM).

2.9 Buffers and Solutions

Blocking solution (for Western blot): 1x PBS, 3 % BSA or non-fat dried milk solution, 0.5 % Tween

Buffer A (for AAV2/8 purification): 5.65 g Bis-Tris propane, 2.42 g Tris up to 1 l with dH_2O, pH 9; filtered through 0.2 µm

Buffer B (for AAV2/8 purification): Buffer A + 175.32 g NaCl; filtered through 0.2 µm

Church Buffer: 21 g of NaH_2PO_4, 48.55 g Na_2HPO_4, 70 g of SDS, 0.5 M EDTA, up to 1 l with dH_2O

HBS (2 x): 16 g NaCl, 0.74 g KCl, 0.2 g $NaH_2PO_4H_2O$, 2 g Dextrose, 10 g HEPES, up to 1 l with dH_2O, pH 7; filtered through 0.2 µm

Laemni buffer (2 x): 125 mM Tris-HCl pH 6.8, 20 % glycerol, 4 % SDS, 10 % 2-mercaptoethanol

LB growth medium: 20 g LB extract (Oxoid Ltd., UK) per litre of dH_2O

PBS (1 x): 85 g NaCl, 4.3 g KH_2PO_4, up to 10 l with dH_2O, pH 7.2

PBS-MK: 1 x PBS, 2.5 mM KCl, 1 mM $MgCl_2$

Proteinase K buffer: 100 mM Tris (pH 7.4), 50 mM EDTA and 0.5 % SDS

Running buffer (for Western blot): 3.3 g Tris, 14.4 g Glycine, 1 g SDS, up to 1 l with dH_2O

Sodium phosphate buffer: 97.1 g Na_2HPO_4, 43.6 g NaH_2PO_4, pH 7.2, up to 1 l with dH_2O

TBE (50 x): 242 g Tris, 57.1 ml Boric Acid, 18.6 g EDTA, up to 1 l with dH_2O

TD Buffer (1 x): 8.2 g NaCl, 0.37 g KCl, 0.12 g K2HPO4, 0.33 g $MgCl_2$, 3 g Tris, up to 1 l with dH_2O, pH 7.5; filtered through 0.2 µm

Transfer buffer (for Western blot): Running buffer + 20 % methanol

3 Virus-mediated RNAi targeting in the retina

3.1 Introduction

In order to achieve efficient and persistent knockdown of a gene of interest in the retina, an shRNA-expressing cassette must be delivered into the target cells. Transduction of certain retinal layers using various viral vectors has proven to be very efficient [93,122,237]. Selective transduction of retinal cell types can also be achieved by capsid pseudotyping of the recombinant AAV vectors used. Tissue specific expression of cassettes in conjunction with capsid pseudotyping can further restrict transgene expression in the desired cell type. Efficient knockdown depends on successful delivery, efficiency of the selected hairpin molecule, as well as on the expression levels of the targeted gene.

In this study, the specificity and stringency of RNAi knockdown was analysed *in vitro* by comparing the silencing effect of the selected shRNA molecule on two different, but highly homologous, GFP transgenes. We also used a GFP transgenic mouse, which constitutively expresses *eGFP* through a CBA promoter, as a model to target endogenous *GFP* expression using viral-mediated RNAi. The high expression levels that a CBA promoter provides, make this model a useful candidate for RNAi experiments since successful downregulation of GFP would indicate the feasibility of silencing highly expressed genes in the retina, such as *rho* or *Prph2*.

3.2 Hairpin expression vectors

The targeting sequence for *eGFP* (siGFP) was kindly provided by Steven Howe (Molecular Immunology unit, Institute of child Health, UCL) after its efficiency was tested synthetically *in vitro* by transfection in HeLa cells stably expressing *eGFP*. A non-targeting control (siCON) sequence was also designed to be tested alongside siGFP in our *in vitro* and *in vivo* experiments (see section 2.2.5; Table 1 for sequences). The siCON target sequence was scanned for homology with murine and human genome databases using the BLAST alignment algorithm (http://blast.ncbi.nlm.nih.gov/Blast.cgi) and no positive hits were returned. However, the siCON molecule was not assessed *in vitro* to investigate whether it incorporates into RISC or whether it elicits any innate immune responses *via* the TLR3 pathway.

3.2.1 mU6pro – RNAi expression vector

In order to make an RNAi expression cassette, a DNA-based template of the siRNA target area needs to be constructed. The main concept behind these short expression cassettes is the transcription of both the sense and antisense strands of the siRNA of interest in one transcript through an RNA polymerase III promoter, like U6 or H1. Upon transcription of the sense and antisense strands separated by an intermediate loop sequence, RNA complementarity causes the single-stranded RNA molecule to fold back onto itself and form an shRNA (Figure 3.1). After export of the shRNA to the cytoplasm, an RNase III enzyme (Dicer; see section 1.4) excises the loop sequence that forms the hairpin giving rise to a mature siRNA duplex.

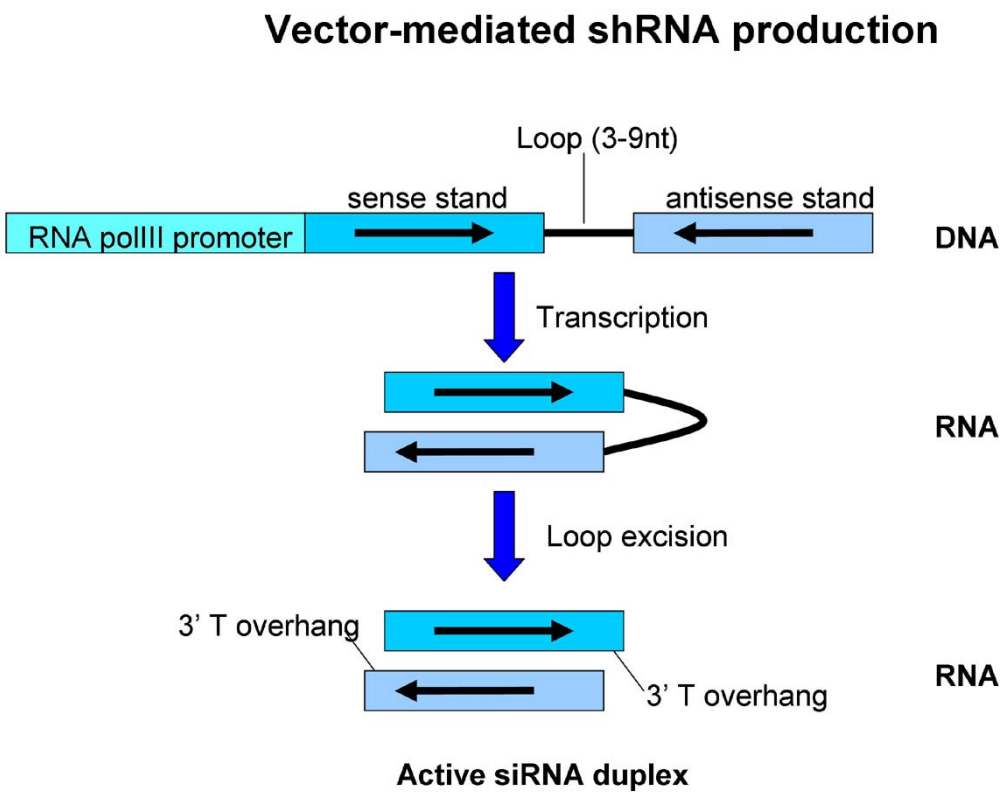

Figure 3.1: Diagram of shRNA production. The U6 promoter-based RNAi cassette transcribes an shRNA molecule in the nucleus. The hairpin is transported to the cytoplasm where it is cleaved by Dicer to produce a mature active siRNA molecule.

The mU6pro vector is an RNAi expression vector employing the polymerase III U6 promoter to transcribe the shRNA of choice [238]. The DNA sequence of the shGFP was cloned downstream of the U6 promoter in the form of annealed oligonucleotides. A subsequent enzyme digestion upstream of the U6 promoter and downstream of the shRNA sequence (AscI/SnaBI) yielded the whole RNAi cassette at a size of around 400 bp (Figure 3.2). This digestion was performed to check the integrity of the cloned cassette, as well as to retrieve the cassette for further cloning into the AAV and lentiviral vector backbones.

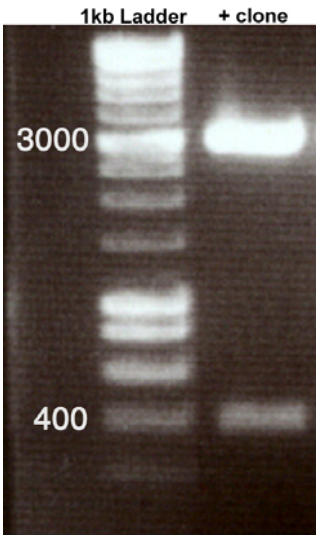

Figure 3.2: Digestion confirming the cloning of shGFP hairpin into the mu6pro plasmid. After ligating the shGFP oligonucleotides downstream of the U6 promoter, the whole shGFP cassette (~400 bp) was excised for further sub-cloning using restriction enzymes AscI that cut upstream of the U6 promoter and SnaBI that cuts downstream of the shGFP hairpin. The 3000 bp band corresponds to the mU6 backbone. The Bioline 1 kb ladder was used to determine the size of the excised fragments. +clone; positive clone.

A positive clone was named mu6.shGFP. The non-targeting control hairpin was cloned in a similar way and the resulting plasmid was named mu6.shCON.

3.2.2 pHR'SIN – lentiviral production vector

After confirming the sequence of each hairpin by sequencing (MWG Biotech, UK, see Chapter 2.2.3), the hairpin cassettes were cloned into the pHR'SIN lentiviral backbone. The pHR'SIN vector contains the 5'- and 3'- LTR sequences from HIV-1 virus together with the central polypurine track (cPPT) fragment from the wild type virus. The 3'LTR of the vector is partially deleted to hinder viral particle replication in the infected host cell. The 3'ΔLTR and the lentiviral production system that is based on a three plasmid co-transfection protocol ensure that the recombinant lentiviral particles are replication incompetent. The successful cloning of either the shGFP or shCON hairpin cassettes into the pHR'SIN backbone was checked by excising the RNAi cassettes after cloning using the restriction sites AscI and XbaI (Figure 3.3).

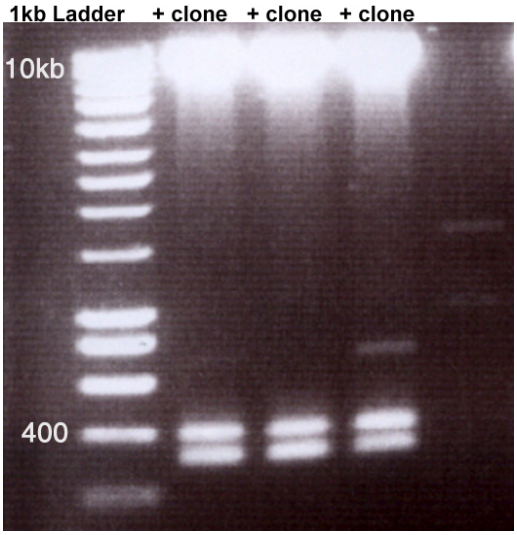

Figure 3.3: Digestion confirming the cloning of shGFP and shCON cassettes into the lentiviral pHR'SIN backbone. Three positive clones are depicted. After restriction digest with AscI and XbaI, the lentiviral backbone (~9 kb), the RNAi cassette (~400 bp) and the 3' LTR (~300 bp) were excised from positive colonies. The Bioline 1 kb ladder was used to determine the size of the excised fragments. +clone; positive clone.

The lentiviral plasmids bearing the RNAi cassette targeting eGFP or the non-targeting control were named pHR'SIN.shGFP and pHR'SIN.shCON, respectively. The integrity of the incorporated RNAi cassettes was checked by sequencing (MWG Biotech, UK, see Chapter 2.2.3).

3.2.3 pD10 – AAV production vector

The relatively small size of the RNAi cassette (400-500 bp) enables the construction of bicistronic vectors in which the RNAi cassette can be placed upstream or downstream of an adjacent RNA polymerase II-based expression cassette. This option allows the co-expression of a reporter gene that will aid in the visualisation and selection of transduced cells. A pre-existing pD10 vector driving the expression of RFP through a CBA promoter (pD10.RFP) was used as the recipient backbone for our RNAi expression cassette. However, since the incorporation of the RNAi cassette was not feasible with the existing restriction sites within the backbone, a polylinker had to be cloned upstream of the CBA-RFP cassette. Five restriction sites were cloned into the pD10 backbone and the resulting plasmid was named

pD10.RFP.poly (Figure 3.4). Polylinker integrity was checked by sequencing (MWG Biotech, UK, see Chapter 2.2.3).

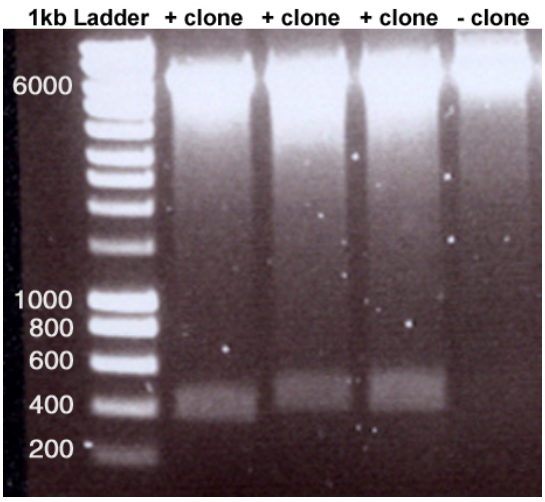

Figure 3.4: Digestion confirming the cloning of polylinker in the pD10.RFP.poly. Three positive (next to ladder) and one negative clone after ligating the designed polylinker with the pD10 backbone. The positive clones exhibited a 400 bp band excised after restriction digest with AscI and SnaBI. The Bioline 1 kb ladder was used to determine the size of the excised fragments. +clone; positive clone. -clone; negative clone.

After further restriction digests to confirm the integrity of all the subcloned fragments (Figure 3.5), AscI and EcoRV were used to digest the pD10.RFP.poly plasmid. Following the ligation of the shGFP expression cassette with AscI and SnaBI overhangs into the pD10 backbone, further restriction enzyme digestion with AscI and PmeI confirmed its successful incorporation and the final rAAV vector plasmid was named pD10.RFP.shGFP (Figure 3.6). Similarly, the shCON expression cassette was cloned into the pD10 backbone using the same restriction sites and the resulting rAAV vector plasmid was named pD10.RFP.shCON. The integrity of the incorporated RNAi cassettes was checked by sequencing (MWG Biotech, UK, see Chapter 2.2.3).

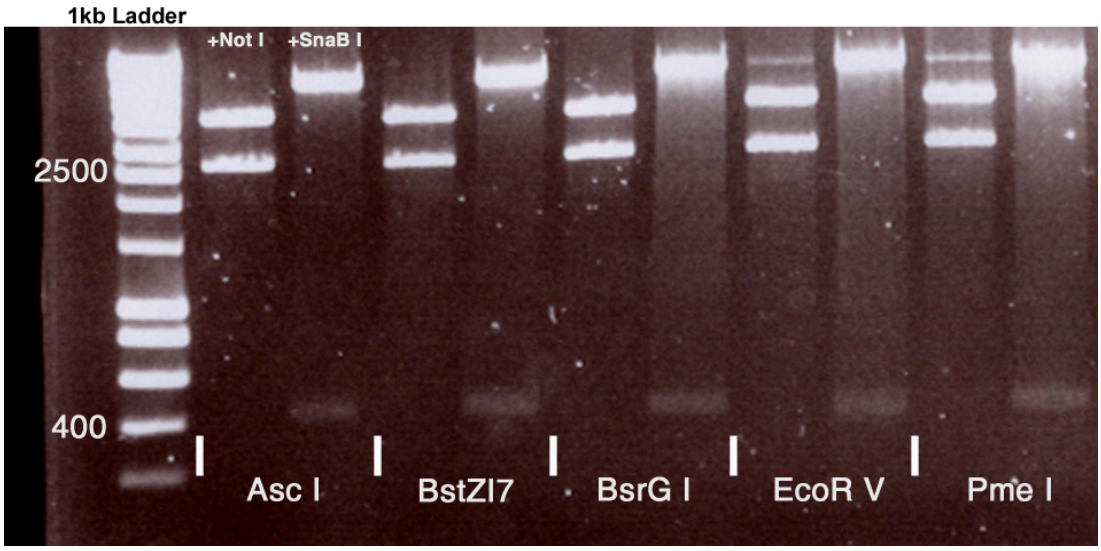

Figure 3.5: pD10 polylinker site integrity. Polylinker incorporation was confirmed by digesting the plasmid with each of the five incorporated sites (AscI, BstZI7, BsrGI, EcoRV and PmeI). The expected sizes for double digests were 3700 bp and 2600 bp after NotI digestion and 6000 bp and 400 bp after SnaBI digestion. The Bioline 1 kb ladder was used to determine the size of the excised fragments.

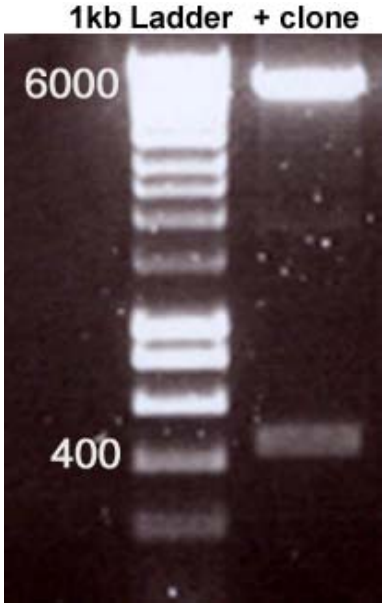

Figure 3.6: Restriction digest to confirm the cloning of the shGFP cassette into the polylinker of pD10. The shGFP cassettes (~400) that had been previously excised from mU6.shGFP using AscI and SnaBI restriction enzymes was cloned into the pD10.RFP.poly plasmid that had been digested with AscI and EcoRV. Upon ligation, both blunt restriction sites on either fragments (SnaBI and EcoRV) are destroyed. Confirmation of the cloning was carried out by digestion of pD10.RFP.shGFP with AscI and PmeI which results in a fragment of ~450 bp. The Bioline 1 kb ladder was used to determine the size of the excised fragments. +clone; positive clone.

3.3 Lentiviral-mediated GFP silencing

3.3.1 In vitro eGFP silencing and stringency of knockdown

In order to test the *eGFP* silencing efficiency of LNT.shGFP *in vitro*, a cell line stably expressing *eGFP* was constructed using a different lentivirus that drives the expression of *eGFP* from an SFFV promoter (LNT.eGFP). Human embryonic kidney fibroblasts (293T) were infected at a limiting multiplicity of infection (MOI) using a ratio of infectious virus particles to cells <1 (see section 2.5.2). The use of limiting MOI makes it likely that the infected cells will be transduced by a single viral particle and hence produce eGFP through a single transgene cassette. A single *eGFP* cassette should be capable of producing enough eGFP to test the efficiency of the shGFP hairpins. The transduced cells were FACS sorted and single $eGFP^+$ cells were propagated to obtain clonal cell populations to ensure that we obtained a cell line that would express eGFP homogeneously (293T/$eGFP^+$). These cells were subsequently transduced with LNT.shGFP at increasing MOIs (1, 5, 10 and 20) and FACS analysed one week after transduction to measure the reduction in the mean fluorescence intensity (MFI) caused by the silencing of the host eGFP expression cassette by shGFP (Figure 3.7).

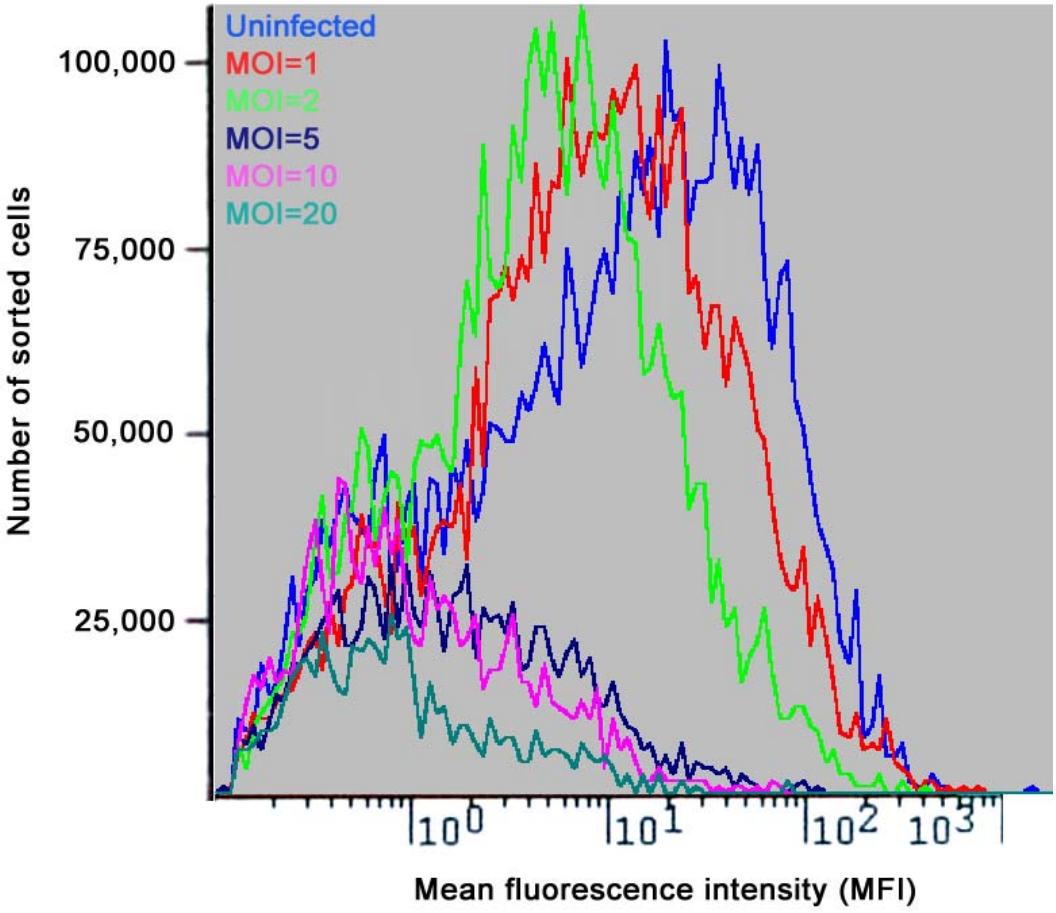

Figure 3.7: FACS plot overlay of GFP expression. Representative overlay of mean fluorescence intensity (MFI) of 293T/GFP$^+$ cells after transduction with LNT.shGFP vectors. GFP expression was gradually reduced in the transduced cells as MOI values increased.

The expression of eGFP in the transduced cells was reduced gradually as the number of virus particles increased. Untransduced 293T/eGFP$^+$ cells were used as a control and their mean fluorescence intensity (MFI) exceeded that of transduced cells (Figure 3.7; blue line). Increasing the MOI, effectively increases the number of shGFP cassettes introduced into the host cells leading to a progressively more potent knockdown of eGFP. 293T/eGFP$^+$ cells already express high levels of an exogenous protein and their viability levels tend to decrease when transduced with a large number of viral particles. This is represented by the reduction in cell numbers for the samples transduced with an MOI higher than 5 (Figure 3.7; MOI=5, 10 or 20). Whilst figure 3.7 depicts a representative overlay of samples, the reduction in

cell numbers after lentiviral infection at an MOI above 5 was observed in all tested samples (n=3). For statistical interpretation see figure 3.8.

The next step of *in vitro* testing concentrated on the stringency of the targeting LNT.shGFP vector. In order to test the stringency of the shGFP hairpin, an additional stable cell line expressing humanised recombinant GFP (hrGFP) was constructed in a similar way to the previous cell line. The resulting cell line was named 293T/hrGFP^{+}. hrGFP is a green fluorescent protein that has been engineered so that it utilises more abundant human tRNAs. Even though eGFP and hrGFP are not derived from the same species, they have approximately 30 % sequence homology.

Both LNT.shGFP and LNT.shCON were packaged into recombinant vectors (see section 2.5.3) and used to transduce the 293T/eGFP^{+} and 293T/hrGFP^{+} cell lines at increasing MOIs. The MFI of each transduced sample was analysed by FACS (Figure 3.8).

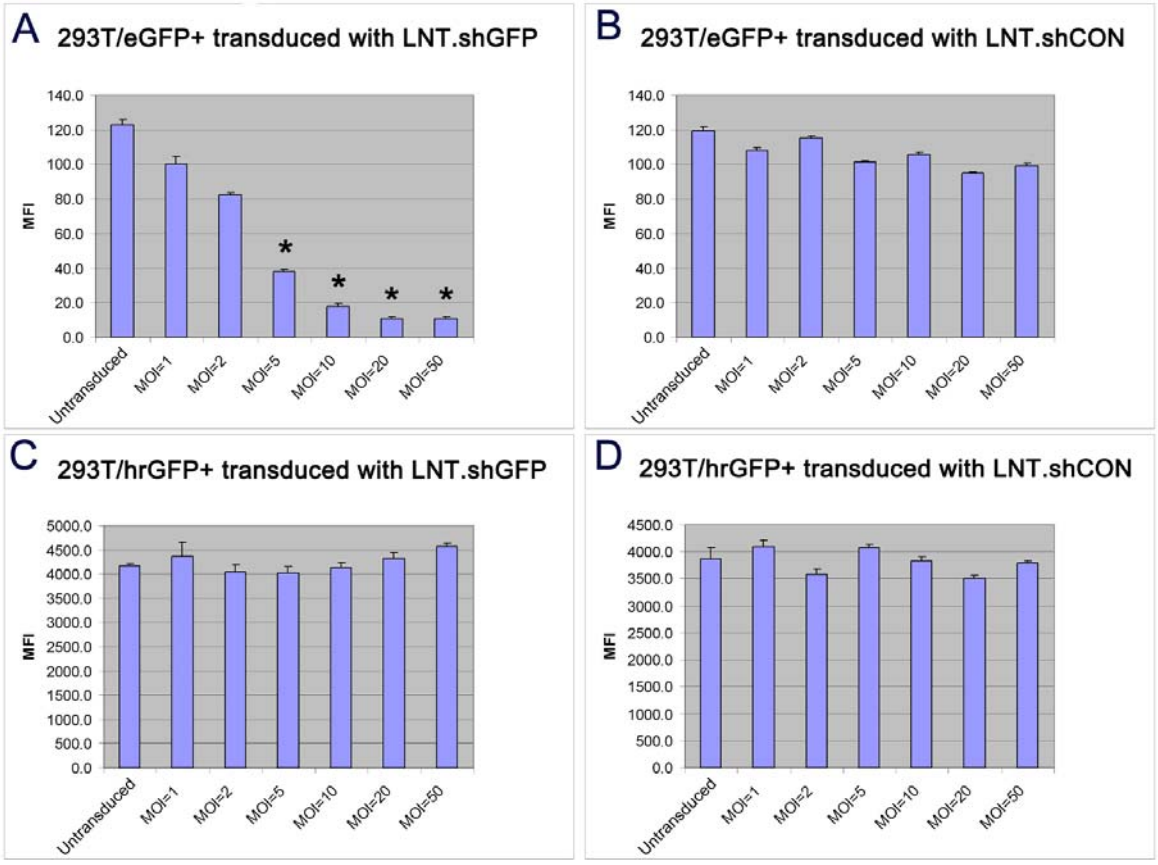

E

```
665         675         685         695         705         715
hrGFP         ACGAGACCGC CATCGCCCAG CTGACCAGCC TGGGCAAGCC CCTGGGCAGC CTGCACGAGT
siGFP         ---------- ----GTTCAT CTG--CACCA CCGGCAAGC- ---------- ----------
```

Figure 3.8: Graphical representation of GFP expression in 293T cells after transduction with eGFP and control targeting lentiviruses. (A) Reduction of eGFP in 293T/eGFP^{+} cells after transduction with the LNT.shGFP at various MOIs. **(B)** Transduction of the same cell line with LNT.shCON did not result in eGFP reduction. **(C, D)** GFP expression in 293T cells expressing hrGFP was not reduced after transduction of LNT.shGFP or LNT.shCON. **(E)** The specificity of the LNT.shGFP towards eGFP was high since there was no reduction in hrGFP levels even though there was partial siGFP:hrGFP homology with up to 7 consecutive nucleotides. Bold nucleotides = mismatches. ***P***<0.001 (Student's *t*-test; n=3, where 3 is the number of infections performed per virus type).

Transduction of 293T/eGFP$^+$ cells with LNT.shGFP resulted in a decrease in MFI (Figure 3.8A) whereas infection with LNT.shCON did not result in any significant eGFP knockdown (Figure 3.8B). Neither LNT.shGFP nor LNT.shCON resulted in a reduction of the MFI in the 293T/hrGFP$^+$ cells (Figure 3.8C,D). Even though the decrease in MFI in figure 3.8A was highly significant (***P***<0.001) for MOIs=5,10 and 20, the reduction in cell numbers at these MOIs should be addressed in the future in order to avoid similar increase in cell death when delivering *in vivo*. Using hrGFP instead of eGFP might improve cell viability as hrGFP is much better tolerated by 293T cells.

Although hrGFP is an engineered GFP protein that allows more efficient production in human derived cells (note MFI differences between graphs in Figure 3.8), it has 30 % homology to the *eGFP* transgene. Therefore, complementarity levels between the *hrGFP* transcript and the target area of shGFP were assessed using BLAST (Figure 3.8E). Even though at the 3'-end of the target area there were seven consecutive nucleotides that were homologous between hrGFP and shGFP, the silencing potential of the hairpin was abolished due to the mismatching in the first half of the target area. This experiment demonstrates how target:hairpin mismatching does not just affect the efficiency of the silencing, but completely abolishes it.

3.3.2 Silencing of eGFP in the RPE in vivo

Titre matched preparations of LNT.shGFP and LNT.shCON (10^8 v.p./ ml), were injected in the subretinal space of young adult mice expressing eGFP throughout the retina. The *C57BL/6*$^{GFP+/GFP+}$animals carry an eGFP transgene driven by a CBA promoter. Vectors were injected subretinally and the effect of vector-mediated *eGFP* silencing was assessed two weeks after administration. Injected eyes were collected, fixed in paraformaldehyde and prepared for cryosectioning through the treated area. GFP expression in the RPE was analysed in eyes injected with either LNT.shGFP or LNT.shCON.

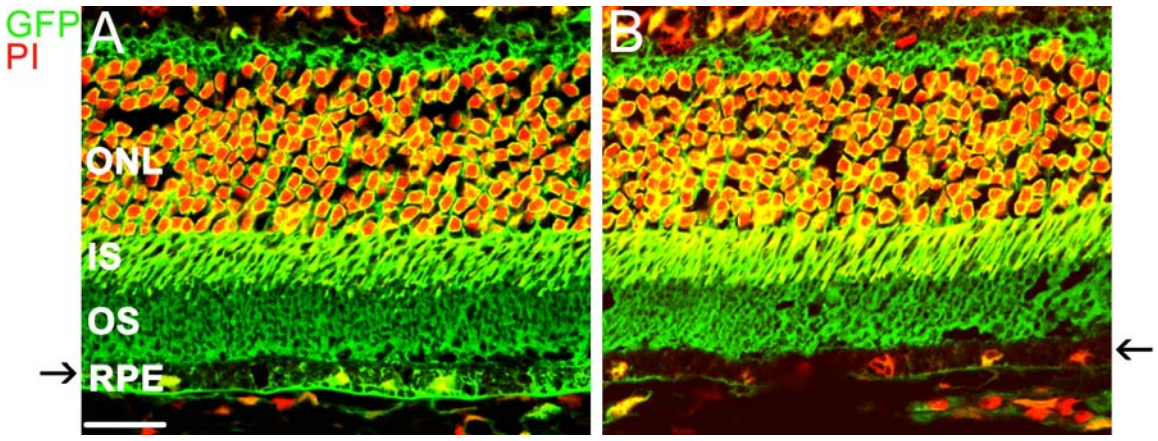

Figure 3.9: *In vivo* silencing of eGFP after subretinal injection of LNT.shGFP in GFP transgenic mice. Confocal imaging of fixed cryosections indicating red nuclear stain (PI) and GFP expression. **(A)** Eyes injected with LNT.shCON presented homogenous GFP expression throughout the retina. **(B)** LNT.shGFP injected eyes showed a marked decrease in RPE-specific GFP expression 14 days p.i. Black arrows indicate the RPE. Size bar; 20 µm. n=4.

In eyes that received LNT.shCON (Figure 3.9A; n=4) there was homogeneous *GFP* expression throughout the retina driven by the constitutive CBA promoter of the integrated *eGFP* expression cassette. No reduction in GFP levels were detected in the RPE within the treated areas. In eyes that received LNT.shGFP (Figure 3.9B; n=4) GFP expression was retained in all the retinal layers apart from the RPE in the area of retinal detachment. Within this area, the RPE was almost devoid of GFP indicating that the lentivirally-delivered shGFP expression cassette was silencing endogenous *GFP* expression. Any residual GFP localisation around the cell membranes could be accounted for by the remaining levels of endogenous expression not silenced by the RNAi cassette as well as GFP molecules that had entered the RPE through outer segment phagocytosis. In addition, the fact that no other retinal layer showed reduced GFP expression within the treated area was consistent with the specificity of the lentiviral vector. The robust and RPE-specific silencing of GFP following delivery of LNT.shGFP indicated that lentiviral vectors can accommodate RNAi cassettes and

efficiently deliver them to the RPE for the silencing of highly expressed endogenous genes.

3.4 AAV-mediated shGFP expression in vivo

After testing the efficiency of GFP knockdown *via* lentiviral-mediated delivery of shGFP, the efficiency of gene silencing was assessed in the context of an AAV vector. Since AAV is the most effective vector for transduction of photoreceptor cells, the successful accommodation of RNAi cassettes in rAAV vectors is essential for future RNAi applications to silence dominant mutations in photoreceptor-specific genes. We chose to test an AAV2/8 platform because of the particularly efficient transduction of photoreceptors using this serotype (see section 1.4.2.2.3).

The targeting plasmids pD10.RFP.shGFP and pD10.RFP.shCON were used to make AAV2/8 preparations (see section 2.4.3) and both viral preparations were titre matched prior to use. In contrast to lentiviral vectors, AAV2/8 could not be tested *in vitro* in human or murine cell lines as infection of cells in culture with this serotype is very inefficient. Whereas low transduction efficiency when using AAV2/2 can be overcome with adenoviral super-infection, in the case of AAV2/8 super-infection does not improve the transduction rate. Therefore, the resulting viral preparations, AAV8.RFP.shGFP and AAV8.RFP.shCON, were tested *in vivo* to assess GFP knockdown in the photoreceptor cell layer.

Two µl of the titre matched AAV2/8 preparations ($5x10^{11}$ v.g./ml), AAV8.RFP.shGFP and AAV8.RFP.shCON, were injected in the subretinal space of *C57BL/6*$^{GFP+/GFP+}$ young adult mice. Vectors were subretinally injected and the effect of AAV-mediated *eGFP* silencing was assessed five weeks after administration. Injected eyes were collected, fixed in paraformaldehyde and prepared for cryosectioning through the treated area. GFP expression in the photoreceptors was analysed in eyes injected with either AAV8.RFP.shGFP or AAV8.RFP.shCON.

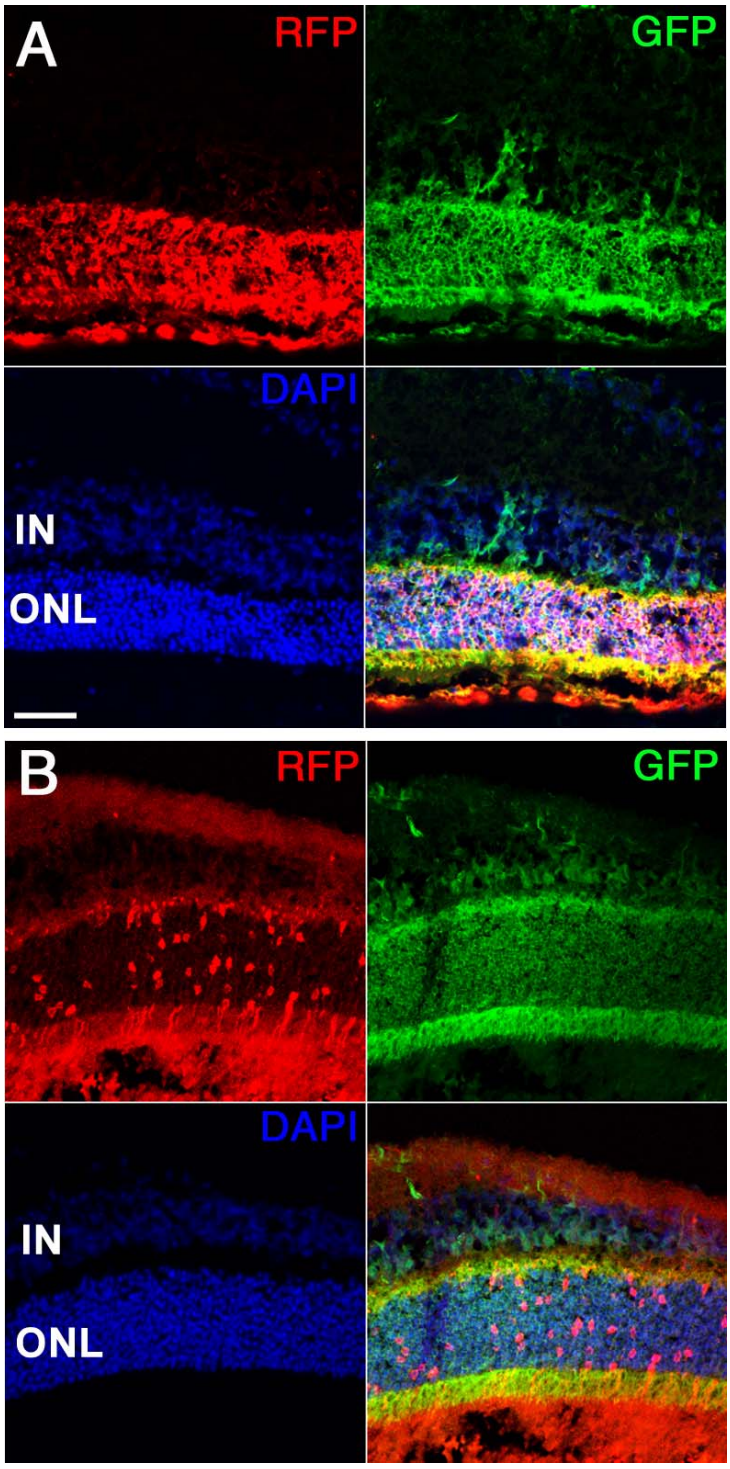

Figure 3.10: ***In vivo*** **transduction efficiency after subretinal injection of AAV8.RFP.shCON or AAV8.RFP.shGFP in GFP transgenic mice.** Confocal imaging of fixed cryosections with DAPI nuclear stain (blue) RFP (red) and GFP expression (green). **(A)** Eyes that received AAV8.RFP.shCON (n=3) had homogenous GFP expression throughout the retina and within the treated area as indicated by the co-expression of RFP. **(B)** In AAV8.RFP.shGFP (n=4) injected eyes there was poor transduction efficiency of photoreceptors that was evident by the relatively low number of cells expressing RFP. Size bar; 20 µm.

Both viruses were engineered to expresse RFP through a CBA promoter in order to visualise the transduced photoreceptors. The control virus AAV8.RFP.shCON resulted in high transduction efficiency within the treated area with the majority of the ONL transduced (Figure 3.10A; n=3). As expected, GFP silencing was not observed in transduced cells after transcription of the shCON hairpin. The AAV8.RFP.shGFP virus preparation did not efficiently transduce photoreceptor cells (Figure 3.10B; n=4). Even though the titre of both vectors was equivalent ($5x10^{11}$ v.g./ml), the infectious capacity of AAV8.RFP.shGFP appeared to be many times less than that of AAV8.RFP.shCON. After thoroughly sectioning all the treated eyes (n=4) it was confirmed that the failure to identify treated areas with equivalent transduction efficiency was not due to ascertainment bias but instead failure to transduce photoreceptors with the same efficiency.

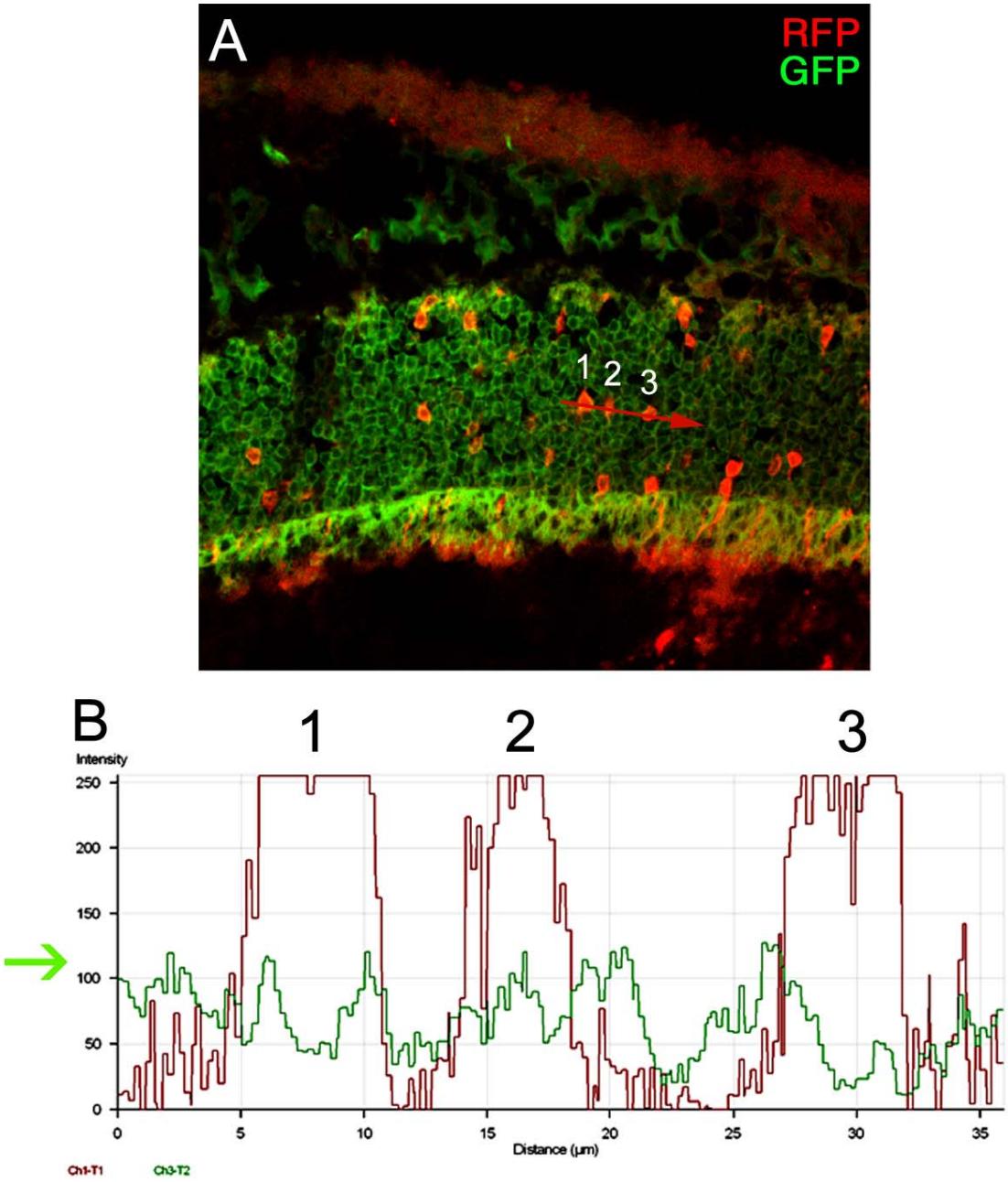

Figure 3.11: Fluorescence profile of transduced photoreceptors after *in vivo* subretinal delivery of AAV8.RFP.shGFP. Confocal image of a fixed cryosection showing RFP (red) and GFP expression (green) and its fluorescence intensity plot. **(A)** An area with RFP-expressing photoreceptors from an AAV8.RFP.shGFP injected eye was selected and a sample area (indicated by red arrow) was selected to analyse the GFP and RFP fluorescence patterns of three RFP^+ photoreceptors. **(B)** The fluorescence analysis indicated that although the selected cells expressed RFP at high levels, the GFP intensity did not fall below basal levels found in adjacent untransduced photoreceptors (green arrow) and hence there was no GFP knockdown taking place within those cells. Either the RNAi cassette was not strong enough to silence GFP or its integrity had been compromised during virus production.

Since the transduction efficiency of AAV8.RFP.shGFP was low, it was not possible to easily visualise GFP downregulation in the few transduced cells because of the high expression levels of GFP from adjacent untransduced cells. In addition, the number of cells expressing RFP was so low that it would not be possible to FACS sort an amount adequate enough to proceed to RNA and protein analysis. Therefore, a fluorescence profile was prepared for selected RFP^+ cells in order to compare the intracellular levels of GFP and RFP (Figure 3.11). Although this technique does not account for all transduced cells, as FACS sorting would do, it does give a detailed analysis of fluorescence for each analysed cell. An area with transduced photoreceptors was selected and the fluorescence measurements were taken from an area indicated by a red arrow set to include three adjacent transduced cells (Figure 3.11A). The fluorescence profile was generated by measuring the relative fluorescence of both GFP and RFP alongside the area of the sampling red arrow. The end result is presented as a plot of fluorescence over absolute length of the selected area (Figure 3.11B). The intracellular green fluorescence measurements could be correlated with the three spikes in RFP expression that corresponded to the three transduced photoreceptors. Extracellular red fluorescence measurements rapidly decreased to background levels as would be expected. The green fluorescence profile fluctuated slightly within cells corresponding to higher GFP concentration close to the nuclear membrane and lower in the centre of the nucleus. However, the overall intracellular GFP profile of transduced cells was not reduced below basal levels indicating that no detectable GFP knockdown occurred.

The integrity of both pD10.RFP.shCON and pD10.RFP.shGFP was re-tested by sequencing the plasmids. Although pD10.RFP.shCON contained both the RNAi and RFP expression cassettes intact, an aberrant sequence was detected in pD10.RFP.shGFP within the RNAi hairpin, the *sense-loop-antisense* motif was mutated to *sense-loop-insertion* abolishing the function of the cassette as no hairpin could be produced. The possible recombination most likely occurred prior to the viral production protocol and after the bacterial-based production of high amounts of the transfected plasmids that

were needed for AAV8 production. Even after repeating the viral production protocol with the original correct clone, the issue was not resolved. It was not clear why the shGFP-bearing pD10 vector would be a lot less stable than the shCON-bearing pD10. Possible reasons and future precautions are discussed below.

3.5 Discussion

In theory, incorporation of any transgene cassette in a viral production vector should be possible as long as it meets the size requirements for the vector of choice. Since the average RNAi expression cassette will not exceed 500 base pairs in length, it is easily accommodated by any viral vector and viral vector-mediated RNAi should be straightforward. Although some studies have successfully demonstrated viral vector-mediated knockdown of endogenous genes using hairpin expression cassettes [233,235,239], others have found it more difficult to match the *in vitro* efficiency of their hairpin to that following *in vivo* vector-mediated delivery [234]. So far, there has been no insight into the reasons why certain sequences do not function equivalently in different genetic or cellular contexts and such problems are viewed as part of a "hit-and-miss" RNAi design rationale.

In the experiments presented in this chapter, the efficiency of delivering an RNAi hairpin into the retina using two different types of viral vectors was tested. The target gene was *eGFP* and we attempted to deliver an shGFP hairpin *in vivo* using lentiviruses and AAV. Incorporation of hairpins into the lentiviral backbone did not present any obstacles and the targeting shGFP hairpin was successfully delivered both *in vitro* and *in vivo*. The integrity of RNAi cassettes in the viral preparations is indicated by the successful knockdown of eGFP that is dose-dependent based on MOI calculations. However, given the increase in cell death in the 293T/eGFP$^+$ cells after infection of the silencing vectors at high MOIs, it would have been more appropriate to use hrGFP as a reporter gene in our assays rather than eGFP. eGFP is known to have a toxic effect when highly expressed in certain cell lines as was the case in this study and demonstrated by reduced numbers of sorted 293T/eGFP$^+$ cells (Figure 3.7). *In vivo*, the RPE-targeting lentiviruses demonstrated almost total knockdown of endogenous *eGFP* expression within the treated area without causing cell toxicity or silencing *eGFP* in adjacent cells (such as the photoreceptors). Even though the reduction in

eGFP protein levels was demonstrated using immunohistochemistry and statistical analysis on fluorescence values of sorted cells, it would have also been useful to confirm gene suppression in mRNA levels by quantitative PCR. Although mRNA silencing can be suggested through the reduction in protein levels, it cannot be confirmed. In addition, comparison of mRNA and protein levels after suppression would provide a correlation between mRNA molecules and protein translation for eGFP; a useful set of data for future eGFP silencing experiments.

Incorporating RNAi cassettes in an AAV vector proved to be more problematic. The AAV vector backbone – pD10 – is prone to recombination due to the ITRs' palindromic sequences. Although this problem can be usually overcome by adjusting the plasmid production protocol (see section 2.2.4), insertion of additional palindromic sequences (like an RNAi hairpin or two identical promoters) can exacerbate the problem of spontaneous recombination. In our vectors, the integrity of both the RNAi cassette and the RFP reporter gene cassette was essential and they were both checked by sequencing after cloning.

The shCON hairpin cassette posed no problems with regard to cloning during the generation of pD10.RFP.shCON. The shGFP hairpin cassette proved to be very difficult to clone particularly in pD10.RFP.poly. Most attempts to clone the hairpin resulted in empty vectors that had failed to incorporate the shGFP cassette. After adjusting the bacterial cloning temperature and the pre-ligation handling of the plasmid fragments (see section 2.2.4), the shGFP was finally incorporated into pD10.RFP.shGFP and a clone with the correct sequence was identified. At this point, it should be noted that all plasmids were sequenced using primers that confirmed part of the CBA promoter, the entire RFP cDNA and the entire RNAi cassette. Apart from confirming the integrity of ITRs by restriction digestion, the remaining sequence of the pD10 backbone was not confirmed.

After *in vivo* delivery the transduction efficiency of AAV8.RFP.shGFP was considerably lower than that of AAV8.RFP.shCON even though the titres of

both viral preparations were identical. The target area of shGFP was compared to the sequence of RFP to ensure that the low transduction efficiency was not a result of RFP knockdown caused by the *eGFP*-targeting hairpin. In addition, no *eGFP* silencing could be measured in the few transduced photoreceptors. After re-sequencing the plasmids we observed that although pD10.RFP.shCON was still correct, pD10.RFP.shGFP had an aberrant sequence inserted after the loop of the hairpin and into the place of the antisense strand. Moreover, the resulting sequences from three separate sequencing reactions were different even though they all occurred at the loop-antisense junction. This indicated that multiple independent recombination events had occurred that abolished the function of the hairpin in all cases. The resulting RNAi cassettes lacked the antisense strand as well as a valid terminator sequence therefore no functional shRNA could be produced.

It is essential for RNAi hairpins to retain their structural integrity in order to ensure efficient target silencing. All the components of the sense-loop-antisense motif are equally essential in any given hairpin as mutations within the sense or antisense strand will affect the thermodynamic coupling in the mature siRNA. The loop sequence is equally important for the hairpins secondary structure and loop mutations may greatly hinder the coupling of the sense and antisense strand. Although the junctions between a hairpin's components are known targets for major enzymes of the RNAi pathway like Drosha and Dicer, their corresponding DNA templates are not thought to act as substrate for DNA-specific recombinases. It is possible that in the case of pD10.RFP.shGFP, the adjacent nucleotides in the loop-antisense junction formed a highly unstable recipient site which accepted donor insertions from at least three different non-specific areas of the pD10 backbone. Even though unrecombined clones were constructed, their stability was low and further recombination effects could have taken place during any of the steps of plasmid and vector production.

Although the integrity of the RNAi cassette was compromised, the RFP cassette was present since the probe used to titre the viral vectors was part

of its CBA promoter and the RFP cDNA was also sequenced. It was, however, evident that most viral particles did not express the RFP cassette. Although we have not been able to determine a specific cause, it is possible that the recombined RNAi cassette which was upstream of the RFP cassette, affected the function of the CBA promoter by altering the secondary structure of the plasmid.

The work described in this chapter analysed the feasibility of lentivirus- and AAV-mediated RNAi *in vivo*. We found that RNAi cassettes can be successfully delivered using lentiviruses or AAV but spontaneous recombination can hinder the efficiency of AAV incorporation for certain hairpins. For this reason sequencing the hairpin at every stage of plasmid preparation is essential. Spontaneous recombination might occur because of the sequence of the hairpin or because of its interaction with another sequence in the viral backbone. Altering the targeting sequence is one option as different sequences might be less recombinogenic, as suggested by the shCON results (see also Chapter 5). However, further analysis in hairpin dynamics and its interactions with viral sequences and/or components of the viral machinery might identify specific sequence patterns that could be incompatible in a viral context and hence aid in the design of RNA hairpins easily accommodated by different viral vectors.

4 Lentiviral vector-mediated RNAi targeting of epithelial tight junctions

4.1 Introduction

The aim of the work described in this chapter is to determine the utility of viral vector-mediated shRNA delivery for probing retinal function and pathophysiology through selective downregulation of target genes. Here, we describe the use of lentiviral vectors to manipulate junctional signalling in mouse RPE *in vivo*. Our results demonstrate that lentiviral vectors expressing RNA hairpins are capable of regulating junctional proteins *in vivo* and indicate that the ZO-1/ZONAB pathway is important for RPE homeostasis and disturbance of this pathway may result in RPE transformation and cause disease.

4.1.1 Epithelial cellular junctions

The blood-retinal barrier (BRB) is maintained in the retina through endothelial cell-cell adhesion in retinal vessels or epithelial cell-cell adhesion of the RPE. There are four major types of junctions that regulate cellular adhesion: adherens junctions (AJ), desmosomes, gap junctions (GJ) and tight junctions (TJ) (see Figure 4.1). In general, junctions consist of 3 types of components: transmembrane anchoring proteins that physically implement cellular adhesion (e.g. E-cadherin, occludin, claudins); cytoskeletal proteins that create an intracellular scaffolding connecting the junctions (e.g. actins, vinculin) and finally, nucleus and adhesion complexes (NACos) that regulate cell density, gene expression and proliferation (e.g. ZONAB, β-catenin,

CDK4) [240,241]. Mutations in genes encoding junctional components and malformation of retinal junctions are implicated in various types of ocular disease (see section 1.2.2.1).

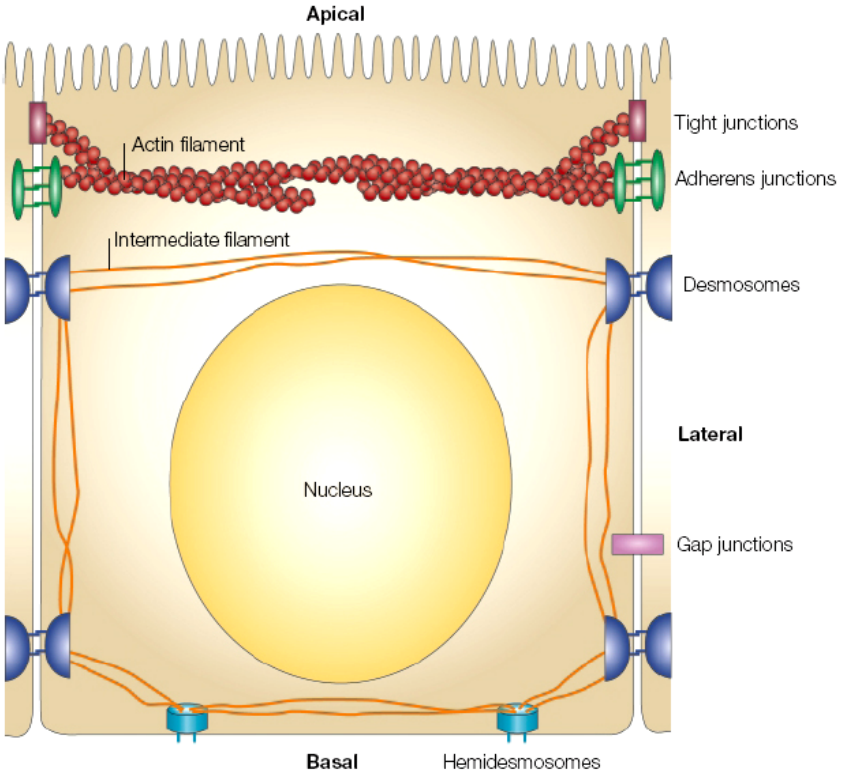

Figure 4.1: Epithelial cellular junctions. Schematic representation of desmosomes, tight, adherens and gap junctions located at the lateral membrane of a polarised epithelial cell. Tight and adherens junctions are situated closer to the apical membrane and are connected to actin filaments of the cytoskeleton. Desmosomes are interconnected through intermediate filaments. Each of the junctions acts as an adhesion point between adjacent epithelial cells. (Adapted from Matter & Balda, 2003) [241]

The formation of junctions allows epithelial cells to polarise and form selective barriers to separate different tissues. Polarisation of epithelial cells creates apical, basal and lateral membrane domains. Often, basal and lateral domains are referred to as the basolateral membrane. In the RPE, the apical membrane forms fine foldings called microvilli that are involved in photoreceptor OS phagocytosis, whereas the basal membrane lies on Bruch's membrane anchoring the neuroretina and supporting its structure.

The lateral sides are in contact with adjacent RPE cells forming a uniform closely packed monolayer underlying and supporting the neuroretina [242].

AJs and desmosomes are the main adhesive junctions between epithelial cells. AJs are often concentrated close to TJs near the apical membrane where they share cytoplasmic interactions with cytoskeletal actin filaments, whereas desmosomes are usually distributed all around the basolateral membrane sharing connections with the intermediate filaments of the cytoskeleton [243]. AJs' and desmosomes' anchoring molecules are cadherins that interact with each other at their extracellular domains. They are known to be involved in tumour suppression and morphoregulation [244]. In addition, it has been suggested that E-cadherin is involved in epithelial tyrosine-kinase dependent endocytosis through its ubiquitination by a zinc-finger family protein, Hakai [245,246]. Intracellularly, cadherins are involved in the sequestration of catenins (β-catenin or plakoglobin (γ-catenin)) which are known to be transcription regulators of proliferative markers. β-catenin has been known to regulate several genes involved in cancer like c-myc, cyclin D1 and matrix metalloproteases [243].

TJs regulate diffusion of molecules through the paracellular pathway and they delineate the apical-basolateral epithelial domains [247]. These two TJ characteristics are known as "gate and fence" functions. They circumvent each cell at the apical end of the lateral membrane forming a dense network that prohibits free compound exchange in the apical-basal orientation. They are composed of three types of transmembrane proteins: occludin, claudins and junction adhesion molecules (JAMs) [243,247]. They all mediate cell-cell adhesion with the first two being involved in the selective paracellular diffusion of molecules. Intracellularly, TJs are connected to a protein complex that consists of membrane-associated guanylate cyclases (MAGUK) and proteins containing PDZ domains (PSD-95, Discs large A, ZO-1 homology). A vast network of other regulators mediates junctional-nuclear communication to regulate expression of genes involved in proliferation, cell cycle and cell density [248].

Zonula occludens-1 (ZO-1) is a major TJ component and has SH3 (Src homology 3) and PDZ domains for protein-protein interactions. ZO-1 has been shown to interact with various signalling molecules that regulate G_1/S phase transition, cellular stress responses and permeability through its SH3 domain [248]. One of its partner molecules is the ZO-1 associated nucleic-acid binding (ZONAB) protein. ZONAB is a Y-box transcription factor that recognises promoter sequences containing an inverted CCAAT box [249]. ZONAB regulates *Erb-2* expression in a cell-density dependent way [250]. In low cell density conditions ZONAB localises in the nucleus where it activates *Erb-2* transcription, leading to cell division. When cellular density increases, ZO-1 sequesters ZONAB as TJ assembly is increased resulting in a downregulation of *Erb-2* and a subsequent slowing of cell proliferation. ZONAB is also regulated by other NACos in TJ specific transcriptional signalling. APG-2, a heat-shock protein encoded by an oncogene, competes with ZONAB for the SH3 domain of ZO-1 in a stress dependent manner thereby promoting proliferation by impeding ZO-1/ZONAB interactions, and hence ZONAB's cytoplasmic sequestration [251]. TJ paracellular permeability is also regulated by Rho family GTPases which are involved in cytoskeletal rearrangements. Guanine nucleotide exchange factor (GEF), a proto-oncogene, has been shown to activate Rho and directly associate with TJs increasing paracellular permeability [252]. Although the mechanism through which Rho GTPases rearrange cytoskeletal filaments to increase diffusion is not clear, the TJ "gate and fence" function does not get compromised in the process meaning that the epithelial monolayer integrity is retained.

4.1.2 The RPE and tight junctions

RPE cells not only support the function of photoreceptors, they also form the outer BRB that prevents fluid from choroidal vessels from entering the retina [253,254]. Breakdown of the BRB can lead to visual loss in a number of

ocular disorders. However, the molecular mechanisms underlying RPE homeostasis are not completely understood.

Binding of ZONAB to ZO-1 results in cytoplasmic sequestration and, hence, inhibition of its transcriptional activity [248,255]. ZONAB interacts with the cell cycle kinase cdk4 and regulates the transcription of cell cycle genes such as cyclin D1 and PCNA, providing a molecular explanation for its role in the proliferation of epithelia cells in culture [249,250,256]. Little is known about the role of ZONAB *in vivo* and although TJ-associated knockout mouse models targeting ZO-2, ZO-3 and ZONAB have demonstrated the developmental importance of ZO-2 and the redundancy of ZO-3, lack of ZONAB expression was found to severely hinder embryonic development only when combined with depletion of YB-1, a cold shock domain protein [257,258]. Mice deficient only in ZONAB exhibited increased spermatocyte apoptosis leading to 50 % male infertility but otherwise no defective epithelial phenotype was observed. When combined with lack of YB-1, lack of ZONAB caused severe mid-to-late embryo development (E11.5) leading to lethality. The double YB-1 and ZONAB knockout phenotype was much more severe than the YB-1 knockout indicating that ZONAB interactions with other cold shock domain proteins are essential for embryo development. In addition, nuclear translocation of ZONAB correlates with increased proliferation in the colonic epithelium of ethanol-fed mice and in adenomas of chronic alcoholics, suggesting a possible involvement in alcohol-induced gastrointestinal transformation [259].

4.2 In vitro shRNA evaluation

4.2.1 mu6pro & pHR'SIN hairpin expression vectors

The targeting sequences for ZO-1 and ZONAB downregulation were kindly provided by Maria Balda and Karl Matter (Department of Cell Biology, Institute of Ophthalmology, UCL). They had previously tested their efficiency in downregulating ZO-1 or ZONAB synthetically *in vitro* by transfecting siRNAs against ZO-1 and ZONAB into MDCK cells (see section 2.2.5; Table 1 for sequences).

Oligonucleotides with the targeting sequences for each gene were subsequently cloned into the mU6pro hairpin expression vector downstream of the U6 polymerase III promoter and the integrity of the ZO-1 and ZONAB hairpin cassettes was established by enzyme digestion of the whole cassette, as described in section 3.2.1. The RNAi cassettes were further subcloned into the pHR'SIN backbone (see section 3.2.2). Prior to the production of recombinant lentiviruses using these two vector plasmids, we employed pHR'SIN.shGFP (see Chapter 3) as an RNAi non-targeting control for our experiments. Because of the interactions between ZO-1 and ZONAB in TJ regulation (see section 3.1), we also generated a lentiviral vector overexpressing ZONAB using an SFFV promoter (see section 2.5.2). This would allow us to assess the physiological effect of ZONAB upregulation on TJ regulation in contrast to downregulation of ZONAB. Thus, we produced four recombinant lentiviruses that we used to elucidate the ZO-1/ZONAB pathway: LNT.shZO-1, LNT.shZONAB, LNT.shGFP and LNT.ZONAB. The integrity of the RNAi cassettes in all the corresponding plasmids, pHR'SIN.shZO-1, pHR'SIN.shZONAB, pHR'SIN.shGFP and pHR'SIN.ZONAB, was confirmed by sequencing (MWG Biotech, UK, see Chapter 2.2.3).

4.2.2 In vitro evaluation of lentiviral efficiency

The four lentiviral vectors were produced using the same production protocol and were titre-matched for all subsequent *in vitro* and *in vivo* experiments. Initially, we wanted to confirm the silencing potential of LNT.shZO-1 and LNT.shZONAB (and lack thereof for LNT.shGFP) as well the overexpression levels of ZONAB after LNT.ZONAB transduction in different epithelial cell lines. A canine kidney cell line (MDCK) and a human breast epithelial cell line (MCF10A) were used for the testing of the lentiviral preparations as they form TJs in culture. A murine embryonic stem cell (ES) line was also used to test the efficiency of LNT.shZO-1 since it expresses ZO-1. LNT.shZO-1 silenced endogenous ZO-1 levels to undetectable levels by Western blotting in both MDCK and MCF10A cells as well as significantly reduced the endogenous levels in ES cells (Figure 4.2A) in comparison with that in LNT.shGFP transduced cells. The target sequences for both ZO-1 and ZONAB were selected from regions of the respective genes that are highly conserved between human, murine and canine orthologues. ZONAB was both overexpressed and downregulated in MDCK cells. After transduction with LNT.ZONAB, intracellular levels of ZONAB were considerably raised as visualised by Western blotting (Figure 4.2B), whereas transfection with LNT.shZONAB reduced endogenous expression to undetectable levels (Figure 4.2C). All western blot experiments were repeated twice.

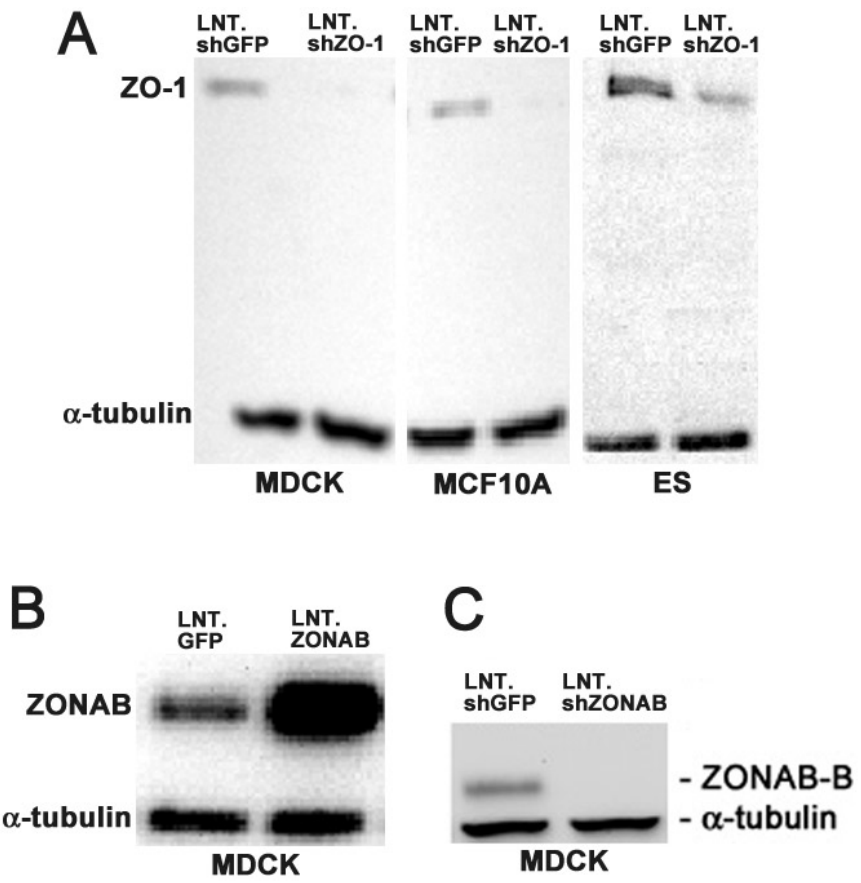

Figure 4.2: Western blots of cell lines transduced with lentiviral vectors. Three cell lines were transduced with either the control LNT.shGFP or LNT.shZO-1 lentiviruses. ZO-1 silencing was observed in all three cell lines in comparison to control **(A)**. Overexpression of ZONAB after transduction of MDCK cells with LNT.ZONAB compared to LNT.GFP transduced cells **(B)**. Silencing of ZONAB in MDCK cells after transduction with LNT.shZONAB **(C)**. All transductions were done at MOI=20. α-tubulin was used as a loading control. MDCK: Madin-Darby canine kidney cells. MCF10A: human mammary epithelial cells. ES: murine embryonic stem cells.

The levels of ZO-1 and ZONAB had been successfully reduced as indicated by Western blotting, but further experiments were needed to assess how their downregulation affected cellular morphology.

4.2.3 Morphological impact of ZO-1 & ZONAB downregulation

Since the tight junctions mediate cell-cell adhesion in epithelia, downregulation of junctional components should impede structural stability in monolayer formation (2-D culturing conditions) or cyst formation (3-D culturing conditions). *In vitro* experiments presented in this section were performed by Maria Balda and Karl Matter, Department of Cell Biology, IoO.

Initially, MDCK cells were transduced with LNT.shZO-1 or LNT.shZONAB and their effect in 2-D cultures was assayed. Direct visualisation of ZO-1 levels using immunocytochemistry on MDCK monolayers transduced with LNT.shZO-1 was carried out alongside cells transduced with LNT.shGFP as a control (Figure 4.3). In healthy confluent MDCK cells, ZO-1 was localised along the cellular membrane clearly indicating the intercellular contact points that form a tightly packed epithelial monolayer. In LNT.shZO-1 transduced MDCK cells the ZO-1 immunostaining of the cellular membranes was intermittent leading to the formation of a loosely packed monoloayer with a reduced cell density.

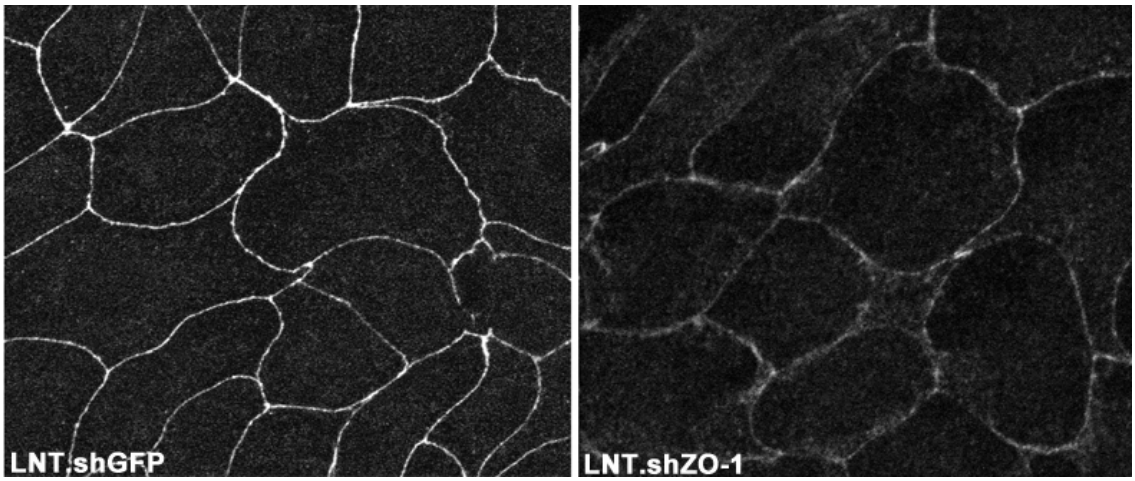

Figure 4.3: ZO-1 immunocytochemistry on MDCK cells. ZO-1 immunofluorescence on confluent MDCK monolayers after transduction of LNT.shZO-1 and LNT.shGFP. A marked reduction in ZO-1 immunofluorescence was observed only following transduction with LNT.shZO-1. MOI=20. Magnification; x40.

Reduction of ZONAB levels could not be visualised by immonofluorescence on the 2D culturing platform because of inadequate immunostaining provided by the ZONAB antibody and also because of the low levels of ZONAB in MDCK cells. However, downregulation of ZONAB resulted in a marked decrease of MDCK cell proliferation in comparison to LNT.shGFP transduced cells (Figure 4.4). For quantification, 5,600 cells/cm^2 were plated in 24 well plates and after 2 days in culture BrdU was added for 2hrs. BrdU incorporation was assessed by counting 500 cells from 6 different areas using the same microscope objective (x20) and scoring for BrdU positive cells. The experiment was done in quadruplicates and the reduction in proliferation in LNT.shZONAB infected cells was found to be statistically highly significant using the student's *t*-test (***P***<0.001, n=4).

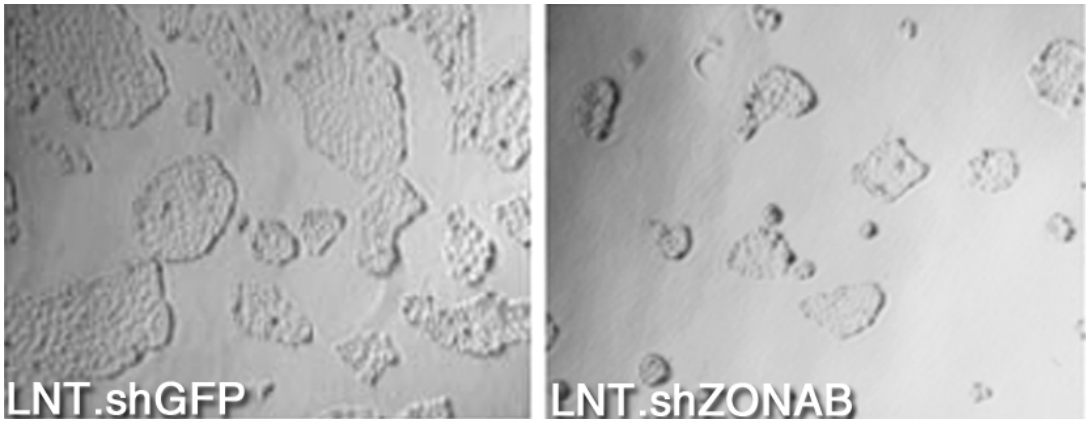

Figure 4.4: ZONAB regulates MDCK cell proliferation. Equal numbers of MDCK cells were transduced with LNT.shGFP or LNT.shZONAB and grown for 3 days. Phase-contrast images indicate a significant decrease in proliferation of MDCK cells transduced with LNT.shZONAB in comparison with LNT.shGFP transduced cells. MOI=20. Magnification: x10.

To further assess the impact of ZO-1 or ZONAB downregulation in MDCK cells, we cultured transduced cell lines in a solid-phase Matrigel-collagen scaffold that allowed the MDCK cells to form cysts rather than monolayers. This approach enables the intercellular associations of MDCK cells to be assessed in a more relevant physiological environment than is possible when using two-dimensional culturing. This experiment also served as an

intermediate step to assess the effect of the vectors prior to delivering them to the murine RPE *in vivo*.

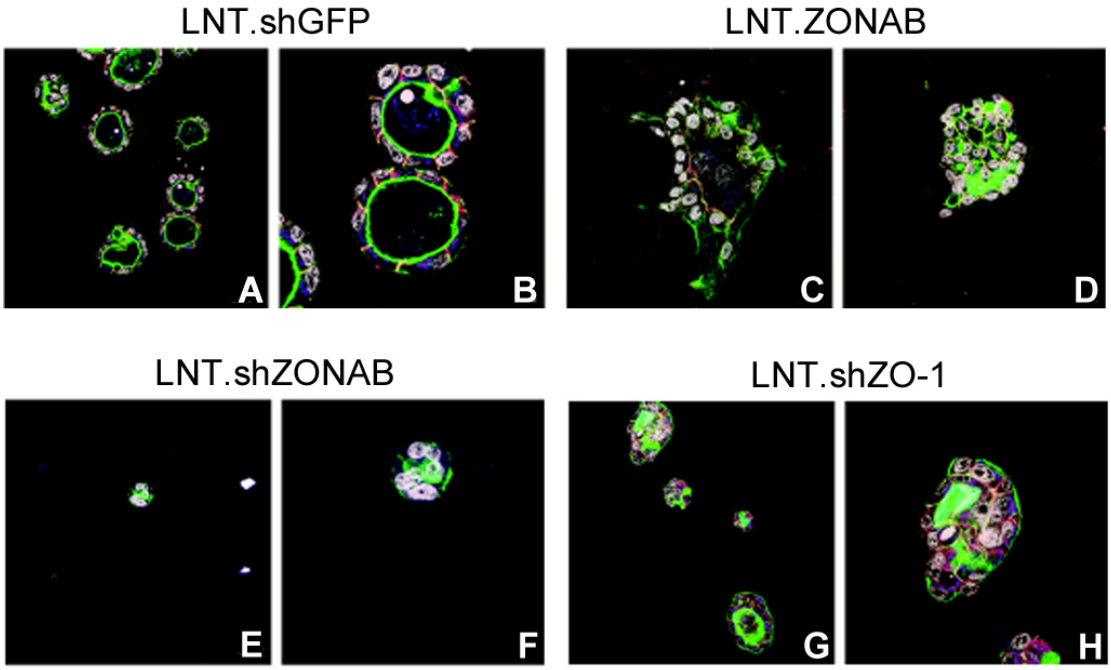

Figure 4.5: Manipulation of ZO-1 or ZONAB affects MDCK cyst formation in 3-D cultures. Matrigel-collagen solid culturing of MDCK cell lines 5 days following transduction with LNT.shGFP, LNT.ZONAB, LNT.shZONAB or LNT.shZO-1. Large field images **(A, C, D, E, G)** and larger magnifications of characteristic structures **(B, F, H)** were taken after immunolabelling with antibodies against β–catenin (red), phalloidin (green) and Hoescht 33528 as nuclear counterstain (white). In MDCK cells transduced with LNT.shGFP normal cyst formation was observed. Irregular structures were found in MDCK cells transduced with LNT.shZO-1, LNT.shZONAB or LNT.ZONAB. They were categorised as spherical structures with no lumen (as in F), single lumen (as in B), multiple lumens (as in H) or other disorganised structure (as in C, D). For quantification of structures see figure 4.6. MOI=20.

Healthy MDCK cells form single lumen cysts when cultured in solid-phase medium as depicted by combined immunostaining of β-catenin and phalloidin (Figure 4.5A,B). For this experiment, the vectors expressing the RNAi cassettes were used to transduce MDCK cells. After five days in culture, MDCK cells formed irregular structures that either lacked a lumen (Figure 4.5F), had multiple irregular lumen (Figure 4.5H) or failed to form any kind of spherical structure (Figure 4.5D). For quantification, 10 pictures from different

areas were taken using low magnification objective (x10) from two independent experiments (Figure 4.6; see Chapter 2.3.8). Statistical analysis was performed for each observed structure type for each condition. After quantification of the observed structures in cells transduced with the RNAi-expressing vectors as well as LNT.ZONAB, it is evident that manipulation of the ZO-1/ZONAB pathway greatly hinders polarity and intercellular organisation in epithelial cells. Furthermore, the similar distribution of cyst morphologies between LNT.ZONAB and LNT.shZO-1 transduced cells supports the proposed mechanism of ZO-1/ZONAB interactions in TJ-regulated pathways for epithelial differentiation and proliferation, where raised intracellular concentration of one gene reduces the concentration of the other. Next we aimed to assess the impact of ZO-1/ZONAB manipulation in the murine RPE *in vivo*.

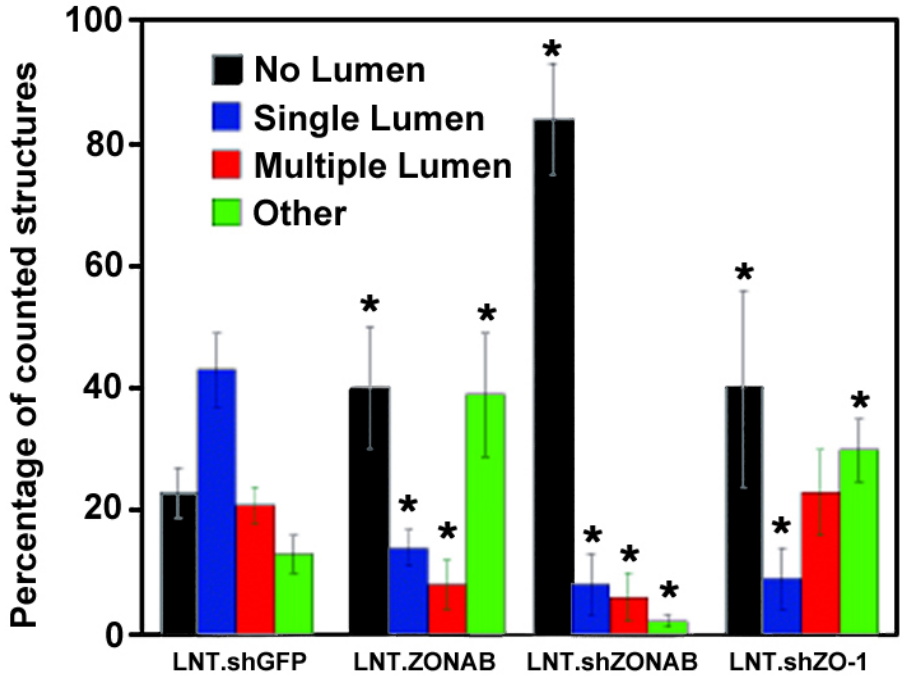

Figure 4.6: Quantification of MDCK cyst morphology in 3-D cultures. Each type of cyst structure was counted from 10 different areas and the percentage occurrence was plotted. Apart from LNT.shGFP-transduced MDCK cysts, all other MDCK lines exhibited a reduced single lumen normal morphology and an increase in irregular structures with no spherical shape, multiple or absent lumen. For representative images of each structure see figure 4.5. Error bars show standard error of the mean. **P*<0.05, n=10.

4.3 ZO-1 & ZONAB silencing in the RPE in vivo

4.3.1 Assessment of lentiviral transduction of the RPE

We first aimed to titrate transduction levels in the RPE using serial dilutions of LNT.hrGFP. Wild-type (wt) mice (n=12) were subretinally injected and transgene expression within the treated area was analysed two weeks post injection (p.i.). Transduction of the entire RPE monolayer was observed following injection of a titre of 10^8 transducing units/ml (T.U./ml) (Fig. 4.7A, B). Injection of a titre of 10^7 T.U./ml resulted in discontinuous transduction of the RPE monolayer (Fig. 4.7C, D). At 10^6 T.U./ml, minimal RPE transduction was observed with expression of hrGFP by the occasional RPE cell (Fig. 4.7E, F). No GFP expression was evident after injection of vector at a titre of 10^5 T.U./ml. Even at the highest titre, GFP expression was only observed in RPE cells, supporting the specificity of the viral vector [122].

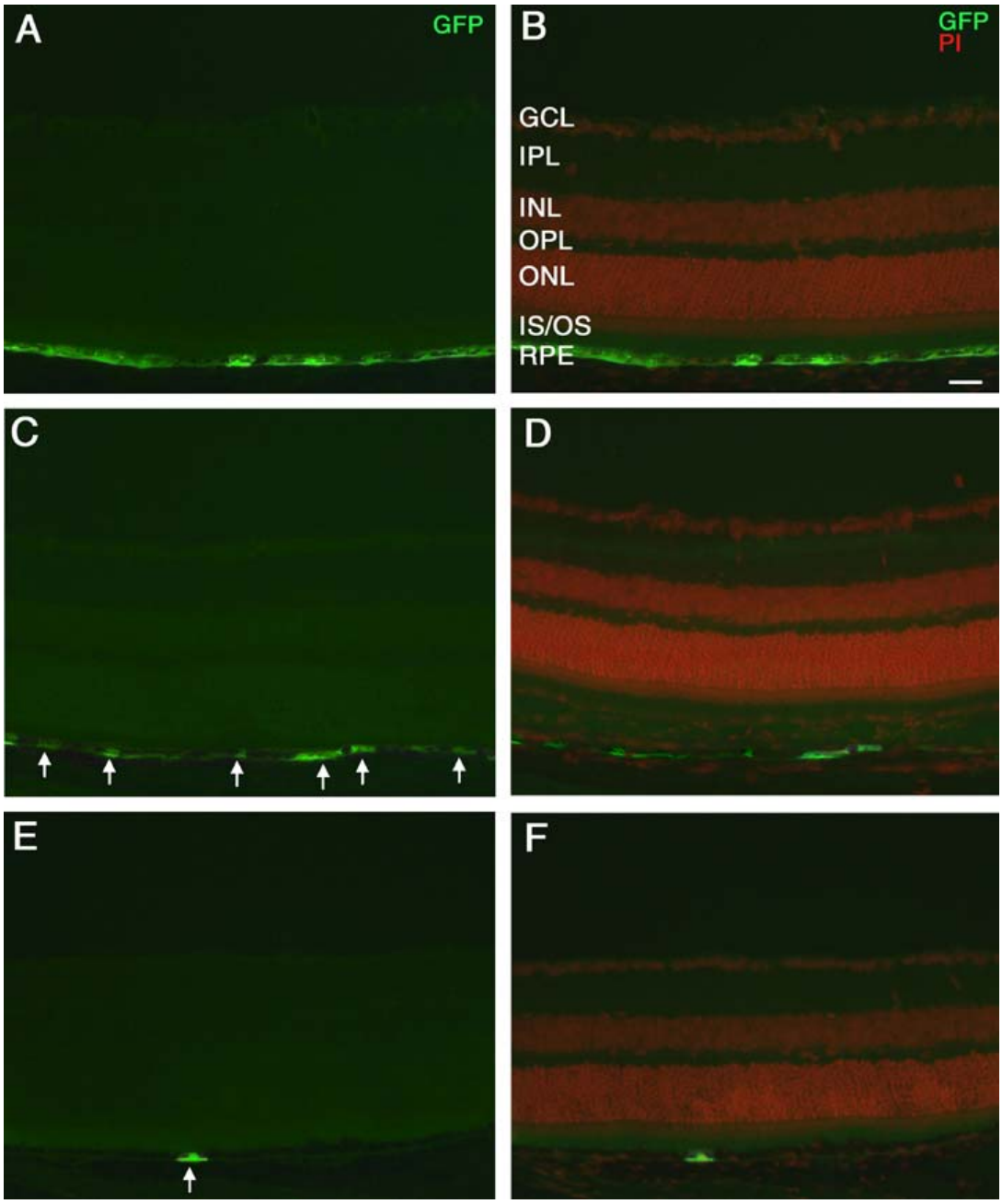

Figure 4.7: RPE transduction following subretinal delivery of LNT.hrGFP. Retinal cryosections were obtained from eyes 14 days after subretinal injection of LNT.hrGFP at titres of 10^8 T.U./ml **(A, B)**, 10^7 T.U./ml **(C, D)** and 10^6 T.U./ml **(E, F)**. Expression of GFP (green) was restricted to the RPE (left panel). Propidium iodide (red) was used as a nuclear counterstain (right panel, merged with GFP). White arrows, GFP-positive cells. GCL, ganglion cell layer; IPL, inner plexiform layer; INL, inner nuclear layer; OPL, outer plexiform layer; ONL, outer nuclear layer; IS, inner segments; OS, outer segments; RPE, retinal pigment epithelium; Size bar, 20 µm. n=4 per treatment group.

In order to assess the role of ZO-1 and ZONAB in RPE cells we used lentiviral vectors expressing shRNAs (LNT.shZO-1, LNT.shZONAB and LNT.shGFP) at two titres. Since a pilot study using a high titre of 10^8 T.U./ml led to severe degeneration of the RPE and the neuroretina, a titre of 10^7 T.U./ml was used in order to obtain discontinuous transduction of the RPE monolayer facilitating phenotypic characterisation. Where indicated, a titre of 10^8 T.U./ml was also used in order to obtain transduction of the entire RPE monolayer and follow the progression of the phenotype observed using the 10^7 T.U./ml titre. This approach enabled a more detailed analysis of the ZO-1/ZONAB pathway and its impact on RPE homeostasis.

4.3.2 ZO-1/ZONAB silencing and RPE proliferation

We tested the ability of the lentiviral vectors to alter the levels of ZO-1 and ZONAB. Four eyes per virus group were injected subretinally in the superior and inferior hemispheres and the eyes were orientated prior to embedding. In this way, and due to the lack of a reporter gene, sections were taken at the centre of the injected hemispheres and close to the optic nerve head to ensure inclusion of the treated area. Ten sections from each treated hemisphere and for each of the four treated eyes were analysed per vector group. Following injection of the control LNT.shGFP virus *in vivo*, basal levels of ZONAB were observed in RPE cells (Fig. 4.8A). Increased levels of ZONAB were observed following subretinal injection of LNT.ZONAB (Fig. 4.8C). Five days after subretinal injection of LNT.shZONAB, ZONAB immunostaining was abolished throughout the treated area (Fig. 4.8E), suggesting efficient silencing by the targeting vector. Following injection of the control LNT.shGFP virus, ZO-1 immunofluorescence in the RPE cells was observed at cell-cell junctions (Fig. 4.8B). No change in ZO-1 immunostaining was observed after injection of LNT.ZONAB and LNT.shZONAB (Fig. 4.8B,D,F), whilst a marked reduction was observed 5 days after subretinal injection of LNT.shZO-1 (Fig. 4.8H). Unexpectedly, increased expression of endogenous ZONAB expression was observed in

the LNT.shZO-1 treated eyes (Fig. 4.8G). These results demonstrate that manipulation of ZONAB or ZO-1 levels in RPE cells *in vivo* can be obtained using HIV-1-based lentiviral vectors.

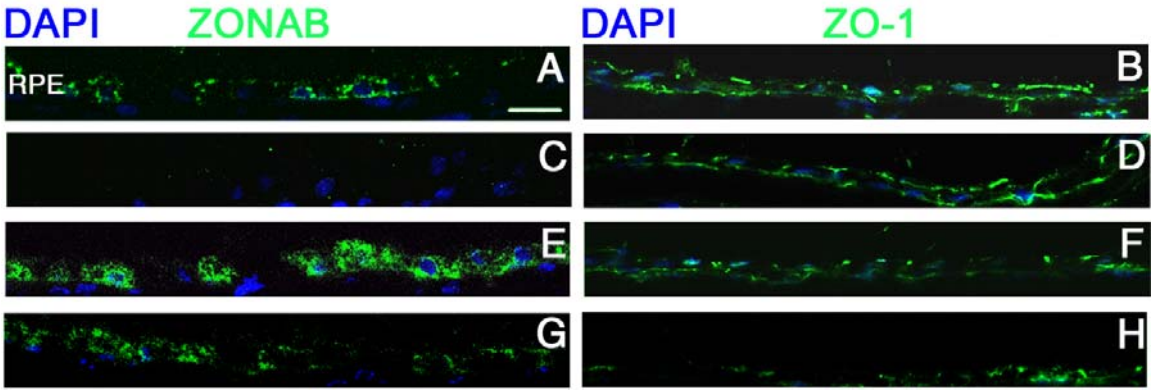

Figure 4.8: Lentiviral-mediated silencing of ZO-1 and ZONAB. Retinal cryosections were obtained from eyes 5 days after the subretinal injections of LNT.shGFP **(A,B)**, LNT.shZONAB **(C,D)**, LNT.ZONAB **(E,F)** or LNT.shZO-1 **(G,H)** at 10^7 T.U./ml. Immunostaining was performed using antibodies against ZONAB (left panel) and ZO-1 (right panel). Following injection of LNT.shGFP, ZONAB can only be detected at low levels in the RPE **(A)** and ZO-1 was observed in the RPE as well as along the outer limiting membrane (not shown) **(B)**. Following subretinal injection of LNT.shZONAB, ZONAB was not detected within the transduced area **(C)** and no significant change in ZO-1 levels was observed **(D)**. Subretinal injection of LNT.ZONAB resulted in an elevation of ZONAB levels in RPE cells **(E)** and did not affect ZO-1 levels **(F)**. Subretinal injection of LNT.siZO-1 resulted in an increase in ZONAB expression **(G)** and a decrease of ZO-1 expression **(H)** compared with control eyes **(B)**. Nuclei were counterstained with DAPI. White arrows, RPE monolayer. Size bar, 20 µm. n=4 per treatment group.

ZO-1/ZONAB signalling controls G_1/S phase transition and differentiation of epithelial cells in culture [249,256]. We therefore analysed RPE differentiation by testing the expression of an RPE-specific marker, RPE65, five days after injection of LNT.shGFP, LNT.ZONAB or LNT.shZO-1 [13]. Four eyes per virus group were injected subretinally in the superior and inferior hemispheres and the eyes were orientated prior to embedding. In this way, and due to the lack of a reporter gene, sections were taken at the centre of the injected hemispheres and close to the optic nerve head to ensure

inclusion of the treated area. Five sections from each treated hemisphere and for each of the four treated eyes were analysed per vector group. Immunostaining of RPE65 in the RPE following injection of LNT.shGFP, LNT.ZONAB or LNT.shZO-1 was not altered (Figure 4.9). However, downregulation of ZONAB following injection of LNT.shZONAB resulted in a reduction of RPE65 expression (Fig. 4.9C), suggesting that ZONAB downregulation results in a reduction of the cell density within the RPE monolayer.

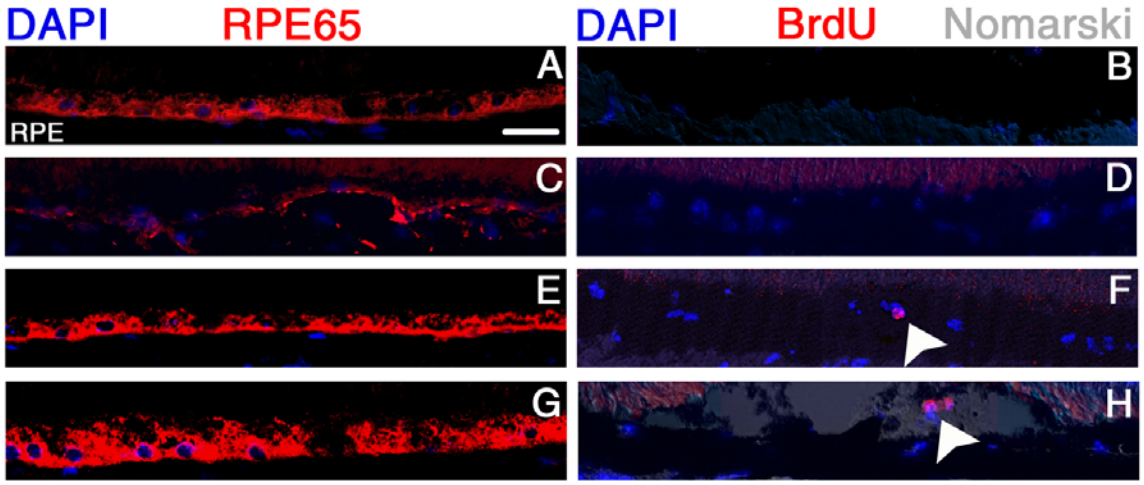

Figure 4.9: Manipulation of ZO-1 and ZONAB expression affects RPE65 expression and RPE proliferation. Retinal cryosections were obtained from eyes 5 days after the subretinal injections of LNT.shGFP **(A,B)**, LNT.shZONAB **(C,D)**, LNT.ZONAB **(E,F)** or LNT.shZO-1 **(G,H)** at 10^7 T.U./ml. BrdU was injected intraperitoneally following the subretinal vector administration. Immunostaining was performed using antibodies against RPE65 (left panel) and BrdU (right panel). In eyes injected with LNT.shGFP, high levels of RPE65 were evident in RPE cells **(A)** and there was no evidence of proliferation judged by the absence of BrdU staining **(B)**. Depletion of ZONAB led to a significant reduction in RPE65 within the targeted area **(C)** and no BrdU positive cells could be found **(D)**. Overexpression of ZONAB did not change RPE65 levels **(E)** but increased the number of BrdU positive cells, indicative of proliferation (**F**, white arrowhead. Inset shows x63 magnification). Delivery of LNT.shZO-1 did not increase RPE65 expression **(G)** but increased BrdU positive cells suggesting RPE proliferation (**H**, white arrowhead). Nuclei were counterstained with DAPI. White arrows, RPE monolayer. Size bar, 20 µm. n=4 per treatment group.

In epithelial cell lines, ZONAB regulates proliferation by stimulating G1/S phase progression. The postnatal RPE is not normally proliferative [260]. We therefore tested whether manipulation of ZONAB and ZO-1 expression in RPE *in vivo* affects cell cycle entry using BrdU incorporation. Whilst injection of control virus and downregulation of ZONAB following injection of LNT.shZONAB did not induce proliferation (Fig. 4.9B,D), proliferating cells were detected in eyes following injection of either LNT.ZONAB (Fig. 4.9F) or LNT.shZO-1 (Fig. 4.9H). We also quantified the number of BrdU-positive cells following injection of the lentiviral vectors (Fig. 4.10), confirming the induction of proliferation by downregulation of ZO-1 and overexpression of ZONAB. Thus, treatments that result in increased ZONAB activity also stimulate proliferation in RPE cells *in vivo*.

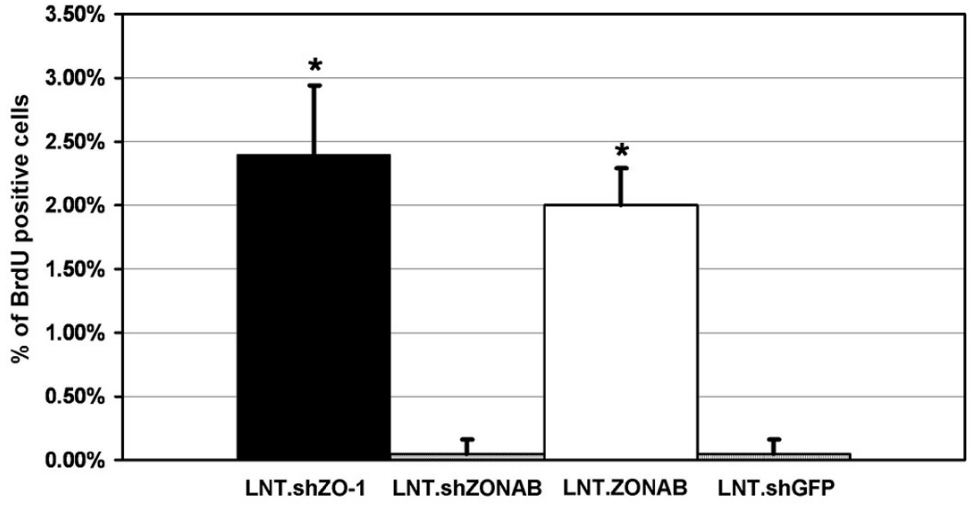

Figure 4.10: Quantification of BrdU positive RPE cells. BrdU positive RPE cells and total RPE cell numbers were counted in the middle of the treated area of retinal cryosections obtained from subretinally injected mice 5 days after vector administration at a titre of 10^7 T.U./ml. Following injection of LNT.shZO-1 or LNT.ZONAB BrdU positive cells increased to 2.4 % and 2.0 % of total RPE cell number, respectively, whereas very few BrdU positive cells were identified in LNT.shGFP (0.05 %) or LNT.shZONAB (0.05 %) treated eyes. (***P***<0.001 compared with LNT.shGFP control. Student's t-test. n=4 [20 measurements from 4 eyes per treatment group]).

4.3.3 TJ deregulation and epithelial-mesenchymal transition

As manipulation of ZONAB affects the expression of the RPE-specific marker, RPE65, and RPE proliferation, we next analysed changes in RPE morphology and retinal integrity after manipulation of ZONAB or ZO-1 following injection of vectors at titres of 10^7 and 10^8 T.U./ml (Fig. 4.11). Semithin sections of treated eyes were analysed to determine morphological changes. Injection of control virus did not affect the morphology of the RPE and the neuroretina (Fig. 4.11A,E). There were, however, mild phenotypical changes following injection of the other vectors at 5 days p.i. (Fig. 4.9) and more pronounced phenotypes after 10 days such as a disrupted RPE monolayer and altered photoreceptor morphology. In LNT.shZONAB treated eyes, the RPE was considerably thinner than normal with evident cell loss and discontinuities in the monolayer (Fig. 4.11B,F; for quantification, see Fig. 4.12). Photoreceptor outer segments appeared disorganised and with extracellular gaps. Accumulation of debris in the inter-retinal space indicated that the phagocytotic function of the RPE was compromised. This, along with reduced levels of RPE65 (Fig. 4.9) suggests loss of normal RPE function. In some areas, the presence of macrophage-like pigmented cells on the apical surface of the RPE suggested the disruption of the posterior BRB and possible leukocyte infiltration. Thus, downregulation of ZONAB appears to cause RPE dysfunction that leads to widespread degeneration of the retina.

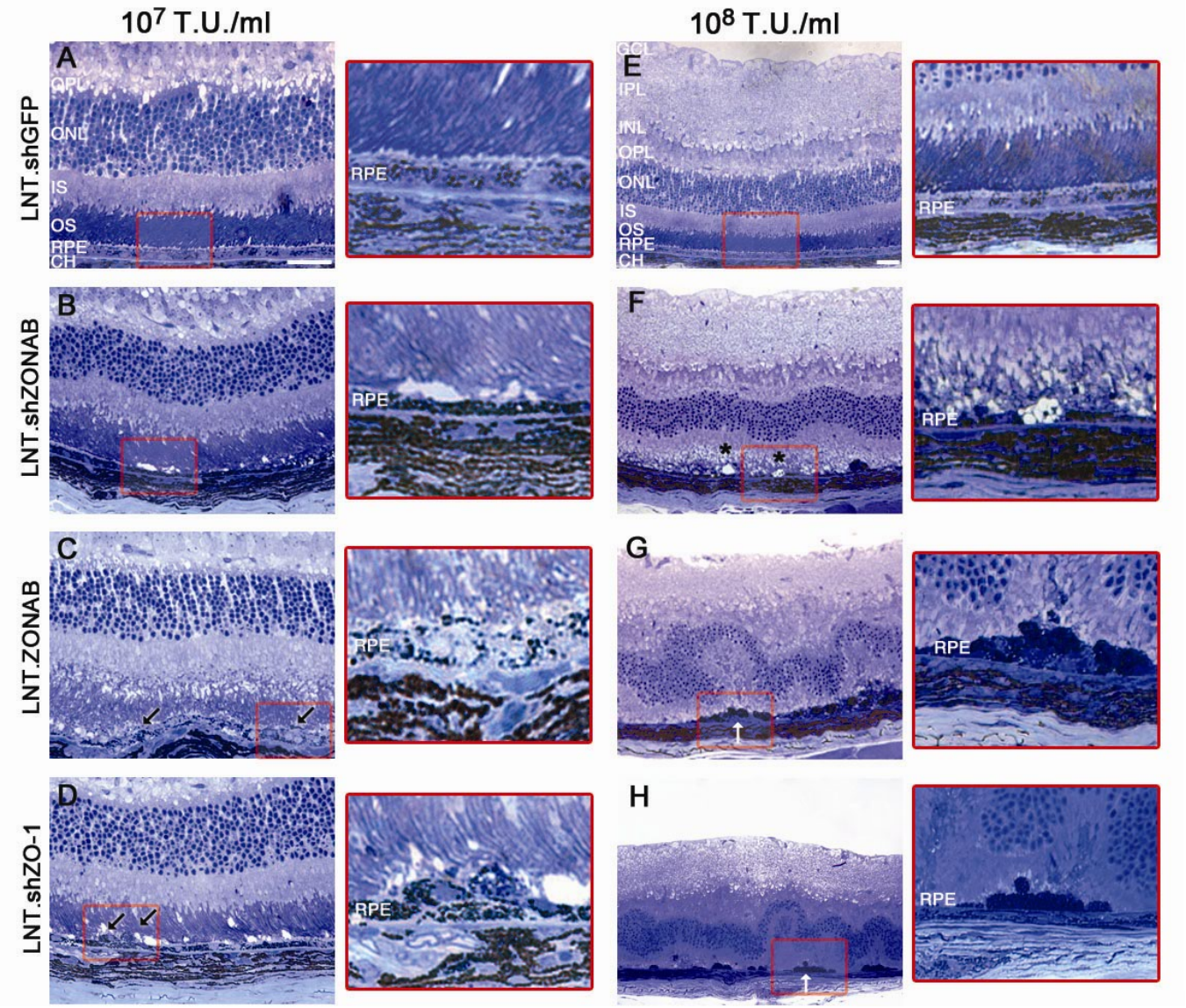

Figure 4.11: Retinal morphology 10 days after subretinal injection of vectors. Retinal semithin sections were obtained after 10 days of subretinal injection of LNT.shGFP **(A,E)**, LNT.shZONAB **(B,F)**, LNT.ZONAB **(C,G)** or LNT.shZO-1 **(D,H)** at 10^7 T.U./ml (left panel, x40 magnification) and 10^8 T.U./ml (right panel, x20 magnification). Areas in red rectangles are shown in higher magnification. The LNT.shGFP treated eyes **(A,E)** exhibit normal retinal architecture showing that there are no adverse effects induced either by the lentiviral vector itself or by the expression of shRNA. In LNT.shZONAB treated eyes **(B,F)**, a thinner RPE monolayer as well as disorganisation of photoreceptor outer segment with intercellular vacuoles (asterisks) were found throughout the treated area. Following injection of either LNT. shZO-1 **(C,G)** or LNT. ZONAB **(D,H)** signs of RPE multilayerisation (black arrows) as well as retinal folding and rosette formation in areas corresponding to those with severe RPE abnormalities (white arrows) were observed. GCL, ganglion cell layer. IPL, inner plexiform layer. INL, inner nuclear layer. OPL, outer plexiform layer. ONL, outer nuclear layer. IS, inner segments. OS, outer segments. RPE, retinal pigment epithelium. CH, choroid. Size bar, 20 µm. n=4 per treatment group.

Injection of LNT.ZONAB (Fig. 4.11C,G) and LNT.shZO-1 (Fig. 4.11D,H) also strongly affected RPE morphology and the two vectors gave similar phenotypes (see figure 4.12 for quantification). Morphological changes were observed after delivery of either vector titre (Fig. 4.11C,D; 10^7 T.U./ml). However, following injection of vector at the higher titre of 10^8 T.U./ml, retinal foldings and rosette formations were evident. These alterations were particularly evident in the outer nuclear layer (ONL), which consists of photoreceptor nuclei. In some areas the RPE lost its monolayer structure and highly pigmented cells could be seen piling up and invading the inner photoreceptor matrix (IPM) (Fig. 4.11G,H). We observed three characteristic structural changes of the RPE monolayers, such as pyknosis, flattening and breaks. Pyknosis was identified as hyperpigmented RPE cells that do not adhere to the monolayer conformation. Figure 4.12 shows the quantification of such phenotypes. Downregulation of ZO-1 or overexpression of ZONAB induced predominantly pyknotic cells, whereas RPE flattening was observed by downregulation of ZONAB. RPE breaks occurred in all three treatment groups adjacent to either pyknotic or flat RPE areas. Thus, the levels of ZO-1 and ZONAB expression are important determinants of RPE cell morphology and differentiation *in vivo*, indicating that the ZO-1/ZONAB pathway is critical for RPE cells to maintain their differentiated phenotype and to fulfil their support function for the neural retina.

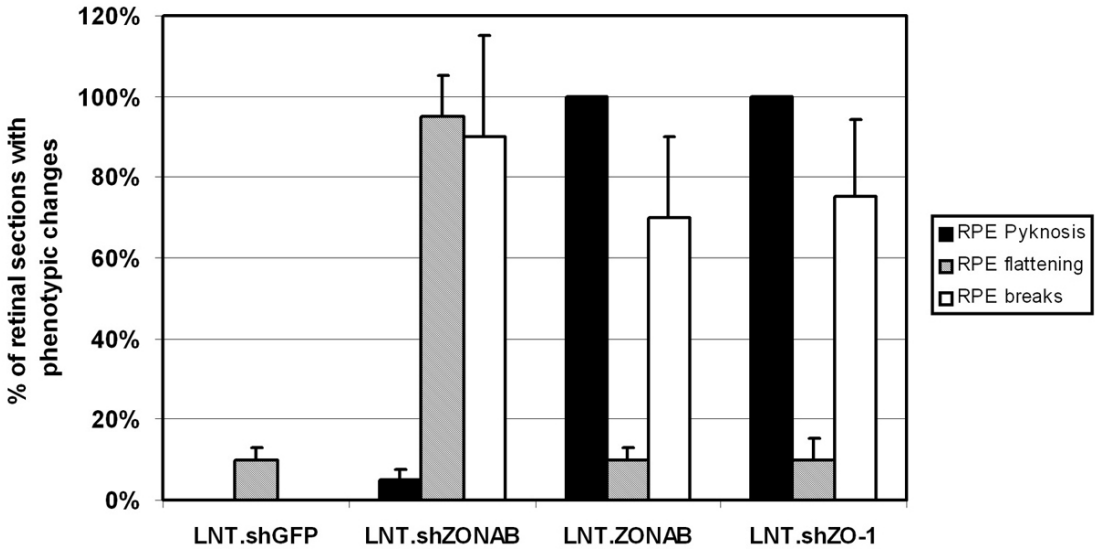

Figure 4.12: RPE features after 10 days of subretinal injection of vectors at 10^8 T.U./ml. Three features were assessed: RPE pyknosis, RPE flattening and RPE breaks. Pyknotic RPE cells were defined as hyperpigmented cells that were not within a continuous monolayer. Percentage of retinal sections in which RPE pyknosis, flattening and breaks were observed is plotted. LNT.shZO-1 and LNT.ZONAB treated eyes contained many pyknotic RPE cells whereas RPE flattening was found consistently in LNT.shZONAB treated eyes. RPE breaks or cell loss occurred adjacent to either pyknotic or flat RPE areas of LNT.shZO-1 and LNT.ZONAB or LNT.shZONAB treated eyes, respectively. (n=4, 20 measurements from 4 eyes per treatment group).

We used transmission electron microscopy (TEM) to assess the ultrastructural changes of the RPE in more detail. Normal RPE consists of a monolayer of tightly packed cells that exhibit a highly polarised epithelial phenotype. They are separated from the choroid by Bruch's membrane (BM) (Fig. 4.13A). Adjacent RPE cells are interconnected via a network of cell-cell intercellular junctions with tight junctions located towards the apical surface of the lateral membrane (Fig. 4.13A,B). The apical membranes of RPE cells are covered with finger-like microvilli that surround the photoreceptor outer segments. RPE cells with reduced expression of ZO-1 or increased expression of ZONAB were flatter and more elongated in comparison with the cuboidal architecture of normal RPE cells suggesting that they had lost polarisation (Fig. 4.13C, D). Basal infoldings were absent or highly disorganised and many cells did not adhere closely to the BM. Apical

microvilli were also absent, disrupted cell-cell junctions and some multilayerisation were observed. The cells were often surrounded by cell debris or extracellular matrix components (Fig. 4.13C). Thus, downregulation of ZO-1 and overexpression of ZONAB in RPE cells *in vivo* appears to not only increase proliferation but also results in dedifferentiation. In contrast, RPE with reduced ZONAB expression retained some of the normal morphological characteristics of RPE cells but microvilli on the apical membrane and the basal infoldings appeared disorganised. Whereas only mature melanin vesicles could be observed in control eyes, different stages of melanin vesicle maturation were observed upon depletion of ZONAB expression (Fig. 4.13E). Microvilli, although reduced in number and size, were present and they surrounded the photoreceptor outer segments at the apical membrane (Fig. 4.13E). Even though the epithelial phenotype was often retained after ZONAB downregulation, these areas appeared thinner due to reduced cell density. Manipulation of ZO-1 or ZONAB expression thus affects RPE differentiation at the ultrastructural level. Moreover, downregulation of ZO-1 or overexpression of ZONAB promotes a mesenchymal-like phenotype similar to cases of epithelial-mesenchymal transition (EMT) [261-263].

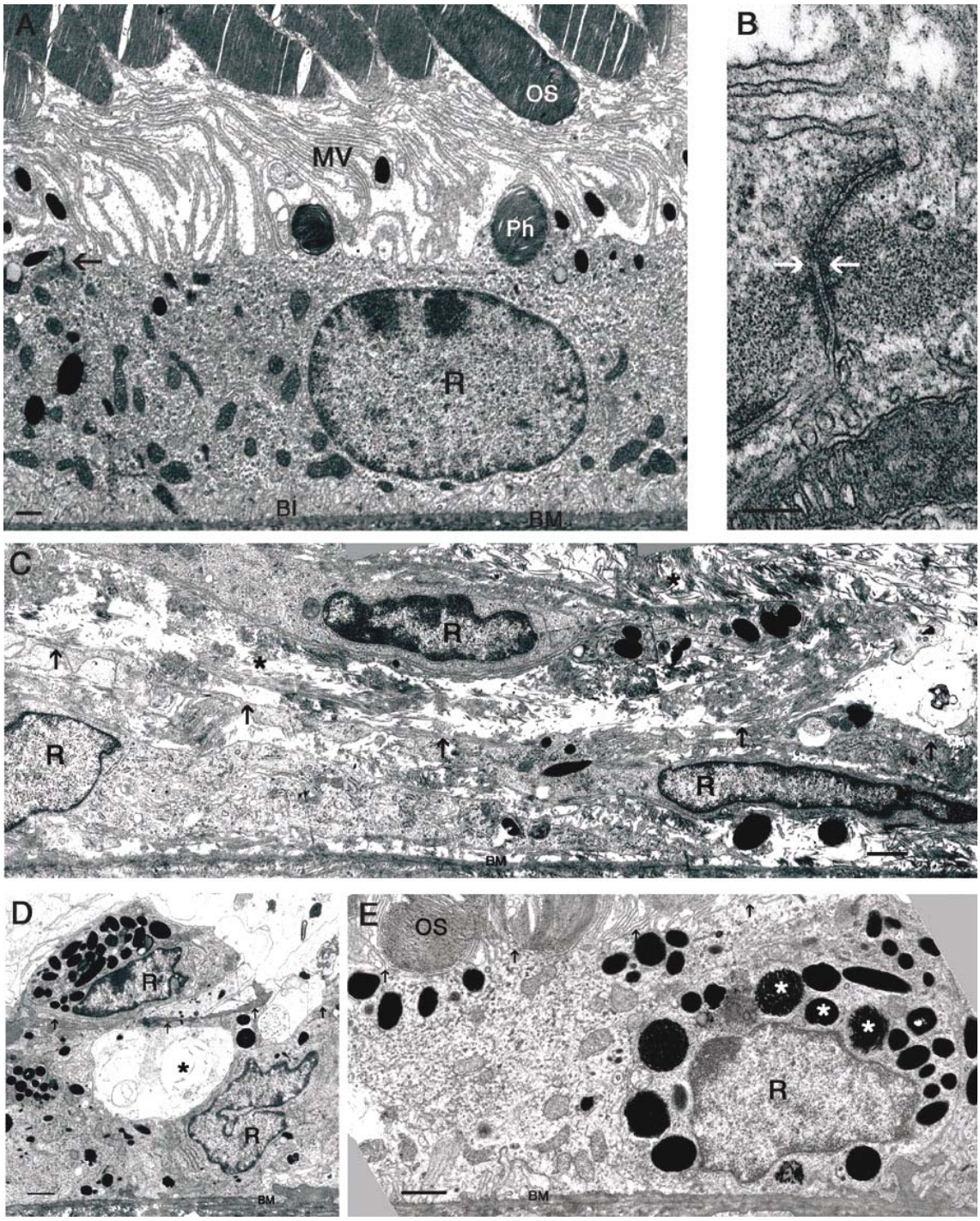

Figure 4.13: Ultrastructure of the RPE after 10 days following subretinal injection of vectors at 10^8 T.U./ml. In LNT.shGFP treated eyes **(A)**, the RPE monolayer lies on Bruch's membrane, has apical microvilli towards the photoreceptor outer segments the cells are interconnected by tight junctions (**A**, black arrow. **B**, white arrows). In eyes either with depleted levels of ZO-1 **(C)** or overexpressing ZONAB **(D)**, the RPE monolayer was highly disorganised with a marked loss of the epithelial monolayer characteristics, areas of RPE cells located on top of each other (see Figure 4.12: RPE pyknosis) and accumulation of extracellular debris was seen (**C**, asterisk). RPE cells appeared flattened and elongated with absent microvilli (black arrows), reduced basal infoldings, and mesenchymal-like

morphology. In addition, numerous vacuoles were present within the cells (**D**, asterisk). In eyes injected with LNT.shZONAB **(E)**, the RPE retained some of its epithelial characteristics, such as, microvilli present on the apical membrane and intracellular basal infoldings. However, melanin vesicle maturation was defective (asterisks). RPE cell size and the overall thickness of the monolayer were reduced (see Figure 6: RPE flattening). R, RPE cell nuclei. OS, photoreceptor outer segments. Mv, microvilli. BM, Bruch's membrane. BI, basal infoldings. Ph, phagosome. Size bar, 1 µm (except in **B**, 200 nm) (n=4 per treatment group).

During mesenchymal transition, epithelial cells start to express specific markers such as vimentin and glial fibrillary acidic protein (GFAP) [261,264]. We therefore analysed expression of these two markers by immunohistochemistry five days after injection. We did not observe vimentin or GFAP immunostaining in RPE from either LNT.shGFP or LNT.shZONAB injected eyes (Fig. X14A,B). Both markers were evident in the RPE following injection of either LNT.shZO-1 or LNT.ZONAB (Fig. 4.14C,D). Increased retinal GFAP staining of Müller cells was also observed in LNT.shZO-1, LNT.ZONAB and LNT.shZONAB injected eyes but not in the LNT.shGFP injected eyes, indicating increased levels of retinal stress caused by the RPE dysfunction (data not shown).

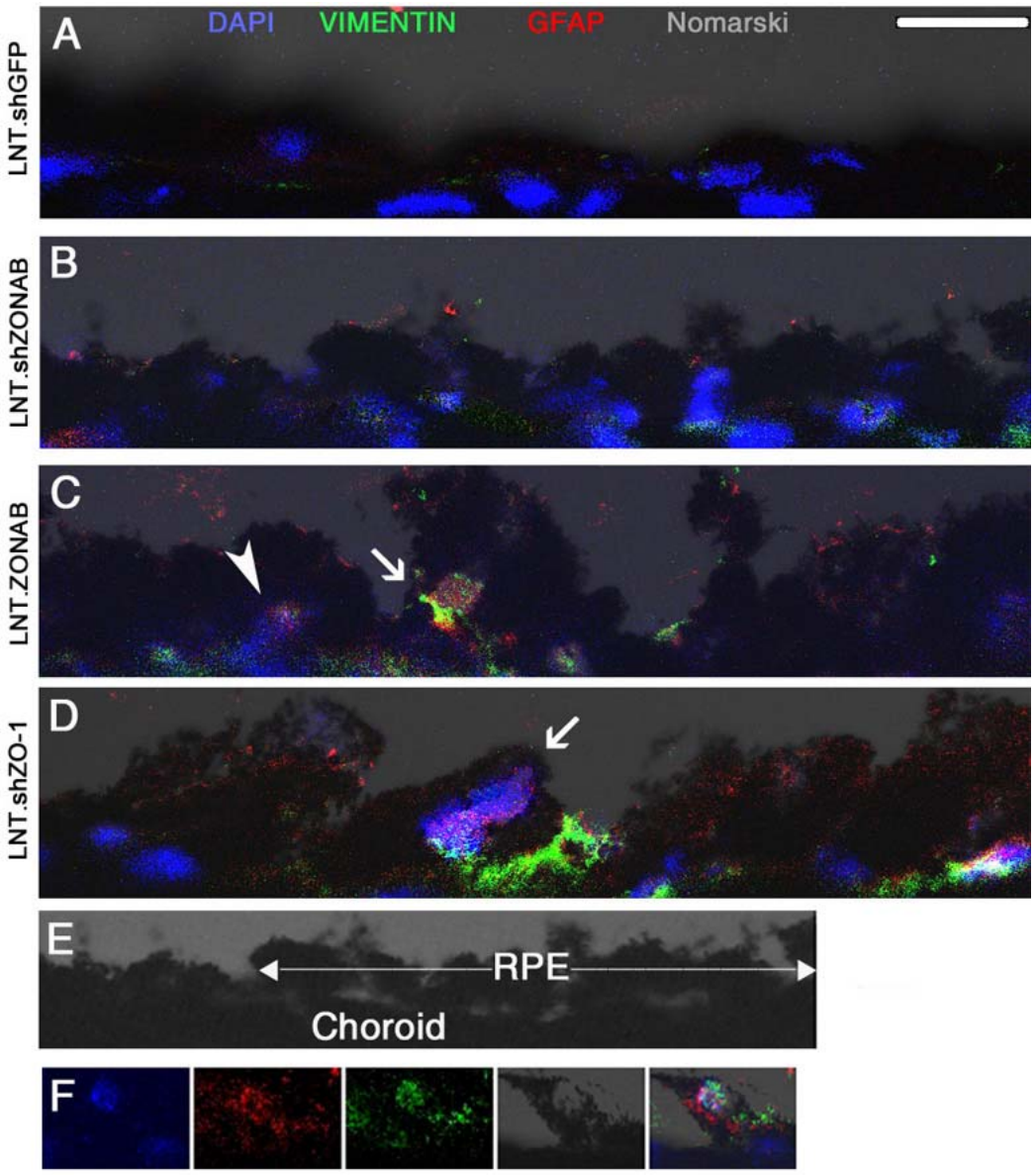

Figure 4.14: Vimentin and GFAP expression in the RPE 5 days following subretinal injection of vectors at 10^7 T.U./ml. Immunostaining on retinal cryosections obtained from treated eyes was performed using antibodies against vimentin and GFAP, two mesenchymal markers that are not expressed in the RPE. In LNT.shGFP **(A)** and in LNT.shZONAB **(B)** treated eyes no staining was observed, whereas vimentin and GFAP (white arrows) were upregulated in RPE cells following injection of LNT.ZONAB **(C)** and LNT.sh.ZO-1 **(D)**. Onset of expression of these mesenchymal markers was different between transduced RPE cells with some cells exhibiting only faint co-expression (**C**, white arrowhead). The LNT.shZONAB Nomarski channel is shown to indicate how the RPE monolayer can be distinguished from the choroid **(E)**. Split-channel image of a positive cell **(F)**. Size bar, 20µm. For panels **E** and **F** a x40 magnification objective was used for imaging. n=4 per treatment group.

4.4 Discussion

Cell-cell adhesion is essential for the morphological integrity as well as the control of proliferation and differentiation of epithelial cells. Here, we demonstrate that alteration of the levels of the TJ components ZO-1 and ZONAB leads to changes in RPE cell proliferation, differentiation and function. Downregulation of ZO-1, or the overexpression of ZONAB, led to the induction of proliferation as well as altered morphology and expression of two epithelial-mesenchymal transition markers, vimentin and GFAP. These changes correlated with areas of RPE cell loss evident on fluorescein angiography. This study describes a novel approach to study the role of TJ proteins in RPE function *in vivo* and demonstrates that the ZO-1/ZONAB signalling pathway plays a critical role in RPE homeostasis.

ZO-1 was the first TJ component to be identified [265]. It was shown to have a regulatory role in epithelial cell proliferation and gene expression in cells in culture [248] and its deficiency in mice causes an embryonic lethal phenotype associated with defected yolk sac angiogenesis and apoptosis of embryonic cells [266]. ZO-1 has multiple protein-protein interaction domains [267]. The SH3 domain is necessary and sufficient to regulate cell proliferation and interacts with the Y-box transcription factor ZONAB [249]. ZONAB was recently identified as a ZO-1–binding NACo protein that acts as a transcriptional activator of genes that regulate epithelial proliferation and differentiation. The cytoplasmic sequestration of ZONAB by ZO-1 regulates its nuclear localisation and, hence, its effect on gene expression. The ZO-1/ZONAB pathway regulates cell cycle progression and epithelial morphogenesis in cells in culture [249,256]. In this study we have demonstrated that downregulation of ZO-1 induced RPE proliferation and dedifferentiation that eventually resulted in cell loss and retinal degeneration. Overexpression of ZONAB resulted in a very similar phenotype, suggesting that ZONAB activation is the main reason for the observed effects in response to depletion of ZO-1 expression in RPE cells. Downregulation of

ZO-1 by LNT.shZO-1 has previously been shown to stimulate the transcriptional activity of ZONAB in epithelial cells in culture as ZO-1 functions as an inhibitor of ZONAB [249,256]. In this study, reduced ZO-1 expression in RPE cells using the same vector also resulted in an increase in ZONAB staining. A possible explanation for this might be that depletion of ZO-1 led to activation of ZONAB, which might in turn have caused a positive feedback loop on its expression as ZONAB is known to be upregulated during proliferation [249,259]. The similarities of the phenotypes observed following manipulation of ZO-1 or ZONAB levels together with their known biochemical and functional interactions suggest that ZO-1 and ZONAB exert their effects on the RPE by, at least in part, a common molecular pathway. This pathway is likely to involve transcriptional activation of ZONAB. However, it might involve alternative mechanisms. For example, ZONAB is a Y-box factor which are also known to participate in cytoplasmic processes such as mRNA translation [268]. Such a possibility is further supported by the strong cytoplasmic staining of ZONAB in RPE cells. In contrast, the complete absence of ZONAB immunostaining following injection of LNT.shZONAB at a titre of 10^7 T.U./ml could be explained by intercellular signalling along the RPE monolayer mediated by TJs. Silencing of ZONAB in transduced RPE cells could possibly trigger endogenous ZONAB inactivation through the ZO-1/ZONAB pathway in adjacent untransduced cells that diminish the basal expression levels of ZONAB.

Certain features of the induced phenotype are common to disorders of the human RPE. Increase in ZONAB activity and ZO-1 downregulation resulted in an RPE cell phenotype that resembled EMT. RPE cells not only started to express the mesenchymal markers vimentin and GFAP, their cuboidal morphology changed to a flattened structure lacking the clear morphological hallmarks of RPE cells such as clear cell junctions, apical microvilli and basal infoldings. Together with the induction of cell proliferation, EMT and co-expression of glial markers like vimentin and GFAP are all features of proliferative vitreoretinopathy (PVR) [261], a condition of exaggerated peri-retinal gliois induced by retinal detachment that is believed to be caused by proliferation and transdifferentiation of RPE cells. Furthermore, aberrant or

reduced retinal ZO-1 expression is associated with the blood-retinal barrier breakdown in diabetic retinopathy [262,269].

The molecular function of ZONAB in healthy RPE is currently not known. In this study we have observed that an increase in ZONAB activity results in increased RPE cell proliferation. As the postnatal RPE is no longer proliferative [270], the observed phenotype suggests that postnatal defects in RPE proliferation lead to RPE dysfunction. ZONAB activation has also previously been linked to the cellular stress response [251]. It is therefore possible that the phenotype we observed might also result from a cellular stress response in the RPE. It will thus be interesting to test if Apg-2, which is responsible for ZONAB activation in response to heat shock, is also important for RPE homeostasis and, if so, what types of retinal stress conditions stimulate Apg-2 to activate ZONAB in the RPE.

In this study, we demonstrated efficient lentiviral-mediated RNA interference and expression of junctional proteins in RPE cells *in vivo* that can be used to study the role of cell-cell adhesion-associated signalling mechanisms in a mature epithelial tissue. The induced phenotypes highlight the importance of ZONAB and ZO-1 in RPE homeostasis *in vivo*. However, additional characterisation of the expression profiles of dedifferentiated RPE cells are required to define the underlying molecular mechanism more clearly. Firstly, even though the reduction in ZO-1 and ZONAB protein levels was demonstrated using immunohistochemistry and, it would have also been useful to confirm gene suppression in mRNA levels by quantitative PCR. Although mRNA silencing can be suggested through the reduction in protein levels, it cannot be confirmed. In addition, comparison of mRNA and protein levels after suppression would provide a correlation between mRNA molecules and protein translation for the ZO-1/ZONAB pathway. In addition, we followed the phenotypes after subretinal delivery of vectors by tissue orientation and identification of phenotypical changes. The use of a reporter gene expression cassette would have made the process easier, but when designing the experiment this option was omitted as we have observed *in vitro* that high expression of reporter genes like eGFP can interfere with the

junctional machinery Furthermore, since immunohistochemistry provides a semi-quantitative approach in demonstrating alterations in gene expression, RNA-based data should also be generated to confirm not only the extent of ZO-1 and ZONAB downregulaiton, but also overexpression of EMT markers like GFAP and vimentin. Future work will include laser capture microdissection (LCM) of RPE cells and subsequent analysis of EMT marker expression by RT-PCR. Further analysis of ZO-1 and ZONAB in human tissues derived from patients with different retinopathies will help to elucidate the functional contributions of this TJ-associated signalling pathway in retinal physiology and pathology. Finally, we demonstrated how shRNA-mediated silencing in a potent viral context provides a very efficient way to study complex mechanisms and disease processes by selectively downregulating key components of a pathway.

5 AAV-mediated RNAi targeting of Prph2

5.1 Introduction

Peripherin-2 (*Prph2*, also known as *peripherin-rds* or rds) is an essential component of the photoreceptor outer segment (OS). It is required for morphogenesis of the OS discs that are produced everyday to replenish the OS tips that are being phagocytosed by the RPE. Mutations in *PRPH2* account for approximately 10 % of adRP cases. The aim of the work described in this chapter is to silence *Prph2* using AAV-mediated RNAi and to establish a robust vector platform for the treatment of patients with gain of function mutations in *PRPH2*.

5.1.1 Photoreceptor disc structure

A unique property of the OS is the presence of an elaborate intracellular membrane system that holds the phototransduction proteins and provides the requisite lipid environment. The maintenance of normal physiological function requires that these post-mitotic cells retain the unique structure of the outer segment regions; stacks of membrane discs in the case of rods and a continuous infolding of membrane in the case of cones. As shedding of older membranous material occurs, new material is synthesised, transported, and incorporated into newly forming OS membranes thereby maintaining the segment at a constant length. These processes are collectively referred to as rod outer segment or cone outer segment renewal.

Prph2 is localised in the periphery of OS rims which provide the structural substrate for the phototransduction cascade to take place. It is 32 kDa and

346 amino acid long tetraspanin-family protein with four transmembrane segments and a large intradiscal (EC-2) domain between the third and fourth membrane-spanning segments [271,272]. There is an *N*-glycosylation site at asparagine on residue 230 and an *O*-glycosylation site at serine on 263 (Figure 5.1).

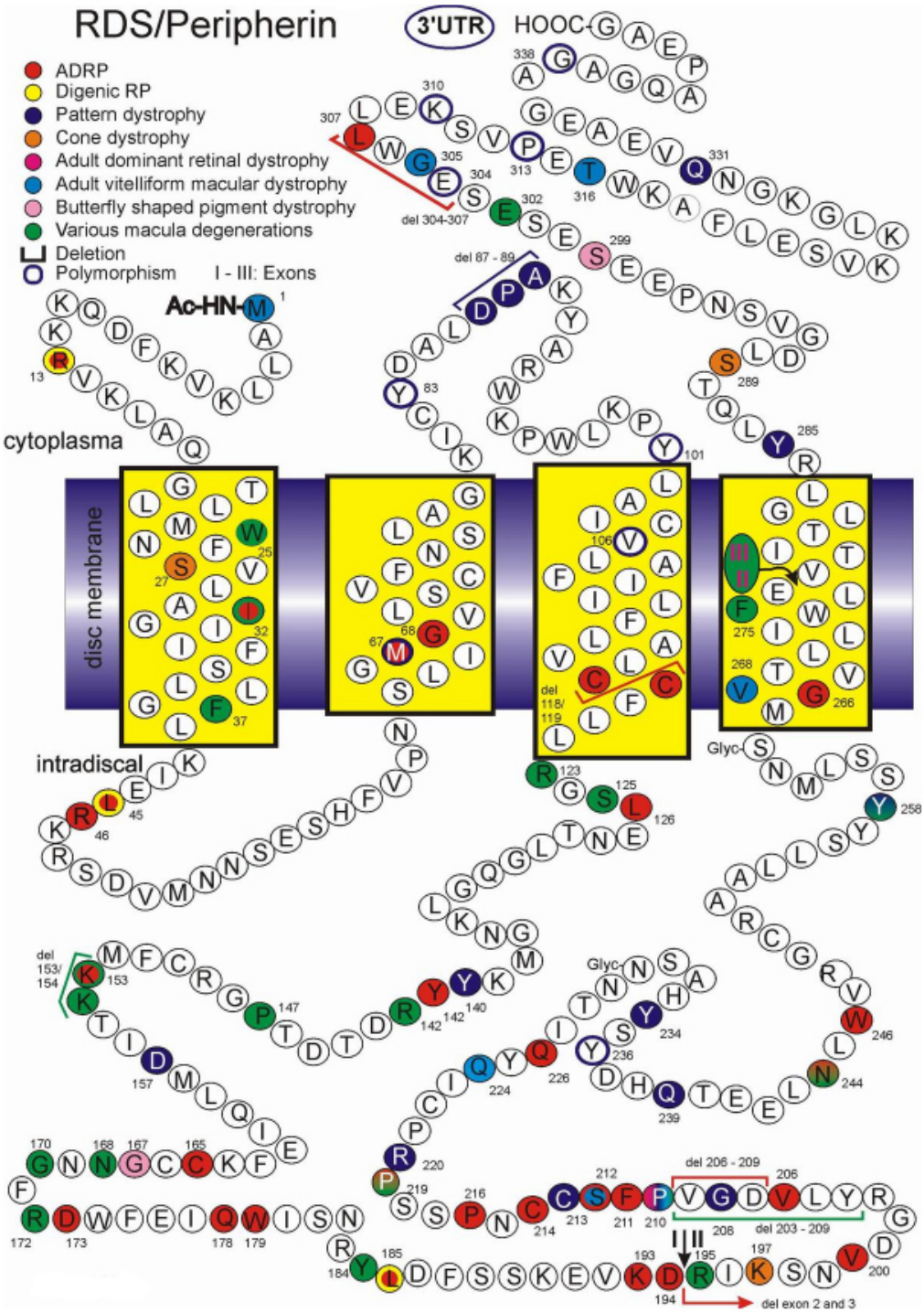

Figure 5.1: Structure of Prph2. Amino acid sequence of the human Prph2 protein. Insertions, deletions and amino acid changes involved in disease are annotated in colour. Murine Prph2 shares 92 % homology with its human orthologue (316 of 346 aa are identical). Glyc, glycosylation site. del, deletion. (Retina International Scientific Newsletter, http://www.retina-international.org)

Prph2 forms homodimers through the formation of disulphide bonds. The polymerisation of Prph2 into higher order oligomers is essential for OS stability. For the formation of these oligomers in rods Prph2 associates with a homologous protein, rod outer segment protein 1 (ROM-1), with which it can form non-covalently bound tetramers [273]. The function of these hetero-tetramers, as opposed to the essential Prph2 homo-tetramers, is not fully understood since absence of ROM-1 has an impact on rod OS ultrastructure but not on OS assembly [274]. It seems that ROM-1 is a non-essential accessory to rod OS morphogenesis catalysing Prph2 polymerisation. However, mutations in *ROM-1* are known to cause digenic retinitis pigmentosa when occurring with *Prph2* mutations as compound heterozygotes (see section 1.2.1).

Another vital step in OS morphogenesis is membrane fusion that gives rise to the highly organised structure of OS. There are around one thousand discs per rod OS and their formation is facilitated by the vesicular flattening properties of Prph2 and the enhancing effect on membrane fusion that ROM-1 has on the oligomer [275,276]. ROM-1 potentiates the fusogenic activity of the C-terminal domain (residues 311-325) of Prph2.

Prph2 maintains the cohesion of the OS discs and its function is essential for photoreceptor cell viability. In the absence of Prph2, OS discs that are being phogocytosed by the RPE layer do not reform. This leads to the degeneration of both rods and cones, although the latter have been shown to compensate for lack of Prph2 by forming open membranous structures that do not align with the RPE [277]. In effect, a diminished matrix area for the phototransduction cascade to take place causes photoreceptor cell dysfunction and death. Most of the information on the function of Prph2 and its essential role on photoreceptor viability has been acquired by studying the *Prph2*$^{Rd2/Rd2}$ or *rds* (retinal degeneration slow) mouse model, a naturally occurring model in which a 9.2 kb viral insertion in exon 2 of the gene abolishes its expression [278]. Recessive in nature, the null mutation of the *rds* mouse causes absence of OS, hence phototransduction events per photoreceptor cell are greatly reduced [271]. This process finally leads to

photoreceptor death probably through a programmed cell death pathway that is not clearly understood [279]. After two months of age, the *rds* mouse loses around 50 % of the photoreceptors.

5.1.2 Peripherin-2 dominant mutations and disease

Patients with missense *PRPH2* mutations develop adRP with late-onset retinal degeneration and signs of night blindness and tunnel vision by 50 years of age [19]. After screening 200 families and 2000 individuals, 67 mutations in *PRPH2* have been identified to date which constitute 8-9 % of adRP in patients [280,281] (Figure 5.1). *PRPH2* adRP can be monogenic in nature or digenic in conjunction with *ROM-1* mutations. In its digenic form, adRP rises from the failure of PRPH2 and ROM-1 to form hetero-tetramers and stabilise the oligomeric transmembrane protein complex that anchors rod OS [282]. Classical RP symptoms like diminished scotopic vision with delayed cone involvement are observed in the patients but sustained visual acuity and visual fields persist through middle age [283].

In order to study the disease processes underlying dominantly inherited Prph2 mutations, animal models engineered to express these mutations have been produced. Dominant gain-of-function mutations in *Prph2* cause slower degeneration in mouse and *Xenopus* models [284,285] with the exception of the Δ307 (deletion at codon 307) mutation that causes faster photoreceptor degeneration than the *rds* null mutation [286]. The P216L mutation is an amino-acid changing point mutation that affects the stability of the protein tetramers. P216L Prph2 is delivered to the OS where its accumulation has a dominant negative effect on OS formation (similar to the effect of the Δ307 mutation). Once in the OS, the mutated *Prph2* affects OS structure by either competing with the wild-type (wt) protein (C150S, L185P), or by incorporating and destabilising the structure (P216L) [285]. Other malformed proteins (e.g. C214S) fail to pass an inner segment checkpoint before OS incorporation. The different levels of severity in retinal degeneration observed in these

models reflect the phenotypical heterogeneity of *Prph2* gain-of-function mutations in patients This indicates their relevance in studying *Prph2*-associated dominant retinopathies.

5.2 In vitro siRNA evaluation

When undertaking RNAi experiments it is essential to select an siRNA target area that provides a high level of mRNA silencing and although most sequences will provide a certain degree of silencing, their efficiency may vary considerably [173,180,233,234,287]. A number of criteria for target selection been proposed (see section 1.5.2) and web-based siRNA design programmes take these into account when designing siRNAs. However, the only way to ensure selection of efficient molecules is to test the selected siRNAs in an *in vitro* cell-based platform that allows mRNA and/or protein level measurements.

5.2.1 Stable cell line generation & siRNA silencing

Human embryonic kidney fibroblasts (293T) were used to generate a cell line that stably expresses the murine *Prph2* cDNA. The *Prph2* cDNA was cloned into a lentiviral HIV-1 based backbone driven by an SFFV promoter (see section 2.5.2) and recombinant vectors were prepared. In order to ensure that there was only one integrated *Prph2* expression cassette, 293T cells were transduced at a limiting MOI (i.e. <1) and allowed to grow for a few days. In order to create a homogenous *Prph2*-expressing 293T cell line, clonal populations of positive cells were propagated from single cells. Although separation of cells expressing a target gene from untransduced cells is easily done using antibody staining and flow cytometry, in the case of *Prph2* this was not possible. The only antibodies available for Prph2 are raised against the C-terminus of the protein. Prph2 is a membrane-bound

protein and the C-terminus is cytoplasmic. Therefore, flow cytometric separation of *viable* Prph2-expressing cells was impossible. In order to overcome this limitation, the transduced 293T cells were plated in a 96-well plate at limiting dilutions and the single cells were propagated. A few cell clones were collected and total protein was extracted. The levels of endogenous Prph2 were assessed using Western blotting and the clonal populations of interest (293T/RDS^{+}) were selected and propagated further (Figure 5.2A). We selected a cell clone that expressed Prph2 at intermediate levels (Clone #8) for two reasons. Firstly, low Prph2 levels would not enable thorough silencing titration of selected siRNAs. Different siRNAs with varying efficiency could reduce the levels below detection leading to false conclusions about their potency. Secondly, too high levels of Prph2 affect 293T viability as it is an exogenous protein not naturally present in human embryonic kidney fibroblasts and its association with cell membranes affects culturing efficiency and cell confluency.

Three siRNA sequences targeting *Prph2* and a non-targeting control were selected using an online siRNA design application and named siRDS4, siRDS5, siRDS6 and siCON, respectively (see section 2.2.5; Table 1). Each of the three siRNAs target different areas of the murine Prph2 mRNA. More specifically, all three target murine Prph2 within the open reading frame with siRDS4 binding at nucleotide positions 674-692, siRDS5 at 365-384 and siRDS6 at 906-925. None of the three selected sequences share 100 % homology with the human orthologue. Murine and human *Prph2* genes share 81 % homology and no target areas that have 100 % complementarity with both genes while fulfulling the sequence design parameters could be found. For future applications in patients with dominant *Prph2* mutations, new siRNAs specifically targeting the human gene would have to be designed. The siCON target sequence was scanned for homology with murine and human genome databases using the BLAST alignment algorithm (http://blast.ncbi.nlm.nih.gov/Blast.cgi) and no positive hits were returned. However, the siCON molecule was not assessed *in vitro* to investigate whether it incorporates into RISC or whether it elicits any innate immune responses *via* the TLR3 pathway. The siRNAs were used to transfect the

293T/RDS$^+$ cell line at a concentration of 20 μM. Duplicate samples for each siRNA transfection were collected and total protein lysates were analysed using Western blotting for Prph2 (Figure 5.2B). Of the three siRNAs, only siRDS6 transfection resulted in significant silencing of *Prph2* at the protein level. Although the experiment should have been repeated to correct for the ambiguity observed in siRDS6 duplicate transfections, it was not repeated and the siRDS6 was selected as the target sequence of choice for the subsequent vector-based experiments.

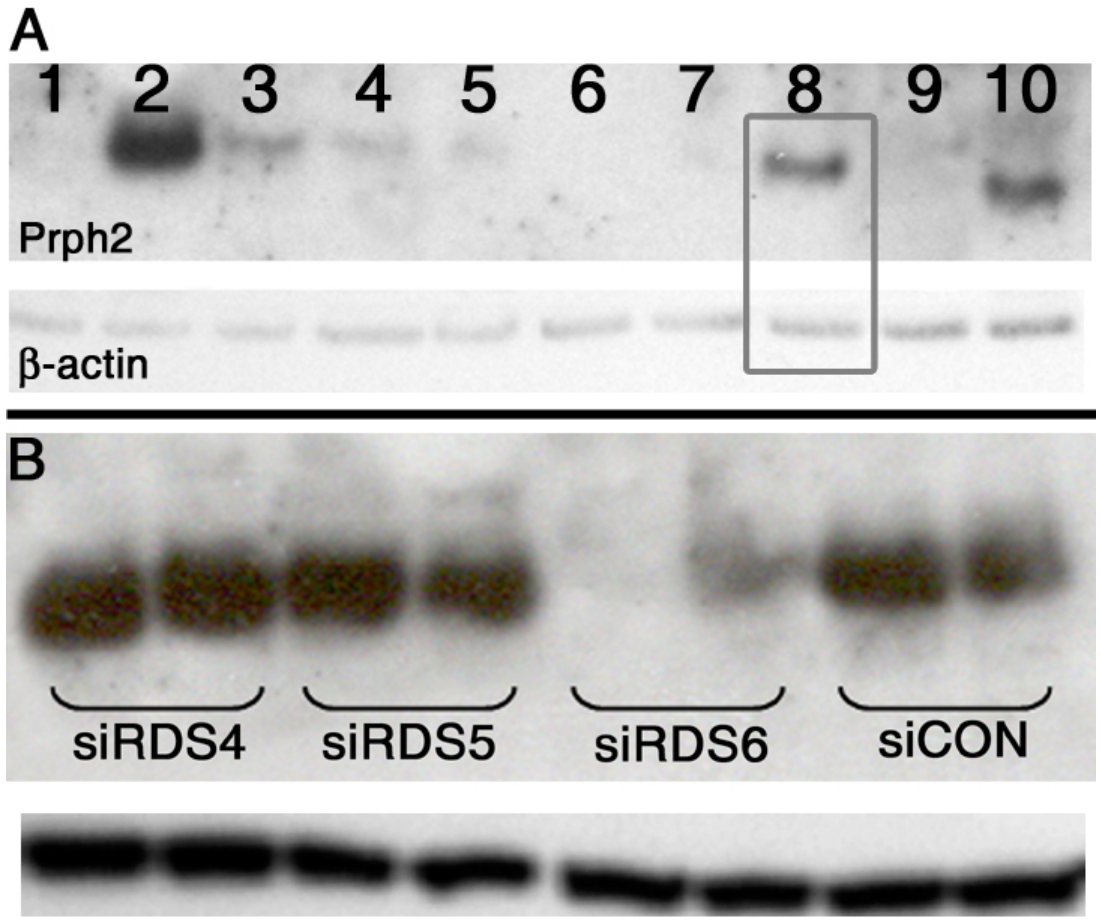

Figure 5.2: Generation of stable *Prph2*-expressing cell line and siRNA knockdown. (A) Western blot for Prph2 on 10 different clonal populations propagated from single 293T cells transduced with the LNT.RDS virus. Clones 2, 3, 4, 5, 8 and 10 expressed *Prph2*. Clone #8 expressed *Prph2* at approximately 5-fold *β-actin* levels and was selected for subsequent experiments. **(B)** Three siRNAs targeting *Prph2* at different regions (siRDS4,5,6) and a non-targeting control (siCON) were transfected into 293T/RDS$^+$ #8 at 20 μM. Only siRDS6 conferred significant silencing.

Having selected the most potent siRNA to silence Prph2, for further experiments we constructed an additional Prph2-expressing 293T cell line that expressed an altered Prph2 cDNA mutated at the target area of siRDS6. This was done in order to be able to test evasion of silencing by siRDS6 using the degeneracy of the code. The rationale lies in the "suppression-and-replacement" concept (see section 1.5.2) where an altered cDNA could be used for gene supplementation to counter effects of haploinsufficiency following downregulation of the mutated allele.

We mutated the cDNA of *Prph2* at the target area of siRDS6 (Figure 5.3). We selected the first three codons (9 nucleotides) in the targeted area for our mutation strategy for two reasons. Firstly, they included the "seed area" of the siRNA and their mismatch would not allow for siRNA:mRNA duplex formation. Secondly, they were in the centre of the siRNA target area which is essential for mRNA cleavage impeding its function, if the siRNA manages to attach itself to the mRNA "seed area".

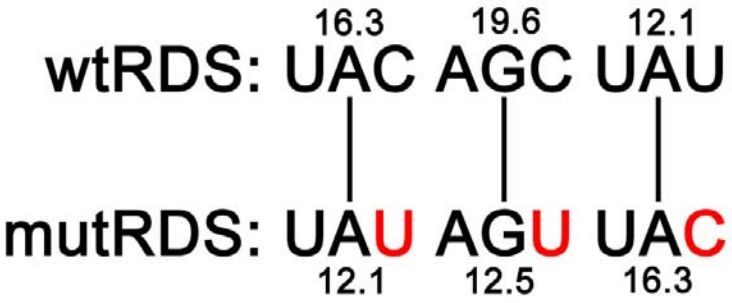

Figure 5.3: Nucleotide alterations between wtRDS and mutRDS. Site-directed PCR mutagenesis in mutRDS to alter nucleotides within the region targeted by siRDS6. Three nucleotides (in red) were altered (at 907-917 bp of *Prph2*) using the degeneracy of the genetic code to retain codon characteristics. Both nineplets encode for Tyrosine–Serine–Tyrosine (amino acids 234-236, see Figure 5.1). The relative abundances of tRNAs for each codon in mice are indicated.

The mutations were inserted using site-directed PCR mutagenesis and the new altered *Prph2* cDNA was named mutRDS (see section 2.2.6). The mutRDS cDNA was used to construct a stable expressing cell line (293T/mutRDS$^+$) in the same way as for 293T/RDS$^+$ (see section 2.5.2). Both cell lines expressed either the wtRDS or mutRDS cDNA from a single integrated copy of an SFFV-based expression cassette. The 293T/mutRDS$^+$ cell line was used later in order to test whether it could evade the silencing effect of the Prph2-targeting hairpin (see section 5.3).

5.2.2 shRDS expression vector

The siRDS6 sequence was cloned downstream of the U6 promoter using the mu6pro vector and the resulting plasmid was named mu6.shRDS6. Correct processing of the shRNA and levels of expression were assessed by plasmid transfection into the 293T/RDS$^+$ cell line (see section 2.3.5 for transfection method). Significant *Prph2* silencing was observed and with increasing efficiency that correlated with the increase in the amount of mu6.shRDS6 (Figure 5.4). A drawback of this experiment is the lack of RNA suppression data to couple the gradual decrease in protein levels following transfection of increasing amounts of mu6.shRDS6. Although the experiment should have been repeated to obtain a western blot of higher quality, it was not repeated and the mu6.shRDS6 plasmid was used to sub-clone the shRDS6 cassette for the subsequent vector-based experiments.

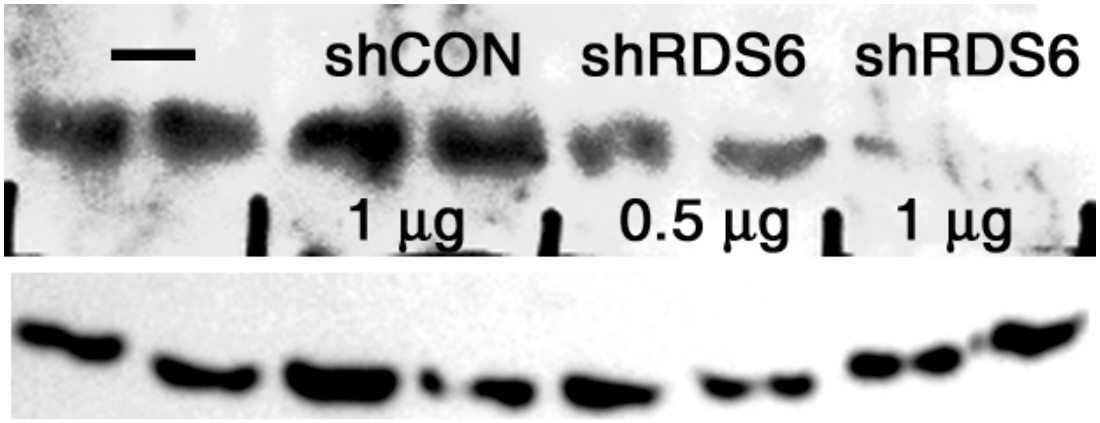

Figure 5.4: Silencing of Prph2 after transfection of hairpin expression cassettes. The stable cell line 293T/RDS^{+} was transfected with 0.5 µg or 1 µg of mu6.shRDS6 or 1 µg of mu6.shCON. No silencing of Prph2 was observed after shCON hairpin expression, whereas a dose-dependent silencing was observed after transfecting 0.5 µg and 1 µg of mu6.shRDS6, respectively. β-actin levels are displayed as a loading control. — = untransfected.

Next, we wanted to address the issue of alternative hairpin design using a miRNA template and whether it would increase the efficiency of the knockdown provided by the shRDS6 hairpin. Therefore, the miR-30 template (see section 1.5.2) was used to construct another hairpin targeting *Prph2*. The resulting hairpin retains the same target area as in shRDS6 and was named miRDS6 (see section 2.2.5; Table 1 for sequence). The same rationale was used to adapt the shCON sequence and the resulting hairpin was named miRCON.

The shRDS6, miRDS6 and miRCON hairpin expression cassettes were cloned into the pD10.RFP.poly backbone (as in section 5.2.3) and the plasmids were named pD10.RFP.shRDS6, pD10.RFP.miRDS6 and pD10.RFP.miRCON, respectively.

5.3 In vitro silencing of Prph2

Although the silencing capacity of the selected siRDS6 sequence was tested *in vitro* synthetically, the hairpin expression levels of the pD10.RFP.shRDS6 and pD10.RFP.miRDS6 plasmids had to be tested prior to the production of rAAV because of the plasmid backbone's viral nature. We had already determined that the pD10 AAV backbone is prone to intramolecular recombinations because of the presence of ITRs, jeopardising the function of the expression cassettes as well as the ability of the plasmid to generate rAAV particles.

All the pD10-based constructs also contained an RFP expression cassette that could be used to correct for variability in transfection efficiency. Hence, after transfection of pD10.RFP.shRDS6, pD10.RFP.miRDS6 and pD10.RFP.miRCON into 293T/RDS^{+} or 293T/mutRDS^{+}, the RFP^{+} cells (Figure 5.5) were selected for using FACS flow cytometry. The representative plots for the 293T/RDS+ cell line are presented in Figure 5.6. The transfections were performed in quadruplicates (n=4) for each plasmid but were not repeated.

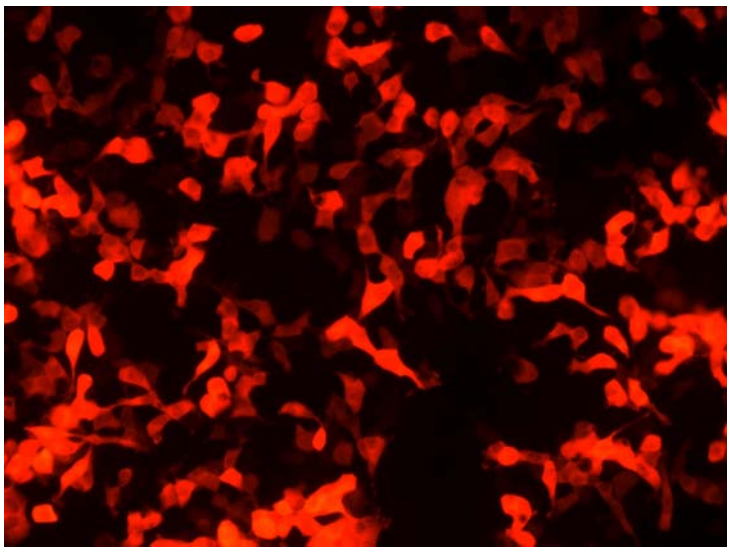

Figure 5.5: Indicative image of 293T/RDS^{+} cells expressing RFP. Twenty-four hours after transfection of 50,000 cells with 1 µg of pD10.RFP.miRCON, cell populations were assessed for RFP expression to confirm transfection efficiency. RFP expression is driven by a CBA promoter.

When sorting for cells, it is important to adjust the collection gate so that only viable cells are retrieved from the total sample population. This preset is important especially if further analysis on the sorted population is to be carried out (e.g. DNA/RNA/protein extractions). In our experiments, a negative control of untransfected 293T/RDS^{+} cells was used to determine both the gate for RFP detection as well as cell viability based on forward and side scatter characteristics (Figure 5.6; top panel). The middle panel indicates the total transfection efficiency of each sample according to the selected gate. Although in theory the sorter is able to select a near 100% pure population positive for the marker of interest, in reality the end population purity may vary. For this reason, it is sensible to re-count a fraction of the sorted cells to get an estimate of the sorting efficiency. The bottom panel in figure 5.6 indicates the end purity of each sample which can be used for post-analysis adjustments in order to correct for the dilution effect of the untransfected cells.

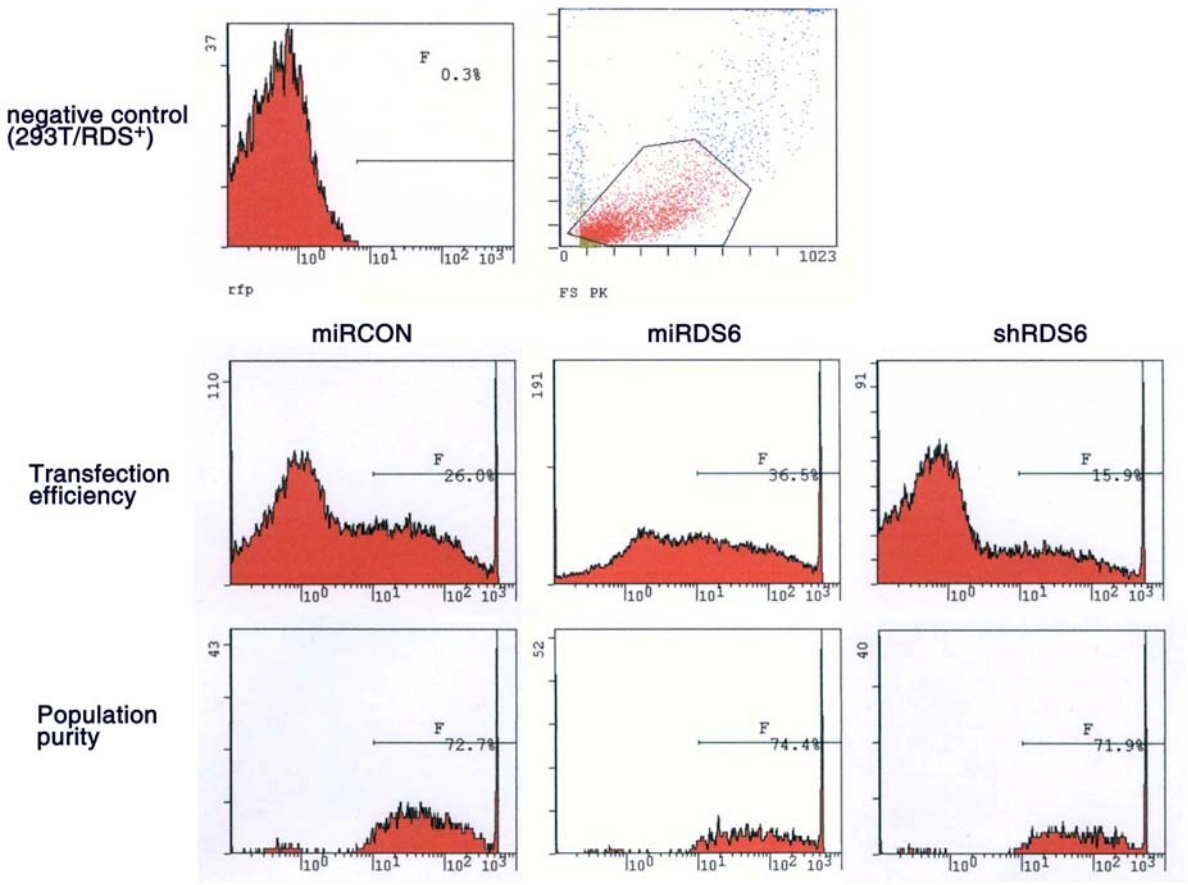

Figure 5.6: FACS plots of RFP$^+$ 293T/RDS$^+$ cells after transfection of RNAi cassettes. Untransfected 293T cells were used as a negative control to set the gate for the collection of healthy cells based on forward and side scatter characteristics. Representative transfection efficiency plots for each of the plasmids (miRCON, miRDS6 and shRDS6) are indicated together with the population purity plots after cell sorting for RFP$^+$ cells (72.7 %, 74.4 % and 71.9 %, respectively). For each sample 10,000 live events were counted.

The purified RFP+ cell populations were used to extract total RNA and generate total cDNA for real-time relative quantification (see section 2.6). Real-time PCR was performed on the cDNA samples using probe-based assays to trace the expression levels of *Prph2* and *β-actin* as a loading control (Figure 5.7).

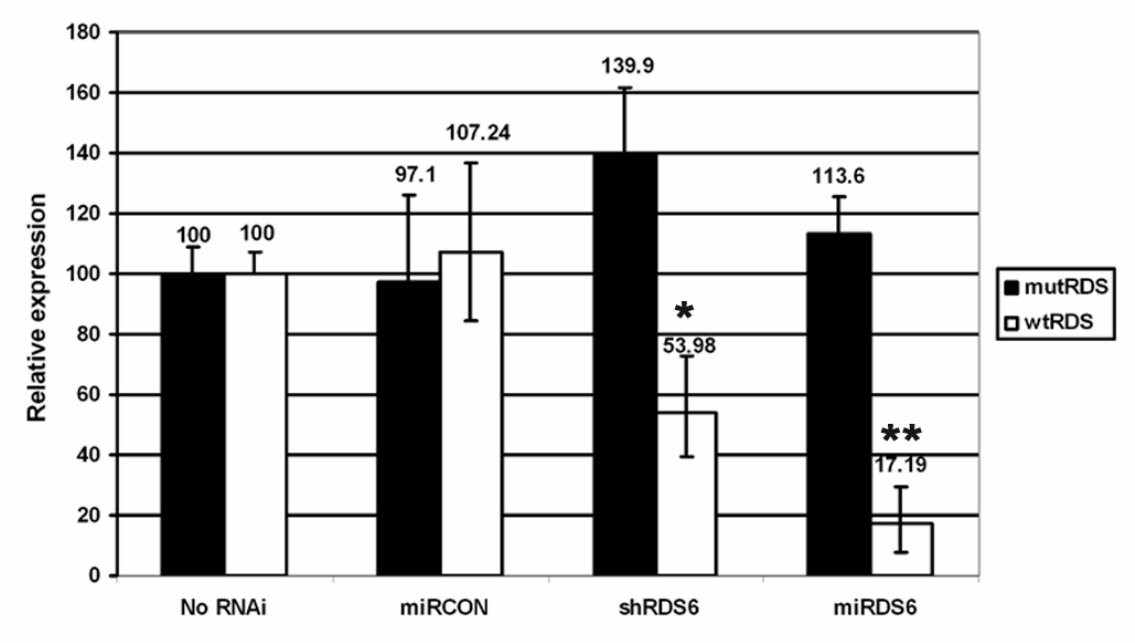

Figure 5.7: Silencing of *Prph2 in vitro* after transfection of RNAi cassettes. Relative expression of wtRDS and mutRDS in 293T/RDS^{+} and 293T/mutRDS^{+} cells, respectively (adjusted to β–actin levels) after transfection of pD10-based plasmids expressing miRCON, shRDS6 and miRDS6 hairpin cassettes. No silencing was observed for mutRDS in any of the transfections whereas wtRDS was only silenced by shRDS6 and miRDS6 constructs at 46 % and 83 % of the untransfected levels, respectively. All sample values were corrected for sorting efficiency. ***P*<0.05. ****P*<0.001 (Student's *t*-test; n=4, where 4 is the number of transfections performed per plasmid type).

The relative expression levels of the wild-type and mutated *Prph2* in comparison to the endogenous *β-actin* levels were measured for each sample. An untransfected sample for both tested cell lines was used to set the 100 % mark for the *Prph2/β-actin* ratio. After transfection of pD10.RFP.miRCON, no silencing of either wtRDS or mutRDS was observed as expected since the target sequence of this hairpin does not bind any murine mRNA sequences. Neither the shRDS6 or miRDS6 RNAi cassettes silenced the mutRDS cDNA indicating that the 3 inserted point mutations in the seed area of the target region abolished any siRNA:mRNA interactions. The wtRDS levels were reduced in both plasmid transfections. The shRDS6 cassette silenced *Prph2* at 46 % of the untransfected endogenous levels, whereas the miRDS6 cassette delivered a silencing of 83 % – an almost 2-fold increase in comparison with the shRDS6-mediated silencing.

The quantification of relative silencing suggested that hairpin design might have an impact on the final silencing capacity presumably because of the efficiency of hairpin processing. The shRDS6 and miRDS6 hairpin share exactly the same targeting sequence and differ only in the design of the hairpin loop, 5' and 3' flanking sequences. However, the alteration in design was able to increase the silencing potential of the same target area by approximately 90 %. Moreover, the control non-targeting miRCON hairpin did not exert any silencing on *Prph2* and the levels were comparable to the untransfected control. Finally, the potency of the RNAi cassettes indicated the integrity of the bicistronic system (RFP & RNAi) in the pD10-based plasmids suggesting that no recombination effects had taken place within the vector backbone and allowed their subsequent use in the preparation of rAAV for *in vivo* administration.

5.4 Efficiency of AAV-mediated silencing of Prph2 in vivo

After ensuring the integrity of the AAV vector plasmids that encode the RNAi cassettes, rAAV preparations were produced for each of the three RNAi expression vectors (pD10.RFP.shRDS6/miRDS6/miRCON). The provirus structure that would persist episomally in the transduced retinal cells after viral transduction is depicted in Figure 5.8.

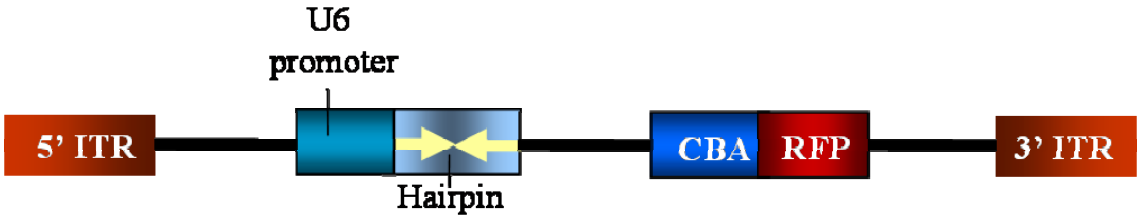

Figure 5.8: Schematic diagram of AAV vectors. Vector expressing a hairpin cassette targeting *Prph2* through an RNA polymerase III U6 promoter. Downstream of the RNAi cassette there is a chicken β–actin promoter (CBA) driving the expression of red fluorescent protein (RFP). ITR; inverted tandem repeats.

Although rAAV2/2 is the most widely used serotype to date in photoreceptor transduction studies, we considered employing rAAV2/8 due to the advantages it confers with regard to transgene expression levels [93,99]. Apart from the fact that the use of such a potent vector would reduce the timeframe for our experiments, it may be useful for treating mouse models with rapid degenerations.

After producing rAAV2/8 preparations for each of the RNAi cassettes, the titre of each preparation was determined so that equivalent numbers of viral particles could be administered.

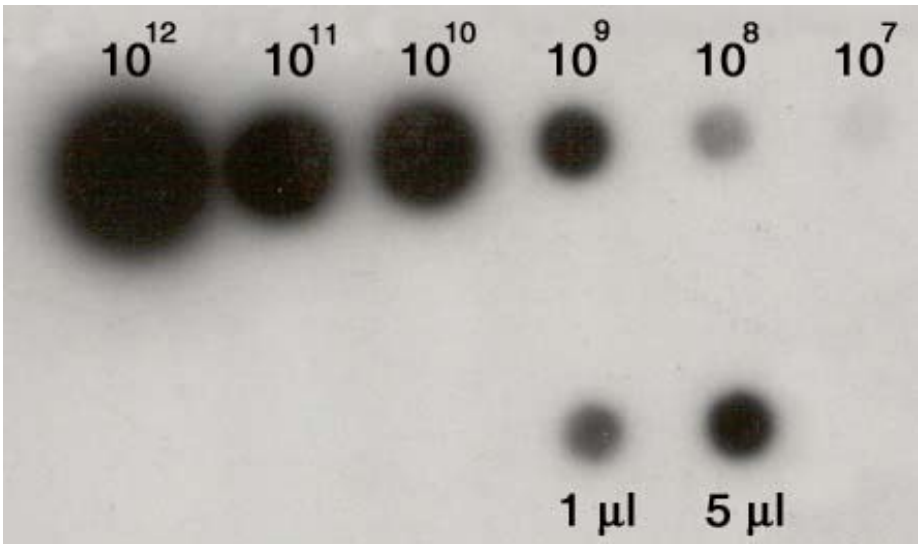

Figure 5.9: Autoradiogram of a dot-blot. The serial dilution of a plasmid DNA of known concentration served as a standard ladder. 1 µl and 5 µl of the virus suspension were loaded and the concentration was estimated by comparing the sample to the dilution series. In this case, it was estimated that the virus suspension had a concentration of $2x10^{11}$ particles/ml.

We delivered 2 µl of each of each vector subretinally at a concentration of $2x10^{11}$ v.g./ml (i.e. $4x10^{8}$ v.g. in 2 µl) into wt young adult mice (n=4 per constuct) (Figure 5.9).

At three weeks p.i., treated retinae (n=4 per treatment group) were dissected out and cells dissociated by treating with trypsin. RFP^{+} photoreceptors were selected from each retina after FACS sorting and the collected transduced photoreceptors were lysed in a manner appropriate for nucleic acid extraction. After total RNA extraction and cDNA generation, real-time PCR was performed on the samples to assess the endogenous *Prph2* levels in comparison with endogenous *β-actin* levels. The relative *Prph2* levels in the AAV2/8.RFP.miRCON control were set as 100 % against which the levels of Prph2 from the cells transduced with the two targeting AAV2/8 viruses were compared (Figure 5.10). AAV2/8.RFP.shRDS6 transduced photoreceptors exhibited a 19.6 % silencing of *Prph2 in vivo* – considerably lower than the equivalent silencing levels in the *in vitro* platform. The AAV2/8.RFP.miRDS6

virus showed a robust silencing of 82.6 % that not only surpassed the degree of silencing achieved by the shRDS6 cassette but also correlated with the *in vitro* silencing efficacy. Although the differences between the *in vitro* and *in vivo* sets of data could be explained by the difference in the host cell (immortalised human embryonic kidney fibroblasts versus murine photoreceptors) or the *Prph2* expression levels, they could also be explained by the difference in the RNAi design. The fact that the miRDS6 virus resulted in consistent and robust *Prph2* silencing might be explained by the nuclear processing advantage over the shRDS6 design based on "miRNA mimetics".

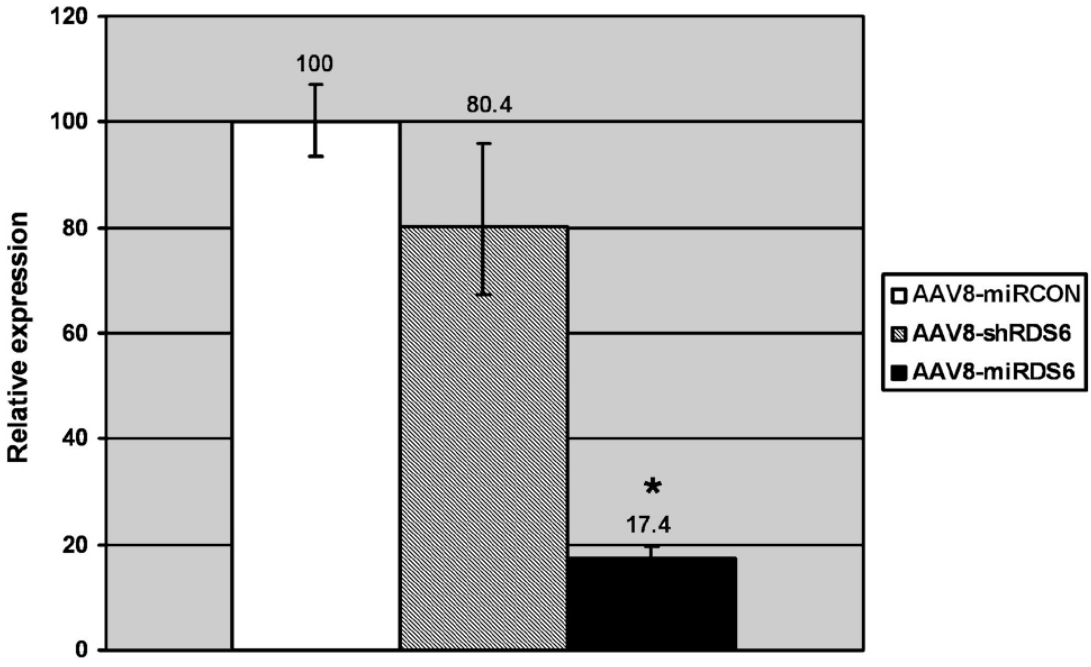

Figure 5.10: Silencing of *Prph2 in vivo* following subretinal injections of AAV2/8-RFP-RNAi viruses. For each treatment group, RFP^+ photoreceptors were collected by FACS sorting from dissociated retinae and *Prph2* expression levels were measured (adjusted to *β–actin* levels). In comparison to AAV2/8.RFP.miRCON injected eyes, *Prph2* levels were silenced 19.6 % and 82.6 % in eyes injected with AAV2/8.RFP.shRDS6 and AAV2/8.RFP.miRDS6, respectively. ***P*<0.001 (Student's *t*-test; n=4).

The morphological impact of *Prph2* knockdown in the retina and the downstream impact on photoreceptor survival was assessed using

immunohistological and ultrastructural analysis at 3 and 5 weeks p.i., respectively.

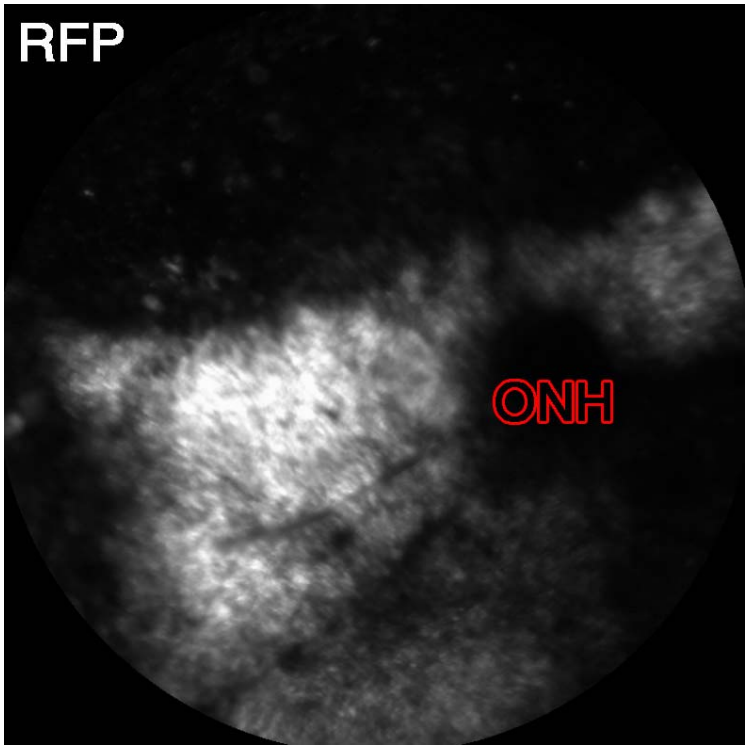

Figure 5.11: Fluorescent fundoscopy imaging of an AAV2/8.RFP.miRCON injected eye 3 weeks p.i. A single 2 µl subretinal injection was performed in the superior hemisphere. AAV2/8 viruses transduce photoreceptor and RPE cells. The RFP fluorescence in the fundus indicates strong expression of the provirus in transduced cells within the treated area. Representative picture shown for all titre-matched injected eyes. ONH, optic nerved head. RFP, red fluorescent protein.

Prior to the collection of treated eyes (n=4 per treatment group) for histological analysis, fluorescent fundoscopy was performed to image RFP expression *in vivo*. All treated eyes exhibited high levels of retinal RFP expression that correlated with the injected hemisphere. A representative fundus picture is shown in Figure 5.11. After collection, the eyes were carefully orientated in a way that the injection area would be included in sections taken around the optic nerve head. Immunohistochemistry for Prph2 was performed on cryosections taken from each eye and they were examined using confocal microscopy (Figure 5.12). At 3 weeks p.i. eyes

treated with the control AAV2/8.RFP.miRCON virus exhibited strong Prph2 staining within the treated area and in RFP^+ photoreceptors that correlated with the natural levels found in unprocedured animals indicating that no silencing of *Prph2* occurred in the transduced photoreceptors. AAV2/8.RFP.shRDS6 administration resulted in some decrease in Prph2 staining within the treated area that still allowed the maintenance of the outer segment layer. AAV2/8.RFP.miRDS6 treated eyes, in contrast, exhibited robust *Prph2* silencing that resulted in extensive decrease in Prph2 staining as well as extensive thinning of the outer segment layer within treated areas. Furthermore, it was also evident that the knockdown in *Prph2* expression had an impact on photoreceptor survival as the thickness of the ONL was slightly reduced. In order to quantify the photoreceptor loss and visualise the outer segment disorganisation, a second set of eyes was prepared for semithin sectioning 5 weeks p.i.

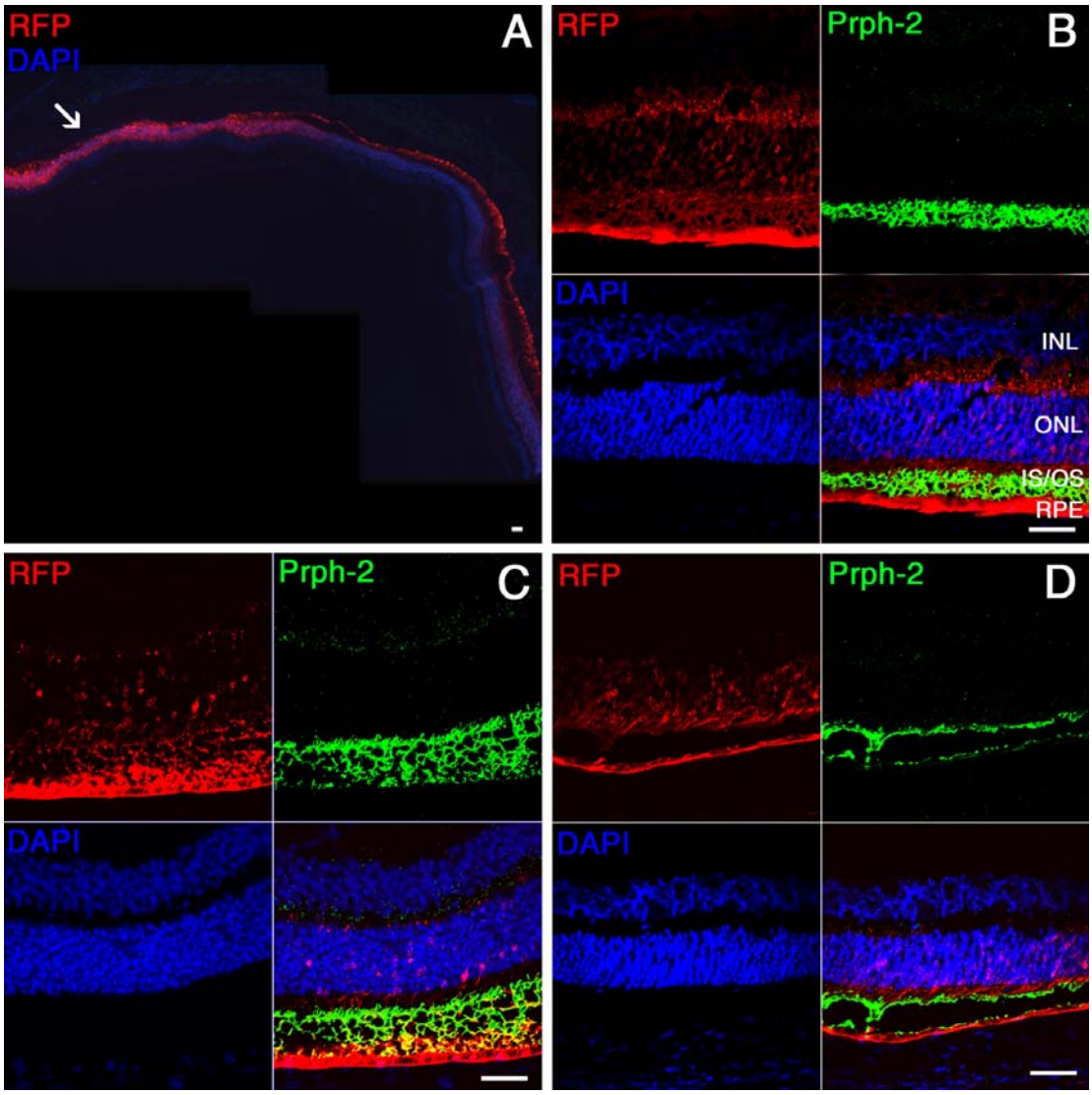

Figure 5.12: Immunohistological analysis of *Prph2* silencing in vivo 3 weeks p.i. (A) Each treated eye received a single 2 µl subretinal injection in the superior hemisphere that led to very high transduction levels of the ONL within the treated area. **(B)** In the AAV2/8.RFP.miRCON treated eyes strong Prph2 straining was observed throughout the treated area confirming that the control RNAi cassette does not lead to *Prph2* silencing. **(C)** In the AAV2/8.RFP.shRDS6 treated eyes some *Prph2* silencing was observed leading to vacuole formation within a loosely-packed outer segment layer. **(D)** In the AAV2/8.RFP.miRDS6 treated eyes low levels of Prph2 immunoreactivity were detected within the treated area confirming the levels of silencing observed in figure 5.10. Size bar, 20 µm (except in **A**; 10 µm). INL, inner nuclear layer. ONL, outer nuclear layer. IS/OS, inner segments/outer segments. RPE, retinal pigment epithelium. n=4 eyes per treatment group.

Low (x20) and high (x40) magnification pictures of representative areas from semithin sections are depicted in Figure 5.13 together with their

corresponding electron micrographs. The retinal architecture in control AAV2/8.RFP.miRCON injected eyes was normal with well organised outer segments and unaffected ONL. In AAV2/8.RFP.shRDS6 treated mice, although the ONL thickness appeared equal to that in the control, the outer segment layer was highly disorganised and reduced in size. Note the fragmented stacks of discs that piled up in the IPM indicating inefficient outer segment regeneration. The reason for outer segment disorganisation lies presumably in the reduced rate of Prph2 assembly at the connecting cilium where normally tightly packed stacks of discs are added to compensate for those lost by RPE phagocytosis. In AAV2/8.RFP.miRDS6 treated eyes the outer segment layer was almost absent with certain areas presenting a thin layer of highly disorganised discs. Such a dramatic loss of outer segments was expected in light of the highly reduced Prph2 immunostaining 3 weeks p.i. In addition, the impact of Prph2 loss on photoreceptor survival was evident by the thinning of the ONL which appeared dramatically reduced in comparison to control eyes. Quantitative measurements of photoreceptor cell numbers from 32 sections (n=4) for each treatment group are presented in Figure 5.14. From these measurements, it is evident that the loss in Prph2 caused rapid photoreceptor degeneration within 5 weeks of treatment in the AAV2/8.RFP.miRDS6 injected eyes leading to a reduction of photoreceptor nuclei to 54 % of the number found in the AAV2/8.RFP.miRCON treated eyes. The rate of *Prph2* silencing by the shRDS6 RNAi cassette did hinder outer segment organisation but was not potent enough to reduce intracellular levels to such an extent that would trigger extensive photoreceptor cell death (95 % of AAV2/8.RFP.miRCON numbers).

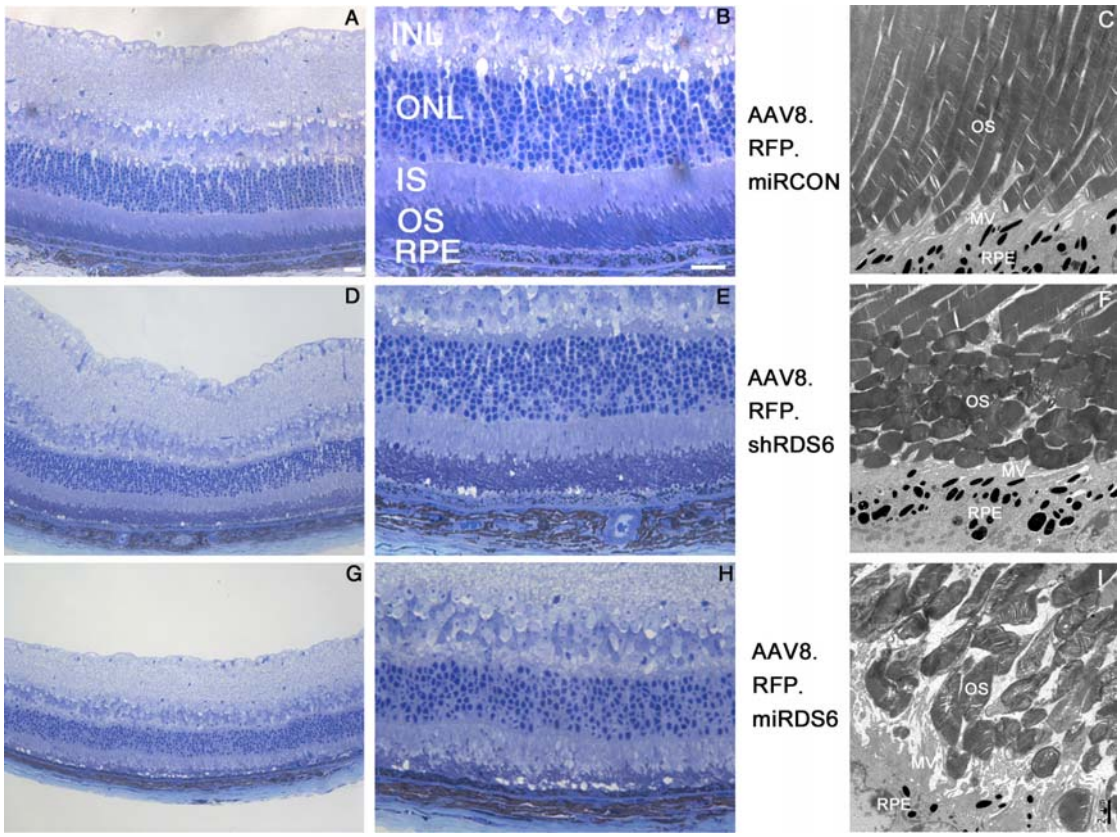

Figure 5.13: Morphological and ultrastructural analysis of *Prph2* silencing in vivo 5 weeks p.i. Semithin (left panel) and EM (right panel) pictures of AAV2/8.RFP.miRCON **(A,B,C)**, AAV2/8.RFP.shRDS6 **(D,E,F)** and AAV2/8.RFP.miRDS6 **(G,H,I)** injected eyes. **(C)** AAV2/8.RFP.miRCON treated eyes showed normal retinal ultrastructure with healthy outer segment morphology. **(F)** AAV2/8.RFP.shRDS6 treated eyes showed highly fragmented outer segments throughout the treated area that accumulated in the IPM. **(I)** AAV2/8.RFP.miRDS6 treated eyes had lost most of the outer segment layer with highly disorganised disc structures accumulating between the inner segments and the RPE. OS, outer segments. Mv, microvilli. RPE, retinal pigment epithelium. Size bar, 20 µm (semithin panel), 2 µm (ultrathin panel). INL, inner nuclear layer. ONL, outer nuclear layer. IS, inner segments. OS, outer segments. RPE, retinal pigment epithelium. n=4 eyes per treatment group.

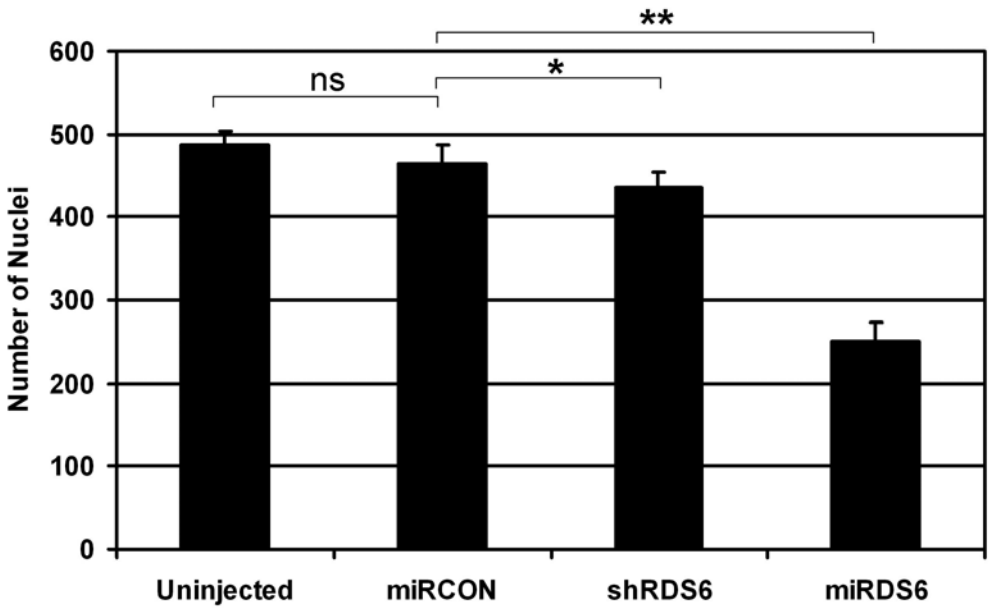

Figure 5.14: Photoreceptor nuclei quantification in AAV.RFP.RNAi treated eyes 5 weeks p.i. The photoreceptor nuclei from pictures of semithin sections for each treated eye were counted and plotted. There was no significant difference between the number of nuclei in uninjected and AAV2/8.RFP.miRCON injected eyes. However, a significant reduction in photoreceptor nuclei numbers was observed for both AAV2/8.RFP.shRDS6 and AAV2/8.RFP.miRDS6 treated eyes showing a 5 % and 46 % reduction in numbers, respectively, in comparison to AAV2/8.RFP.miRCON injected eyes. Nuclei counts from 32 pictures of semithin sections taken around the optic nerve head for each treatment group. ***P*<0.05. ****P*<0.001 (Student's t-test; n=4 per treatment group).

5.5 Discussion

In this study, the direct comparison of the shRDS6 and miRDS6 hairpins enables us to assess how the difference in RNAi design can affect the silencing of the same targeting sequence *in vitro* and *in vivo*. The standard 6 nt loop-design of shRDS6 silenced endogenous *Prph2* levels by 46 % *in vitro* and 20 % *in vivo*. The miR30-adapted miRDS6, however, silenced endogenous *Prph2* levels by 83 % *in vitro* and *in vivo*. Whereas shRDS6 lost half of its potency across experimental platforms, miRDS6 was highly consistent in silencing *Prph2*. Of course, the difference in shRDS6 downregulation could be accounted for by the difference in initial *Prph2* expression levels that differ between the stable-expressing cell line used in the *in vitro* experiments from the endogenous levels in a wt murine retina. However, both design strategies were tested and the miR-based strategy appears to consistently and efficiently silence *Prph2* in both *in vitro* and *in vivo* experimental platforms.

Not only was miRDS6-mediated silencing consistent between *in vitro* and *in vivo* sets of data, it also delivered a significant morphological effect in the treated retinae in comparison to shRDS6. Silencing of *Prph2* did not only occur at the mRNA level but also at the protein level as demonstrated by a reduction in Prph2 immunohistochemistry levels and reduced numbers of photoreceptorss caused by lack of Prph2 after 5 weeks of treatment. The use of rAAV2/8 provided high levels of hairpin expression and led to a 46 % reduction in photoreceptor cell numbers. Such a reduction in photoreceptor cell numbers is bound to have an impact on visual function, however it would have been useful to quantify the visual loss using ERGs. Although previous studies in animal models have demonstrated knockdown of mutations in photoreceptor-specific genes, this is the first study to demonstrate a significant morphological impact on photoreceptors following silencing of a highly expressed gene.

The adaptability of miRDS6 in different experimental contexts (human cells and mouse retinae) lies in its miR30-based design. The two main enzymes in miRNA processing are Drosha and Dicer. In miRNA mimetics, the sequences are altered so that the molecule has restriction sites compatible with those recognised by Drosha and Dicer. Correct Drosha processing together with the natural loop sequence increases the levels of nuclear export, possibly by Exportin 5. Correct Dicer processing increases RISC incorporation and, hence, silencing effect. The role of the hairpin's secondary structure is very important in the RNAi pathway and miRNA-based design has been shown to mitigate shRNA-induced toxicity in murine brain [194,288]. McBride and colleagues noted that the brain was very sensitive in shRNA-related toxicity even by a non-targeting hairpin. A miR30-based design abolished the toxicity caused by the shRNA indicating that cellular processing of the hairpin plays a role in off-targeting or pathway saturation. In an elaboration of that study, Boudreau and colleagues showed that shRNAs disrupt miRNA biogenesis causing neurotoxicity in mouse cerebella [288]. The concept of minimising toxicity by entering the natural pathway of RNAi at an earlier point is of considerable interest for potential clinical application, and considering their increased potency [193], miRNA approaches are likely to attract increasing attention.

The use of the miRNA-based design is not a necessity and to date numerous studies have efficiently downregulated genes *in vitro* and *in vivo* using shRNAs. However, each tissue has different sensitivity to toxicity and each target may trigger different stress pathways. Adapting the design to utilise a more natural template could minimise unwanted secondary effects as well as delivering higher levels of silencing when required. Although this study did not focus on testing various miRNA sequence templates, there is an important experiment missing from the comparison studies between miR30-based and standard design hairpins. RNase protection assays for the *in vivo* part of this study would have provided useful information on the amount of mature siRNAs generated from each cassette (miRDS6 vs. shRDS6). Such work will be carried out in the future to determine whether it is the amount of siRNAs that it is increased or their ability to enter RISC more efficiently.

Further work should be carried out to evaluate hairpin expression in relation to endogenous miRNA levels. The expression of the hairpin depends on the promoter used and the copy number of the RNAi cassette. Silencing should be achieved with the lowest possible hairpin expression levels in order to avoid saturating the endogenous miRNA pathway [289]. Optimised promoters and the comparison of their expression levels with those provided by endogenous miRNA promoters using real-time PCR, could optimise dosage in order to avoid side-effects associated with intracellular toxicity and activation of the host immune system.

6 Discussion

6.1 Therapeutic gene silencing

Whereas gene replacement approaches have been used successfully for treating animal models of recessive disorders, the treatment of dominant retinopathies is often more complicated. In dominant disease, the mutated allele may exert a toxic effect on the cell and in these cases gene supplementation on its own may not suffice. The requirement for an inhibiting agent that abolishes the expression of the mutant gene has led to the development of gene silencing techniques such as ribozyme and antisense RNA technologies. Whilst ribozyme and antisense RNA intervention have been used in animal models of retinal degeneration to ablate mutant rhodopsin alleles and downregulate caspase-3, the levels of inhibition did not lead to significant amelioration of the phenotype [136-140].

Around ten years ago, the development of RNAi paved the way for the development of much more effective methods for ablating gene expression. The recent success of RNAi is very promising as the technique is still developing and RNAi vectors are constantly being optimised in order to deliver stable gene silencing over longer periods of time and with minimal adverse effects.

There have been several studies to date that have employed RNAi for the treatment of animal models of adRP [232-236,290]. All of the published studies used standard shRNA design for their expression vectors and AAV-mediated delivery to the retina. The two most promising have emerged during the last couple of years from Jane Farrar's group in Ireland [235,236]. O'Reilly and colleagues used a "suppression and replacement" approach in order to rescue a transgenic mouse expressing the rhodopsin P23H mutation using AAV2/5-mediated delivery [235]. The "suppression and replacement"

approach aims to downregulate all endogenous mRNAs of the gene of interest, irrespective of allelic origin, prior to gene supplementation with a codon-modified cDNA. Due to the stringency of the RNAi mechanism, a few point mutations in the cDNA can abolish shRNA silencing while retaining the wt amino acid sequence of the protein. In their study, a potent shRNA targeting rhodopsin was used to efficiently silence all endogenous transcripts (<10 % of control levels) while the codon-modified cDNA (8 nt mismatches with the shRNA) evaded silencing. Although there was a significant photoreceptor rescue after 10 days of treatment, no later timepoints were assessed to follow the persistence of the rhodopsin knockdown. Earlier this year, Chadderton and colleagues demonstrated the most promising and persistent amelioration of phenotype in the transgenic mouse expressing the human Pro347Ser mutation [236]. The group used the same AAV2/5-based RNAi vector as in the study by O'Reilly and colleagues to silence the human mutation but with a reporter gene in place of the codon-modified cDNA. The reason for this was that their model was heterozygous for the dominant human mutation that was bred on a wt background ($Pro347Ser^{+/-}Rho^{+/+}$) and hence no further supplementation was required. By silencing the Pro347Ser toxic allele, they observed a 2-fold increase in ERG amplitudes in treated eyes in comparison to control eyes ten weeks after subretinal delivery [236]. Although this study successfully demonstrated *in vivo* silencing of a mutated allele that directly contributed to functional rescue of the model, the amelioration in visual function was brought about by the wt background haplotype for rhodopsin and not by supplementation with an engineered cDNA as would probably be required for clinical applications. It will be interesting to see future results in which the silencing of a dominant allele is coupled with supplementation to treat any underlying genetic haploinsufficiency.

Treating patients with dominant retinopathies in the future will mainly depend on the efficiency and safety of vectors delivering hairpin expression cassettes in the affected retinal cells or on more potent neurotrophic agents. However, dominant retinal disorders are not the only ocular conditions amenable to treatment by RNAi. A number of other applications are currently advancing

towards the clinic. These focus on focusing on angiogenesis and especially the delivery of anti-angiogenic agents such as siRNAs targeting VEGF [225-229], a key regulator of neovascularisation. It has been shown to be downregulated following delivery of siRNAs or virus-mediated delivery of shRNAs in models of CNV [227-229]. It is likely that the first clinical trials using RNAi in the eye will involve intravitreal injection of siRNAs targeting VEGF in AMD patients to halt CNV, the hallmark of “wet” AMD. To date, there are two promising siRNA molecules targeting VEGF, bevasiranib and AGN211745, and both are currently in pre-clinical development [291,292].

6.2 miRNA mimetics

RNA interference involves a complex pathway that takes place in both the cell nucleus and the cytoplasm (see Chapter 1.4) and its components are still being characterised. During the last five years, the discovery of endogenous miRNA molecules that regulate gene expression has led to an alternative shRNA design that results in more potent and stringent silencing. In order to optimise siRNA design and reduce adverse toxic effects while maintaining silencing capacity, non-standard designs, such as asymmetric siRNAs or miRNA-based hairpins, have been devised [293]. A number of studies on hairpin design have shown that target sequences incorporated in a miRNA-based design can deliver more potent silencing in comparison with the standard design, while reducing toxic side-effects [193,194,288,289]. The reasons why miRNA-based hairpins may confer more efficient silencing or reduce shRNA-related toxicity are not yet known. It is possible that the 3'- and 5'- sequences as well as miRNA-based loops facilitate Drosha digestion or nuclear export by Exportin5, respectively, thereby increasing the cytoplasmic concentration of the mature hairpin. It has been suggested that mimicking the endogenous miRNA pathway might reduce saturation-dependent toxicity [194].

AAV vectors have been used extensively to transduce photoreceptors and in this study we selected AAV2/8 particles to deliver RNAi expression cassettes to the murine retina to silence *Prph2* which is the second most highly expressed gene in the retina (after rhodopsin) and hence a useful candidate gene to test the efficacy of hairpin-mediated silencing *in vivo*. We constructed an AAV vector with two separate expression cassettes: a reporter gene (RFP) expression cassette to follow transduction efficiency and onset of expression within the treated areas, and an RNAi cassette to silence *Prph2*. The selected RNAi target sequence that was validated *in vitro* (RDS6) was placed in the AAV hairpin expression cassette using two design strategies: One in which the hairpin is formed using the standard short hairpin design (sense–6nt-loop–antisense; shRDS6), and another in which the hairpin

design was based on the sequence of the endogenous miR30a (miRDS6). Both vector plasmids were used to generate AAV2/8 particles and the preparations that were titre matched and subsequently delivered in the subretinal space of wt mice. In this way, we aimed to compare the design strategies (sh vs. miR) and their effect on the efficacy of our *Prph2* target sequence (RDS6). Although both shRDS6 and miRDS6 hairpins silenced *Prph2 in vitro* and *in vivo*, we found that the miR30-based design significantly increased the potency of suppression achieved. The severity of outer segment malformation caused by *Prph2* knockdown also had an impact on photoreceptor viability with the miRDS6-treated eyes showing almost a 50 % reduction in nuclei counts compared to controls. Although loss of visual function was not assessed using ERGs since this study concentrated on proof of concept rather than rescuing a model of disease, it would have been useful to follow outer segment degeneration due to lack of Prph2 in association with a decrease in visual responses. That way, comparisons between the treated mice and the *rds* mouse model could have been drawn.

These results demonstrate miRNA-based silencing of a retinal gene *in vivo* for the first time as well as the use of AAV2/8 particles for the delivery of an RNAi cassette in the neuroretina. Although the miR30-based design significantly increased the silencing potential of our *Prph2* target area, we cannot conclude that every RNAi application will benefit from a miRNA-based design. An experiment omitted from this study that would have provided a preliminary answer to this question was RNase protection assays. Had RNase protection assays been performed for both the miRDS6 and shRDS6 hairpins, it would have been possible to identify whether the miR30-based design resulted in higher amounts of mature siRDS6 being produced or whether the miR30-based design increases processing efficiency without necessarily increasing the final output of mature siRNAs. However, this study adds weight to the rationale that miRNA-based silencing might enhance the efficiency of RNAi, especially in cases where target selection is very limited. For example, in allelic-dependent silencing of a point mutation the target area cannot be altered as the mutation has to be placed in the middle of the hairpin. Alternative miRNA-based design would be one way to enhance the

knockdown effect of the hairpin if the levels achieved by conventional hairpin design are not high enough.

6.3 Using RNAi to study pathophysiology

Stable genetic silencing can be used not only for therapeutic interventions to treat dominant disorders, but also in studies to elucidate molecular pathways and disease processes. As with therapeutic approaches, an RNAi cassette has to be delivered efficiently into the target tissue using an appropriate vector. Lentiviruses have been used extensively for the transduction of the RPE and one recent study successfully used a lentiviral vector to deliver an RNAi cassette targeting FGF-2 [239]. The potential advantages of using RNAi to study gene function and molecular pathways is the reduced cost and shorter time required in comparison to more conventional methods, such as generation of transgenic animal models using homologous DNA recombination.

We employed lentiviruses to deliver RNAi cassettes targeting ZO-1 and ZONAB into the RPE of wild-type (wt) mice in an effort to shed light on the complex TJ signalling pathways that regulate proliferation and differentiation of the monolayer. Using a combination of downregulating and upregulating transgene cassettes, we observed the effect of the transcription factor ZONAB on RPE cell proliferation, density and polarity. Studies on molecular signalling pathways involving transcription factors, like ZONAB, are not feasible using conventional transgenic lines as they are essential during development. Complex inducible systems would be required in order to study the effects of tissue-specific downregulation. Using RNAi, we studied the function of ZONAB in mature RPE cells *in vivo* and its potential role in disease processes.

Given the known associations of ZONAB and ZO-1 in regulating epithelial cell density, we studied their role *in vivo* in the RPE of wt mice by downregulating both genes independently and following the impact of downregulation on retinal integrity and RPE monolayer stability. We also overexpressed ZONAB in a separate cohort of mice in order to compare its

effect with downregulation of ZO-1. This way, we confirmed the “inverse-ratio” connection for the action of ZO-1 and ZONAB that had only been previously shown *in vitro* [248-251,256]. Whereas downregulation of ZONAB reduced the RPE cell density and overall thickness leading to breaks in the posterior blood-retina-barrier (BRB), downregulation of ZO-1 or overexpression of ZONAB triggered RPE proliferation and at later stages induced EMT. The results suggested that TJ regulation in the RPE plays a major role in RPE proliferation, cell density and overall homeostasis elucidating the mechanisms that can cause RPE loss or posterior proliferative vitroretinopathy (PVR). The ZO-1/ZONAB pathway provides the RPE with a regulatory pathway linking cell density (sensed by TJ component recruitment in the cell membrane) and proliferation (initiated by transcriptional activation of proliferation markers in the nucleus). The intracellular trafficking of the transcription factor ZONAB tightly regulates the pathway in two ways: either by being localised in the nucleus when cell density is low triggering RPE proliferation, or by being sequestered in the cytoplasm to bind ZO-1 when cell density is high. RPE homeostasis is highly dependent on cell cycle regulation as reduced cell density may lead to breaks in the BRB and an immunological insult on the retina, whereas increased proliferation may lead to retinal gliotic scars affecting retinal function. Altough the experiments performed provide evidence of the essential role of ZO-1/ZONAB pathway in RPE homeostasis qualitatively, there was a lack of quantitative data to further dissect the dynamics between ZO-1 and ZONAB and the relative concentrations required for RPE monolayer integrity. Immunohistochemistry does not provide a quantitative method for gene expression and this is the reason why no statistical interpretation was performed in Figures 4.8 and 4.9. Although the lack of a reporter gene in our vectors (as used in Chapter 5) is debatable due to possible interference with the signalling pathway (see section 4.4), RNA suppression data would have been invaluable as an additional demonstration of gene knockdown and further proof that all the analyses were performed within the treated area. These points will be taken into account for future work on this project where laser captured RPE cells will be analysed more closely for induction of EMT marker expression using RT-PCR. The lack of RNA suppression data is a drawback not only for this

project but also for experiments presented in Chapter 3. Hence, all future work on data presented in this thesis will aim to correct that.

In addition to new conclusions drawn on monolayer integrity from our RNAi-mediated results on either RPE proliferation or topical RPE atrophy, this is the first experimental model that displays RPE dedifferentiation and retinal degeneration as a direct result of EMT.

6.4 Future directions

Many current studies are trying to optimise the efficiency and stringency of RNAi. However, since the therapeutic applications of RNAi may require the delivery of targeting cassettes as part of a vector rather than as naked nucleic acids, the impact of the hairpin sequence on vector integrity should also be examined. In this study during preliminary reporter gene silencing experiments, we encountered obstacles in the generation of a particular AAV vector plasmid targeting *eGFP*. Upon inspection, it became evident that the selected target sequence was highly recombinogenic at the specific sense-loop junction area. Although it is known that viral vectors are prone to recombination due to the presence of palindromic sequences such as LTRs or ITRs, in this case no tandem repeat sequences were involved in the recombination events. In addition, even though the recombination junction was identical in all three tested clones, the resultant aberrant sequence varied. This might indicate that the recombinogenic effect depended mostly on the hairpin sequence rather than the vector plasmid backbone. Since we encountered no problems in incorporating any other hairpins into the AAV vector backbone, neither did we observe any such obstacles in the generation of lentiviral vectors, these results suggest that selected target RNAi sequences should also be tested in their destination vectors and not only in synthetic (i.e. siRNA) form prior to selection.

The importance of RNAi in gene characterisation and especially therapeutic intervention has been extensively studied in various research fields apart from ophthalmology. The design of the shRNA molecule can vary as well as the delivery method of choice depending on the target tissue. However, there are still issues to be addressed regarding the molecular kinetics of the RNAi pathway, hairpin expression levels and off-targeting. Studies on the endogenous miRNA transcripts and their respective targets have shed light on the enzymatic complexes that catalyse basic steps in the pathway (Drosha, Exportin5, Dicer and RISC) [146,147,152,154,157]. Studies on RNA-protein interactions between shRNA and RNAi enzymes can reveal the

importance of each nucleotide in the guide strand (antisense) while at the same time testing the redundancy of the passenger strand (sense). In other words, each nucleotide of the guide strand plays a role in guiding the RISC complex to recognise and bind to the target mRNA while the passenger strand has not functional role apart from its requirement in hairpin formation. An example of a study contributing to siRNA optimisation is the development of asymmetric siRNAs (asiRNAs) that retain their silencing capacity even though the sense strand is considerably smaller than the antisense [293]. Chang and colleagues demonstrated that while retaining the 19+2 nucleotide format for the antisense strand, they were able to construct efficient asiRNAs with a sense strand of 13 nucleotides. The advantage was that the asiRNAs did not lose any of their silencing capacity in comparison to their symmetrical counterparts, while the off-targeting and pathway saturation caused by the sense strand was reduced to a minimum.

One of the main concerns with RNAi technology is the level of off-targeting that can be triggered by any given siRNA/shRNA molecule. The “seed region” of an siRNA molecule (2-8 nt positions) is part of the molecule associated with off-targeting especially when it shares complementarity with the 3’ UTR region of a gene (other than the gene of interest) [184,185]. The reason for this was found to be the non-perfect complementarity between either strand of a hairpin with a gene’s 3’UTR. These associations mimic the endogenous miRNA-mediated silencing that is brought about by translational repression rather than mRNA degradation. Nowadays, algorithms for siRNA design exclude candidates with partial complementarity within the first 8 nucleotides in order to address this issue. A few studies have demonstrated alarming levels of off-targeting and systemic toxicity after delivery of siRNAs [207,209,211-214] and more recently one reason for siRNA-induced toxicity was found to be the activation of the Toll-like receptor 3 (TLR3) [210]. TLR3 is a cell surface double-stranded viral RNA sensor that protects the cell from viral infections. Naked siRNAs are able to activate the extracellular part of TLR3 causing non-specific mRNA degradation and eventually leading to cell death. This process is initiated by TLR3 and propagated through the interferon response system for the protection of the host. Kleinman *et al.* also

demonstrated that the minimum siRNA length required for TLR3 activation was 21 nt of conventional design [210]. Smaller siRNAs did not activate the receptor. Although the authors clearly demonstrated TLR3 activation by naked RNA, they did not test corresponding shRNAs or siRNAs delivered using transfection reagents. Some of the problems underlined here can be circumvented by adapting to a miRNA-based design [288] or simply by selecting a different target area. It is highly probable that there are still more components of the RNAi pathway to be discovered and until their functions are also incorporated in algorithm-based bioinformatics tools to ensure safer siRNA design, target area selection for RNAi experiments will depend on a "hit-and-miss" approach.

In the future, inclusion of miRNA target sequences in transgene constructs may target expression to specific cell types depending on their miRNA expression profile. This approach may result in finely tuned transgene expression beyond the targeting capabilities of the delivery vector. This technique has been recently demonstrated in haematopoietic lineages and its efficiency indicates the feasibility of miRNA-based transgene regulation depending on the type and developmental stage of the host cell [294,295]. miRNA profiling has shown that there is varying miRNA expression between RPE, peripheral, central neuroretina and the macula (Shunbin Xu; unpublished data). Since the miRNA transcriptome of the retina has been mapped [150,296], it would be possible in the future to deliver a transgene or shRNA expression cassette to the retina and based on the miRNA adaptor sequence inserted in the expression cassette, so that the transgene is silenced in different parts of the retina. In effect, after viral delivery of the transgene in all parts of the retina, transgene expression could be further regulated not based on transduced cell type or promoter of choice, but instead based on the miRNA sequence attached to it.

RNAi is a promising technique for therapeutic intervention for the treatment of gain of function retinal disorders. The results presented in this study suggest

further optimisation studies to be conducted on target area selection parameters, nucleotide positioning, siRNA:mRNA associations, dosage and evasion of off-targeting. With the experience gained from the *RPE65* clinical trials concerning vector delivery and safety and the promising results obtained from RNAi-mediated knockdown in animal models, it is likely that the first RNAi-based clinical trials to treat adRP patients will take place within the next decade.

Reference list

1. **Chow, R. L. and R. A. Lang**. 2001. Early eye development in vertebrates. Annu. Rev. Cell Dev. Biol. **17**:255-296.

2. **Fernald, R. D.** 2006. Casting a genetic light on the evolution of eyes. Science **313**:1914-1918.

3. **Masland, R. H.** 2001. The fundamental plan of the retina. Nat. Neurosci. **4**:877-886.

4. **West, E. L., R. A. Pearson, R. E. MacLaren, J. C. Sowden, and R. R. Ali**. 2009. Cell transplantation strategies for retinal repair. Prog. Brain Res. **175**:3-21.

5. **Kanan, Y., A. Kasus-Jacobi, G. Moiseyev, K. Sawyer, J. X. Ma, and M. R. Al-Ubaidi**. 2008. Retinoid processing in cone and Muller cell lines. Exp. Eye Res. **86**:344-354.

6. **Applebury, M. L., M. P. Antoch, L. C. Baxter, L. L. Chun, J. D. Falk, F. Farhangfar, K. Kage, M. G. Krzystolik, L. A. Lyass, and J. T. Robbins**. 2000. The murine cone photoreceptor: a single cone type expresses both S and M opsins with retinal spatial patterning. Neuron **27**:513-523.

7. **Szel, A., P. Rohlich, A. R. Caffe, B. Juliusson, G. Aguirre, and V. T. van**. 1992. Unique topographic separation of two spectral classes of cones in the mouse retina. J. Comp Neurol. **325**:327-342.

8. **Luna, J. D., C. C. Chan, N. L. Derevjanik, J. Mahlow, C. Chiu, B. Peng, T. Tobe, P. A. Campochiaro, and S. A. Vinores**. 1997. Blood-retinal barrier (BRB) breakdown in experimental autoimmune uveoretinitis: comparison with vascular endothelial growth factor, tumor necrosis factor alpha, and interleukin-1beta-mediated breakdown. J. Neurosci. Res. **49**:268-280.

9. **Bailey, T. A., N. Kanuga, I. A. Romero, J. Greenwood, P. J. Luthert, and M. E. Cheetham**. 2004. Oxidative stress affects the junctional integrity of retinal pigment epithelial cells. Invest Ophthalmol. Vis. Sci. **45**:675-684.

10. **Kent, D., S. A. Vinores, and P. A. Campochiaro**. 2000. Macular oedema: the role of soluble mediators. Br. J. Ophthalmol. **84**:542-545.

11. **Konrad, M., A. Schaller, D. Seelow, A. V. Pandey, S. Waldegger, A. Lesslauer, H. Vitzthum, Y. Suzuki, J. M. Luk, C. Becker, K. P. Schlingmann, M. Schmid, J. Rodriguez-Soriano, G. Ariceta, F. Cano, R. Enriquez, H. Juppner, S. A. Bakkaloglu, M. A. Hediger, S. Gallati, S. C. Neuhauss, P. Nurnberg, and S. Weber**. 2006. Mutations in the tight-junction gene claudin 19 (CLDN19) are associated with renal magnesium wasting, renal failure, and severe ocular involvement. Am. J. Hum. Genet. **79**:949-957.

12. **Pugh, E. N. Jr. and T. D. Lamb**. 2000. Phototransduction in Vertebrate Rods and Cones: Molecular Mechanisms of Amplification, Recovery and Light Adaptation., p. 183-255. Handbook of Biological Physics, vol. 3, Molecular Mechanisms of Visual Transduction.

13. **Moiseyev, G., Y. Takahashi, Y. Chen, S. Gentleman, T. M. Redmond, R. K. Crouch, and J. X. Ma**. 2006. RPE65 is an iron(II)-dependent isomerohydrolase in the retinoid visual cycle. J. Biol. Chem. **281**:2835-2840.

14. **Lamb, T. D. and E. N. Pugh, Jr.** 2004. Dark adaptation and the retinoid cycle of vision. Prog. Retin. Eye Res. **23**:307-380.

15. **Moiseyev, G., Y. Chen, Y. Takahashi, B. X. Wu, and J. X. Ma**. 2005. RPE65 is the isomerohydrolase in the retinoid visual cycle. Proc. Natl. Acad. Sci. U. S. A **102**:12413-12418.

16. **Pepperberg, D. R. and R. K. Crouch**. 2001. An illuminating new step in visual-pigment regeneration. Lancet **358**:2098-2099.

17. **Bessant, D. A., R. R. Ali, and S. S. Bhattacharya**. 2001. Molecular genetics and prospects for therapy of the inherited retinal dystrophies. Curr. Opin. Genet. Dev. **11**:307-316.

18. **Daiger, S. P., S. J. Bowne, and L. S. Sullivan**. 2007. Perspective on genes and mutations causing retinitis pigmentosa. Arch. Ophthalmol. **125**:151-158.

19. **Hartong, D. T., E. L. Berson, and T. P. Dryja**. 2006. Retinitis pigmentosa. Lancet **368**:1795-1809.

20. **Mordes, D., X. Luo, A. Kar, D. Kuo, L. Xu, K. Fushimi, G. Yu, P. Sternberg, Jr., and J. Y. Wu**. 2006. Pre-mRNA splicing and retinitis pigmentosa. Mol. Vis. **12**:1259-1271.

21. **Kalloniatis, M. and E. L. Fletcher**. 2004. Retinitis pigmentosa: understanding the clinical presentation, mechanisms and treatment options. Clin. Exp. Optom. **87**:65-80.

22. **Dryja, T. P., T. L. McGee, E. Reichel, L. B. Hahn, G. S. Cowley, D. W. Yandell, M. A. Sandberg, and E. L. Berson**. 1990. A point mutation of the rhodopsin gene in one form of retinitis pigmentosa. Nature **343**:364-366.

23. **Kennan, A., A. Aherne, and P. Humphries**. 2005. Light in retinitis pigmentosa. Trends Genet. **21**:103-110.

24. **Bessant, D. A., A. M. Payne, K. P. Mitton, Q. L. Wang, P. K. Swain, C. Plant, A. C. Bird, D. J. Zack, A. Swaroop, and S. S. Bhattacharya**. 1999. A mutation in NRL is associated with autosomal dominant retinitis pigmentosa. Nat. Genet. **21**:355-356.

25. **Chiang, S. W., D. Y. Wang, W. M. Chan, P. O. Tam, K. K. Chong, D. S. Lam, and C. P. Pang**. 2006. A novel missense RP1 mutation in retinitis pigmentosa. Eye **20**:602-605.

26. **Sullivan, L. S., S. J. Bowne, C. R. Seaman, S. H. Blanton, R. A. Lewis, J. R. Heckenlively, D. G. Birch, D. Hughbanks-Wheaton, and S. P. Daiger**. 2006. Genomic rearrangements of the PRPF31 gene account for 2.5% of autosomal dominant retinitis pigmentosa. Invest Ophthalmol. Vis. Sci. **47**:4579-4588.

27. **Aherne, A., A. Kennan, P. F. Kenna, N. McNally, D. G. Lloyd, I. L. Alberts, A. S. Kiang, M. M. Humphries, C. Ayuso, P. C. Engel, J. J. Gu, B. S. Mitchell, G. J. Farrar, and P. Humphries**. 2004. On the molecular pathology of neurodegeneration in IMPDH1-based retinitis pigmentosa. Hum. Mol. Genet. **13**:641-650.

28. **Hamel, C. P.** 2007. Cone rod dystrophies. Orphanet. J. Rare. Dis. **2**:7.

29. **Michaelides, M., A. J. Hardcastle, D. M. Hunt, and A. T. Moore**. 2006. Progressive cone and cone-rod dystrophies: phenotypes and underlying molecular genetic basis. Surv. Ophthalmol. **51**:232-258.

30. **Kobayashi, A., T. Higashide, D. Hamasaki, S. Kubota, H. Sakuma, W. An, T. Fujimaki, M. J. McLaren, R. G. Weleber, and G. Inana**. 2000. HRG4 (UNC119) mutation found in cone-rod dystrophy causes retinal degeneration in a transgenic model. Invest Ophthalmol. Vis. Sci. **41**:3268-3277.

31. **Michaelides, M., D. M. Hunt, and A. T. Moore**. 2003. The genetics of inherited macular dystrophies. J. Med. Genet. **40**:641-650.

32. **Donoso, L. A., A. O. Edwards, A. Frost, T. Vrabec, E. M. Stone, G. S. Hageman, and T. Perski**. 2001. Autosomal dominant Stargardt-like macular dystrophy. Surv. Ophthalmol. **46**:149-163.

33. **McMahon, A., I. A. Butovich, N. L. Mata, M. Klein, R. Ritter, III, J. Richardson, D. G. Birch, A. O. Edwards, and W. Kedzierski**. 2007. Retinal pathology and skin barrier defect in mice carrying a Stargardt disease-3 mutation in elongase of very long chain fatty acids-4. Mol. Vis. **13**:258-272.

34. **Marmorstein, A. D., L. Y. Marmorstein, M. Rayborn, X. Wang, J. G. Hollyfield, and K. Petrukhin**. 2000. Bestrophin, the product of the Best vitelliform macular dystrophy gene (VMD2), localizes to the basolateral plasma membrane of the retinal pigment epithelium. Proc. Natl. Acad. Sci. U. S. A **97**:12758-12763.

35. **Qu, Z., L. T. Chien, Y. Cui, and H. C. Hartzell**. 2006. The anion-selective pore of the bestrophins, a family of chloride channels associated with retinal degeneration. J. Neurosci. **26**:5411-5419.

36. **Weber, B. H., G. Vogt, R. C. Pruett, H. Stohr, and U. Felbor**. 1994. Mutations in the tissue inhibitor of metalloproteinases-3 (TIMP3) in patients with Sorsby's fundus dystrophy. Nat. Genet. **8**:352-356.

37. **Qi, J. H., Q. Ebrahem, N. Moore, G. Murphy, L. Claesson-Welsh, M. Bond, A. Baker, and B. nand-Apte**. 2003. A novel function for tissue inhibitor of metalloproteinases-3 (TIMP3): inhibition of angiogenesis by blockage of VEGF binding to VEGF receptor-2. Nat. Med. **9**:407-415.

38. **Berson, E. L., B. Rosner, M. A. Sandberg, C. Weigel-DiFranco, A. Moser, R. J. Brockhurst, K. C. Hayes, C. A. Johnson, E. J. Anderson, A. R. Gaudio, W. C. Willett, and E. J. Schaefer**. 2004. Clinical trial of docosahexaenoic acid in patients with retinitis pigmentosa receiving vitamin A treatment. Arch. Ophthalmol. **122**:1297-1305.

39. **Berson, E. L., B. Rosner, M. A. Sandberg, C. Weigel-DiFranco, A. Moser, R. J. Brockhurst, K. C. Hayes, C. A. Johnson, E. J. Anderson, A. R. Gaudio, W. C. Willett, and E. J. Schaefer**. 2004. Further evaluation of docosahexaenoic acid in patients with retinitis pigmentosa receiving vitamin A treatment: subgroup analyses. Arch. Ophthalmol. **122**:1306-1314.

40. **Azadi, S., L. E. Johnson, F. Paquet-Durand, M. T. Perez, Y. Zhang, P. A. Ekstrom, and V. T. van**. 2007. CNTF+BDNF treatment and neuroprotective pathways in the rd1 mouse retina. Brain Res. **1129**:116-129.

41. **Bok, D., D. Yasumura, M. T. Matthes, A. Ruiz, J. L. Duncan, A. V. Chappelow, S. Zolutukhin, W. Hauswirth, and M. M. LaVail**. 2002. Effects of adeno-associated virus-vectored ciliary neurotrophic factor on retinal structure and function in mice with a P216L rds/peripherin mutation. Exp. Eye Res. **74**:719-735.

42. **Buch, P. K., R. E. MacLaren, Y. Duran, K. S. Balaggan, A. MacNeil, F. C. Schlichtenbrede, A. J. Smith, and R. R. Ali**. 2006. In contrast to AAV-mediated Cntf expression, AAV-mediated Gdnf expression enhances gene replacement therapy in rodent models of retinal degeneration. Mol. Ther. **14**:700-709.

43. **Frasson, M., J. A. Sahel, M. Fabre, M. Simonutti, H. Dreyfus, and S. Picaud**. 1999. Retinitis pigmentosa: rod photoreceptor rescue by a calcium-channel blocker in the rd mouse. Nat. Med. **5**:1183-1187.

44. **Lau, D., L. H. McGee, S. Zhou, K. G. Rendahl, W. C. Manning, J. A. Escobedo, and J. G. Flannery**. 2000. Retinal degeneration is slowed in transgenic rats by AAV-mediated delivery of FGF-2. Invest Ophthalmol. Vis. Sci. **41**:3622-3633.

45. **LaVail, M. M., K. Unoki, D. Yasumura, M. T. Matthes, G. D. Yancopoulos, and R. H. Steinberg**. 1992. Multiple growth factors, cytokines, and neurotrophins rescue photoreceptors from the damaging effects of constant light. Proc. Natl. Acad. Sci. U. S. A **89**:11249-11253.

46. **LaVail, M. M., D. Yasumura, M. T. Matthes, C. Lau-Villacorta, K. Unoki, C. H. Sung, and R. H. Steinberg**. 1998. Protection of mouse photoreceptors by survival factors in retinal degenerations. Invest Ophthalmol. Vis. Sci. **39**:592-602.

47. **Rhee, K. D., A. Ruiz, J. L. Duncan, W. W. Hauswirth, M. M. LaVail, D. Bok, and X. J. Yang**. 2007. Molecular and cellular alterations induced by sustained expression of ciliary neurotrophic factor in a mouse model of retinitis pigmentosa. Invest Ophthalmol. Vis. Sci. **48**:1389-1400.

48. **Sanz, M. M., L. E. Johnson, S. Ahuja, P. A. Ekstrom, J. Romero, and V. T. van**. 2007. Significant photoreceptor rescue by treatment with a combination of antioxidants in an animal model for retinal degeneration. Neuroscience **145**:1120-1129.

49. **Schlichtenbrede, F. C., A. MacNeil, J. W. Bainbridge, M. Tschernutter, A. J. Thrasher, A. J. Smith, and R. R. Ali**. 2003. Intraocular gene delivery of ciliary neurotrophic factor results in significant loss of retinal function in normal mice and in the Prph2Rd2/Rd2 model of retinal degeneration. Gene Ther. **10**:523-527.

50. **Binder, S., B. V. Stanzel, I. Krebs, and C. Glittenberg**. 2007. Transplantation of the RPE in AMD. Prog. Retin. Eye Res.

51. **MacLaren, R. E., A. C. Bird, P. J. Sathia, and G. W. Aylward**. 2005. Long-term results of submacular surgery combined with macular translocation of the retinal pigment epithelium in neovascular age-related macular degeneration. Ophthalmology **112**:2081-2087.

52. **Klassen, H. J., T. F. Ng, Y. Kurimoto, I. Kirov, M. Shatos, P. Coffey, and M. J. Young**. 2004. Multipotent retinal progenitors express developmental markers, differentiate into retinal neurons, and preserve light-mediated behavior. Invest Ophthalmol. Vis. Sci. **45**:4167-4173.

53. **Mizumoto, H., K. Mizumoto, M. A. Shatos, H. Klassen, and M. J. Young**. 2003. Retinal transplantation of neural progenitor cells derived from the brain of GFP transgenic mice. Vision Res. **43**:1699-1708.

54. **Sakaguchi, D. S., S. J. Van Hoffelen, and M. J. Young**. 2003. Differentiation and morphological integration of neural progenitor cells transplanted into the developing mammalian eye. Ann. N. Y. Acad. Sci. **995**:127-139.

55. **MacLaren, R. E., R. A. Pearson, A. MacNeil, R. H. Douglas, T. E. Salt, M. Akimoto, A. Swaroop, J. C. Sowden, and R. R. Ali**. 2006. Retinal repair by transplantation of photoreceptor precursors. Nature **444**:203-207.

56. **Osakada, F., H. Ikeda, M. Mandai, T. Wataya, K. Watanabe, N. Yoshimura, A. Akaike, Y. Sasai, and M. Takahashi**. 2008. Toward the generation of rod and cone

photoreceptors from mouse, monkey and human embryonic stem cells. Nat. Biotechnol. **26**:215-224.

57. **Ott, M. G., M. Schmidt, K. Schwarzwaelder, S. Stein, U. Siler, U. Koehl, H. Glimm, K. Kuhlcke, A. Schilz, H. Kunkel, S. Naundorf, A. Brinkmann, A. Deichmann, M. Fischer, C. Ball, I. Pilz, C. Dunbar, Y. Du, N. A. Jenkins, N. G. Copeland, U. Luthi, M. Hassan, A. J. Thrasher, D. Hoelzer, K. C. Von, R. Seger, and M. Grez**. 2006. Correction of X-linked chronic granulomatous disease by gene therapy, augmented by insertional activation of MDS1-EVI1, PRDM16 or SETBP1. Nat. Med. **12**:401-409.

58. **Kaplitt, M. G., A. Feigin, C. Tang, H. L. Fitzsimons, P. Mattis, P. A. Lawlor, R. J. Bland, D. Young, K. Strybing, D. Eidelberg, and M. J. During**. 2007. Safety and tolerability of gene therapy with an adeno-associated virus (AAV) borne GAD gene for Parkinson's disease: an open label, phase I trial. Lancet **369**:2097-2105.

59. **Rosenecker, J., S. Huth, and C. Rudolph**. 2006. Gene therapy for cystic fibrosis lung disease: current status and future perspectives. Curr. Opin. Mol. Ther. **8**:439-445.

60. **Cavazzana-Calvo, M., S. Hacein-Bey, B. G. de Saint, F. Gross, E. Yvon, P. Nusbaum, F. Selz, C. Hue, S. Certain, J. L. Casanova, P. Bousso, F. L. Deist, and A. Fischer**. 2000. Gene therapy of human severe combined immunodeficiency (SCID)-X1 disease. Science **288**:669-672.

61. **Gaspar, H. B., K. L. Parsley, S. Howe, D. King, K. C. Gilmour, J. Sinclair, G. Brouns, M. Schmidt, K. C. Von, T. Barington, M. A. Jakobsen, H. O. Christensen, G. A. Al, H. N. White, J. L. Smith, R. J. Levinsky, R. R. Ali, C. Kinnon, and A. J. Thrasher**. 2004. Gene therapy of X-linked severe combined immunodeficiency by use of a pseudotyped gammaretroviral vector. Lancet **364**:2181-2187.

62. **Thrasher, A. J., C. M. Casimir, C. Kinnon, G. Morgan, A. W. Segal, and R. J. Levinsky**. 1995. Gene transfer to primary chronic granulomatous disease monocytes. Lancet **346**:92-93.

63. **Aiuti, A., S. Slavin, M. Aker, F. Ficara, S. Deola, A. Mortellaro, S. Morecki, G. Andolfi, A. Tabucchi, F. Carlucci, E. Marinello, F. Cattaneo, S. Vai, P. Servida, R. Miniero, M. G. Roncarolo, and C. Bordignon**. 2002. Correction of ADA-SCID by stem cell gene therapy combined with nonmyeloablative conditioning. Science **296**:2410-2413.

64. **Hacein-Bey-Abina, S., D. F. Le, F. Carlier, C. Bouneaud, C. Hue, J. P. De Villartay, A. J. Thrasher, N. Wulffraat, R. Sorensen, S. Dupuis-Girod, A. Fischer, E. G. Davies, W. Kuis, L. Leiva, and M. Cavazzana-Calvo**. 2002. Sustained correction of X-linked severe combined immunodeficiency by ex vivo gene therapy. N. Engl. J. Med. **346**:1185-1193.

65. **Hacein-Bey-Abina, S., K. C. Von, M. Schmidt, M. P. McCormack, N. Wulffraat, P. Leboulch, A. Lim, C. S. Osborne, R. Pawliuk, E. Morillon, R. Sorensen, A. Forster, P. Fraser, J. I. Cohen, B. G. de Saint, I. Alexander, U. Wintergerst, T. Frebourg, A. Aurias, D. Stoppa-Lyonnet, S. Romana, I. Radford-Weiss, F. Gross, F. Valensi, E. Delabesse, E. Macintyre, F. Sigaux, J. Soulier, L. E. Leiva, M. Wissler, C. Prinz, T. H. Rabbitts, D. F. Le, A. Fischer, and M. Cavazzana-Calvo**. 2003. LMO2-associated clonal T cell proliferation in two patients after gene therapy for SCID-X1. Science **302**:415-419.

66. **Thornhill, S. I., A. Schambach, S. J. Howe, M. Ulaganathan, E. Grassman, D. Williams, B. Schiedlmeier, N. J. Sebire, H. B. Gaspar, C. Kinnon, C. Baum, and**

A. J. Thrasher. 2008. Self-inactivating gammaretroviral vectors for gene therapy of X-linked severe combined immunodeficiency. Mol. Ther. **16**:590-598.

67. **Zhang, F., S. I. Thornhill, S. J. Howe, M. Ulaganathan, A. Schambach, J. Sinclair, C. Kinnon, H. B. Gaspar, M. Antoniou, and A. J. Thrasher**. 2007. Lentiviral vectors containing an enhancer-less ubiquitously acting chromatin opening element (UCOE) provide highly reproducible and stable transgene expression in hematopoietic cells. Blood **110**:1448-1457.

68. **Jacobson, S. G., S. L. Boye, T. S. Aleman, T. J. Conlon, C. J. Zeiss, A. J. Roman, A. V. Cideciyan, S. B. Schwartz, A. M. Komaromy, M. Doobrajh, A. Y. Cheung, A. Sumaroka, S. E. Pearce-Kelling, G. D. Aguirre, S. Kaushal, A. M. Maguire, T. R. Flotte, and W. W. Hauswirth**. 2006. Safety in nonhuman primates of ocular AAV2-RPE65, a candidate treatment for blindness in Leber congenital amaurosis. Hum. Gene Ther. **17**:845-858.

69. **Le, M. G., K. Stieger, A. J. Smith, M. Weber, J. Y. Deschamps, D. Nivard, A. Mendes-Madeira, N. Provost, Y. Pereon, Y. Cherel, R. R. Ali, C. Hamel, P. Moullier, and F. Rolling**. 2007. Restoration of vision in RPE65-deficient Briard dogs using an AAV serotype 4 vector that specifically targets the retinal pigmented epithelium. Gene Ther. **14**:292-303.

70. **Bainbridge, J. W., A. J. Smith, S. S. Barker, S. Robbie, R. Henderson, K. Balaggan, A. Viswanathan, G. E. Holder, A. Stockman, N. Tyler, S. Petersen-Jones, S. S. Bhattacharya, A. J. Thrasher, F. W. Fitzke, B. J. Carter, G. S. Rubin, A. T. Moore, and R. R. Ali**. 2008. Effect of gene therapy on visual function in Leber's congenital amaurosis. N. Engl. J. Med. **358**:2231-2239.

71. **Hauswirth, W. W., T. S. Aleman, S. Kaushal, A. V. Cideciyan, S. B. Schwartz, L. Wang, T. J. Conlon, S. L. Boye, T. R. Flotte, B. J. Byrne, and S. G. Jacobson**. 2008. Treatment of leber congenital amaurosis due to RPE65 mutations by ocular subretinal injection of adeno-associated virus gene vector: short-term results of a phase I trial. Hum. Gene Ther. **19**:979-990.

72. **Maguire, A. M., F. Simonelli, E. A. Pierce, E. N. Pugh, Jr., F. Mingozzi, J. Bennicelli, S. Banfi, K. A. Marshall, F. Testa, E. M. Surace, S. Rossi, A. Lyubarsky, V. R. Arruda, B. Konkle, E. Stone, J. Sun, J. Jacobs, L. Dell'Osso, R. Hertle, J. X. Ma, T. M. Redmond, X. Zhu, B. Hauck, O. Zelenaia, K. S. Shindler, M. G. Maguire, J. F. Wright, N. J. Volpe, J. W. McDonnell, A. Auricchio, K. A. High, and J. Bennett**. 2008. Safety and efficacy of gene transfer for Leber's congenital amaurosis. N. Engl. J. Med. **358**:2240-2248.

73. **Maguire, A. M., K. A. High, A. Auricchio, J. F. Wright, E. A. Pierce, F. Testa, F. Mingozzi, J. L. Bennicelli, G. S. Ying, S. Rossi, A. Fulton, K. A. Marshall, S. Banfi, D. C. Chung, J. I. Morgan, B. Hauck, O. Zelenaia, X. Zhu, L. Raffini, F. Coppieters, B. E. De, K. S. Shindler, N. J. Volpe, E. M. Surace, C. Acerra, A. Lyubarsky, T. M. Redmond, E. Stone, J. Sun, J. W. McDonnell, B. P. Leroy, F. Simonelli, and J. Bennett**. 2009. Age-dependent effects of RPE65 gene therapy for Leber's congenital amaurosis: a phase 1 dose-escalation trial. Lancet **374**:1597-1605.

74. **Simonelli, F., A. M. Maguire, F. Testa, E. A. Pierce, F. Mingozzi, J. L. Bennicelli, S. Rossi, K. Marshall, S. Banfi, E. M. Surace, J. Sun, T. M. Redmond, X. Zhu, K. S. Shindler, G. S. Ying, C. Ziviello, C. Acerra, J. F. Wright, J. W. McDonnell, K. A. High, J. Bennett, and A. Auricchio**. 2010. Gene Therapy for Leber's Congenital Amaurosis is Safe and Effective Through 1.5 Years After Vector Administration. Mol. Ther. **18**:643-650.

75. **Farjo, R., J. Skaggs, A. B. Quiambao, M. J. Cooper, and M. I. Naash**. 2006. Efficient non-viral ocular gene transfer with compacted DNA nanoparticles. PLoS. ONE. **1**:e38.

76. **Matsuda, T. and C. L. Cepko**. 2004. Electroporation and RNA interference in the rodent retina in vivo and in vitro. Proc. Natl. Acad. Sci. U. S. A **101**:16-22.

77. **Andrieu-Soler, C., R. A. Bejjani, B. T. de, N. Normand, D. BenEzra, and F. Behar-Cohen**. 2006. Ocular gene therapy: a review of nonviral strategies. Mol. Vis. **12**:1334-1347.

78. **Glover, D. J., H. J. Lipps, and D. A. Jans**. 2005. Towards safe, non-viral therapeutic gene expression in humans. Nat. Rev. Genet. **6**:299-310.

79. **Kachi, S., Y. Oshima, N. Esumi, M. Kachi, B. Rogers, D. J. Zack, and P. A. Campochiaro**. 2005. Nonviral ocular gene transfer. Gene Ther. **12**:843-851.

80. **Spencer, B., S. Agarwala, M. Miskulin, M. Smith, and C. R. Brandt**. 2000. Herpes simplex virus-mediated gene delivery to the rodent visual system. Invest Ophthalmol. Vis. Sci. **41**:1392-1401.

81. **Fraefel, C., A. Mendes-Madeira, O. Mabon, A. Lefebvre, M. G. Le, M. Ackermann, P. Moullier, and F. Rolling**. 2005. In vivo gene transfer to the rat retina using herpes simplex virus type 1 (HSV-1)-based amplicon vectors. Gene Ther. **12**:1283-1288.

82. **Spencer, B., S. Agarwala, L. Gentry, and C. R. Brandt**. 2001. HSV-1 vector-delivered FGF2 to the retina is neuroprotective but does not preserve functional responses. Mol. Ther. **3**:746-756.

83. **Cai, S. and C. R. Brandt**. 2008. Induction of interleukin-6 in human retinal epithelial cells by an attenuated Herpes simplex virus vector requires viral replication and NFkappaB activation. Exp. Eye Res. **86**:178-188.

84. **Raper, S. E., N. Chirmule, F. S. Lee, N. A. Wivel, A. Bagg, G. P. Gao, J. M. Wilson, and M. L. Batshaw**. 2003. Fatal systemic inflammatory response syndrome in a ornithine transcarbamylase deficient patient following adenoviral gene transfer. Mol. Genet. Metab **80**:148-158.

85. **Ali, R. R., M. B. Reichel, A. P. Byrnes, C. J. Stephens, A. J. Thrasher, D. Baker, D. M. Hunt, and S. S. Bhattacharya**. 1998. Co-injection of adenovirus expressing CTLA4-Ig prolongs adenovirally mediated lacZ reporter gene expression in the mouse retina. Gene Ther. **5**:1561-1565.

86. **Lamartina, S., M. Cimino, G. Roscilli, E. Dammassa, D. Lazzaro, R. Rota, G. Ciliberto, and C. Toniatti**. 2007. Helper-dependent adenovirus for the gene therapy of proliferative retinopathies: stable gene transfer, regulated gene expression and therapeutic efficacy. J. Gene Med. **9**:862-874.

87. **Kumar-Singh, R. and D. B. Farber**. 1998. Encapsidated adenovirus mini-chromosome-mediated delivery of genes to the retina: application to the rescue of photoreceptor degeneration. Hum. Mol. Genet. **7**:1893-1900.

88. **Bennett, J., T. Tanabe, D. Sun, Y. Zeng, H. Kjeldbye, P. Gouras, and A. M. Maguire**. 1996. Photoreceptor cell rescue in retinal degeneration (rd) mice by in vivo gene therapy. Nat. Med. **2**:649-654.

89. **Cashman, S. M., S. L. Sadowski, D. J. Morris, J. Frederick, and R. Kumar-Singh**. 2002. Intercellular trafficking of adenovirus-delivered HSV VP22 from the

retinal pigment epithelium to the photoreceptors--implications for gene therapy. Mol. Ther. **6**:813-823.

90. **Campochiaro, P. A., Q. D. Nguyen, S. M. Shah, M. L. Klein, E. Holz, R. N. Frank, D. A. Saperstein, A. Gupta, J. T. Stout, J. Macko, R. DiBartolomeo, and L. L. Wei**. 2006. Adenoviral vector-delivered pigment epithelium-derived factor for neovascular age-related macular degeneration: results of a phase I clinical trial. Hum. Gene Ther. **17**:167-176.

91. **Cashman, S. M., L. McCullough, and R. Kumar-Singh**. 2007. Improved retinal transduction in vivo and photoreceptor-specific transgene expression using adenovirus vectors with modified penton base. Mol. Ther. **15**:1640-1646.

92. **McCarty, D. M., S. M. Young, Jr., and R. J. Samulski**. 2004. Integration of adeno-associated virus (AAV) and recombinant AAV vectors. Annu. Rev. Genet. **38**:819-845.

93. **Auricchio, A., G. Kobinger, V. Anand, M. Hildinger, E. O'Connor, A. M. Maguire, J. M. Wilson, and J. Bennett**. 2001. Exchange of surface proteins impacts on viral vector cellular specificity and transduction characteristics: the retina as a model. Hum. Mol. Genet. **10**:3075-3081.

94. **Lai, C. M., Y. K. Lai, and P. E. Rakoczy**. 2002. Adenovirus and adeno-associated virus vectors. DNA Cell Biol. **21**:895-913.

95. **Mistry, A. R., A. M. De, E. Feudner, R. R. Ali, and A. J. Thrasher**. 2002. High-titer stocks of adeno-associated virus from replicating amplicons and herpes vectors. Methods Mol. Med. **69**:445-460.

96. **Auricchio, A., E. O'Connor, M. Hildinger, and J. M. Wilson**. 2001. A single-step affinity column for purification of serotype-5 based adeno-associated viral vectors. Mol. Ther. **4**:372-374.

97. **Kaludov, N., B. Handelman, and J. A. Chiorini**. 2002. Scalable purification of adeno-associated virus type 2, 4, or 5 using ion-exchange chromatography. Hum. Gene Ther. **13**:1235-1243.

98. **Zolotukhin, S., M. Potter, I. Zolotukhin, Y. Sakai, S. Loiler, T. J. Fraites, Jr., V. A. Chiodo, T. Phillipsberg, N. Muzyczka, W. W. Hauswirth, T. R. Flotte, B. J. Byrne, and R. O. Snyder**. 2002. Production and purification of serotype 1, 2, and 5 recombinant adeno-associated viral vectors. Methods **28**:158-167.

99. **Natkunarajah, M., P. Trittibach, J. McIntosh, Y. Duran, S. E. Barker, A. J. Smith, A. C. Nathwani, and R. R. Ali**. 2008. Assessment of ocular transduction using single-stranded and self-complementary recombinant adeno-associated virus serotype 2/8. Gene Ther. **15**:463-467.

100. **Yokoi, K., S. Kachi, H. S. Zhang, P. D. Gregory, S. K. Spratt, R. J. Samulski, and P. A. Campochiaro**. 2007. Ocular gene transfer with self-complementary AAV vectors. Invest Ophthalmol. Vis. Sci. **48**:3324-3328.

101. **Ali, R. R., M. B. Reichel, A. J. Thrasher, R. J. Levinsky, C. Kinnon, N. Kanuga, D. M. Hunt, and S. S. Bhattacharya**. 1996. Gene transfer into the mouse retina mediated by an adeno-associated viral vector. Hum. Mol. Genet. **5**:591-594.

102. **Flannery, J. G., S. Zolotukhin, M. I. Vaquero, M. M. LaVail, N. Muzyczka, and W. W. Hauswirth**. 1997. Efficient photoreceptor-targeted gene expression in vivo by recombinant adeno-associated virus. Proc. Natl. Acad. Sci. U. S. A **94**:6916-6921.

103. **Ali, R. R., G. M. Sarra, C. Stephens, M. D. Alwis, J. W. Bainbridge, P. M. Munro, S. Fauser, M. B. Reichel, C. Kinnon, D. M. Hunt, S. S. Bhattacharya, and A. J. Thrasher**. 2000. Restoration of photoreceptor ultrastructure and function in retinal degeneration slow mice by gene therapy. Nat. Genet. **25**:306-310.

104. **Pang, J. J., B. Chang, A. Kumar, S. Nusinowitz, S. M. Noorwez, J. Li, A. Rani, T. C. Foster, V. A. Chiodo, T. Doyle, H. Li, R. Malhotra, J. T. Teusner, J. H. McDowell, S. H. Min, Q. Li, S. Kaushal, and W. W. Hauswirth**. 2006. Gene therapy restores vision-dependent behavior as well as retinal structure and function in a mouse model of RPE65 Leber congenital amaurosis. Mol. Ther. **13**:565-572.

105. **Pawlyk, B. S., A. J. Smith, P. K. Buch, M. Adamian, D. H. Hong, M. A. Sandberg, R. R. Ali, and T. Li**. 2005. Gene replacement therapy rescues photoreceptor degeneration in a murine model of Leber congenital amaurosis lacking RPGRIP. Invest Ophthalmol. Vis. Sci. **46**:3039-3045.

106. **Sun, X., B. Pawlyk, X. Xu, X. Liu, O. V. Bulgakov, M. Adamian, M. A. Sandberg, S. C. Khani, M. H. Tan, A. J. Smith, R. R. Ali, and T. Li**. 2009. Gene therapy with a promoter targeting both rods and cones rescues retinal degeneration caused by AIPL1 mutations. Gene Ther.

107. **Alexander, J. J., Y. Umino, D. Everhart, B. Chang, S. H. Min, Q. Li, A. M. Timmers, N. L. Hawes, J. J. Pang, R. B. Barlow, and W. W. Hauswirth**. 2007. Restoration of cone vision in a mouse model of achromatopsia. Nat. Med. **13**:685-687.

108. **Kjellstrom, S., R. A. Bush, Y. Zeng, Y. Takada, and P. A. Sieving**. 2007. Retinoschisin Gene Therapy and Natural History in the Rs1h-KO Mouse: Long-term Rescue from Retinal Degeneration. Invest Ophthalmol. Vis. Sci. **48**:3837-3845.

109. **Bainbridge, J. W., A. Mistry, F. C. Schlichtenbrede, A. Smith, C. Broderick, A. M. De, A. Georgiadis, P. M. Taylor, M. Squires, C. Sethi, D. Charteris, A. J. Thrasher, D. Sargan, and R. R. Ali**. 2003. Stable rAAV-mediated transduction of rod and cone photoreceptors in the canine retina. Gene Ther. **10**:1336-1344.

110. **Nathwani, A. C., J. T. Gray, C. Y. Ng, J. Zhou, Y. Spence, S. N. Waddington, E. G. Tuddenham, G. Kemball-Cook, J. McIntosh, M. Boon-Spijker, K. Mertens, and A. M. Davidoff**. 2006. Self-complementary adeno-associated virus vectors containing a novel liver-specific human factor IX expression cassette enable highly efficient transduction of murine and nonhuman primate liver. Blood **107**:2653-2661.

111. **Stieger, K., M. G. Le, F. Lasne, M. Weber, J. Y. Deschamps, D. Nivard, A. Mendes-Madeira, N. Provost, L. Martin, P. Moullier, and F. Rolling**. 2006. Long-term doxycycline-regulated transgene expression in the retina of nonhuman primates following subretinal injection of recombinant AAV vectors. Mol. Ther. **13**:967-975.

112. **Yuasa, K., M. Yoshimura, N. Urasawa, S. Ohshima, J. M. Howell, A. Nakamura, T. Hijikata, Y. Miyagoe-Suzuki, and S. Takeda**. 2007. Injection of a recombinant AAV serotype 2 into canine skeletal muscles evokes strong immune responses against transgene products. Gene Ther. **14**:1249-1260.

113. **Donsante, A., D. G. Miller, Y. Li, C. Vogler, E. M. Brunt, D. W. Russell, and M. S. Sands**. 2007. AAV vector integration sites in mouse hepatocellular carcinoma. Science **317**:477.

114. **Pien, G. C., E. Basner-Tschakarjan, D. J. Hui, A. N. Mentlik, J. D. Finn, N. C. Hasbrouck, S. Zhou, S. L. Murphy, M. V. Maus, F. Mingozzi, J. S. Orange, and K. A. High**. 2009. Capsid antigen presentation flags human hepatocytes for

destruction after transduction by adeno-associated viral vectors. J. Clin. Invest **119**:1688-1695.

115. **Stieger, K., J. Schroeder, N. Provost, A. Mendes-Madeira, B. Belbellaa, M. G. Le, M. Weber, J. Y. Deschamps, B. Lorenz, P. Moullier, and F. Rolling**. 2009. Detection of intact rAAV particles up to 6 years after successful gene transfer in the retina of dogs and primates. Mol. Ther. **17**:516-523.

116. **Cideciyan, A. V., T. S. Aleman, S. L. Boye, S. B. Schwartz, S. Kaushal, A. J. Roman, J. J. Pang, A. Sumaroka, E. A. Windsor, J. M. Wilson, T. R. Flotte, G. A. Fishman, E. Heon, E. M. Stone, B. J. Byrne, S. G. Jacobson, and W. W. Hauswirth**. 2008. Human gene therapy for RPE65 isomerase deficiency activates the retinoid cycle of vision but with slow rod kinetics. Proc. Natl. Acad. Sci. U. S. A **105**:15112-15117.

117. **Stieger, K., M. A. Colle, L. Dubreil, A. Mendes-Madeira, M. Weber, M. G. Le, J. Y. Deschamps, N. Provost, D. Nivard, Y. Cherel, P. Moullier, and F. Rolling**. 2008. Subretinal delivery of recombinant AAV serotype 8 vector in dogs results in gene transfer to neurons in the brain. Mol. Ther. **16**:916-923.

118. **Quinonez, R. and R. E. Sutton**. 2002. Lentiviral vectors for gene delivery into cells. DNA Cell Biol. **21**:937-951.

119. **Sinn, P. L., S. L. Sauter, and P. B. McCray, Jr.** 2005. Gene therapy progress and prospects: development of improved lentiviral and retroviral vectors--design, biosafety, and production. Gene Ther. **12**:1089-1098.

120. **Dull, T., R. Zufferey, M. Kelly, R. J. Mandel, M. Nguyen, D. Trono, and L. Naldini**. 1998. A third-generation lentivirus vector with a conditional packaging system. J. Virol. **72**:8463-8471.

121. **Naldini, L., U. Blomer, F. H. Gage, D. Trono, and I. M. Verma**. 1996. Efficient transfer, integration, and sustained long-term expression of the transgene in adult rat brains injected with a lentiviral vector. Proc. Natl. Acad. Sci. U. S. A **93**:11382-11388.

122. **Bainbridge, J. W., C. Stephens, K. Parsley, C. Demaison, A. Halfyard, A. J. Thrasher, and R. R. Ali**. 2001. In vivo gene transfer to the mouse eye using an HIV-based lentiviral vector; efficient long-term transduction of corneal endothelium and retinal pigment epithelium. Gene Ther. **8**:1665-1668.

123. **Bemelmans, A. P., C. Kostic, S. V. Crippa, W. W. Hauswirth, J. Lem, F. L. Munier, M. W. Seeliger, A. Wenzel, and Y. Arsenijevic**. 2006. Lentiviral gene transfer of RPE65 rescues survival and function of cones in a mouse model of Leber congenital amaurosis. PLoS. Med. **3**:e347.

124. **Pang, J., M. Cheng, S. E. Haire, E. Barker, V. Planelles, and J. C. Blanks**. 2006. Efficiency of lentiviral transduction during development in normal and rd mice. Mol. Vis. **12**:756-767.

125. **Tschernutter, M., F. C. Schlichtenbrede, S. Howe, K. S. Balaggan, P. M. Munro, J. W. Bainbridge, A. J. Thrasher, A. J. Smith, and R. R. Ali**. 2005. Long-term preservation of retinal function in the RCS rat model of retinitis pigmentosa following lentivirus-mediated gene therapy. Gene Ther. **12**:694-701.

126. **Yanez-Munoz, R. J., K. S. Balaggan, A. MacNeil, S. J. Howe, M. Schmidt, A. J. Smith, P. Buch, R. E. MacLaren, P. N. Anderson, S. E. Barker, Y. Duran, C. Bartholomae, K. C. Von, J. R. Heckenlively, C. Kinnon, R. R. Ali, and A. J. Thrasher**. 2006. Effective gene therapy with nonintegrating lentiviral vectors. Nat. Med. **12**:348-353.

127. **Philpott, N. J. and A. J. Thrasher**. 2007. Use of nonintegrating lentiviral vectors for gene therapy. Hum. Gene Ther. **18**:483-489.

128. **Ramezani, A., T. S. Hawley, and R. G. Hawley**. 2003. Performance- and safety-enhanced lentiviral vectors containing the human interferon-beta scaffold attachment region and the chicken beta-globin insulator. Blood **101**:4717-4724.

129. **Mok, H. P., S. Javed, and A. Lever**. 2007. Stable gene expression occurs from a minority of integrated HIV-1-based vectors: transcriptional silencing is present in the majority. Gene Ther. **14**:741-751.

130. **Millington-Ward, S., B. O'Neill, G. Tuohy, N. Al-Jandal, A. S. Kiang, P. F. Kenna, A. Palfi, P. Hayden, F. Mansergh, A. Kennan, P. Humphries, and G. J. Farrar**. 1997. Strategems in vitro for gene therapies directed to dominant mutations. Hum. Mol. Genet. **6**:1415-1426.

131. **Opalinska, J. B. and A. M. Gewirtz**. 2005. Rationally targeted, conformationally constrained, oxetane-modified oligonucleotides demonstrate efficient gene-silencing activity in a cellular system. Ann. N. Y. Acad. Sci. **1058**:39-51.

132. **Bhisitkul, R. B., G. S. Robinson, R. S. Moulton, K. P. Claffey, E. S. Gragoudas, and J. W. Miller**. 2005. An antisense oligodeoxynucleotide against vascular endothelial growth factor in a nonhuman primate model of iris neovascularization. Arch. Ophthalmol. **123**:214-219.

133. **Mei, H., Y. Xing, J. Yang, A. Wang, Y. Xu, and A. Heiligenhaus**. 2009. Influence of antisense oligonucleotides targeting tumor necrosis factor-alpha on experimental herpetic-induced chorioretinitis of mouse eye. Pathobiology **76**:45-50.

134. **Phylactou, L. A., M. W. Kilpatrick, and M. J. Wood**. 1998. Ribozymes as therapeutic tools for genetic disease. Hum. Mol. Genet. **7**:1649-1653.

135. **Drenser, K. A., A. M. Timmers, W. W. Hauswirth, and A. S. Lewin**. 1998. Ribozyme-targeted destruction of RNA associated with autosomal-dominant retinitis pigmentosa. Invest Ophthalmol. Vis. Sci. **39**:681-689.

136. **Bantounas, I., C. P. Glover, S. Kelly, S. Iseki, L. A. Phylactou, and J. B. Uney**. 2005. Assessing adenoviral hammerhead ribozyme and small hairpin RNA cassettes in neurons: inhibition of endogenous caspase-3 activity and protection from apoptotic cell death. J. Neurosci. Res. **79**:661-669.

137. **Lewin, A. S., K. A. Drenser, W. W. Hauswirth, S. Nishikawa, D. Yasumura, J. G. Flannery, and M. M. LaVail**. 1998. Ribozyme rescue of photoreceptor cells in a transgenic rat model of autosomal dominant retinitis pigmentosa. Nat. Med. **4**:967-971.

138. **Olsson, J. E., J. W. Gordon, B. S. Pawlyk, D. Roof, A. Hayes, R. S. Molday, S. Mukai, G. S. Cowley, E. L. Berson, and T. P. Dryja**. 1992. Transgenic mice with a rhodopsin mutation (Pro23His): a mouse model of autosomal dominant retinitis pigmentosa. Neuron **9**:815-830.

139. **LaVail, M. M., D. Yasumura, M. T. Matthes, K. A. Drenser, J. G. Flannery, A. S. Lewin, and W. W. Hauswirth**. 2000. Ribozyme rescue of photoreceptor cells in P23H transgenic rats: long-term survival and late-stage therapy. Proc. Natl. Acad. Sci. U. S. A **97**:11488-11493.

140. **Gorbatyuk, M., V. Justilien, J. Liu, W. W. Hauswirth, and A. S. Lewin**. 2007. Preservation of photoreceptor morphology and function in P23H rats using an allele independent ribozyme. Exp. Eye Res. **84**:44-52.

141. **Fire, A., S. Xu, M. K. Montgomery, S. A. Kostas, S. E. Driver, and C. C. Mello**. 1998. Potent and specific genetic interference by double-stranded RNA in Caenorhabditis elegans. Nature **391**:806-811.

142. **Boutla, A., C. Delidakis, I. Livadaras, M. Tsagris, and M. Tabler**. 2001. Short 5'-phosphorylated double-stranded RNAs induce RNA interference in Drosophila. Curr. Biol. **11**:1776-1780.

143. **Hammond, S. M., S. Boettcher, A. A. Caudy, R. Kobayashi, and G. J. Hannon**. 2001. Argonaute2, a link between genetic and biochemical analyses of RNAi. Science **293**:1146-1150.

144. **Bernstein, E., A. A. Caudy, S. M. Hammond, and G. J. Hannon**. 2001. Role for a bidentate ribonuclease in the initiation step of RNA interference. Nature **409**:363-366.

145. **Hutvagner, G., J. McLachlan, A. E. Pasquinelli, E. Balint, T. Tuschl, and P. D. Zamore**. 2001. A cellular function for the RNA-interference enzyme Dicer in the maturation of the let-7 small temporal RNA. Science **293**:834-838.

146. **Cullen, B. R.** 2005. RNAi the natural way. Nat. Genet. **37**:1163-1165.

147. **Grosshans, H. and F. J. Slack**. 2002. Micro-RNAs: small is plentiful. J. Cell Biol. **156**:17-21.

148. **Sevignani, C., G. A. Calin, L. D. Siracusa, and C. M. Croce**. 2006. Mammalian microRNAs: a small world for fine-tuning gene expression. Mamm. Genome **17**:189-202.

149. **Lagos-Quintana, M., R. Rauhut, W. Lendeckel, and T. Tuschl**. 2001. Identification of novel genes coding for small expressed RNAs. Science **294**:853-858.

150. **Xu, S.** 2009. microRNA expression in the eyes and their significance in relation to functions. Prog. Retin. Eye Res. **28**:87-116.

151. **Boden, D., O. Pusch, R. Silbermann, F. Lee, L. Tucker, and B. Ramratnam**. 2004. Enhanced gene silencing of HIV-1 specific siRNA using microRNA designed hairpins. Nucleic Acids Res. **32**:1154-1158.

152. **Kim, V. N.** 2004. MicroRNA precursors in motion: exportin-5 mediates their nuclear export. Trends Cell Biol. **14**:156-159.

153. **Grishok, A., A. E. Pasquinelli, D. Conte, N. Li, S. Parrish, I. Ha, D. L. Baillie, A. Fire, G. Ruvkun, and C. C. Mello**. 2001. Genes and mechanisms related to RNA interference regulate expression of the small temporal RNAs that control C. elegans developmental timing. Cell **106**:23-34.

154. **Kolb, F. A., H. Zhang, K. Jaronczyk, N. Tahbaz, T. C. Hobman, and W. Filipowicz**. 2005. Human dicer: purification, properties, and interaction with PAZ PIWI domain proteins. Methods Enzymol. **392**:316-336.

155. **Mourelatos, Z., J. Dostie, S. Paushkin, A. Sharma, B. Charroux, L. Abel, J. Rappsilber, M. Mann, and G. Dreyfuss**. 2002. miRNPs: a novel class of ribonucleoproteins containing numerous microRNAs. Genes Dev. **16**:720-728.

156. **Peters, L. and G. Meister**. 2007. Argonaute proteins: mediators of RNA silencing. Mol. Cell **26**:611-623.

157. **Yuan, Y. R., Y. Pei, J. B. Ma, V. Kuryavyi, M. Zhadina, G. Meister, H. Y. Chen, Z. Dauter, T. Tuschl, and D. J. Patel**. 2005. Crystal structure of A. aeolicus argonaute, a site-specific DNA-guided endoribonuclease, provides insights into RISC-mediated mRNA cleavage. Mol. Cell **19**:405-419.

158. **Doench, J. G. and P. A. Sharp**. 2004. Specificity of microRNA target selection in translational repression. Genes Dev. **18**:504-511.

159. **Gottwein, E., X. Cai, and B. R. Cullen**. 2006. A novel assay for viral microRNA function identifies a single nucleotide polymorphism that affects Drosha processing. J. Virol. **80**:5321-5326.

160. **Krutzfeldt, J., N. Rajewsky, R. Braich, K. G. Rajeev, T. Tuschl, M. Manoharan, and M. Stoffel**. 2005. Silencing of microRNAs in vivo with 'antagomirs'. Nature **438**:685-689.

161. **Weiler, J., J. Hunziker, and J. Hall**. 2006. Anti-miRNA oligonucleotides (AMOs): ammunition to target miRNAs implicated in human disease? Gene Ther. **13**:496-502.

162. **Loscher, C. J., K. Hokamp, P. F. Kenna, A. C. Ivens, P. Humphries, A. Palfi, and G. J. Farrar**. 2007. Altered retinal microRNA expression profile in a mouse model of retinitis pigmentosa. Genome Biol. **8**:R248.

163. **Loscher, C. J., K. Hokamp, J. H. Wilson, T. Li, P. Humphries, G. J. Farrar, and A. Palfi**. 2008. A common microRNA signature in mouse models of retinal degeneration. Exp. Eye Res. **87**:529-534.

164. **Krutzfeldt, J., S. Kuwajima, R. Braich, K. G. Rajeev, J. Pena, T. Tuschl, M. Manoharan, and M. Stoffel**. 2007. Specificity, duplex degradation and subcellular localization of antagomirs. Nucleic Acids Res. **35**:2885-2892.

165. **Hartig, J. V., Y. Tomari, and K. Forstemann**. 2007. piRNAs--the ancient hunters of genome invaders. Genes Dev. **21**:1707-1713.

166. **Aravin, A. A., R. Sachidanandam, A. Girard, K. Fejes-Toth, and G. J. Hannon**. 2007. Developmentally regulated piRNA clusters implicate MILI in transposon control. Science **316**:744-747.

167. **Klenov, M. S., S. A. Lavrov, A. D. Stolyarenko, S. S. Ryazansky, A. A. Aravin, T. Tuschl, and V. A. Gvozdev**. 2007. Repeat-associated siRNAs cause chromatin silencing of retrotransposons in the Drosophila melanogaster germline. Nucleic Acids Res. **35**:5430-5438.

168. **Kim, V. N.** 2006. Small RNAs just got bigger: Piwi-interacting RNAs (piRNAs) in mammalian testes. Genes Dev. **20**:1993-1997.

169. **Lau, N. C., A. G. Seto, J. Kim, S. Kuramochi-Miyagawa, T. Nakano, D. P. Bartel, and R. E. Kingston**. 2006. Characterization of the piRNA complex from rat testes. Science **313**:363-367.

170. **Watanabe, T., A. Takeda, T. Tsukiyama, K. Mise, T. Okuno, H. Sasaki, N. Minami, and H. Imai**. 2006. Identification and characterization of two novel classes of small RNAs in the mouse germline: retrotransposon-derived siRNAs in oocytes and germline small RNAs in testes. Genes Dev. **20**:1732-1743.

171. **Yao, M. C., P. Fuller, and X. Xi**. 2003. Programmed DNA deletion as an RNA-guided system of genome defense. Science **300**:1581-1584.

172. **Tabara, H., E. Yigit, H. Siomi, and C. C. Mello**. 2002. The dsRNA binding protein RDE-4 interacts with RDE-1, DCR-1, and a DExH-box helicase to direct RNAi in C. elegans. Cell **109**:861-871.

173. **Aronin, N.** 2006. Target selectivity in mRNA silencing. Gene Ther. **13**:509-516.

174. **Cullen, B. R.** 2006. Induction of stable RNA interference in mammalian cells. Gene Ther. **13**:503-508.

175. **Reynolds, A., D. Leake, Q. Boese, S. Scaringe, W. S. Marshall, and A. Khvorova**. 2004. Rational siRNA design for RNA interference. Nat. Biotechnol. **22**:326-330.

176. **Ui-Tei, K., Y. Naito, F. Takahashi, T. Haraguchi, H. Ohki-Hamazaki, A. Juni, R. Ueda, and K. Saigo**. 2004. Guidelines for the selection of highly effective siRNA sequences for mammalian and chick RNA interference. Nucleic Acids Res. **32**:936-948.

177. **Holen, T., S. E. Moe, J. G. Sorbo, T. J. Meza, O. P. Ottersen, and A. Klungland**. 2005. Tolerated wobble mutations in siRNAs decrease specificity, but can enhance activity in vivo. Nucleic Acids Res. **33**:4704-4710.

178. **Dykxhoorn, D. M. and J. Lieberman**. 2006. Running Interference: Prospects and Obstacles to Using Small Interfering RNAs as Small Molecule Drugs. Annu. Rev. Biomed. Eng.

179. **Boese, Q., D. Leake, A. Reynolds, S. Read, S. A. Scaringe, W. S. Marshall, and A. Khvorova**. 2005. Mechanistic insights aid computational short interfering RNA design. Methods Enzymol. **392**:73-96.

180. **Schwarz, D. S., H. Ding, L. Kennington, J. T. Moore, J. Schelter, J. Burchard, P. S. Linsley, N. Aronin, Z. Xu, and P. D. Zamore**. 2006. Designing siRNA that distinguish between genes that differ by a single nucleotide. PLoS. Genet. **2**:e140.

181. **Abdelgany, A., M. Wood, and D. Beeson**. 2003. Allele-specific silencing of a pathogenic mutant acetylcholine receptor subunit by RNA interference. Hum. Mol. Genet. **12**:2637-2644.

182. **Dykxhoorn, D. M., L. D. Schlehuber, I. M. London, and J. Lieberman**. 2006. Determinants of specific RNA interference-mediated silencing of human beta-globin alleles differing by a single nucleotide polymorphism. Proc. Natl. Acad. Sci. U. S. A **103**:5953-5958.

183. **Kim, D. H. and J. J. Rossi**. 2003. Coupling of RNAi-mediated target downregulation with gene replacement. Antisense Nucleic Acid Drug Dev. **13**:151-155.

184. **Birmingham, A., E. M. Anderson, A. Reynolds, D. Ilsley-Tyree, D. Leake, Y. Fedorov, S. Baskerville, E. Maksimova, K. Robinson, J. Karpilow, W. S. Marshall, and A. Khvorova**. 2006. 3' UTR seed matches, but not overall identity, are associated with RNAi off-targets. Nat. Methods **3**:199-204.

185. **Pei, Y. and T. Tuschl**. 2006. On the art of identifying effective and specific siRNAs. Nat. Methods **3**:670-676.

186. **Siolas, D., C. Lerner, J. Burchard, W. Ge, P. S. Linsley, P. J. Paddison, G. J. Hannon, and M. A. Cleary**. 2005. Synthetic shRNAs as potent RNAi triggers. Nat. Biotechnol. **23**:227-231.

187. **Chang, K., S. J. Elledge, and G. J. Hannon**. 2006. Lessons from Nature: microRNA-based shRNA libraries. Nat. Methods **3**:707-714.

188. **Silva, J. M., M. Z. Li, K. Chang, W. Ge, M. C. Golding, R. J. Rickles, D. Siolas, G. Hu, P. J. Paddison, M. R. Schlabach, N. Sheth, J. Bradshaw, J. Burchard, A. Kulkarni, G. Cavet, R. Sachidanandam, W. R. McCombie, M. A. Cleary, S. J. Elledge, and G. J. Hannon**. 2005. Second-generation shRNA libraries covering the mouse and human genomes. Nat. Genet. **37**:1281-1288.

189. **Zeng, Y., R. Yi, and B. R. Cullen**. 2003. MicroRNAs and small interfering RNAs can inhibit mRNA expression by similar mechanisms. Proc. Natl. Acad. Sci. U. S. A **100**:9779-9784.

190. **Sano, M., Y. Kato, H. Akashi, M. Miyagishi, and K. Taira**. 2005. Novel methods for expressing RNA interference in human cells. Methods Enzymol. **392**:97-112.

191. **Vlassov, A. V., B. Korba, K. Farrar, S. Mukerjee, A. A. Seyhan, H. Ilves, R. L. Kaspar, D. Leake, S. A. Kazakov, and B. H. Johnston**. 2007. shRNAs targeting hepatitis C: effects of sequence and structural features, and comparision with siRNA. Oligonucleotides. **17**:223-236.

192. **Xia, X. G., H. Zhou, H. Ding, e. B. Affar, Y. Shi, and Z. Xu**. 2003. An enhanced U6 promoter for synthesis of short hairpin RNA. Nucleic Acids Res. **31**:e100.

193. **Shan, Z., Q. Lin, C. Deng, X. Li, W. Huang, H. Tan, Y. Fu, M. Yang, and X. Y. Yu**. 2008. An efficient method to enhance gene silencing by using precursor microRNA designed small hairpin RNAs. Mol. Biol. Rep.

194. **McBride, J. L., R. L. Boudreau, S. Q. Harper, P. D. Staber, A. M. Monteys, I. Martins, B. L. Gilmore, H. Burstein, R. W. Peluso, B. Polisky, B. J. Carter, and B. L. Davidson**. 2008. Artificial miRNAs mitigate shRNA-mediated toxicity in the brain: implications for the therapeutic development of RNAi. Proc. Natl. Acad. Sci. U. S. A **105**:5868-5873.

195. **Zeng, Y., E. J. Wagner, and B. R. Cullen**. 2002. Both natural and designed micro RNAs can inhibit the expression of cognate mRNAs when expressed in human cells. Mol. Cell **9**:1327-1333.

196. **Zeng, Y. and B. R. Cullen**. 2003. Sequence requirements for micro RNA processing and function in human cells. RNA. **9**:112-123.

197. **Desai, D., K. Zhang, S. Barik, A. Srivastava, M. E. Bolander, and G. Sarkar**. 2004. Intragenic codon bias in a set of mouse and human genes. J. Theor. Biol. **230**:215-225.

198. **Brummelkamp, T. R., R. Bernards, and R. Agami**. 2002. A system for stable expression of short interfering RNAs in mammalian cells. Science **296**:550-553.

199. **van de Wetering, M., I. Oving, V. Muncan, M. T. Pon Fong, H. Brantjes, L. D. van, F. C. Holstege, T. R. Brummelkamp, R. Agami, and H. Clevers**. 2003. Specific inhibition of gene expression using a stably integrated, inducible small-interfering-RNA vector. EMBO Rep. **4**:609-615.

200. **Matsukura, S., P. A. Jones, and D. Takai**. 2003. Establishment of conditional vectors for hairpin siRNA knockdowns. Nucleic Acids Res. **31**:e77.

201. **An, D. S., Y. Xie, S. H. Mao, K. Morizono, S. K. Kung, and I. S. Chen**. 2003. Efficient lentiviral vectors for short hairpin RNA delivery into human cells. Hum. Gene Ther. **14**:1207-1212.

202. **Brummelkamp, T. R., R. Bernards, and R. Agami**. 2002. Stable suppression of tumorigenicity by virus-mediated RNA interference. Cancer Cell **2**:243-247.

203. **Shin, K. J., E. A. Wall, J. R. Zavzavadjian, L. A. Santat, J. Liu, J. I. Hwang, R. Rebres, T. Roach, W. Seaman, M. I. Simon, and I. D. Fraser**. 2006. A single lentiviral vector platform for microRNA-based conditional RNA interference and coordinated transgene expression. Proc. Natl. Acad. Sci. U. S. A **103**:13759-13764.

204. **Grimm, D., K. Pandey, and M. A. Kay**. 2005. Adeno-associated virus vectors for short hairpin RNA expression. Methods Enzymol. **392**:381-405.

205. **Michel, U., I. Malik, S. Ebert, M. Bahr, and S. Kugler**. 2005. Long-term in vivo and in vitro AAV-2-mediated RNA interference in rat retinal ganglion cells and cultured primary neurons. Biochem. Biophys. Res. Commun. **326**:307-312.

206. **Tomar, R. S., H. Matta, and P. M. Chaudhary**. 2003. Use of adeno-associated viral vector for delivery of small interfering RNA. Oncogene **22**:5712-5715.

207. **Bridge, A. J., S. Pebernard, A. Ducraux, A. L. Nicoulaz, and R. Iggo**. 2003. Induction of an interferon response by RNAi vectors in mammalian cells. Nat. Genet. **34**:263-264.

208. **Judge, A. D., V. Sood, J. R. Shaw, D. Fang, K. McClintock, and I. MacLachlan**. 2005. Sequence-dependent stimulation of the mammalian innate immune response by synthetic siRNA. Nat. Biotechnol. **23**:457-462.

209. **Sledz, C. A., M. Holko, M. J. de Veer, R. H. Silverman, and B. R. Williams**. 2003. Activation of the interferon system by short-interfering RNAs. Nat. Cell Biol. **5**:834-839.

210. **Kleinman, M. E., K. Yamada, A. Takeda, V. Chandrasekaran, M. Nozaki, J. Z. Baffi, R. J. Albuquerque, S. Yamasaki, M. Itaya, Y. Pan, B. Appukuttan, D. Gibbs, Z. Yang, K. Kariko, B. K. Ambati, T. A. Wilgus, L. A. DiPietro, E. Sakurai, K. Zhang, J. R. Smith, E. W. Taylor, and J. Ambati**. 2008. Sequence- and target-independent angiogenesis suppression by siRNA via TLR3. Nature **452**:591-597.

211. **Kim, D. H., M. Longo, Y. Han, P. Lundberg, E. Cantin, and J. J. Rossi**. 2004. Interferon induction by siRNAs and ssRNAs synthesized by phage polymerase. Nat. Biotechnol. **22**:321-325.

212. **Doench, J. G., C. P. Petersen, and P. A. Sharp**. 2003. siRNAs can function as miRNAs. Genes Dev. **17**:438-442.

213. **Jackson, A. L., S. R. Bartz, J. Schelter, S. V. Kobayashi, J. Burchard, M. Mao, B. Li, G. Cavet, and P. S. Linsley**. 2003. Expression profiling reveals off-target gene regulation by RNAi. Nat. Biotechnol. **21**:635-637.

214. **Grimm, D., K. L. Streetz, C. L. Jopling, T. A. Storm, K. Pandey, C. R. Davis, P. Marion, F. Salazar, and M. A. Kay**. 2006. Fatality in mice due to oversaturation of cellular microRNA/short hairpin RNA pathways. Nature **441**:537-541.

215. **Dickins, R. A., M. T. Hemann, J. T. Zilfou, D. R. Simpson, I. Ibarra, G. J. Hannon, and S. W. Lowe**. 2005. Probing tumor phenotypes using stable and regulated synthetic microRNA precursors. Nat. Genet. **37**:1289-1295.

216. **McCaffrey, A. P. and M. A. Kay**. 2002. A story of mice and men. Gene Ther. **9**:1563.

217. **Xiang, S., J. Fruehauf, and C. J. Li**. 2006. Short hairpin RNA-expressing bacteria elicit RNA interference in mammals. Nat. Biotechnol. **24**:697-702.

218. **Xu, Z. and X. G. Xia**. 2005. RNAi therapy: dominant disease gene gets silenced. Gene Ther. **12**:1159-1160.

219. **Banerjea, A., M. J. Li, G. Bauer, L. Remling, N. S. Lee, J. Rossi, and R. Akkina**. 2003. Inhibition of HIV-1 by lentiviral vector-transduced siRNAs in T lymphocytes differentiated in SCID-hu mice and CD34+ progenitor cell-derived macrophages. Mol. Ther. **8**:62-71.

220. **Boden, D., O. Pusch, F. Lee, L. Tucker, and B. Ramratnam**. 2004. Efficient gene transfer of HIV-1-specific short hairpin RNA into human lymphocytic cells using recombinant adeno-associated virus vectors. Mol. Ther. **9**:396-402.

221. **Denovan-Wright, E. M. and B. L. Davidson**. 2006. RNAi: a potential therapy for the dominantly inherited nucleotide repeat diseases. Gene Ther. **13**:525-531.

222. **Ralph, G. S., P. A. Radcliffe, D. M. Day, J. M. Carthy, M. A. Leroux, D. C. Lee, L. F. Wong, L. G. Bilsland, L. Greensmith, S. M. Kingsman, K. A. Mitrophanous, N. D. Mazarakis, and M. Azzouz**. 2005. Silencing mutant SOD1 using RNAi protects against neurodegeneration and extends survival in an ALS model. Nat. Med. **11**:429-433.

223. **Raoul, C., T. bbas-Terki, J. C. Bensadoun, S. Guillot, G. Haase, J. Szulc, C. E. Henderson, and P. Aebischer**. 2005. Lentiviral-mediated silencing of SOD1 through RNA interference retards disease onset and progression in a mouse model of ALS. Nat. Med. **11**:423-428.

224. **Xia, H., Q. Mao, S. L. Eliason, S. Q. Harper, I. H. Martins, H. T. Orr, H. L. Paulson, L. Yang, R. M. Kotin, and B. L. Davidson**. 2004. RNAi suppresses polyglutamine-induced neurodegeneration in a model of spinocerebellar ataxia. Nat. Med. **10**:816-820.

225. **Campochiaro, P. A.** 2006. Potential applications for RNAi to probe pathogenesis and develop new treatments for ocular disorders. Gene Ther. **13**:559-562.

226. **Dykxhoorn, D. M., D. Palliser, and J. Lieberman**. 2006. The silent treatment: siRNAs as small molecule drugs. Gene Ther. **13**:541-552.

227. **Reich, S. J., J. Fosnot, A. Kuroki, W. Tang, X. Yang, A. M. Maguire, J. Bennett, and M. J. Tolentino**. 2003. Small interfering RNA (siRNA) targeting VEGF effectively inhibits ocular neovascularization in a mouse model. Mol. Vis. **9**:210-216.

228. **Shen, J., R. Samul, R. L. Silva, H. Akiyama, H. Liu, Y. Saishin, S. F. Hackett, S. Zinnen, K. Kossen, K. Fosnaugh, C. Vargeese, A. Gomez, K. Bouhana, R. Aitchison, P. Pavco, and P. A. Campochiaro**. 2006. Suppression of ocular neovascularization with siRNA targeting VEGF receptor 1. Gene Ther. **13**:225-234.

229. **Cashman, S. M., L. Bowman, J. Christofferson, and R. Kumar-Singh**. 2006. Inhibition of choroidal neovascularization by adenovirus-mediated delivery of short hairpin RNAs targeting VEGF as a potential therapy for AMD. Invest Ophthalmol. Vis. Sci. **47**:3496-3504.

230. **Hanze, J., B. G. Eul, R. Savai, S. Krick, P. Goyal, F. Grimminger, W. Seeger, and F. Rose**. 2003. RNA interference for HIF-1alpha inhibits its downstream signalling and affects cellular proliferation. Biochem. Biophys. Res. Commun. **312**:571-577.

231. **Palfi, A., M. Ader, A. S. Kiang, S. Millington-Ward, G. Clark, M. O'Reilly, H. P. McMahon, P. F. Kenna, P. Humphries, and G. J. Farrar**. 2006. RNAi-based suppression and replacement of rds-peripherin in retinal organotypic culture. Hum. Mutat. **27**:260-268.

232. **Cashman, S. M., E. A. Binkley, and R. Kumar-Singh**. 2005. Towards mutation-independent silencing of genes involved in retinal degeneration by RNA interference. Gene Ther. **12**:1223-1228.

233. **Gorbatyuk, M., V. Justilien, J. Liu, W. W. Hauswirth, and A. S. Lewin**. 2007. Suppression of mouse rhodopsin expression in vivo by AAV mediated siRNA delivery. Vision Res. **47**:1202-1208.

234. **Tessitore, A., F. Parisi, M. A. Denti, M. Allocca, V. U. Di, L. Domenici, I. Bozzoni, and A. Auricchio**. 2006. Preferential silencing of a common dominant rhodopsin mutation does not inhibit retinal degeneration in a transgenic model. Mol. Ther. **14**:692-699.

235. **O'Reilly, M., A. Palfi, N. Chadderton, S. Millington-Ward, M. Ader, T. Cronin, T. Tuohy, A. Auricchio, M. Hildinger, A. Tivnan, N. McNally, M. M. Humphries, A. S. Kiang, P. Humphries, P. F. Kenna, and G. J. Farrar**. 2007. RNA interference-mediated suppression and replacement of human rhodopsin in vivo. Am. J. Hum. Genet. **81**:127-135.

236. **Chadderton, N., S. Millington-Ward, A. Palfi, M. O'Reilly, G. Tuohy, M. M. Humphries, T. Li, P. Humphries, P. F. Kenna, and G. J. Farrar**. 2009. Improved Retinal Function in a Mouse Model of Dominant Retinitis Pigmentosa Following AAV-delivered Gene Therapy. Mol. Ther.

237. **Bainbridge, J. W., M. H. Tan, and R. R. Ali**. 2006. Gene therapy progress and prospects: the eye. Gene Ther. **13**:1191-1197.

238. **Yu, J. Y., S. L. DeRuiter, and D. L. Turner**. 2002. RNA interference by expression of short-interfering RNAs and hairpin RNAs in mammalian cells. Proc. Natl. Acad. Sci. U. S. A **99**:6047-6052.

239. **Paskowitz, D. M., K. P. Greenberg, D. Yasumura, D. Grimm, H. Yang, J. L. Duncan, M. A. Kay, M. M. LaVail, J. G. Flannery, and D. Vollrath**. 2007. Rapid and stable knockdown of an endogenous gene in retinal pigment epithelium. Hum. Gene Ther. **18**:871-880.

240. **Matter, K. and M. S. Balda**. 2003. Functional analysis of tight junctions. Methods **30**:228-234.

241. **Matter, K. and M. S. Balda**. 2003. Signalling to and from tight junctions. Nat. Rev. Mol. Cell Biol. **4**:225-236.

242. **Peng, S., C. Rahner, and L. J. Rizzolo**. 2003. Apical and basal regulation of the permeability of the retinal pigment epithelium. Invest Ophthalmol. Vis. Sci. **44**:808-817.

243. **Balda, M. S. and K. Matter**. 2003. Epithelial cell adhesion and the regulation of gene expression. Trends Cell Biol. **13**:310-318.

244. **Jamora, C. and E. Fuchs**. 2002. Intercellular adhesion, signalling and the cytoskeleton. Nat. Cell Biol. **4**:E101-E108.

245. **Fujita, Y., G. Krause, M. Scheffner, D. Zechner, H. E. Leddy, J. Behrens, T. Sommer, and W. Birchmeier**. 2002. Hakai, a c-Cbl-like protein, ubiquitinates and induces endocytosis of the E-cadherin complex. Nat. Cell Biol. **4**:222-231.

246. **Pece, S. and J. S. Gutkind**. 2002. E-cadherin and Hakai: signalling, remodeling or destruction? Nat. Cell Biol. **4**:E72-E74.

247. **Balda, M. S. and K. Matter**. 2000. Transmembrane proteins of tight junctions. Semin. Cell Dev. Biol. **11**:281-289.

248. **Matter, K. and M. S. Balda**. 2007. Epithelial tight junctions, gene expression and nucleo-junctional interplay. J. Cell Sci. **120**:1505-1511.

249. **Balda, M. S., M. D. Garrett, and K. Matter**. 2003. The ZO-1-associated Y-box factor ZONAB regulates epithelial cell proliferation and cell density. J. Cell Biol. **160**:423-432.

250. **Balda, M. S. and K. Matter**. 2000. The tight junction protein ZO-1 and an interacting transcription factor regulate ErbB-2 expression. EMBO J. **19**:2024-2033.

251. **Tsapara, A., K. Matter, and M. S. Balda**. 2006. The heat-shock protein Apg-2 binds to the tight junction protein ZO-1 and regulates transcriptional activity of ZONAB. Mol. Biol. Cell **17**:1322-1330.

252. **Benais-Pont, G., A. Punn, C. Flores-Maldonado, J. Eckert, G. Raposo, T. P. Fleming, M. Cereijido, M. S. Balda, and K. Matter**. 2003. Identification of a tight junction-associated guanine nucleotide exchange factor that activates Rho and regulates paracellular permeability. J. Cell Biol. **160**:729-740.

253. **Pastor, J. C.** 1998. Proliferative vitreoretinopathy: an overview. Surv. Ophthalmol. **43**:3-18.

254. **Rizzolo, L. J.** 2007. Development and role of tight junctions in the retinal pigment epithelium. Int. Rev. Cytol. **258**:195-234.

255. **Arakawa, Y., K. Kajino, S. Kano, H. Tobita, J. Hayashi, M. Yasen, M. Moriyama, Y. Arakawa, and O. Hino**. 2004. Transcription of dbpA, a Y box binding protein, is positively regulated by E2F1: implications in hepatocarcinogenesis. Biochem. Biophys. Res. Commun. **322**:297-302.

256. **Sourisseau, T., A. Georgiadis, A. Tsapara, R. R. Ali, R. Pestell, K. Matter, and M. S. Balda**. 2006. Regulation of PCNA and cyclin D1 expression and epithelial morphogenesis by the ZO-1-regulated transcription factor ZONAB/DbpA. Mol. Cell Biol. **26**:2387-2398.

257. **Lu, Z. H., J. T. Books, and T. J. Ley**. 2006. Cold shock domain family members YB-1 and MSY4 share essential functions during murine embryogenesis. Mol. Cell Biol. **26**:8410-8417.

258. **Xu, J., P. J. Kausalya, D. C. Phua, S. M. Ali, Z. Hossain, and W. Hunziker**. 2008. Early embryonic lethality of mice lacking ZO-2, but Not ZO-3, reveals critical and nonredundant roles for individual zonula occludens proteins in mammalian development. Mol. Cell Biol. **28**:1669-1678.

259. **Pannequin, J., N. Delaunay, C. Darido, T. Maurice, P. Crespy, M. A. Frohman, M. S. Balda, K. Matter, D. Joubert, J. F. Bourgaux, J. P. Bali, and F. Hollande**. 2007. Phosphatidylethanol accumulation promotes intestinal hyperplasia by inducing ZONAB-mediated cell density increase in response to chronic ethanol exposure. Mol. Cancer Res. **5**:1147-1157.

260. **Defoe, D. M., L. B. Adams, J. Sun, S. N. Wisecarver, and E. M. Levine**. 2007. Defects in retinal pigment epithelium cell proliferation and retinal attachment in mutant mice with p27(Kip1) gene ablation. Mol. Vis. **13**:273-286.

261. **Casaroli-Marano, R. P., R. Pagan, and S. Vilaro**. 1999. Epithelial-mesenchymal transition in proliferative vitreoretinopathy: intermediate filament protein expression in retinal pigment epithelial cells. Invest Ophthalmol. Vis. Sci. **40**:2062-2072.

262. **Lee, H., S. J. O'Meara, C. O'Brien, and R. Kane**. 2007. The role of gremlin, a BMP antagonist, and epithelial-to-mesenchymal transition in proliferative vitreoretinopathy. Invest Ophthalmol. Vis. Sci. **48**:4291-4299.

263. **Lee, J. M., S. Dedhar, R. Kalluri, and E. W. Thompson**. 2006. The epithelial-mesenchymal transition: new insights in signaling, development, and disease. J. Cell Biol. **172**:973-981.

264. **Wu, K. H., M. C. Madigan, F. A. Billson, and P. L. Penfold**. 2003. Differential expression of GFAP in early v late AMD: a quantitative analysis. Br. J. Ophthalmol. **87**:1159-1166.

265. **Stevenson, B. R., J. D. Siliciano, M. S. Mooseker, and D. A. Goodenough**. 1986. Identification of ZO-1: a high molecular weight polypeptide associated with the tight junction (zonula occludens) in a variety of epithelia. J. Cell Biol. **103**:755-766.

266. **Katsuno, T., K. Umeda, T. Matsui, M. Hata, A. Tamura, M. Itoh, K. Takeuchi, T. Fujimori, Y. I. Nabeshima, T. Noda, S. Tsukita, and S. Tsukita**. 2008. Deficiency of Zonula Occludens-1 Causes Embryonic Lethal Phenotype Associated with Defected Yolk Sac Angiogenesis and Apoptosis of Embryonic Cells. Mol. Biol. Cell **19**:2465-2475.

267. **Anderson, J. M., C. M. Van Itallie, and A. S. Fanning**. 2004. Setting up a selective barrier at the apical junction complex. Curr. Opin. Cell Biol. **16**:140-145.

268. **Kohno, K., H. Izumi, T. Uchiumi, M. Ashizuka, and M. Kuwano**. 2003. The pleiotropic functions of the Y-box-binding protein, YB-1. Bioessays **25**:691-698.

269. **Antonetti, D. A., A. J. Barber, L. A. Hollinger, E. B. Wolpert, and T. W. Gardner**. 1999. Vascular endothelial growth factor induces rapid phosphorylation of tight junction proteins occludin and zonula occluden 1. A potential mechanism for vascular permeability in diabetic retinopathy and tumors. J. Biol. Chem. **274**:23463-23467.

270. **Defoe, D. M., L. B. Adams, J. Sun, S. N. Wisecarver, and E. M. Levine**. 2007. Defects in retinal pigment epithelium cell proliferation and retinal attachment in mutant mice with p27(Kip1) gene ablation. Mol. Vis. **13**:273-286.

271. **Connell, G., R. Bascom, L. Molday, D. Reid, R. R. McInnes, and R. S. Molday**. 1991. Photoreceptor peripherin is the normal product of the gene responsible for retinal degeneration in the rds mouse. Proc. Natl. Acad. Sci. U. S. A **88**:723-726.

272. **Travis, G. H., J. G. Sutcliffe, and D. Bok**. 1991. The retinal degeneration slow (rds) gene product is a photoreceptor disc membrane-associated glycoprotein. Neuron **6**:61-70.

273. **Boesze-Battaglia, K., F. P. Stefano, C. Fitzgerald, and S. Muller-Weeks**. 2007. ROM-1 potentiates photoreceptor specific membrane fusion processes. Exp. Eye Res. **84**:22-31.

274. **Clarke, G., A. F. Goldberg, D. Vidgen, L. Collins, L. Ploder, L. Schwarz, L. L. Molday, J. Rossant, A. Szel, R. S. Molday, D. G. Birch, and R. R. McInnes**. 2000. Rom-1 is required for rod photoreceptor viability and the regulation of disk morphogenesis. Nat. Genet. **25**:67-73.

275. **Boesze-Battaglia, K., A. F. Goldberg, J. Dispoto, M. Katragadda, G. Cesarone, and A. D. Albert**. 2003. A soluble peripherin/Rds C-terminal polypeptide promotes membrane fusion and changes conformation upon membrane association. Exp. Eye Res. **77**:505-514.

276. **Wrigley, J. D., T. Ahmed, C. L. Nevett, and J. B. Findlay**. 2000. Peripherin/rds influences membrane vesicle morphology. Implications for retinopathies. J. Biol. Chem. **275**:13191-13194.

277. **Farjo, R. and M. I. Naash**. 2006. The role of Rds in outer segment morphogenesis and human retinal disease. Ophthalmic Genet. **27**:117-122.

278. **Ma, J., J. C. Norton, A. C. Allen, J. B. Burns, K. W. Hasel, J. L. Burns, J. G. Sutcliffe, and G. H. Travis**. 1995. Retinal degeneration slow (rds) in mouse results from simple insertion of a t haplotype-specific element into protein-coding exon II. Genomics **28**:212-219.

279. **Portera-Cailliau, C., C. H. Sung, J. Nathans, and R. Adler**. 1994. Apoptotic photoreceptor cell death in mouse models of retinitis pigmentosa. Proc. Natl. Acad. Sci. U. S. A **91**:974-978.

280. **Sohocki, M. M., S. P. Daiger, S. J. Bowne, J. A. Rodriquez, H. Northrup, J. R. Heckenlively, D. G. Birch, H. Mintz-Hittner, R. S. Ruiz, R. A. Lewis, D. A. Saperstein, and L. S. Sullivan**. 2001. Prevalence of mutations causing retinitis pigmentosa and other inherited retinopathies. Hum. Mutat. **17**:42-51.

281. **Sullivan, L. S., S. J. Bowne, D. G. Birch, D. Hughbanks-Wheaton, J. R. Heckenlively, R. A. Lewis, C. A. Garcia, R. S. Ruiz, S. H. Blanton, H. Northrup, A. I. Gire, R. Seaman, H. Duzkale, C. J. Spellicy, J. Zhu, S. P. Shankar, and S. P. Daiger**. 2006. Prevalence of disease-causing mutations in families with autosomal dominant retinitis pigmentosa: a screen of known genes in 200 families. Invest Ophthalmol. Vis. Sci. **47**:3052-3064.

282. **Goldberg, A. F. and R. S. Molday**. 1996. Defective subunit assembly underlies a digenic form of retinitis pigmentosa linked to mutations in peripherin/rds and rom-1. Proc. Natl. Acad. Sci. U. S. A **93**:13726-13730.

283. **Kajiwara, K., L. B. Hahn, S. Mukai, G. H. Travis, E. L. Berson, and T. P. Dryja**. 1991. Mutations in the human retinal degeneration slow gene in autosomal dominant retinitis pigmentosa. Nature **354**:480-483.

284. **Kedzierski, W., M. Lloyd, D. G. Birch, D. Bok, and G. H. Travis**. 1997. Generation and analysis of transgenic mice expressing P216L-substituted rds/peripherin in rod photoreceptors. Invest Ophthalmol. Vis. Sci. **38**:498-509.

285. **Loewen, C. J., O. L. Moritz, B. M. Tam, D. S. Papermaster, and R. S. Molday**. 2003. The role of subunit assembly in peripherin-2 targeting to rod photoreceptor disk membranes and retinitis pigmentosa. Mol. Biol. Cell **14**:3400-3413.

286. **McNally, N., P. F. Kenna, D. Rancourt, T. Ahmed, A. Stitt, W. H. Colledge, D. G. Lloyd, A. Palfi, B. O'Neill, M. M. Humphries, P. Humphries, and G. J. Farrar**. 2002. Murine model of autosomal dominant retinitis pigmentosa generated by targeted deletion at codon 307 of the rds-peripherin gene. Hum. Mol. Genet. **11**:1005-1016.

287. **Elbashir, S. M., J. Harborth, W. Lendeckel, A. Yalcin, K. Weber, and T. Tuschl**. 2001. Duplexes of 21-nucleotide RNAs mediate RNA interference in cultured mammalian cells. Nature **411**:494-498.

288. **Boudreau, R. L., I. Martins, and B. L. Davidson**. 2009. Artificial microRNAs as siRNA shuttles: improved safety as compared to shRNAs in vitro and in vivo. Mol. Ther. **17**:169-175.

289. **Cullen, B. R.** 2006. Enhancing and confirming the specificity of RNAi experiments. Nat. Methods **3**:677-681.

290. **Tam, L. C., A. S. Kiang, A. Kennan, P. F. Kenna, N. Chadderton, M. Ader, A. Palfi, A. Aherne, C. Ayuso, M. Campbell, A. Reynolds, A. McKee, M. M. Humphries, G. J. Farrar, and P. Humphries**. 2008. Therapeutic benefit derived

from RNAi-mediated ablation of IMPDH1 transcripts in a murine model of autosomal dominant retinitis pigmentosa (RP10). Hum. Mol. Genet. **17**:2084-2100.

291. **Barakat, M. R. and P. K. Kaiser**. 2009. VEGF inhibitors for the treatment of neovascular age-related macular degeneration. Expert. Opin. Investig. Drugs **18**:637-646.

292. **Dejneka, N. S., S. Wan, O. S. Bond, D. J. Kornbrust, and S. J. Reich**. 2008. Ocular biodistribution of bevasiranib following a single intravitreal injection to rabbit eyes. Mol. Vis. **14**:997-1005.

293. **Chang, C. I., J. W. Yoo, S. W. Hong, S. E. Lee, H. S. Kang, X. Sun, H. A. Rogoff, C. Ban, S. Kim, C. J. Li, and D. K. Lee**. 2009. Asymmetric shorter-duplex siRNA structures trigger efficient gene silencing with reduced nonspecific effects. Mol. Ther. **17**:725-732.

294. **Brown, B. D., M. A. Venneri, A. Zingale, S. L. Sergi, and L. Naldini**. 2006. Endogenous microRNA regulation suppresses transgene expression in hematopoietic lineages and enables stable gene transfer. Nat. Med. **12**:585-591.

295. **Brown, B. D., B. Gentner, A. Cantore, S. Colleoni, M. Amendola, A. Zingale, A. Baccarini, G. Lazzari, C. Galli, and L. Naldini**. 2007. Endogenous microRNA can be broadly exploited to regulate transgene expression according to tissue, lineage and differentiation state. Nat. Biotechnol. **25**:1457-1467.

296. **Xu, S., P. D. Witmer, S. Lumayag, B. Kovacs, and D. Valle**. 2007. MicroRNA (miRNA) transcriptome of mouse retina and identification of a sensory organ-specific miRNA cluster. J. Biol. Chem. **282**:25053-25066.

Abbreviations

aa	amino acid
AAV	adeno-associated virus
ABCR	ATP-binding cassette transporter
Ad	adenovirus
ADA	adenosine deaminase
ADP	adenosine-5'-diphosphate
adRP	autosomal dominant retinitis pigmentosa
Ago	argonaute
AJ	adherens junction
AMD	age related macular degeneration
AMD	age-related macular degeneration
Arr	arrestin
arRP	autosomal recessive retinitis pigmentosa
ATP	adenosine-5'-triphosphate
Aub	aubergine
BDNF	brain-derived neurotrophic factor
bFGF	basic fibroblast growth factor
BHK	baby hamster kidney cells
Bmp	bone morphogenetic protein
BNB	blood-neural barrier
bp	base pair
BRB	brain-retina barrier
BrdU	5-bromo-2-deoxyuridine solution
cAMP	cyclic AMP
cDNA	complementary DNA
CFH	complement factor H
CGD	chronic granulomatous disease
cGMP	cyclic GMP
CMV	cytomegalovirus
CMZ	ciliary margin zone
CNS	central nervous system
CNTF	ciliary neurotrophic factor
CNV	choroidal neovascularisation
CORD	cone-rod dystrophy
CRALBP	cellular retinaldehyde binding protein
CRBP	cellular retinol-binding protein
CRX	cone-rod otx-like homeobox
Cx	connexin
DMEM	Dulbecco’s Modified Eagle’s Medium
DMSO	dimethylsulfoxide
DNA	deoxyribonucleic acid
ds	double stranded
EAM	encapsidated adenoviral mini-chromosome
EAU	experimental autoimmune uveoretinitis
eGFP	enhanced green fluorescent protein

EIAV	equine infectious anaemia virus
ERG	electroretinogram
ES	embryonic stem cell
Exp	exportin
FACS	fluorescence-activated cell sorter
FBS	fetal bovine serum
Fgf	fibroblast growth factor
FITC	fluorescein isothiocyanate
FIV	feline immunodeficiency virus
GC	ganglion cell
GCAP	guanylate cyclase activator protein
GDNF	glial-cell line derived neurotrophic factor
GDP	guanosine- 5'-diphosphate
GJ	gap junction
GMP	guanosine 5'-monophosphate
GTP	guanosine-5'-triphosphate
HEK	human embryonic kidney cells
HIV	human immunodeficiency virus
hr	hour
hrGFP	human recombinised green fluorescent protein
HRP	horseradish peroxidase
HSV	herpes simplex virus
IL	interleukin
ILM	inner limiting membrane
IMPDH1	inosine monophosphate dehydrogenase 1
INL	inner nuclear layer
IPL	inner plexiform layer
IPM	inter photoreceptor matrix
IRBP	interphotoreceptor retinoid-binding protein
IS	inner segments
ITR	inverted terminal repeats
JAM	junction adhesion molecule
kb	kilobase
kDa	kilodalton
l	litre
LCM	laser capture microdissection
LRAT	lecithin-retinol acyltransferase
LTR	long tandem repeats
m	meter
m-	milli
µ-	micro-
MAGUK	membrane-associated guanylate cyclase
MD	macular degeneration
MDCK	Madin-Darby canine kidney cells
Mertk	mer-receptor tyrosine kinase
min	minute
miRNA	micro RNA
miRNP	miRNA ribonucleoprotein
MOI	multiplicity of infection
mRNA	messenger RNA

mut	mutant
Mv	microvilli
n-	nano-
NACos	nucleus and adhesion complexes
ncRNA	non-coding RNA
NF	nerve fibre layer
NRL	neural retina leucine zipper transcription factor
nt	nucleotide
OIR	oxygen-induced retinopathy
OLM	outer limiting membrane
ONL	outer nuclear layer
OPL	outer plexiform layer
OS	outer segments
P	postnatal day
PAZ	Piwi Argonaute and Zwille
PCR	polymerase chain reaction
PDE	phosphodiesterase
PEDF	pigment epithelium derived factor
PEG	Polyethylene glycol
Ph	phagosome
pi	post injection
piRNA	Piwi-interacting RNA
Prph2	peripherin2
PTGS	post transcriptional gene silencing
R*	metarhodopsin
rAAV	recombinant AAV
rasiRNA	repeat-associated siRNA
RCS	royal college of surgeons
rd	retinal degeneration
RDH	retinol dehydrogenase
RDS	retinal degeneration slow
Rec	recoverin
retGC	retinal guanylate cyclase
RFP	red fluorescent protein
RGC	retinal ganglion cells
RGR	retinal G-protein-coupled receptor
Rho	rhodopsin
RISC	RNA induced silencing complex
RK	rhodopsin kinase
RNA	ribonucleic acid
RNAi	RNA interference
ROM-1	retinal outer segment membrane protein-1
RP	retinitis pigmentosa
RPC	retinal progenitor cell
RPE	retinal pigment epithelium
RPGR	retinitis pigmentosa GTPase regulator
RPGRIP	RPGR-interacting protein
rRNA	ribosomal RNA
RT	reverse transcriptase
RVE	retinal vascular endothelium

scAAV	self-complementary AAV
SCID	severe combined immunodeficiency
SFFV	spleen focus-forming virus
sFLT	soluble fms-like tyrosine kinase 1
Shh	sonic hedgehog
shRNA	short hairpin RNA
SIN	self inactivating
siRNA	short interfering RNA
ss	single strand
TEM	transmission electron microscopy
TIMP3	tissue inhibitor of metalloproteinase 3
TJ	tight junction
TNF-α	tumor necrosis factor alpha
tRNA	transfer RNA
UCOE	ubiquitously-acting chromatin opening element
UTR	untranslated regions
VEGF	vascular endothelial growth factor
vp	viral particles
VSV-G	vesicular-stomatitis virus G-protein
w/v	weight/volume
WPRE	Woodchuck hepatitis virus post-transcriptional element
wt	wild-type
xl	X-linked
ZO-1	zonula occludens-1
ZONAB	ZO-1 associated nucleic-acid binding

Publications arising from this project

Regulation of PCNA and cyclin D1 expression and epithelial morphogenesis by the ZO-1-regulated transcription factor ZONAB/DbpA. Tony Sourisseau, Anastasios Georgiadis, Anna Tsapara, Robin R. Ali, Richard Pestell, Karl Matter, Maria S. Balda. *Molecular and Cellular Biology*. 2006. 26(6):2387-98

AAV-mediated knockdown of Peripherin-2 *in vivo* using miRNA-based hairpin design. Anastasios Georgiadis, Marion Tschernutter, James W. B. Bainbridge, Scott J. Robbie, Adrian J. Thrasher, Alexander J. Smith, Robin R. Ali. *Gene Therapy.* 2009. In Press.

The tight junction-regulated ZO-1/ZONAB pathway regulates retinal pigment epithelium homeostasis in mice. Anastasios Georgiadis, Marion Tschernutter, James W. B. Bainbridge, Kamaljit S. Balaggan, Freya Mowat, Peter M.G. Munro, Adrian J. Thrasher, Karl Matter, Maria S. Balda, Robin R. Ali. 2009. *Manuscript in preparation for Molecular and Cellular Biology.*

Appendix

Plasmids used in viral-mediated RNA interference:

RNAi expression plasmids – mu6pro

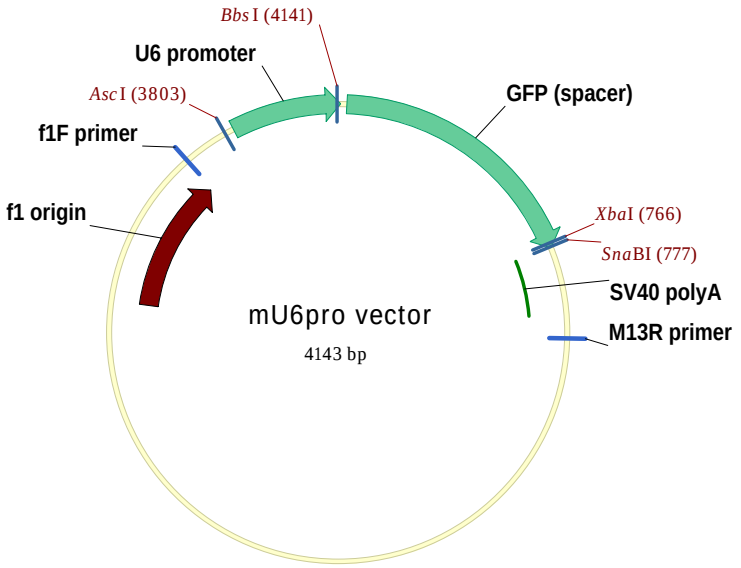

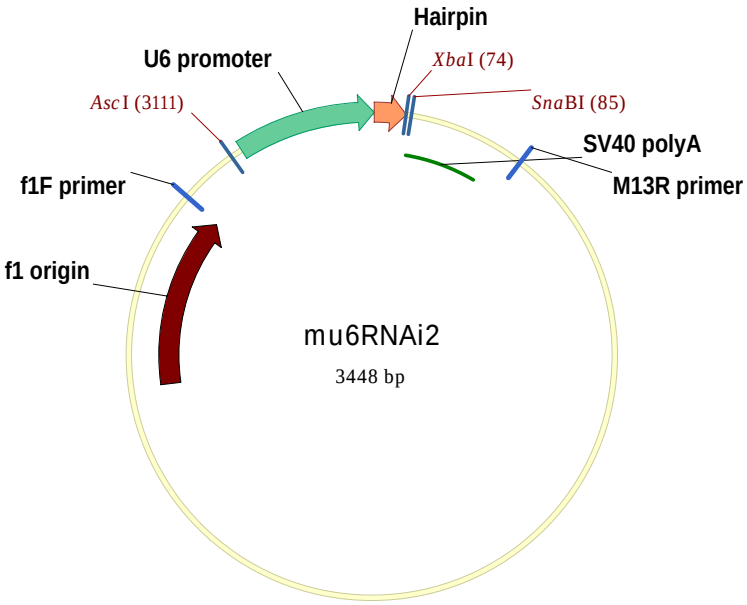

AAV backbone plasmids – pD10

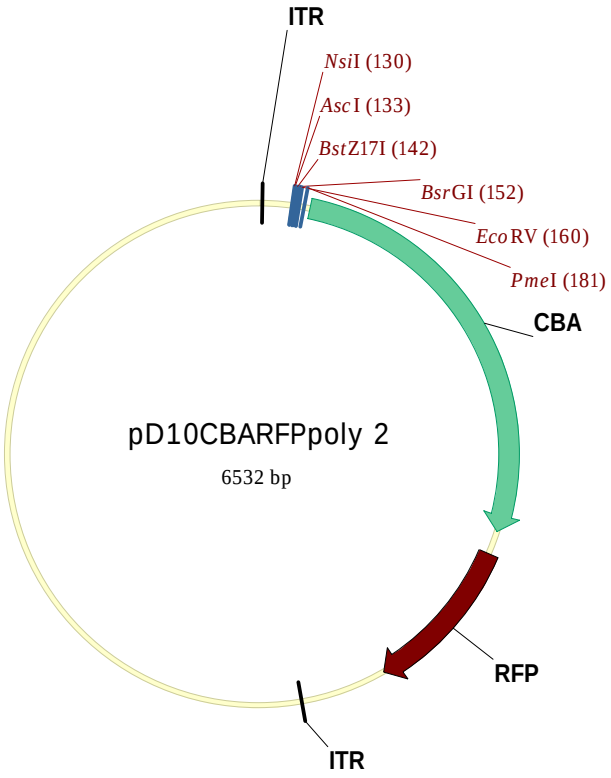

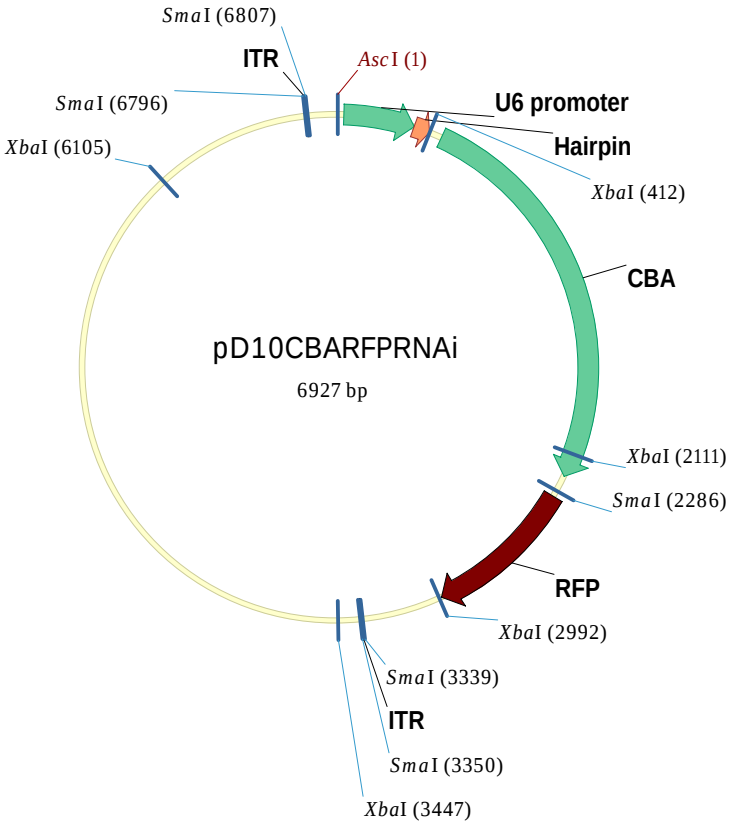

Lentivirus backbone plasmids – pHR'SIN

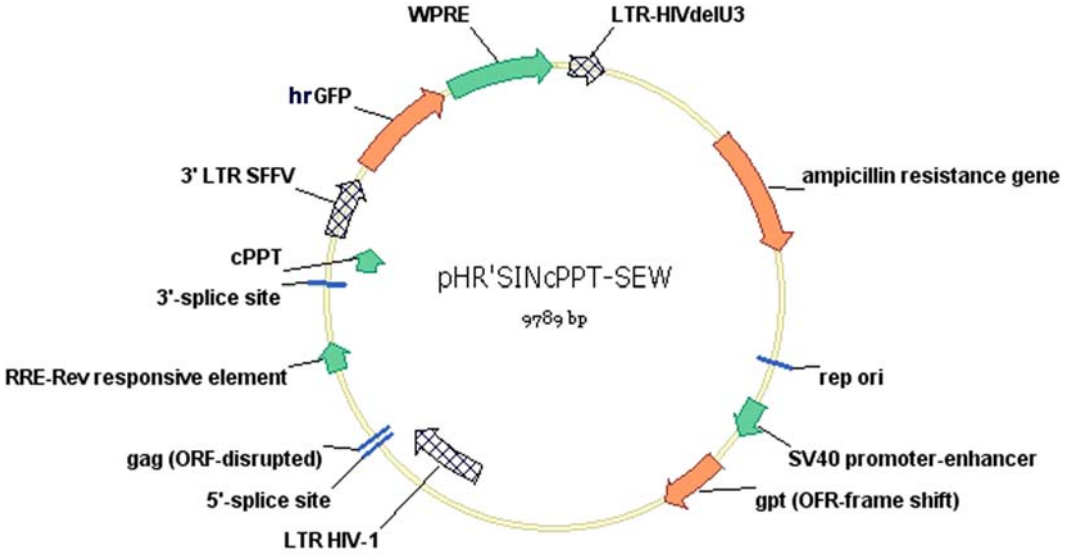

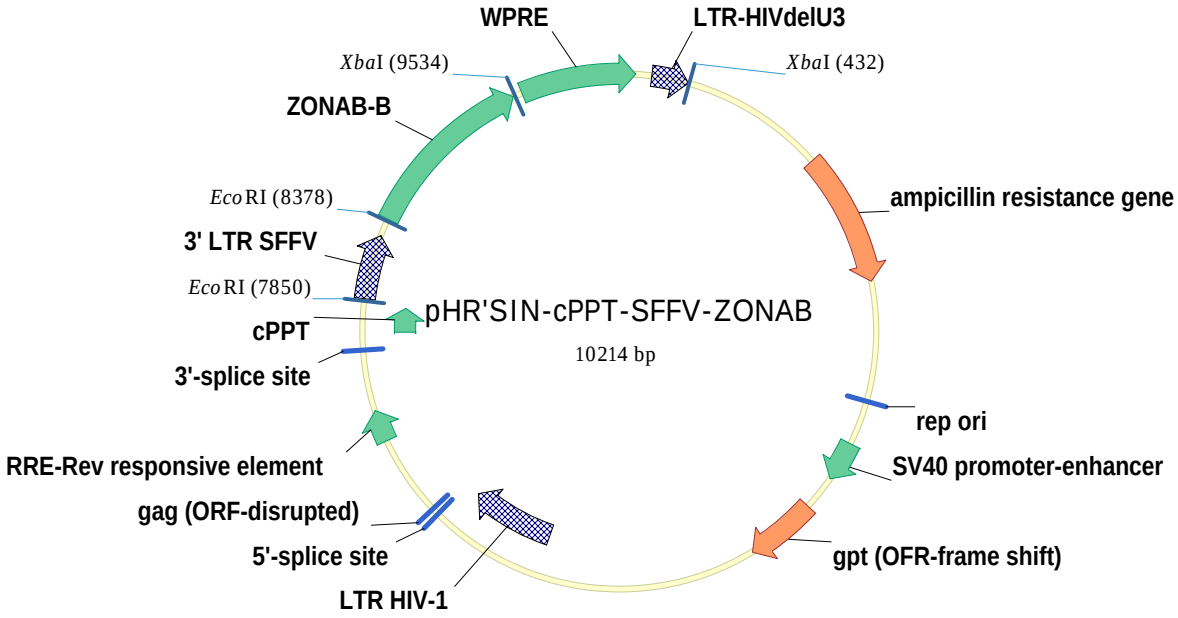

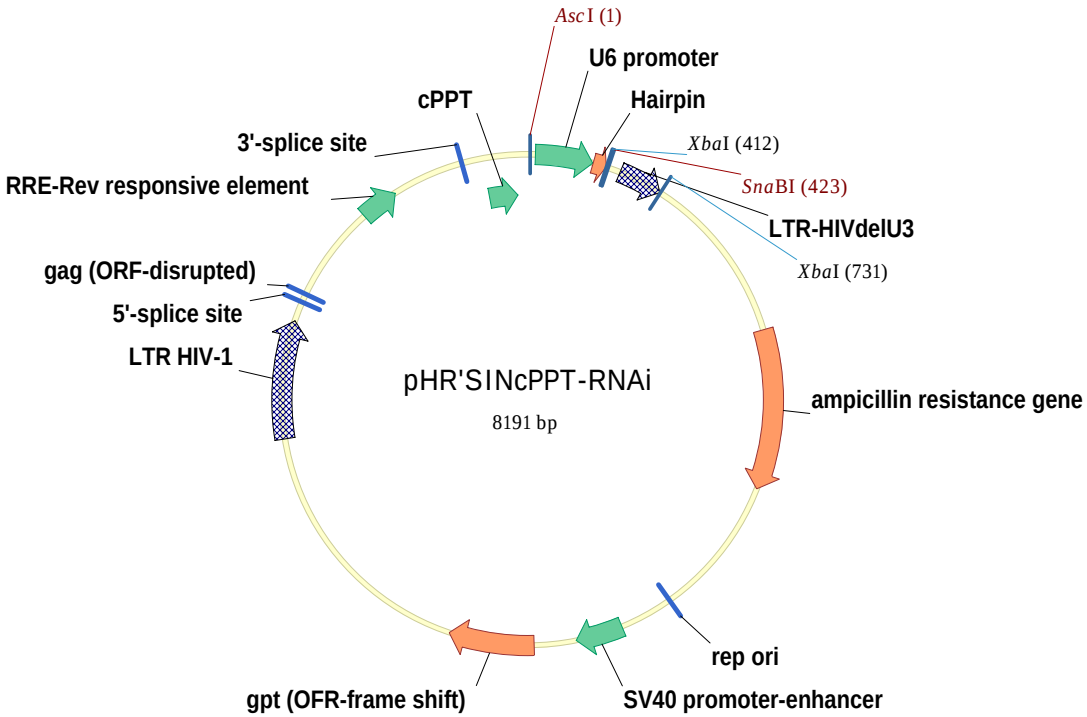
AscI (1)
U6 promoter
cPPT
Hairpin
3'-splice site
XbaI (412)
RRE-Rev responsive element
SnaBI (423)
LTR-HIVdelU3
XbaI (731)
gag (ORF-disrupted)
5'-splice site
LTR HIV-1
pHR'SINcPPT-RNAi
8191 bp
ampicillin resistance gene
rep ori
gpt (OFR-frame shift)
SV40 promoter-enhancer